

# Oil And Gas Geoscience Reports 2010



**Ministry of Energy, Mines and Petroleum Resources**  
Resource Development and Geoscience Branch



© British Columbia Ministry of Energy, Mines and Petroleum Resources  
Oil and Gas Division  
Resource Development and Geoscience Branch  
Victoria, British Columbia, April 2010

Please use the following citation format when quoting or reproducing parts of this document:

Fefchak, C. and Zonneveld, J-P. (2010): Sedimentary geology of the Artex Member, Brassey Field, northeastern British Columbia; Geoscience Reports 2010, BC Ministry of Energy, Mines and Petroleum Resources, pages 1-10.

Colour digital copies of this publication in Adobe Acrobat PDF format are available, free of charge, from the BC Ministry of Energy, Mines and Petroleum Resources website at:

*<http://www.em.gov.bc.ca/subwebs/oilandgas/pub/reports.htm>*

## FOREWORD

This volume of Geoscience Reports is published annually by the Resource Development and Geoscience Branch of the Oil and Gas Division, British Columbia Ministry of Energy, Mines and Petroleum Resources. This publication highlights petroleum-related geological activities carried out in British Columbia by ministry staff and affiliated universities, federal government and industry researchers. The 2010 volume contains seven articles that cover a wide range of topics focussing mainly on new play concepts and unconventional gas development in the Horn River Basin, the northern Foothills and the Dawson – Ft. St. John region (Montney play area). Other contributions include a paper on Triassic porosity-trend mapping to identify possible sites for carbon sequestration and a paper on oil and gas prospectivity in the Nechako Basin.

The first paper in the volume by Chelsea Fefchak and John-Paul Zonneveld, both from the University of Alberta, focuses on the sedimentology of the Upper Triassic Artex Member of the Charlie Lake Formation in northeastern British Columbia. The economic significance of the Artex Member is exemplified by prolific hydrocarbon production in the Brassey Field. The authors show that the Artex Member at the Brassey Field is an aeolian sand dune succession. The paper demonstrates the importance of lithofacies interpretations and highlights how paleo-topographic depressions control deposition of the Artex reservoir facies.

Evaluation of potential source rocks in pre-Givetian (Middle Devonian) strata in northeast BC is critical to furthering the exciting play concept that tremendous hydrocarbon accumulations may occur in these strata. Filippo Ferri from the BC Resource Development and Geoscience Branch and Martyn Golding from the University of British Columbia, address this important question in an evaluation of the hydrocarbon source rock potential of Ordovician and Silurian sediments in Halfway River map area in the northern foothills. Over 500 metres of silty dolomite, calcareous siltstone, and quartzite of the upper Skoki Formation and Road River Group were examined. Calcareous siltstones of the Road River Group are shown to have the best source rock characteristics. More basinal equivalents of the Skoki Formation, farther west in the Kechika Trough, are identified as potential source-rocks that require further testing.

New data on surface equivalents of the prolific Montney and Doig formations are provided by Filippo Ferri (BC Resource Development and Geoscience Branch), Martyn Golding and James Mortensen (University of British Columbia), John-Paul Zonneveld (University of Alberta) and Michael Orchard (Geological Survey of Canada). Ferri and his co-authors studied a key section of the Toad Formation in the Halfway River map area. Sedimentologic descriptions, spectral gamma-ray measurements, and samples for Rock-Eval analysis and thermal maturation determination were obtained for a 600 m thick sequence of the Toad Formation. The sequence of calcareous siltstones and fine sandstones is interpreted as a coarsening-upward succession of distal turbidites, which become more proximal in the upper part of the section. A correlation of the surface sequence with subsurface sections is also presented.

Two articles directly relating to development within the Horn River shale basin deal with potential sand sources for hydraulic fracturing (paper by Hickin *et al.*) and water budget information in the basin (see paper by Johnson).

A timely study of potential hydraulic fracture sand sources is provided by Adrian Hickin, Filippo Ferri and Travis Ferbey, from the BC Ministry of Energy, Mines and Petroleum Resources, and Rod Smith from the Geological Survey of Canada. The study was prompted by a dramatic increase in the demand for hydraulic fracture proppant (frac sand), required to develop the enormous unconventional gas resources of the Horn River and Montney plays. A preliminary assessment of bedrock and unconsolidated samples collected during previous regional projects is presented. Thin sections and distribution maps of prospective bedrock units are provided. For unconsolidated samples, geochemistry and grain-size data and grain photographs are also provided. Results suggest that quartz arenites of the Liard, Monteith and Monach formations and feldspathic arenites of the Charlie Lake Formation are the most prospective bedrock units of those assessed. The most prospective Quaternary sand units include: well-rounded, quartz-rich sands in the Komie area on the western edge of the Horn River Basin; fine-grained quartz sand in the Fontas dune field; and quartz-rich glaciofluvial deltaic sands from the Redwillow area south of Dawson Creek. Other dune fields in the Kiskatinaw and Pine River areas and eskers, in and around the Horn River Basin, are also identified as potential exploration targets.

...more

A second paper, applicable to the Horn River Basin, is a conceptual water model for the basin presented by Elizabeth Johnson of the BC Resource Development and Geoscience Branch. This paper provides a valuable information base needed for water management in areas of shale gas development in northeast British Columbia. Johnson discusses water modelling, important information sources, specific features that will affect hydrological predictions in the region and information gaps. Results of the analyses show that precipitation is not uniform across the basin, and that evapotranspiration is a very important component, at times exceeding precipitation. Other important parameters in the water balance include groundwater flow, which maintains stream water quality and quantity, and frost/permafrost, which controls subsurface flow, infiltration and recharge rates.

Ed Janicki from the BC Resource Development and Geoscience Branch provides an update on Triassic porosity-trend mapping initially conducted 2008. The work is intended to identify possible sites for carbon sequestration. Wireline logs from an additional 200 wells were added to the initial study of 600 wells to improve data density and extend the study area. The best prospects for carbon storage identified in the paper are thick, porous sections of the Halfway and Baldonnel formations near the southern end of the studied area. Secure locations might also include more isolated, lightly drilled areas around the edge of existing Triassic oil and gas producing regions.

The most recent results of a multi-year project aimed at evaluating the oil and gas prospectivity of the Nechako Basin, in British Columbia's interior, are provided in the paper by Riddell from the BC Resource Development and Geoscience Branch. This paper presents a summary of 17 radiometric dates and 69 apatite fission-track analyses. The new radiometric ages provide constraints on the distribution of prospective rocks and the locations of important structures. The apatite fission-track data constrain the time limits of a rock's most recent passage through oil and gas windows and indicate whether it has been heated enough for hydrocarbon generation since trap-forming tectonic events occurred.

**Vic M. Levson**

Executive Director,  
Resource Development and Geoscience Branch,  
Oil and Gas Division,  
British Columbia Ministry of Energy, Mines and Petroleum Resources

# TABLE OF CONTENTS

## GEOSCIENCE REPORTS 2010

|  |     |
|--|-----|
| SEDIMENTARY GEOLOGY OF THE ARTEX MEMBER, BRASSEY FIELD, NORTHEASTERN BRITISH COLUMBIA ..... 1<br><i>by Chelsea Fefchak, and John-Paul Zonneveld</i>  | 1   |
| EVALUATION OF ORDOVICIAN AND SILURIAN STRATIGRAPHY FOR HYDROCARBON SOURCE-ROCK POTENTIAL IN THE NORTHERN<br>HALFWAY RIVER MAP AREA, BRITISH COLUMBIA (NTS 094B/13) ..... 11<br><i>by Filippo Ferri, Martyn Golding</i>                         | 11  |
| TOAD FORMATION (MONTNEY AND DOIG EQUIVALENT) IN THE NORTHWESTERN HALFWAY RIVER MAP AREA,<br>BRITISH COLUMBIA (NTS 094B/14) ..... 21<br><i>by Filippo Ferri, Martyn L. Golding, James K. Mortensen, John-Paul Zonneveld, Michael J. Orchard</i> | 21  |
| PRELIMINARY ASSESSMENT OF POTENTIAL HYDRAULIC FRACTURE SAND SOURCES AND THEIR DEPOSITIONAL ORIGIN,<br>NORTHEAST BRITISH COLUMBIA ..... 35<br><i>by Adrian S. Hickin, Fil Ferri, Travis Ferbey and I. Rod Smith</i>                             | 35  |
| TRIASSIC POROSITY TRENDS IN NORTHEASTERN BRITISH COLUMBIA UPDATE FEBRUARY 2009..... 93<br><i>by E. Janicki</i>   | 93  |
| CONCEPTUAL WATER MODEL FOR THE HORN RIVER BASIN, NORTHEAST BRITISH COLUMBIA (PARTS OF NTS 094I, J, O, P) ..... 99<br><i>by Elizabeth Johnson</i>   | 99  |
| SUMMARY OF APATITE FISSION-TRACK ANALYSES AND RADIOMETRIC DATES FROM THE NECHAKO REGION, BRITISH COLUMBIA (NTS 92O, N;<br>93B, C, E, F, G, L) AND IMPLICATIONS FOR OIL AND GAS PROSPECTIVITY ..... 123<br><i>by J.M. Riddell</i>               | 123 |



# SEDIMENTARY GEOLOGY OF THE ARTEX MEMBER, BRASSEY FIELD, NORTHEASTERN BRITISH COLUMBIA

*Chelsea Fefchak<sup>1</sup>, and John-Paul Zonneveld<sup>1</sup>*

---

## ABSTRACT

*Hydrocarbon production from the lower Charlie Lake Formation (Upper Triassic) of northeastern British Columbia occurs primarily from sandstone units such as the Artex Member. The Brassey Field is one of the more prolific fields producing from the Artex Member. At the Brassey Field, the Artex Member comprises an aeolian sand dune succession encased in an anhydritic and dolomitic interdune/supratidal package. Despite the economic importance of this member, few studies have focused on the sedimentology of this interval; consequently, the facies relationships, geological history and depositional controls of this member remain unconstrained.*

*Detailed core analysis and petrography augmented with wireline log correlations have aided in the development of a preliminary facies model for the Artex Member at the Brassey Field. Ten lithofacies grouped into three facies associations have been identified. These facies associations are interpreted to record deposition in aeolian sand dune, interdune/supratidal sabhka, lagoon and lake, and transgressive shoreface environments. Reservoir-quality lithofacies are limited to aeolian sandstone interval (Brassey Member) usually 1 to 3 m thick. Net reservoir thickness is a function of total sandstone thickness minus the proportion of sandstone characterized by porosity-occluding cements (primarily anhydrite). These cements are interpreted to be early postdepositional and related to dissolution of gypsum and anhydrite interbeds that interfinger with other rock types in the interdune/supratidal flat successions. The Artex Member in Brassey Field is preserved within a local topographic depression on the surface of the underlying Halfway Formation. Recognition of these hollows is critical to aid in the development of predictable models for the Artex Member sand.*

Fefchak, C. and Zonneveld, J-P. (2010): Sedimentary geology of the Artex Member, Brassey Field, northeastern British Columbia; Geoscience Reports 2010, BC Ministry of Energy, Mines and Petroleum Resources, pages 1–10.

<sup>1</sup>chnology Research Group, Department of Earth and Atmospheric Sciences, University of Alberta, Edmonton, AB

**Key Words:** Sedimentology, Facies Analysis, Aeolian, Brassey Field, Charlie Lake Formation, Artex Member, Triassic

---

## INTRODUCTION

The Middle–Upper Triassic (Late Ladinian to Carnian) Charlie Lake Formation occurs most extensively in northeastern British Columbia. It is a lithologically diverse succession of primarily unfossiliferous mixed siliciclastic, carbonaceous and evaporitic rocks. Historically, these rocks have been interpreted to represent a sabhka or back-barrier depositional environment (Arnold, 1994; Higgs, 1990). Adjacent formations consist of the older (underlying) Middle Triassic (Ladinian) Halfway Formation and the younger (overlying) Upper Triassic (Carnian) Baldonnel Formation. These units are composed of rock types that are easily distinguished from the Charlie Lake Formation and thus formation contacts are easily distinguished in drillcore and on petrophysical logs. The Halfway Formation has been described as a fossiliferous marine sandstone succession that is a temporal equivalent to the Charlie Lake Formation (Arnold, 1994; Caplan and Moslow, 1997). Consequently, the transition to the Charlie Lake Formation represents a

marine-nonmarine regression that is gradational in some areas of the basin but appears to be sharp and abrupt in others. The contact between the Halfway Formation and the Charlie Lake Formation is conformable in many areas (Arnold, 1994) including the study area, although it has been argued to be unconformable in other areas. The overlying Charlie Lake–Baldonnel Formation contact consists of an abrupt shift to fossiliferous limestone and dolomite (Zonneveld and Orchard, 2002). This contact is conformable and gradational in many parts of the basin but is demarcated by an abrupt erosional surface in others (Davies, 1997a; Zonneveld and Orchard, 2002).

Triassic strata account for approximately 40% of oil reserves in British Columbia, making this unit both of economic and academic interest (Zonneveld et al., 2004). Several sand-dominated, commonly hydrocarbon-bearing members of the Charlie Lake Formation occur above the thick Halfway Formation sandstone succession (e.g., the Siphon, Blueberry and Artex members). As recognized by several authors (e.g., Dixon, 2007), facies descriptions in

the Charlie Lake Formation have been lacking, mainly due to the fact that the majority of drill-core intervals have been focused on the zone below the 'A' marker, a locally fossiliferous limestone of marine derivation. Several studies have focused on the regional extent and stratigraphy of the Charlie Lake Formation sandstone bodies and the relationship of the Charlie Lake Formation to underlying strata (Higgs, 1990; Young, 1997; Dixon, 2007).

The best known of these sandstone intervals consists of the Artex Member, which occurs in the basal beds of the Charlie Lake Formation. The Artex Member produces hydrocarbons in several of parts of the basin, commonly exploited as a secondary target encountered in Halfway Formation exploration and development wells. Hydrocarbon production at the Brassey Field (Figure 1), the focus of the present study, produces primarily from the Artex Member. This field has been the focus of several investigations since its discovery in the late 1980s (e.g., Higgs, 1990; Woofter and MacGillvray, 1990). It has produced over 78 MBLs to date (Accumap, 2010).

Previous studies have focused on stratigraphic, engineering and development aspects of the Artex sands at Brassey Field (e.g., Higgs, 1990; Woofter and MacGillvray, 1990). This investigation focuses on the process sedimentology and petrography of reservoir and host-rock types and tests the premise that the Artex Member at the Brassey Field consists of a buried aeolian dune succession. A clearer understanding of the sedimentary framework of this unit is essential for petroleum exploration and development. To date, predictive facies models are lacking for this reservoir interval.

## METHODS

Fourteen drill-cores from within and around the Brassey Field were examined in detail and sampled for petrographic analyses. Ten distinct facies and subfacies (summarized below) have been identified. The drill-cores used in this study penetrate various portions of Artex member, the reservoir unit in the Brassey Field. In order to aid in developing criteria for establishing proximity indicators and constructing a predictive facies model, the core selected represent Artex strata found in producing oil pools as well as those outside the pools.

The Wentworth scale was used to describe variations in grain size. Additionally, to describe the bioturbated strata, a bioturbation index (BI) has been used (Taylor and Goldring, 1993). This index quantifies the degree of reworking by assigning a relative number to bioturbated sediment.

Textural components often used to describe and interpret aeolian environments are typically less visible in drill-core than in outcrop because natural weathering can highlight seminal criteria such as grain-size variations in

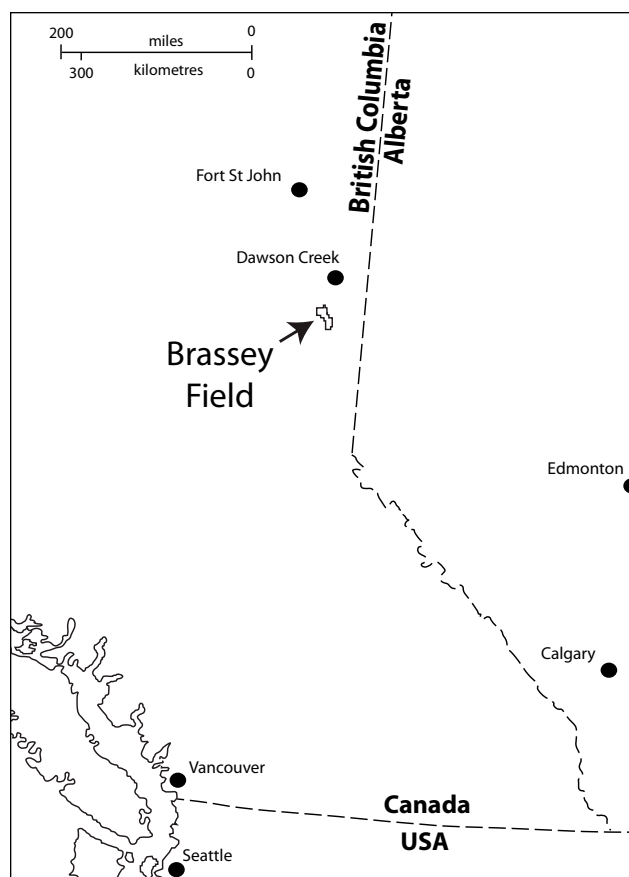


Figure 1. Location of the Brassey Field, northeastern British Columbia; modified from Woofter and MacGillvray (1990).

the laminae. In addition, intense internal heterogeneities, due in part to advanced postdepositional diagenesis, has affected reservoir quality and has likely destroyed some of the textures and structures useful for interpretation. Despite this, it is apparent that the distribution of the reservoir facies remains the primary control on the extent, shape and quality of the reservoir.

## Facies Descriptions

### Facies 1: Dolomitic bioturbated siltstone (F1)

Facies 1 is a dolomitic bioturbated siltstone with common silt or very fine grained sand laminae. This facies is characterized by a mottled or clotted texture. The 'mottling' is a result of areally variable syndepositional bioturbation (Zonneveld et al., 2001). The traces are dominated by relatively simple forms (such as *Planolites*) with variable orientations including horizontal, vertical and inclined. The bioturbation index ranges from light to moderate (BI 1–BI 3). Sedimentary structures (visible within lightly mottled intervals) include oscillatory ripples. Facies 1 is commonly interbedded with both light and dark mud beds, 3–6 cm thick. A single subfacies (F1a) was identified to further describe the variations in this facies. Subfacies F1a is

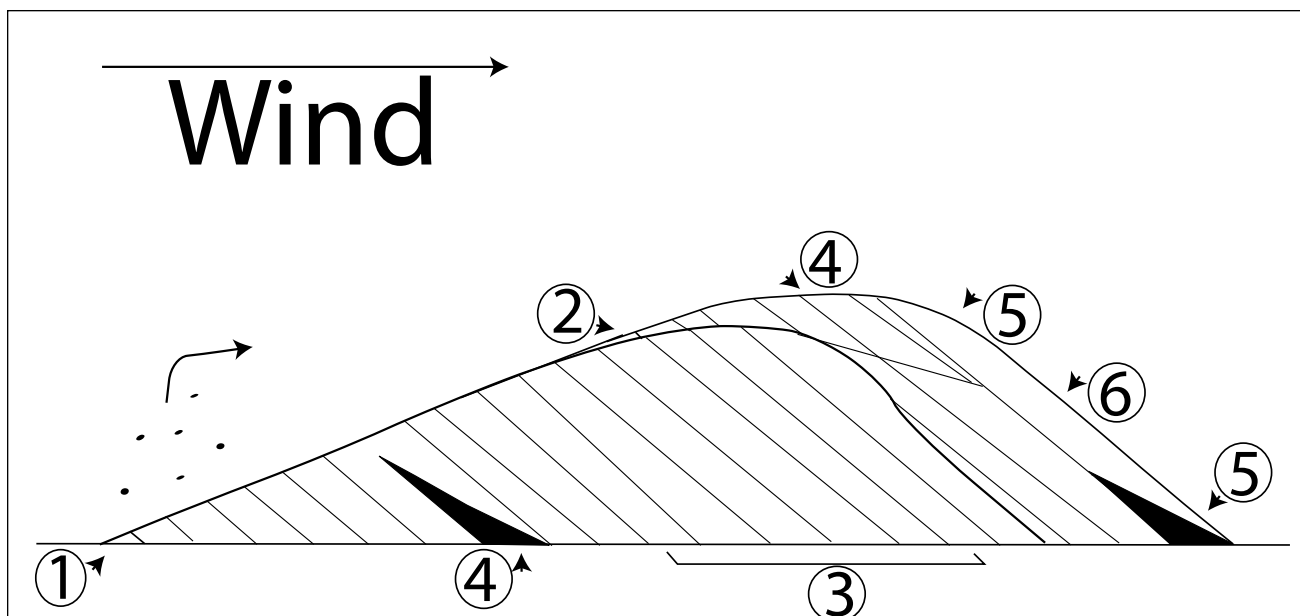


Figure 2. Simplified aeolian dune showing depositional and architectural features. The dune depicted in this schematic has undergone migration on the draa with unidirectional wind influence: 1) First-order bounding surface; showing a draa-interdune contact; 2) second-order bounding surface; dune-dune; 3) third-order bounding surfaces are aeolian laminations; 4) wind-influenced strata-spatial location of wind ripple or planar strata, found at the crest or apron of subsequent dunes, where wind influence is at its strongest; 5) location of grainfall laminae; 6) location of sandflow laminae.

a dolomitic, bioturbated siltstone with vuggy porosity. The vugs range in size from 0.4 to 1.0 cm. They are most commonly filled with calcite or anhydrite cement, but unfilled examples were also observed. Patches of moderate porosity characterize this subfacies; however, permeability is lacking.

Facies 2: Well-sorted fine- to medium-grained sandstone (F2)

Facies 2 is characterized by very fine to medium-grained sand. The cement consists primarily of patchy anhydrite and/or calcite. Cementation is the primary porosity inhibitor within this reservoir subfacies; thus the porosity ranges from nearly zero to relatively high (>15% from a visual estimation of thin sections). The pervasiveness of the anhydrite cement ranges from light to heavy. Significant variation occurs in nodule morphology with diameters ranging from about 1 to 3 cm. In this facies, the porosity is dominantly dependent on the degree of anhydrite cementation. This facies comprises the Artex Member and is the primary reservoir unit in the Brassey Field. Variability in the Artex Member sandstone has resulted in differentiation of two subfacies within this facies.

Subfacies 2a consists primarily of fine- to medium-grained, moderately to well-sorted, trough cross-stratified sand, with average foreset inclinations of ~20–25°. Low-angle (<10°) cross-strata (with identical grain-size, oil staining and porosity) occur intermittently interbedded with the steeper beds. Sedimentary structures include common

oscillatory ripples. This unit is often stained with micrinite bitumen, as noted by Klein and Woofter (1989). Additionally, subfacies F2a has an erosive contact with the underlying facies. The average thickness of this unit is variable, but is usually approximately 1–3 m. This subfacies comprises the primary reservoir rock type in the Artex Member at the Brassey Field.

Subfacies 2b consists of generally massive, fine- to medium-grained sandstone. Rare examples of convolute bedding, distinguished by faint, distorted laminae, are associated with oscillatory ripples. Upon microcopy study, F2b was characterized by poorly sorted sand with a bimodal nature. Anhydrite and/or calcite cementation is more pervasive in this subfacies, resulting in poor porosity and minimal permeability.

Facies 3: Dolomitic anhydrite siltstone (F3)

Facies 3 consists primarily of dolomitic siltstone with abundant calcite-replaced anhydrite nodules. The nodules are relatively small (<0.5 cm) and are circular to subcircular. This facies displays low porosity and virtually no permeability. This facies is devoid of sedimentary and biogenic structures. It is predominantly light grey in colour but was observed to have a reddish hue in some samples.

Facies 4: Planar to low-angle fine-grained sandstone (F4)

Facies 4 is characterized by very fine to fine-grained sandstone. The bedding in this facies consists of planar laminae and low-angle crossbeds (<8°). Although difficult to discern, faint coarsening-upward trends are visible

in some places. Anhydrite cement in the form of nodules (<1 cm) is common. Rare to common coarser laminae (up to medium grained) occur within this facies. The average thickness of this facies is about 20 cm (F2 is considerably thicker). It has gradational, nonerosional contacts with the adjoining facies.

*Facies 5: Planar to convolute laminated dolomitic mudstone (F5)*

Facies 5 is composed of grey, laminated, interbedded dolomitic mudstone. This facies is often characterized by soft sediment deformation structures, including highly convolute bedding. Dewatering structures, which exhibit fluidized mudstone that has been subjected to sudden loading resulting in a sinuous and tapered morphology, are also common. Thin-section analysis shows that microscopic dissolution seams characterized by organic residue (microstylolites) are common in this facies. This mudstone also exhibits intervals dominated by planar bedding with little to no deformation. In many examples, a thin (0.25 cm), dark, organic-rich band occurs at the upper contact of this facies. The dolomitic mudstone intervals are relatively thin (10–20 cm) and commonly overlie an erosional surface that truncates subjacent facies.

*Facies 6: Laminated dolomitic mudstone and siltstone (F6)*

This facies consists of parallel laminated siltstone with alternating mudstone laminae. Differential compaction of the two lithologies has resulted in an elongate lens-like appearance of the silt. Faint oscillatory ripples are sometimes visible within the siltstone, especially near the upper surface of this facies where ripples are truncated by subsequently deposited erosive facies.

*Facies 7: Planar-bedded anhydrite (F7)*

Facies 7 consists of planar-bedded anhydrite. It is a relatively thin facies, commonly 10–15 cm in total thickness. Thin-section analysis reveals that the anhydrite crystals have been deposited horizontally, with no biogenic structures visible. This facies has zero porosity and permeability, and likely acts as a barrier to any fluid flow within the reservoir. Contacts with the adjoining formations are nonerosive.

*Facies 8: Calcareous siltstone/limestone (F8)*

This facies is characterized by fossiliferous, dolomitic bioclastic wackestone, packstone and rarely grainstone consisting of poorly sorted silt- and clay-sized grains. Recrystallized fossil debris (echinoderms, brachiopods, bivalves and gastropods) and framework grains of calcite are most visible in microscopic analysis. Dolomitized mudstone rip-

up clasts are common, particularly at the base of this facies. Facies 8 is invariably characterized by an erosive base and is commonly situated on convolute-bedded mudstone (F5).

*Facies 9: Massive undifferentiated siltstone (F9)*

This facies is characterized by dolomitized siltstone. The siltstone is massive in nature, with no discernible bedding or internal structure. Variations in the lithology include rare mud drapes and common pyrite occurrences, with rare, poorly sorted, very fine grained sandstone laminae. Unlike F1, the sand laminae do not appear to be biogenically sorted (bioturbated), but rather occur as discrete, planar, structureless lenses. The contacts with the subsequently deposited facies are conformable.

*Facies 10: Dolomitic siltstone with convolute-bedded nodules (F10)*

This facies is composed of interbedded crystalline calcite (replacing anhydrite) and dolomitic siltstone. The anhydrite appears to have been deposited initially as horizontal beds that underwent subsequent disturbances resulting in contorted layers of calcite-replaced anhydrite. The facies thickness varies, but most commonly ranges between 9 and 12 cm in thickness. It is usually found above subfacies F2b (fine-grained convolute-bedded sandstone).

## ***Facies Associations***

*Facies association I (FA-I)*

Facies association I (comprising F2a and F4) is interpreted as an aeolian dune succession deposited within an arid coastal environment. The Artex Member and several other intervals within the Charlie Lake Formation exhibit depositional characteristics consistent with deposition in an aeolian dune setting (Higgs, 1990; Arnold, 1994; Zonneveld and Gingras, 2002; Zonneveld et al., 2004). Aeolian dunes have textures and sedimentary structures that provide evidence for the location on the dune where these facies were most likely deposited. Subfacies 2a (high-angle cross-stratified sand) provides the strongest evidence for an aeolian interpretation for this facies association. This type of deposit is unusual outside aeolian environments. Other key criteria include overall excellent sorting and well-rounded grains (Figure 4a). In addition, the nature of the anhydrite cement (i.e., mimicking primary bedding orientation) is consistent with cementation trends in other aeolian regimes (Fryberger, 1992).

Two major sedimentary processes create high-angle deposits on the lee side of sand dunes: grainfall laminae and sandflow (also known as avalanche crossbedding), which both have the ability to form cross-stratified deposits with abnormally high inclinations. The sedimentary process re-

sulting in the texture seen in F2a is mostly likely due to the grainfall of sand grains. These deposits were created by sand grains dropping from the air, most often in the lee side of the dunes (Pye and Tsoar, 1990). This type of lamination is characterized by unsorted grains with rare grading (Brookfield, 1992). Packing is mostly loose, with an average primary depositional porosity of approximately 40%. Sandflow laminae, which are characterized by thicker, more irregular deposits, have a slightly higher porosity. Another distinguishing factor between these two processes are the angles at which the strata are deposited. In grainfall lamination, the angle of deposition is 28° or less. In sandflow deposits, angles of deposition can reach up to 35°. Based on the drillcore examined at the Brassey Field, the inclined strata have a dip of 20–25°, indicating the most likely process of deposition was grainfall lamination (Figure 3).

The spatial location of the grainfall laminae depends on the morphology of the dune. Typically, grainfall strata accumulate on the lee side of the dune just over the crest. Once the accumulation meets and exceeds the angle of repose, grains cascade down the steep dune and create an erosionally based 2–5 cm thick sandflow deposit (Pye and Tsoar, 1990). Grainfall strata commonly interfinger with sandflow laminae (Brookfield, 1992).

The planar to slightly inclined nature of sandstone beds in F4 is interpreted to be wind-ripple laminae deposited on the aeolian dune surface. These bedforms are dependent on variable wind speeds during dune deposition. When wind speeds increase and are too strong for ripple creation and migration, these tightly packed, inversely graded packages are formed. Likewise, with a decrease in wind speed it is possible to create climbing-ripple laminae. Unlike subaqueous climbing ripples, foresets in aeolian climbing ripples are difficult to distinguish because of their low relief (Brookfield, 1992). In addition, the stoss and the crest are commonly eroded during migration of the ripple, preserving only planar-laminated beds. The planar bed lamination and climbing ripples are wind-ripple deposits and are found either at the crest of the dune or near the dune apron (i.e., the basal portion of the lee side of the dune).

#### Facies Association II (FA-II)

Facies association II consists of nine facies (F1, F2b, F3 and F5–F10). This facies association is herein interpreted as interdune deposits. The nature of the facies indicates that seasonal hydration, resulting in development of numerous shallow ephemeral lakes and lagoons, was commonplace (Zonneveld et al., 2004). The Lower Charlie Lake interdune area was a highly variable environment, with multiple controls on lateral lithological variability. It is proposed that the Artex sands were deposited in a sand-limited desert, which typically have interdune areas that are characterized by numerous small dunes, deflation lags and coarse sand sheets (Brookfield, 1992). It is the area where the water ta-

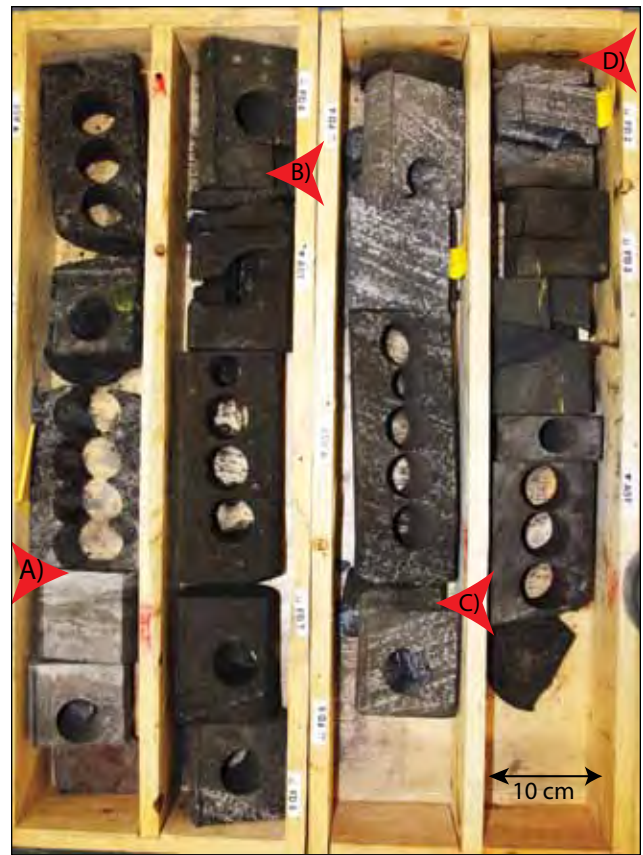


Figure 3. Drill-core from 6-1-77-19W6 showing various sedimentological features: A) Contact between the interdune/dune; interdune F1, bioturbated silt/sand; reservoir subfacies F2a sits above F1; B) F2b, massive sand; C) third-order bounding surface, reactivation surface; possibly due to wind direction variation; D) ripple cross lamination, facies F4.

ble directly interacts seasonally with the environment/sediment-air interface (Brookfield, 1992).

Two facies (F1 and F9) are interpreted to be subaqueous interdune deposits (i.e., ephemeral lagoon). Locally pervasive bioturbation interpreted to be syndepositional in nature, and abundant oscillatory ripples, are consistent with subaqueous deposits (Higgs, 1990). The presence of burrows in F1 and the lack of biogenic structures in F9 is attributed herein to water chemistry in the ephemeral lakes and lagoons (Zonneveld et al., 2004). Within F1, bioturbation became prevalent after a very short lag time wherein burrowing organisms are first established and, consequently, pervasive burrowing ensued. This is similar to seasonally rejuvenated ephemeral lagoons and lakes in the Coorong region of Australia (Warren, 1988). The unbioturbated mud and silt of F9 reflects deposits in which chemical conditions were simply too harsh (too saline or too acidic) for the development of infaunal populations. Locally abundant pyrite observed within F9 is consistent with sulphate-rich waters in this facies and with an evaporating ephemeral lake or lagoon succession (Higgs, 1990). In the Coorong region, increased salinity associated with seasonal evapora-

tion results in the decimation of infaunal populations and the lagoons and lakes become devoid of invertebrate life (Warren, 1988). The mud drapes on ripples in F9 also supports interpretation of an overall low-energy environment such as a lagoon.

Facies 2b has been interpreted as slump deposits that originated on the dune and were transported into interdune areas. The poorly sorted, massive nature of the sands is consistent with slumping, most likely after the dune had been saturated with rain, although we recognize that other atmospheric (wind storms) or seismic phenomena could have also initiated the slumps. The bimodal nature of this facies (Figure 4a) is consistent with interdune deposits. Convolute, load-casted basal contacts to this facies are also consistent with sudden sediment movement onto soupy, unconsolidated substrata, likely ephemeral lagoon or lake deposits.

Sabkha deposits in the study area are represented by F3 and F10. These sabkha deposits develop in the interdune area during seasonal drying of ephemeral water bodies. The nodular morphology of anhydrite in F3 suggests that it was deposited as subsequent drying of the interdune occurred. Local red coloration of F3 (also noted by Dixon, 2007) is most likely due to incipient soil development within these areas (Zonneveld et al., 2004). The fluidized appearance of the recrystallized anhydrite observed in F10 is likely a result of periodic influxes of groundwater likely due to rain during an overall dry interval.

Mudstone and siltstone (F5 and F6) were deposited within interdune areas during intervals in which the interdune lagoons and lakes were infilled with water. Laminated mudstone included within F6 was deposited under primarily quiescent conditions. Heterolithic, flaser- to lenticular-bedded, interlaminated mudstone/siltstone reflect fluctuating energy conditions, possibly within intertidal flats on the margins of a tidally influenced lagoon. The convolute mudstone included within F5 is the result of the sudden burial of water-saturated sediment.

Seasonal desiccation of the lagoons and lakes resulted in the deposition of laminar anhydrite beds (F7). The horizontal nature of the delicate anhydrite crystals in most examples suggest that this facies was deposited during a time of seasonal dryness, when the ephemeral water body was absent. Although it is unusual in anhydrite deposits, there are several occurrences of ripples and low-angle crossbeds in this facies, which suggests aeolian reworking and re-deposition.

#### *Facies Association III (FA-III)*

Facies association III consists of a single facies (F8). This facies occurs within a single horizon, near the top of the study interval, and has been informally referred to as the A-marker member of the Charlie Lake Formation. The presence of marine fossils (echinoderms and brachiopods)

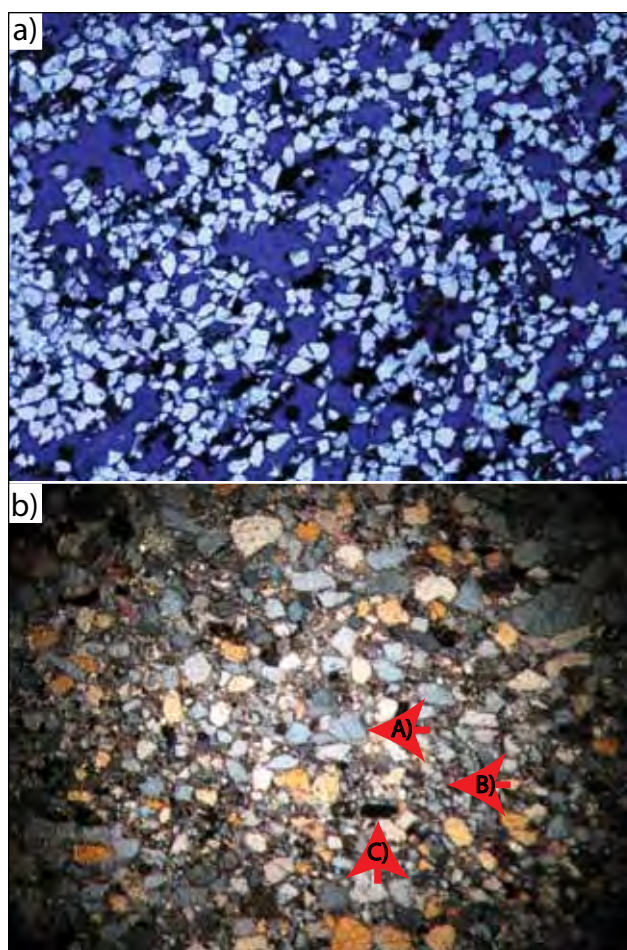


Figure 4. Photomicrographs from the Artex Member at the Brassey a) Thin-section taken from F2a, grading difficult to see but heavy minerals are at an inclined angle; postdepositional diagenesis has improved porosity; 6-1-77-19W6, 50x plane-polarized light; b) Thin section from FA-II (interdune) showing the poorly sorted, bimodal nature of the interdune area (A, B) and the presence of heavy minerals (C).

in association with fossils of facies-crossing organisms (bivalves and gastropods) reflects a marine transgression within the study area (Zonneveld and Gingras, 2002). The A-marker member occurs throughout the subsurface of northeastern British Columbia. It is thin throughout (rarely exceeding 2–7 m in thickness) and both overlies and underlies sedimentary successions deposited in marginal marine and nonmarine depositional settings, underscoring the short-lived nature of this regional marine incursion.

## AEOLIAN FACIES MODELS

Aeolian facies models were among the last clastic models to be developed (Brookfield, 1992). This is due in part to the nature of climatic variations and controls in aeolian systems and to difficulties in assessing the sedimentary structures and bedforms in present-day dune systems. However, a framework has been established to help with the identi-

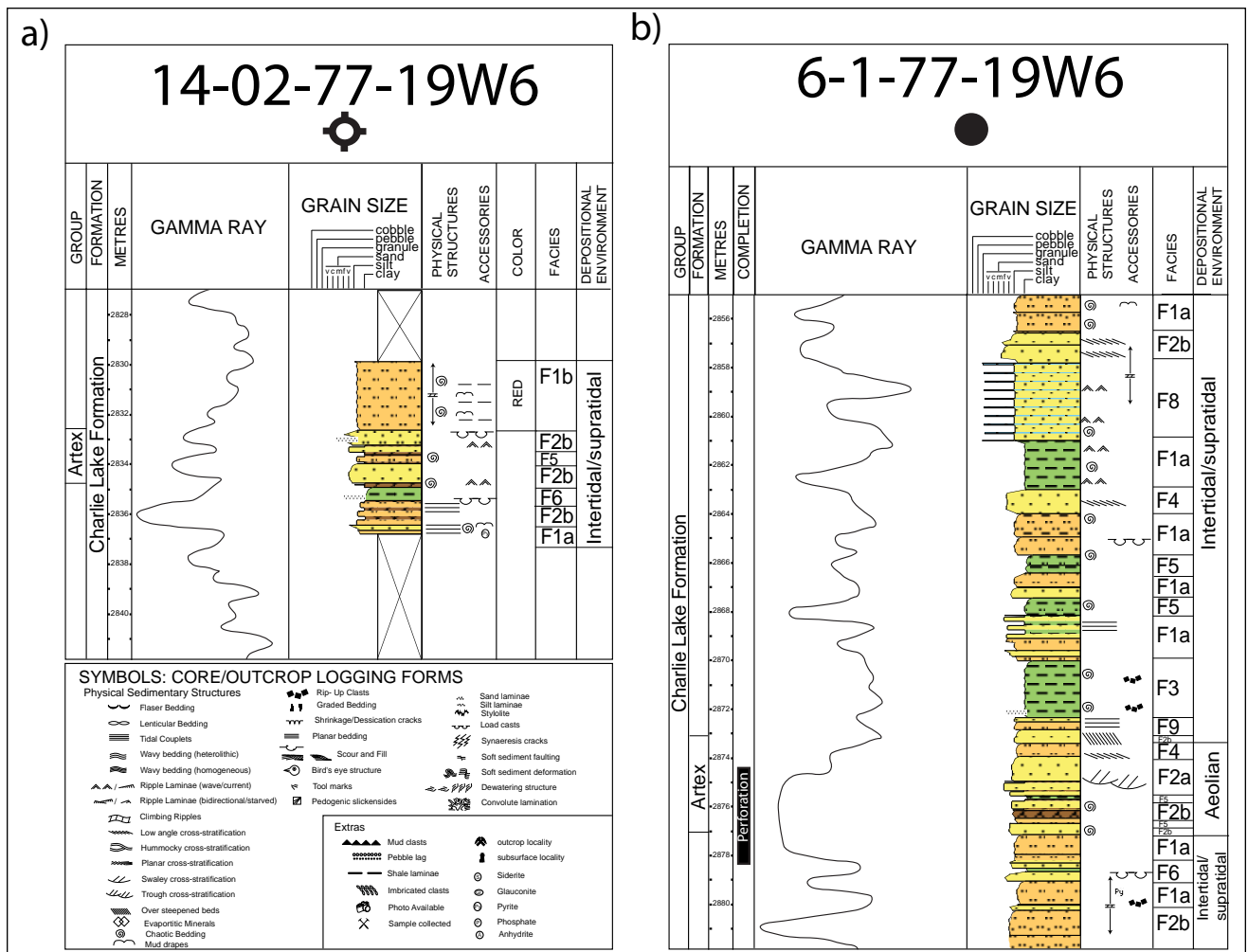


Figure 5. Core descriptions through the Brassey Field wells a) Well 14-02-77-19W6 is an abandoned well showing the lateral limits of the Brassey Field reservoir because it does not contain the reservoir facies F2a but only some intermittent F2b sands; b) well 6-1-77-19W6 is a producing well (with the corresponding gamma log) showing a full intersection through reservoir subfacies F2a.

fication and interpretation of aeolian systems. Brookfield (1992) identified several fundamental observations necessary for an aeolian dune interpretation. These include the identification of sedimentological processes that produce larger-scale bedforms found in aeolian strata that are the result of migration and amalgamation of smaller, variable-sized bedforms. The processes create unique strata, facies, grainfall, grainflow and ripple lamination. The boundaries of these strata can be assessed to deduce the nature, and possibly infer the morphology, of the dunes.

Three bounding surfaces can be identified within aeolian successions (Figure 2). The formation of first-order bounding surfaces is attributed to the migration of the draa (the largest-scale bedform identified), which varies from 10 to 450 m in height (Brookfield, 1992). The boundary of the draa is usually identified as being between interdune and dune deposits, demarcated by the contact of two dunes. Second-order bounding surfaces are formed by migration of the dune on the draa surface. Dunes are characterized by being larger than ripples but smaller than the draa on which

they formed. Heights vary from 0.1 to 100 m. Second-order bounding surfaces usually form on the lee, or down wind, side of the draa. Third-order bounding surfaces represent aeolian lamination and are often reactivation surfaces. The aeolian lamination will often consist of bundles of laminae (laminae sets) formed by the erosion and subsequent reactivation of the crossbed (Brookfield, 1992). Mapping of the second- and third-order sequences is controlled by well density and distance; therefore, is not mappable in some fields, as pointed out by Woofter and MacGillvray (1990). Because of the considerable size of the draa, first-order bounding sequences should be mappable on a larger scale. In the Brassey Field, the dune-interdune contact is distinct in both drill-cores and well logs (Figures 3–5). Identification of lower-order bounding surfaces has been accomplished in parts of the Brassey Field; however, work is ongoing to substantiate the veracity of these correlations and assess their role in reservoir compartmentalization.

As mentioned above, deserts are characterized and influenced by numerous climatic conditions, including

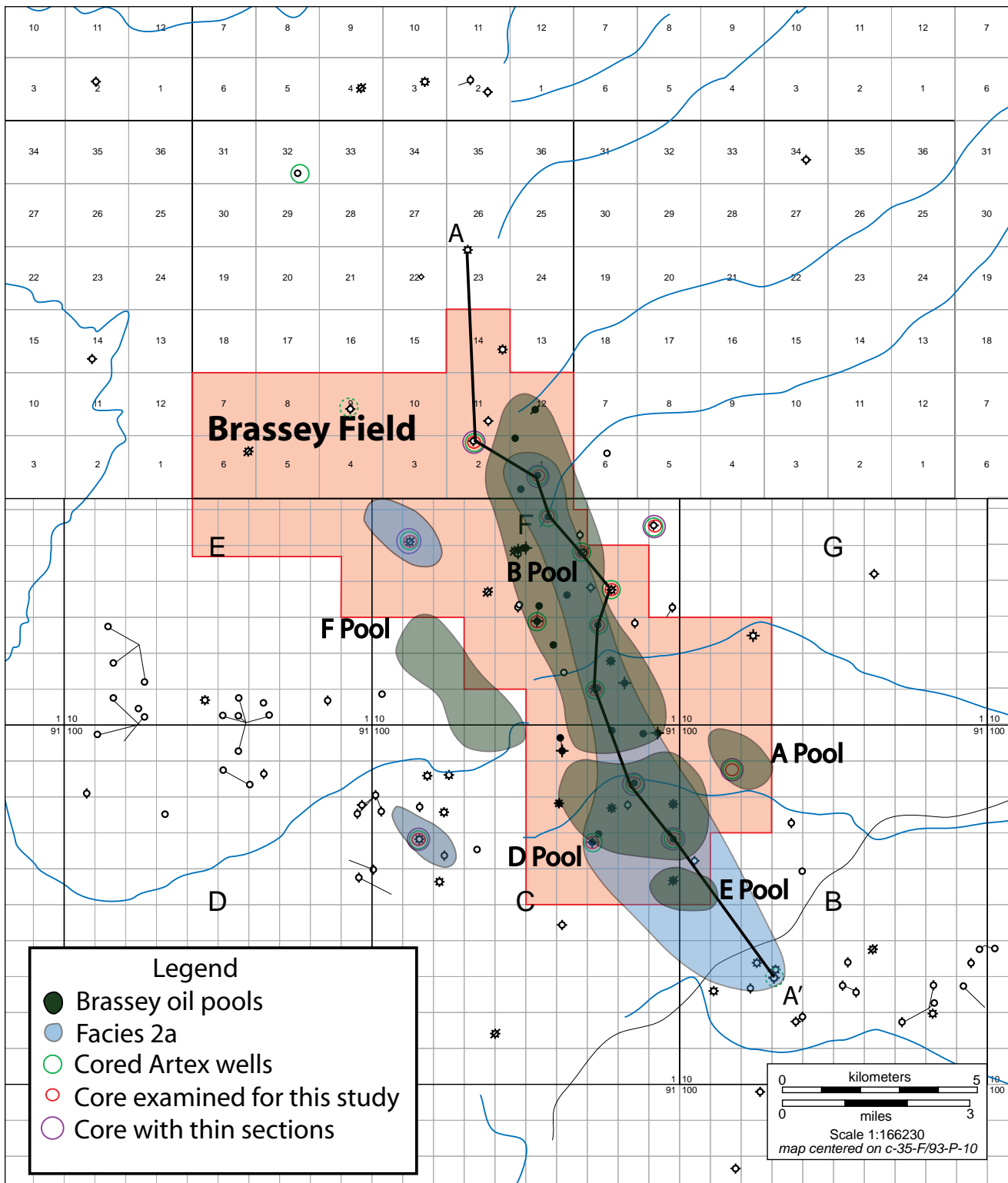


Figure 6. Facies and oil pool map of the Brassey Field.

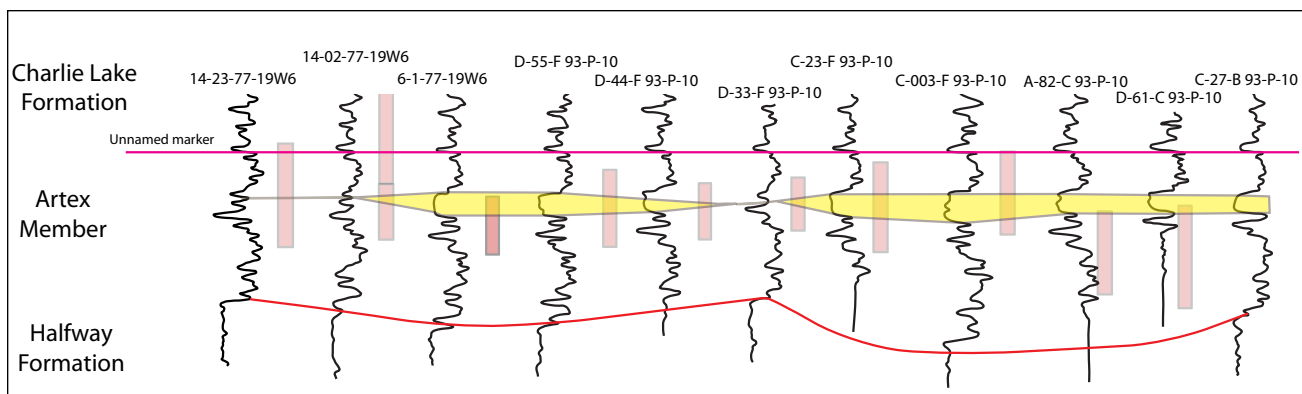


Figure 7. Northeast-southwest cross section through pools B and D of the Brassey Field. An unnamed field-wide marker is used as a stratigraphic datum (indicated by a pink line). The marker corresponds to a slightly sandier silt bed within facies F1.

sediment supply, wind strength and direction, and basin morphology. Within erg systems, several types of dunes commonly coexist, depending on local and regional wind patterns. The morphology of the dunes are related to the wind direction (Brookfield, 1992). Previous research showing sand thickness in the area around the Brassey Field has suggested a substantial erg system in which the Brassey Field was deposited (Higgs, 1990). The size and areal extent of this dune field remains conjectural (Higgs, 1990; Arnold, 1992). Dominantly unidirectional wind orientation often results in the formation of transverse and barchanoid dunes, whereas longitudinal and star dunes are more likely to form under variable wind conditions (Brookfield, 1992). Conflicting studies have postulated that the wind directions during the deposition of Charlie Lake Formation sands were both northeasterly (in the northern portion of British Columbia) and westerly (Arnold, 1994). Observation of the facies distribution (Figure 6, 7) in combination with oriented drill core data (Woofter and MacGillvray, 1990) suggests the predominant wind direction forming the dunes at the Brassey Field was from the northeast. This suggests that the dunes formed at an oblique angle to the dominant wind direction (Woofter and MacGillvray, 1990). The relationship between wind direction and the preserved shape of the Brassey Field (and its component pools) has not yet been resolved.

## CONCLUSION

The Artex sands of the Charlie Lake Formation have been identified as aeolian sands. Facies mapping of the Brassey Field show that reservoir subfacies F2a coincides with the pools within the field. As proposed by Woofter and MacGillvray (1990), the primary wind direction is from the northeast and the resulting dunes formed at an oblique angle to the wind. The interdune zone was mostly likely a seasonally wet system, as suggested by some of the structures observed (i.e., dewatering structures).

A northeast-southwest cross section through the pools of the Brassey Field (Figure 7) indicates that the primary control on the deposition of these sands appears to be depressions in the topography at the time of deposition. The use of a field-wide datum as a stratigraphic marker clearly shows that no thinning of the adjacent strata occurs above or below the Artex sand reservoir facies. This indicates that reservoir predictability is dependent on paleotopography.

## REFERENCES

- Accumap, commercial database for oil and gas information, accessed February 2010.
- Arnold, K.J. (1994): Origin and distribution of aeolian sandstones in the Triassic Charlie Lake Formation, northeastern British Columbia; MSc thesis, *University of Alberta*, 320 pages.
- Brookfield, M.E. (1992): *Eolian systems*; in *Facies Models: Response to Sea Level Change*, Walker, R.G. and James, N.P., Geological Association of Canada. Geotext 1: pages 143–156.
- Caplan, M.L. and Moslow, T.F. (1997): Tectonic controls on preservation of the Middle Triassic Halfway Formation reservoir facies, Peejay Field, northeastern British Columbia: a new hydrocarbon exploration interpretation; *Bulletin of Canadian Petroleum Geology*, Volume 45, pages 595–613.
- Davies, G.R. (1997a): The Upper Triassic Baldonnel and Pardonet formations, Western Canada Sedimentary Basin; *Bulletin of Canadian Petroleum Geology*, Volume 45, pages 643–674.
- Davies, G.R. (1997b): Aeolian sedimentation and bypass, Triassic of Western Canada; *Bulletin of Canadian Petroleum Geology*, Volume 45, pages 624–642.
- Dixon, J. (2007): Regional facies trends in the lowermost beds of the Upper Triassic Charlie Lake Formation, in the subsurface of Western Canada; *Bulletin of Canadian Petroleum Geology*, Volume 55, pages 1–20.
- Fryberger, S.G. (1993): A review of aeolian bounding surfaces, with examples from the Permian Minnelusa Formation, USA; in *Characterization of fluvial and aeolian reservoirs*, North, C.P. and Prosser, D.J., Editors, *Geological Society of London Special Publication*, Volume 73, pages 167–197.
- Higgs, R. (1990): Sedimentology and petroleum geology of the Artex Member (Charlie Lake Formation), northeast British Columbia; in *Petroleum Geology Special Papers 1990*, BC Ministry of Energy, Mines and Petroleum Resources, pages 1–26.
- Klein, M. and Woofter, D. (1989): The Triassic Brassey Oilfield of northeast British Columbia — a light oil discovery: its evolution from exploration to development; in *Exploration Update '89*; *Canadian Society of Exploration Geophysicists — Canadian Society of Petroleum Geologists*, Calgary, Alberta, Program and Abstracts, page 134.
- Pye, K. and Tsoar, H. (1990): *Aeolian Sand and Sand Dunes*; London, *Unwin Hyman Ltd.*, 396 pages.
- Taylor, A.M. and Goldring, R. (1993): Description and analysis of bioturbation and ichnofabric; *Journal of the Geological Society*, February 1993, Volume 150, pages 141–148.
- Warren, J.K. (1988): Sedimentology of *Coorong* dolomite in the Salt Creek region, South Australia; *Carbonates and Evaporites*, Volume 3, pages 175–199.
- Woofter, D.M. and MacGillivray, J. (1990): Brassey Canada: development of an aeolian sand — a team approach; *Society of Petroleum Engineers 65<sup>th</sup> Annual Technical Conference*, pages 163–174.
- Young, F.G. (1997). An iconoclastic view of mid-Triassic stratigraphy, Umbach-Wargen area, British Columbia. *Bulletin of Canadian Petroleum Geology*, Volume 45, pages 577–594.
- Zonneveld, J-P., Carrelli, G.G. and Riediger, C. (2004): Sedimentology of the Upper Triassic Charlie Lake, Baldonnel & Pardonet Formations from outcrop exposures in the southern Trutch region, northeastern British Columbia; in *Central Foreland NATMAP: Stratigraphic and Structural Evolution of the Cordilleran Foreland — Part 1*, Lane, L.S., Editor, *Bulletin of Canadian Petroleum Geology*, Volume 52, pages 343–375.
- Zonneveld, J-P. and Gingras, M.K. (2002): Sedimentology and ichnology of the Triassic of northeastern British Columbia: constructing a depositional and stratigraphic framework; *Canadian Society of Petroleum Geology Diamond Jubilee Convention*, 160 pages.
- Zonneveld, J-P., Gingras, M.K. and Pemberton, S.G. (2001): Depositional framework & trace fossil assemblages in a mixed siliciclastic-carbonate marginal marine depositional system, Middle Triassic, NE British Columbia; *Palaeogeography, Palaeoclimatology, Palaeoecology*, Volume 166, pages 249–276.
- Zonneveld, J-P. and Orchard, M.J. (2002): Stratal relationships of the Baldonnel Formation (Upper Triassic), Williston Lake, northeastern British Columbia; *Geological Survey of Canada Current Research 2002-A8*: 15 pages.

# EVALUATION OF ORDOVICIAN AND SILURIAN STRATIGRAPHY FOR HYDROCARBON SOURCE-ROCK POTENTIAL IN THE NORTHERN HALFWAY RIVER MAP AREA, BRITISH COLUMBIA (NTS 094B/13)

Filippo Ferri<sup>1</sup>, Martyn L. Golding<sup>2</sup>

---

## ABSTRACT

*Over 500 m of Middle Ordovician to Lower Silurian silty dolomite, calcareous siltstone and quartzite of the upper Skoki Formation and the Road River Group were examined and sampled for hydrocarbon source-rock potential in the northern Halfway River map area. Road River Formation units investigated are basinal equivalents of the Nonda and Muncho-McConnell formations and an unnamed quartzite-dolomite unit. Source-rock potential for the upper Skoki Formation is poor, whereas limited data from the overlying calcareous siltstone of the Road River Group exhibit values that suggest they originally may have had fair to good source-rock characteristics. Further sampling is required to verify these limited results and to test the more basinal, Lower–Middle Ordovician succession for source-rock potential.*

Ferri, F. and Golding, M. (2010): Evaluation of Ordovician and Silurian stratigraphy for hydrocarbon source-rock potential in the northern Halfway River map area, British Columbia (NTS 094B/13); in *Geoscience Reports 2010, BC Ministry of Energy, Mines and Petroleum Resources*, pages 11–20.

<sup>1</sup>BC Ministry of Energy, Mines and Petroleum Resources, Victoria, BC

<sup>2</sup>Department of Earth and Ocean Sciences, University of British Columbia, Vancouver, BC

**Key Words:** British Columbia, Rocky Mountains, Halfway River, 094B/13, Lower Paleozoic, Road River Group, Skoki Formation, stratigraphy, measured section, Rock-Eval, petroleum system, hydrocarbons.

---

## INTRODUCTION

In 2005, the BC Ministry of Energy, Mines and Petroleum Resources published a preliminary assessment of the petroleum potential of pre-Givetian strata in northeast British Columbia (Ibrahimbas and Walsh, 2005). This report focused on the stratigraphy and reservoir development of the strata and noted that prospective zones exist within carbonate rocks of the Lower Keg River–Chinchaga, Chinchaga and Stone formations, quartz arenite of the Wokpash Formation and unnamed Cambrian units (Ibrahimbas and Walsh, 2005). Although the authors noted high gas recoveries from some carbonate horizons (4.18 mmcf/day), no potential source rock has been identified in the subsurface to date. The recognition of pre-Givetian source rocks would lay the foundation for petroleum systems of this age and increase the probability that economic hydrocarbon accumulations exist.

Unpublished Rock-Eval data from surface samples of Ordovician and Silurian strata in the Trutch map area (NTS 094G) reportedly contained total organic carbon (TOC) of up to 10% (Ibrahimbas and Walsh, 2005). In light of this, a section of basinal Ordovician and Silurian strata was chosen for systematic sampling of potential source rocks in an attempt to corroborate this unpublished data

and establish the presence of a Lower Paleozoic petroleum system. Rationale for the sampling area was based on proximity to Lower Triassic strata 20 km to the east, the detailed study of which formed the main focus of the 2009 field program (Ferri et al., 2010).

## LOCATION

The section sampled is located in the northwest corner of the Halfway River map area (NTS 094B/13), near the Graham River headwaters, approximately 10 km south of Robb Lake (Figure 1). Access was by helicopter and the section was measured and sampled through the set-up of a camp about 1.5 km to the northeast.

## GENERAL GEOLOGY

The area sampled is found in the eastern Northern Rocky Mountains, north-northwest of the Bernard anticline (Figures 2, 3). Lower–Middle Paleozoic strata exposed in the immediate area represent off-shelf equivalents to continental carbonate deposits in the Western Canada Sedimentary Basin. The demarcation line between shelf and basinal deposition moved through time and carbonate debris flows

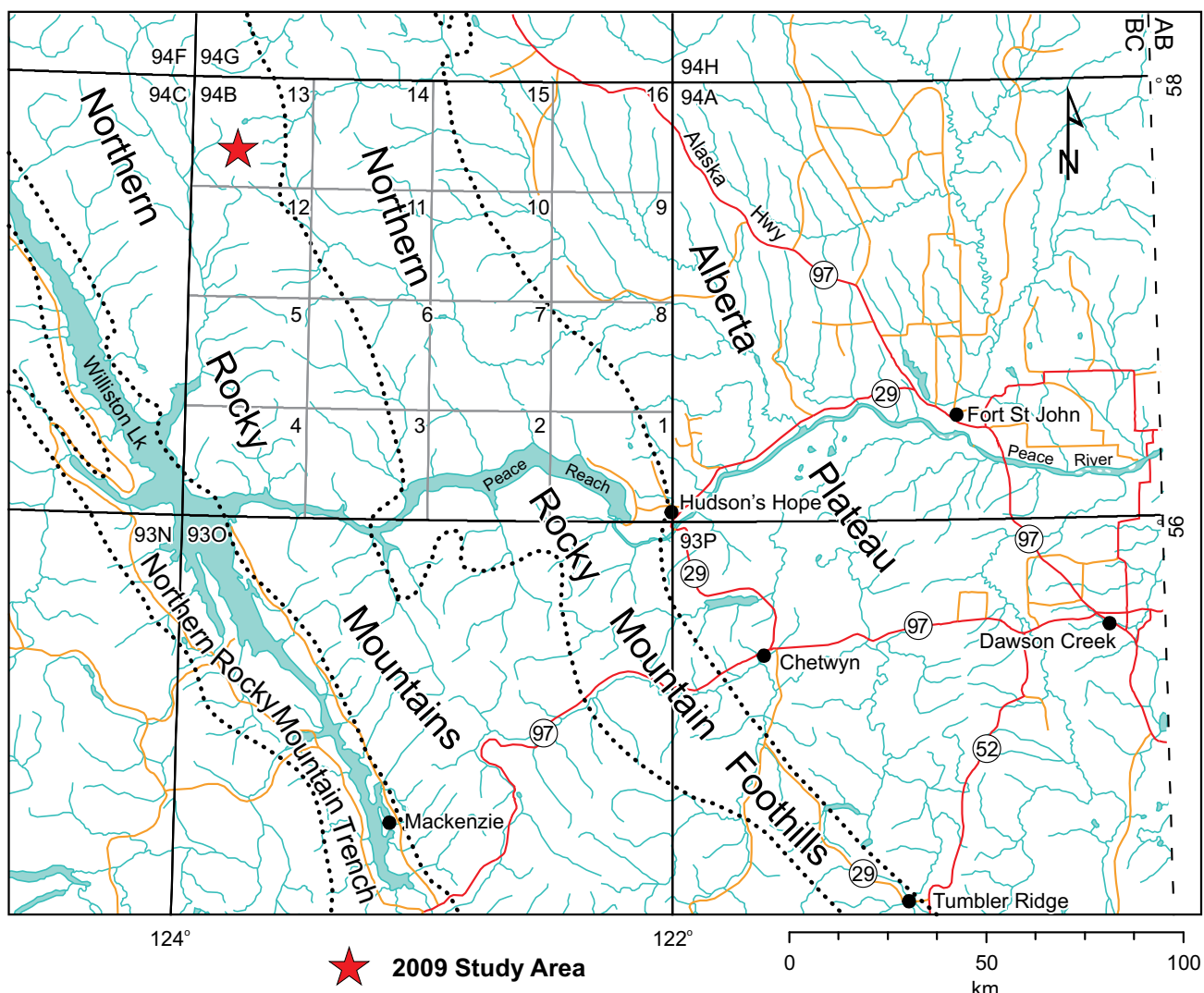
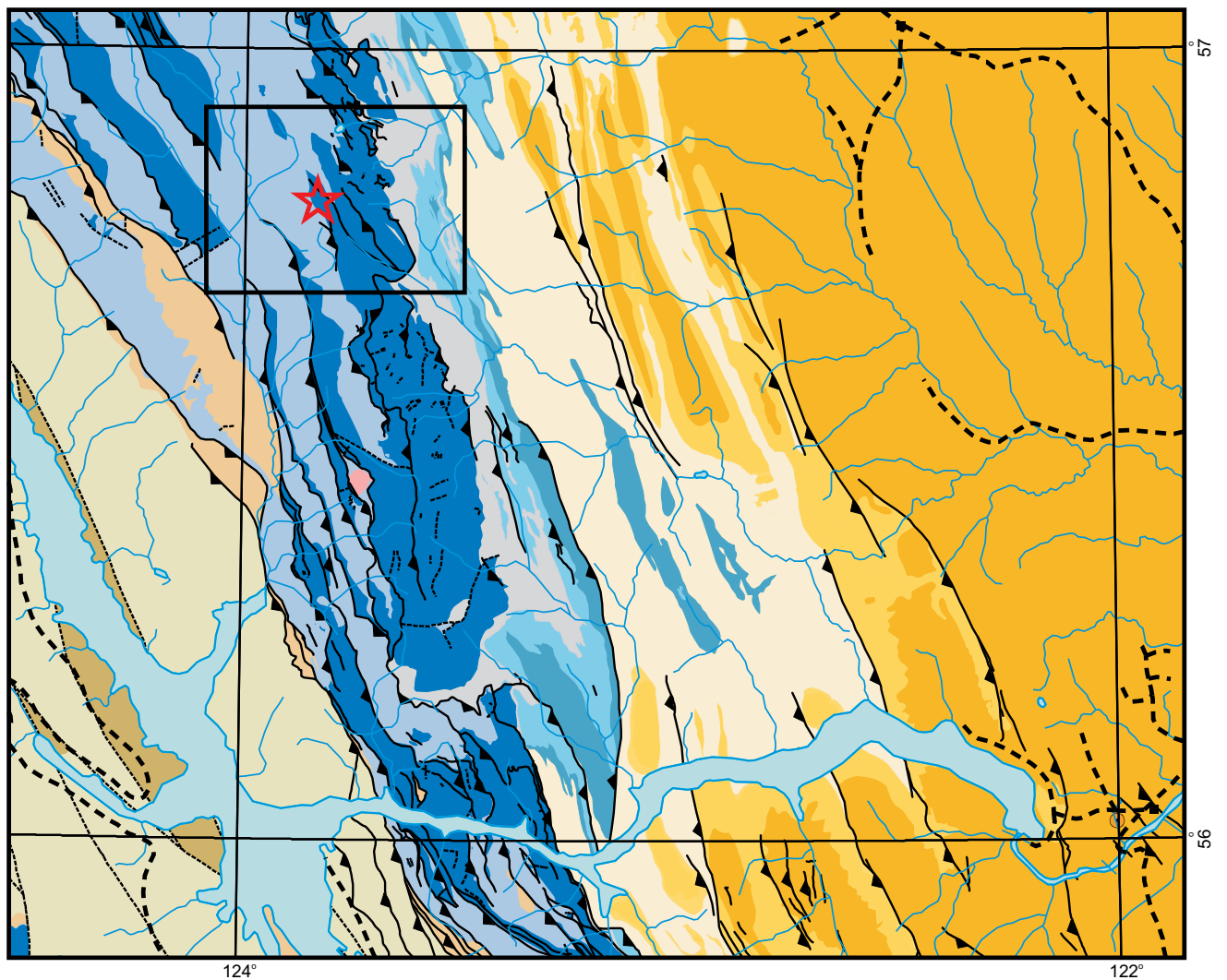


Figure 1. Location of the study area within northeast British Columbia.

suggests the shelf edge was relatively abrupt (Figure 4; Cecile and Norford, 1979). Thompson (1989) broadly referred to the off-shelf sedimentary rocks as ‘Road River strata’. More recent work (see Pyle and Barnes, 2000) redefined this stratigraphy and renamed these strata as the Road River Group and defined a series of formations (Figure 5). Some of the rock types observed in this report can be directly correlated with these new units, whereas the relationship to other units is more problematic.

Rocks examined during the 2009 field season encompassed an overturned section of the Lower Ordovician Skoki Formation and the lower–middle part of the Road River Group. Thompson (1989) informally referred to this Road River strata as, from bottom to top, the graptolitic shale-quartzite unit (Middle–Upper Ordovician), the carbonaceous limestone unit (Lower Silurian), the breccia unit (Lower Silurian) and the brown siltstone unit (Upper Silurian to Lower Devonian). Correlation of these units with the work of Pyle and Barnes (2000) is shown in Figure 5.

The Skoki Formation and overlying Silurian to Devonian Nonda, Muncho-McConnell, Stone and Dunedin formations define a carbonate shelf sequence that ‘shales out’ westward into the Road River Group. Dark grey shale, calcareous shale, siltstone, limestone and quartzite of the graptolitic shale-quartzite unit (Ospika Formation) are basal equivalents of a more proximal quartzite-dolomite unit (Thompson, 1989). The overlying carbonaceous limestone and carbonate breccia units (Pesika Formation) are off-shelf equivalents of the Nonda Formation. This limestone breccia suggests the presence of a well-developed carbonate escarpment during deposition of the Nonda Formation that shed carbonate debris to the west (Cecile and Norford, 1979). The overlying orange to tan weathering, brown calcareous siltstones of the brown siltstone unit (Kwadacha Formation) are time-equivalent to the Muncho-McConnell Formation. The westward equivalents of this unit represent the typical ‘Silurian siltstone’ division of the Road River Group that is found throughout the more basal Kechika Trough and Selwyn Basin (Ferri et al., 1999).



**Layered Rocks**

- Cretaceous - Tertiary
- Cretaceous
- Jurassic - Cretaceous
- Triassic
- Carboniferous - Permian
- Carboniferous
- Devonian - Carboniferous

- Ordovician - Middle Devonian
- Cambrian - Ordovician
- Cambrian
- Late Proterozoic

**Intrusive Rocks**

- Mississippian

- Road
- Thrust fault
- Fault

★ 2009 Study Area

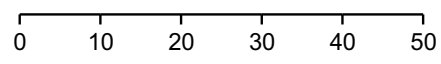


Figure 2. General geology of the Halfway River map area, British Columbia. Geology from the BC Geological Survey MapPlace website (MapPlace, 2010;www.mapplace.ca).

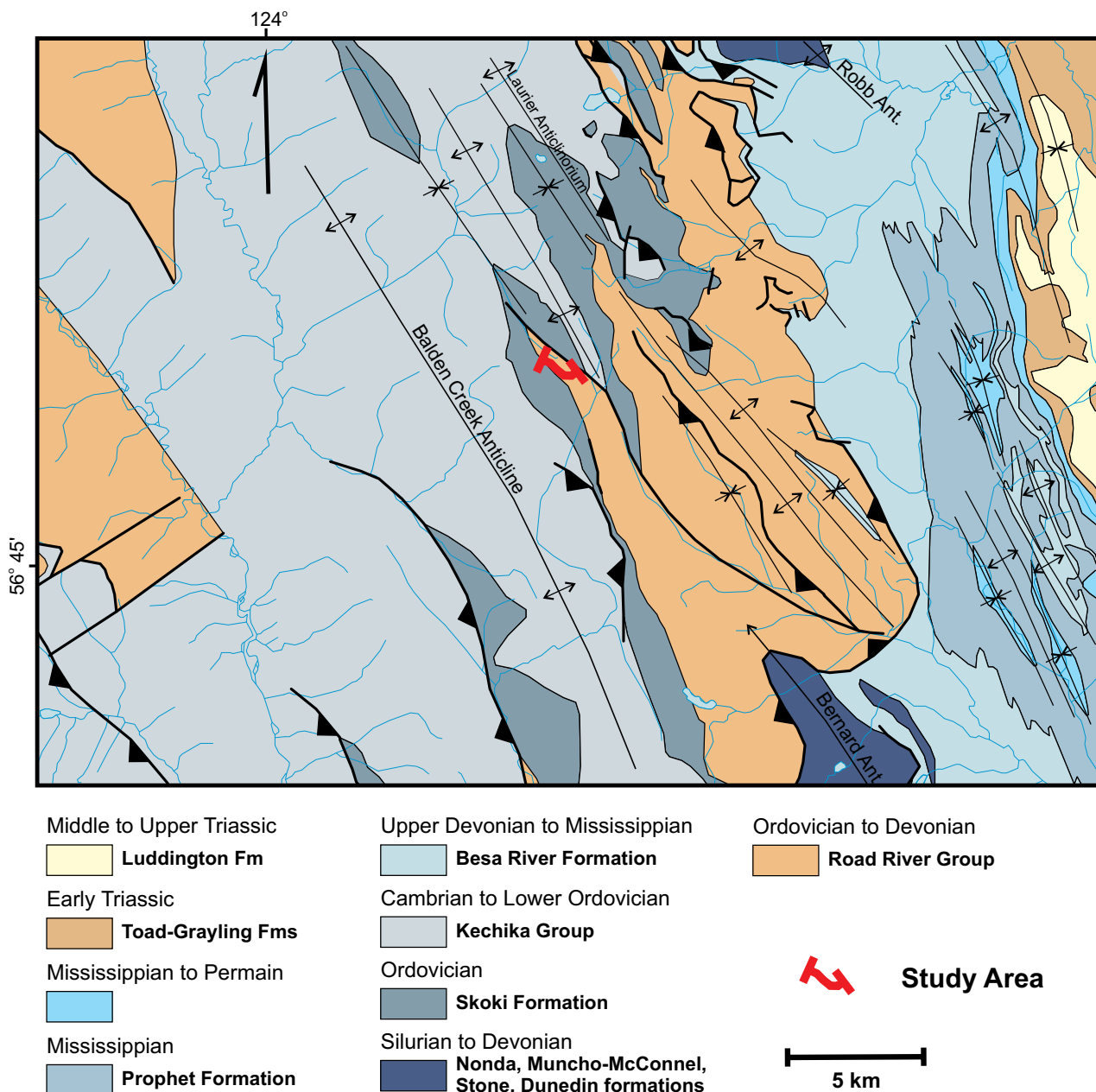


Figure 3. General geology in the immediate vicinity of the study area.

## DETAILED SECTION

Approximately 540 m of semicontinuous section were measured near the headwaters of Graham River (Figures 6, 7). The UTM coordinates (NAD 83) are 449184E, 6296474N for the base of the section and 450321E, 629349N for the top. The lower 220 m, below a thick quartzite of the graptolitic shale-quartzite unit, were measured continuously, with samples of material taken every 5 m for Rock-Eval analysis. Above the quartzite, outcrop is less continuous and thicknesses are based on detailed mapping and are thus more approximate. The carbonaceous limestone unit is crumbly and poorly exposed in this area, and lithological descriptions are based on limited exposures.

Although the sampled section encompasses the upper part of the Skoki Formation, aspects of this section, particularly the carbonate debris flows below the thick quartzite, bear a strong lithological resemblance to similar deposits within the Chesterfield Member described by Pyle and Barnes (2000), the latter being a basal equivalent to the Skoki Formation. This suggests that these rocks in the study area reflect an initial shale-out of the upper Skoki Formation. Conodont samples were collected and may provide evidence for these correlations.

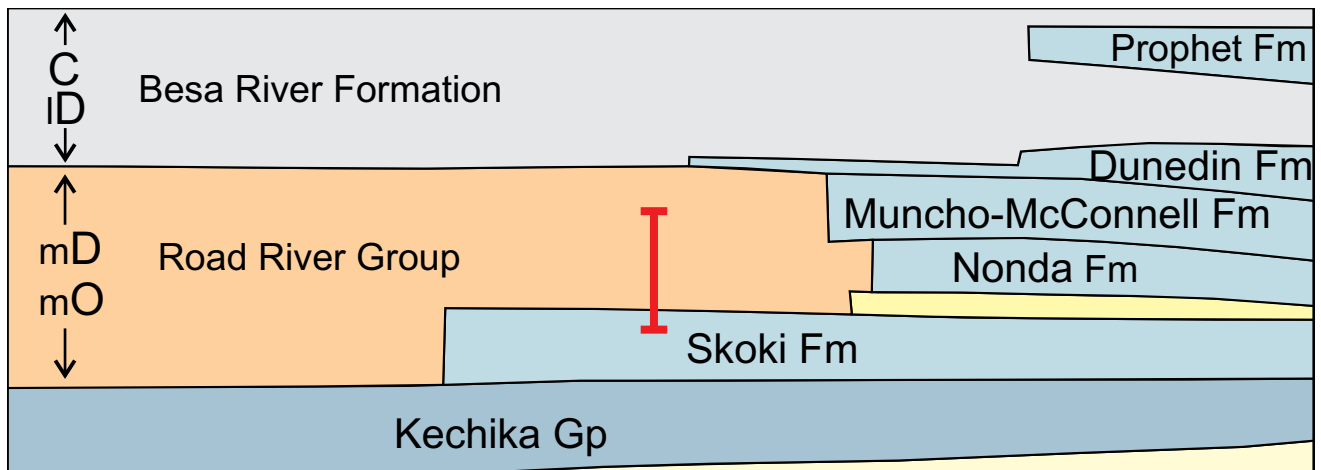


Figure 4. Schematic representation of Lower Paleozoic carbonate to shale transition in the Halfway River map area, British Columbia; adapted from Thompson (1989). Abbreviations: mO – Middle Ordovician; mD – Middle Devonian; ID – Lower Devonian; C – Carboniferous.

### Skoki Formation

In the northern Halfway River map area, the Skoki Formation is divided into three members: a middle pale grey dolostone bounded on the top and the bottom by dark grey dolostone (Thompson, 1989). The upper dark grey siliceous dolostone unit was sampled for source-rock potential. The middle part of the Skoki Formation consists of wavy-bedded, light grey to buff weathering, medium- to thick-bedded dolostone to dolomitic siltstone. Considerable rubble of this unit was observed at the base of the section, including a section of carbonate breccia floating in a matrix of light green sericitic shale to siltstone, suggesting a volcanic origin (Figure 8). Mafic volcanic rocks have been mapped within the middle Skoki Formation west of Bernard anticline (Thompson, 1989).

### UPPER SKOKI FORMATION

The upper Skoki Formation consists of approximately 200 m grey to dark grey weathering, silty dolomite and lesser amounts of carbonate breccias (Figure 9, 10). Silty dolomite is thin bedded, platy and commonly has very thin dark grey shaly partings. Locally the dolomite is quite siliceous. Shale interbeds appear to thicken into centimetre-thick layers at the top of the unit.

The middle–upper part of this siltstone succession is punctuated by 1 to >30 m thick horizons of tan to buff weathering, grey dolomitic crinoidal packstone to grainstone interbedded locally with carbonate breccia or conglomerate (Figures 10, 11). These are commonly massive in nature, with local wavy bedding developed. The nature of these deposits, and surrounding thin-bedded dark grey silty dolomite, are similar to off-shelf rock types described by Cecile and Norford (1979) in the Ware map area (94F) located just west of the Skoki Formation ‘shale-out’. This suggests the carbonate breccia represents debris flows off

|                   | Basinal Sequence      |                   | Shelf Sequence         |
|-------------------|-----------------------|-------------------|------------------------|
|                   | Pyle and Barnes, 2000 | Thompson, 1989    |                        |
| Middle Devonian   |                       |                   | Muncho - McConnell Fms |
| Lower Devonian    |                       | Brown Siltstone   |                        |
| Upper Silurian    | Kwadacha Formation    |                   |                        |
| Lower Silurian    | Pesika Formation      | Breccia           | Nonda Fm               |
| Upper Ordovician  | Ware                  | Carbon. Imst      |                        |
|                   | Finbow Shale          | Graptolitic shale | Quartzite-dlmt         |
| Middle Ordovician | Chesterfield          | Quartzite         | ?                      |
| Lower Ordovician  | Finlay Limestone      | Skoki Fm          | Skoki Fm               |
|                   | Cloudmaker            |                   |                        |
| Cambrian          | Kechika Gp            | Kechika Gp        | Kechika Gp             |

Figure 5. Correlation chart showing relationships between shelf strata and Road River stratigraphy as defined by Thompson (1989) and Pyle and Barnes (2000). Abbreviations: Carbon. Imst, Carbonaceous Limestone unit; Quartzite-dlmt, Quartzite-Dolomite unit.

the carbonate bank edge and that the upper part of the Skoki Formation may be transitioning to basinal environments.

### Graptolitic shale-quartzite unit

Some 230 m of siltstone, carbonate clastic rocks and quartzite make up the graptolitic shale-quartzite unit in the

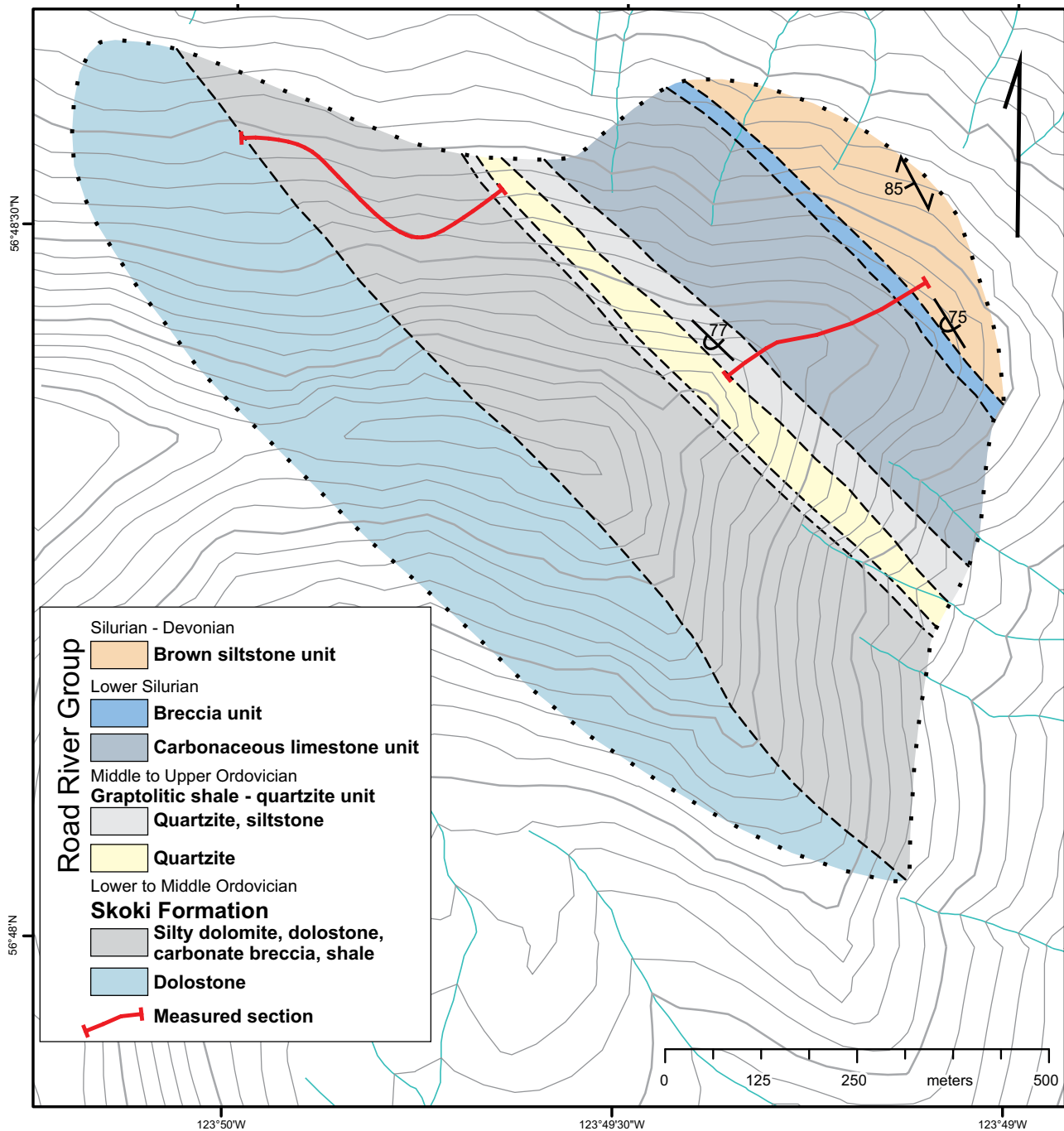


Figure 6. Geology in the vicinity of the studied section.

study area. The lowest part consists of dark grey silty dolomite and shale overlain by approximately 75 m of tan to brown or grey weathering, grey to beige quartzite. It is massive in appearance and thick bedded, consisting of sugary, medium- to fine-grained quartz (>99%) with minor white lithic sediments. Above this is a rubbly zone consisting of quartzite boulders and dark grey to black shale, which on structural sections suggests a unit approximately 35 m thick. Thompson (1989) indicates that these quartzitic deposits are turbiditic in nature and correlative with a quartz-dolomite unit on the shelf sequence located unconformably

above the Skoki Formation.

Quartzite is succeeded by approximately 95 m of a poorly exposed section of blocky to platy, dark grey to black calcareous siltstone that is locally very rubbly and/or cleaved. The section consists of scree punctuated by several semicontinuous outcrops (from 355 to 360 m and from 400 to 440 m; Figure 7).

### *Carbonaceous limestone unit*

Succeeding the graptolitic shale-quartzite unit is a poorly exposed section of thinly bedded grey to dark grey silty limestone assigned here to the carbonaceous limestone unit. The thickness of this unit is approximately 65 m, which is based on structural sections as no exposure or rubble was found below the base of the breccia unit.

### *Breccia unit*

This unit is approximately 20 m thick and consists of grey to dark grey weathering, grey lime mudstone breccia to conglomerate. Clasts are rounded to tabular, up to 20 cm in size, floating or clast supported, and surrounded by a sparry to crinoidal packstone or grainstone matrix.

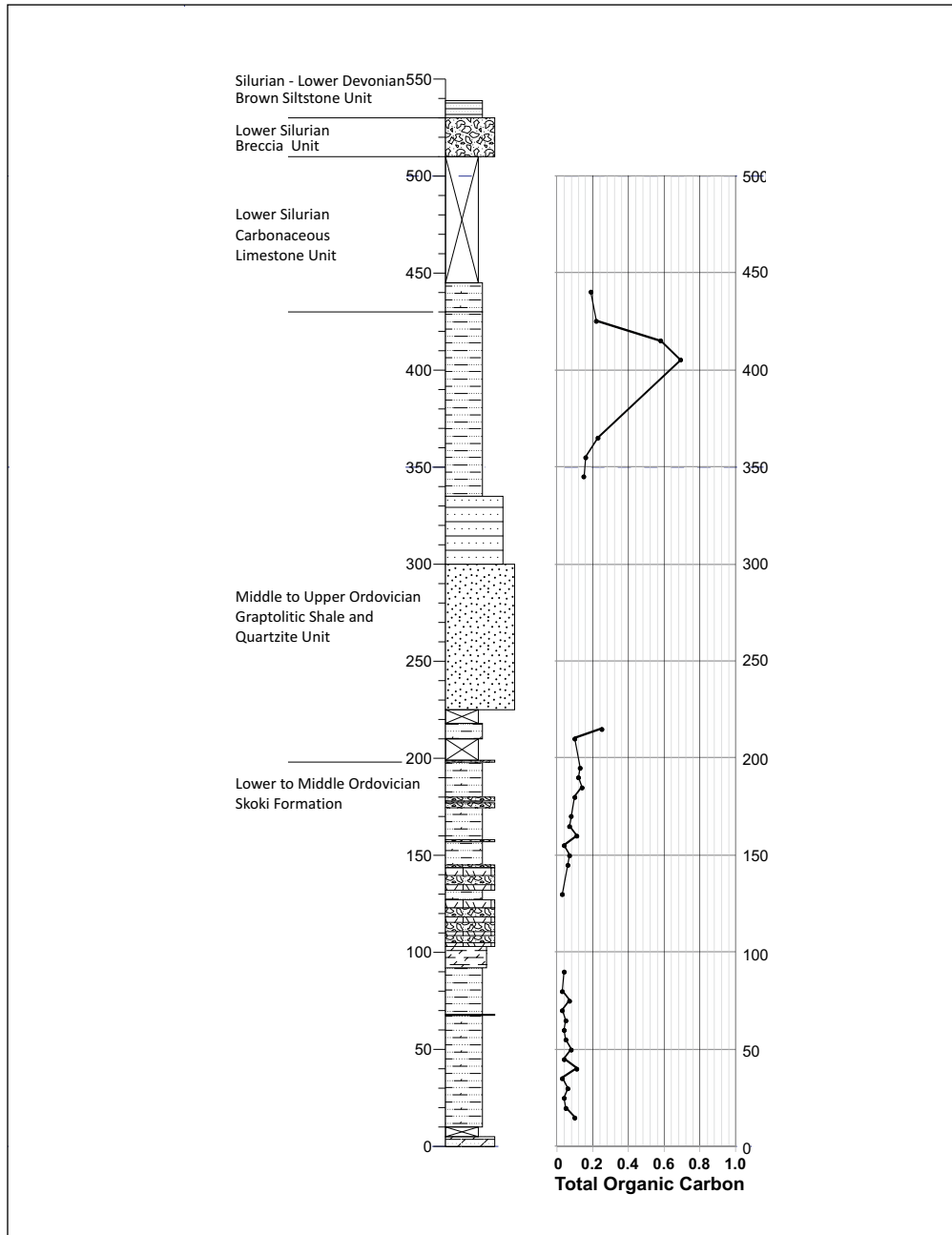


Figure 7. Schematic stratigraphic section sampled for Rock-Eval analysis. The right-hand side of the figure shows the abundance of total organic carbon within collected samples.



Figure 8. Carbonate breccia boulder from the Skoki Formation. The matrix of this breccia is sericitic, suggesting a volcanic origin.



Figure 9. Platy calcareous to dolomitic siltstone of the upper Skoki Formation.



Figure 10. Carbonate breccia to conglomerate horizons within the upper Skoki Formation. Note how these horizons pinch out along strike.



Figure 11. Close-up photo of breccia within the upper Skoki Formation showing the nature of clasts.

## ROCK-EVAL DATA

The presence of cleavage in these rocks indicates that temperatures probably exceeded the upper dry gas window. Due to the high thermal maturity, no generative capacity would remain in any organic-rich horizon and the organic carbon content is the only parameter that can be used to measure the original source-rock potential (Table 1).

Total organic carbon values from the Skoki Formation are all less than 0.2% and are of questionable significance. Even if the original TOC values were 2–4 times higher prior to thermal maturation (Jarvie, 1991), most of these samples suggest that Skoki Formation rock types originally had poor source-rock potential (0.06–0.25% TOC). Total organic carbon values are higher just below and above the thick quartzite, with values in the range of 0.23–0.67%, suggesting original values of 0.5–1.5%. Although only a limited number of samples returned these higher values, they originate from a section approximately 100 m thick.

## DISCUSSION

Total organic carbon values obtained from Upper Ordovician calcareous black shale and siltstone in the northern Halfway River map area suggest these rock types may originally have been fair to good hydrocarbon source rocks (Peters, 1986). This is assuming the kerogen within the sequence was oil prone and had high initial hydrogen to carbon ratios. Although only a limited amount of data is available, the relatively thick section (~100 m) indicates the potential presence of a large volume of organic matter that could have been part of a petroleum system, although the low amount of original TOC may not have been sufficient to make the unit an effective source rock (because it expelled its generated hydrocarbons). Further sampling is required to verify these initial results.

TABLE 1. ROCK-EVAL DATA FOR SAMPLES COLLECTED ACROSS THE SECTION. SAMPLES ANALYZED USING ROCK-EVAL 6 APPARATUS AT GEOLOGICAL SURVEY OF CANADA LABORATORIES IN CALGARY, ALBERTA.

| Height in section | Sample    | Qty  | Tmax | S1   | S2   | S3   | PI   | S2/S3 | PC(%) | TOC(%) | HI  | OI  |
|-------------------|-----------|------|------|------|------|------|------|-------|-------|--------|-----|-----|
| 440               | 09FF-163g | 70.9 | 430  | 0.01 | 0.03 | 0.22 | 0.15 | 0.14  | 0.01  | 0.19   | 16  | 116 |
| 425               | 09FF-163f | 70.6 | 337  | 0.00 | 0.00 | 0.26 | 0.31 | 0.00  | 0.01  | 0.22   | 0   | 118 |
| 415               | 09FF-163e | 70.6 | 502  | 0.00 | 0.03 | 0.27 | 0.16 | 0.11  | 0.02  | 0.58   | 5   | 47  |
| 405               | 09FF-163d | 70.8 | 501  | 0.00 | 0.02 | 0.48 | 0.13 | 0.04  | 0.02  | 0.69   | 3   | 70  |
| 365               | 09FF-163c | 70.8 | 492  | 0.00 | 0.01 | 0.48 | 0.17 | 0.02  | 0.02  | 0.23   | 4   | 209 |
| 355               | 09FF-163b | 70.4 | 494  | 0.01 | 0.03 | 0.32 | 0.15 | 0.09  | 0.01  | 0.16   | 19  | 200 |
| 345               | 09FF-163a | 70.5 | 440  | 0.00 | 0.02 | 0.42 | 0.09 | 0.05  | 0.01  | 0.15   | 13  | 280 |
| 215               | 09FF-165  | 70.0 | 494  | 0.00 | 0.01 | 0.51 | 0.22 | 0.02  | 0.02  | 0.25   | 4   | 204 |
| 210               | 09FF-166  | 70.6 | 494  | 0.00 | 0.02 | 0.35 | 0.16 | 0.06  | 0.01  | 0.10   | 20  | 350 |
| 195               | 09FF-167  | 71.2 | 427  | 0.00 | 0.02 | 0.30 | 0.13 | 0.07  | 0.01  | 0.13   | 15  | 231 |
| 190               | 09FF-168  | 70.1 | 444  | 0.00 | 0.03 | 0.31 | 0.14 | 0.10  | 0.02  | 0.12   | 25  | 258 |
| 185               | 09FF-169  | 69.9 | 425  | 0.00 | 0.03 | 0.22 | 0.14 | 0.14  | 0.01  | 0.14   | 21  | 157 |
| 180               | 09FF-171  | 70.9 | 425  | 0.00 | 0.02 | 0.23 | 0.12 | 0.09  | 0.01  | 0.10   | 20  | 230 |
| 170               | 09FF-172  | 70.2 | 423  | 0.00 | 0.02 | 0.03 | 0.13 | 0.67  | 0.00  | 0.08   | 25  | 38  |
| 165               | 09FF-173  | 70.2 | 432  | 0.01 | 0.04 | 0.22 | 0.13 | 0.18  | 0.01  | 0.07   | 57  | 314 |
| 160               | 09FF-174  | 70.2 | 494  | 0.00 | 0.01 | 0.27 | 0.18 | 0.04  | 0.01  | 0.11   | 9   | 245 |
| 155               | 09FF-175  | 70.7 | 494  | 0.00 | 0.01 | 0.17 | 0.18 | 0.06  | 0.01  | 0.04   | 25  | 425 |
| 150               | 09FF-176  | 70.6 | 440  | 0.00 | 0.02 | 0.24 | 0.12 | 0.08  | 0.01  | 0.07   | 29  | 343 |
| 145               | 09FF-177  | 70.0 | 440  | 0.00 | 0.02 | 0.20 | 0.15 | 0.10  | 0.01  | 0.06   | 33  | 333 |
| 130               | 09FF-178  | 70.9 | 437  | 0.00 | 0.01 | 0.20 | 0.14 | 0.05  | 0.01  | 0.03   | 33  | 667 |
| 90                | 09FF-179  | 70.2 | 434  | 0.00 | 0.04 | 0.23 | 0.10 | 0.17  | 0.02  | 0.04   | 100 | 575 |
| 80                | 09FF-180  | 70.8 | 436  | 0.00 | 0.03 | 0.25 | 0.11 | 0.12  | 0.01  | 0.03   | 100 | 833 |
| 75                | 09FF-181  | 70.4 | 429  | 0.01 | 0.03 | 0.21 | 0.16 | 0.14  | 0.01  | 0.07   | 43  | 300 |
| 70                | 09FF-182  | 70.5 | 433  | 0.00 | 0.03 | 0.28 | 0.09 | 0.11  | 0.01  | 0.03   | 100 | 933 |
| 65                | 09FF-184  | 70.3 | 423  | 0.00 | 0.02 | 0.27 | 0.17 | 0.07  | 0.01  | 0.05   | 40  | 540 |
| 60                | 09FF-185  | 70.7 | 416  | 0.00 | 0.01 | 0.16 | 0.20 | 0.06  | 0.01  | 0.04   | 25  | 400 |
| 55                | 09FF-186  | 70.7 | 439  | 0.01 | 0.03 | 0.23 | 0.17 | 0.13  | 0.01  | 0.05   | 60  | 460 |
| 50                | 09FF-187  | 70.2 | 413  | 0.00 | 0.01 | 0.26 | 0.18 | 0.04  | 0.02  | 0.08   | 12  | 325 |
| 45                | 09FF-188  | 70.9 | 441  | 0.00 | 0.02 | 0.00 | 0.11 | 0.00  | 0.00  | 0.04   | 50  | 0   |
| 40                | 09FF-189  | 70.3 | 437  | 0.00 | 0.01 | 0.34 | 0.16 | 0.03  | 0.02  | 0.11   | 9   | 309 |
| 35                | 09FF-190  | 70.9 | 444  | 0.00 | 0.02 | 0.21 | 0.15 | 0.10  | 0.01  | 0.03   | 67  | 700 |
| 30                | 09FF-191  | 71.1 | 494  | 0.00 | 0.01 | 0.23 | 0.20 | 0.04  | 0.01  | 0.06   | 17  | 383 |
| 25                | 09FF-192  | 71.0 | 452  | 0.00 | 0.01 | 0.30 | 0.10 | 0.03  | 0.01  | 0.04   | 25  | 750 |
| 20                | 09FF-194  | 71.0 | 442  | 0.00 | 0.02 | 0.21 | 0.12 | 0.10  | 0.02  | 0.05   | 40  | 420 |
| 15                | 09FF-195  | 70.6 | 437  | 0.00 | 0.01 | 0.29 | 0.10 | 0.03  | 0.02  | 0.10   | 10  | 290 |

Qty = mg; TOC = Total Organic Carbon, weight per cent; S1, S2 = mg hydrocarbons (HC)/g rock; S3 = mg CO<sub>2</sub>/g rock;

PI = Production Index = S1/(S1+S2);

PC = Pyrolyzable Carbon(weight per cent) = ((0.83\*(S1+S2))+(S3\*.273)+ ((S3CO+(S3'CO/2))\*0.4286))/10

Tmax = °C; HI = Hydrogen Index = (100\*S2)/TOC; OI = Oxygen Index = (100\*S3)/TOC

The high TOC values reported from the Trutch map area (94G) were not encountered during 2009 sampling. This may be a reflection of the more shelfward nature of the section sampled in 2009, with transition to Nonda and Muncho-McConnell formation carbonate rocks occurring only 10–20 km to the east. Furthermore, the Skoki Formation does not shale out for another 10–20 km westward. This western, more basinal setting (i.e., Kechika Trough), contains a thinner, more condensed section with zones higher in organic matter, particularly in the Lower–Middle Ordovician and Silurian (see Ferri et al, 1999). Further sampling is required to test these more western Lower–Middle Ordovician sections equivalent to the Skoki Formation for hydrocarbon source-rock potential.

## ACKNOWLEDGMENTS

The authors would thank Bob Batchelor of Whitney Helicopters for excellent service and making our stay in the mountains much more enjoyable. We also thank Leanne Pyle, Alf Hartling, Warren Walsh and Lavern Stasiuk for reviewing early versions of this manuscript.

## REFERENCES

- Cecile, M.P. and Norford, B.S. (1979): Basin to platform transition, Lower Paleozoic strata of Ware and Trutch map areas, northeastern British Columbia; *in* Current Research, Part A, *Geological Survey of Canada*, Paper 79-1A, pages 219–226.
- Ferri, F., Golding, M., Mortensen, J., Zonneveld, J.P. and Orchard, M. (2010): The Toad Formation in northwestern Halfway River map area (94B/14); *in* Geoscience Reports 2010, *BC Ministry of Energy, Mines and Petroleum Resources*, pages xx–xx.
- Ferri, F., Rees, C., Nelson, J. and Legun, A. (1999): Geology and mineral deposits of the northern Kechika Trough between Gataga River and the 60<sup>th</sup> parallel; *BC Ministry of Energy, Mines and Petroleum Resources*, Bulletin 107, 122 pages.
- Ibrahimbas, A. and Walsh, W. (2005): Stratigraphy and reservoir assessment of pre-Givetian strata in northern British Columbia; *in* Summary of Activities 2005, BC Ministry of Energy and Mines, pages 1–16.
- Jarvie, D.M. (1991): Total organic carbon (TOC) analysis; *in* Source Migration Processes and Evaluation Techniques, *Treatise of Petroleum Geology, Handbook of Petroleum Geology*, Merrill, R.K., Editor; *American Association of Petroleum Geologists*, pages 113–118.
- Peters, K.E. (1986): Guidelines for evaluating petroleum source rocks using programmed pyrolysis; *American Association of Petroleum Geologists Bulletin*, Volume 70, pages 318–329.
- Pyle, L.J. and Barnes, C.R. (2000): Upper Cambrian to Lower Silurian stratigraphic framework of platform-to-basin facies, northeastern British Columbia; *Bulletin of Canadian Petroleum Geology*, Volume 48, Number 2, pages 123–149.
- Thompson, R.I. (1989): Stratigraphy, tectonic evolution and structural analysis of the Halfway River map area (94B), northern Rocky Mountains, British Columbia; *Geological Survey of Canada*, Memoir 425, 119 pages.

# TOAD FORMATION (MONTNEY AND DOIG EQUIVALENT) IN THE NORTHWESTERN HALFWAY RIVER MAP AREA, BRITISH COLUMBIA (NTS 094B/14)

Filippo Ferri<sup>1</sup>, Martyn L. Golding<sup>2</sup>, James K. Mortensen<sup>2</sup>, John-Paul Zonneveld<sup>3</sup>, Michael J. Orchard<sup>4</sup>

---

## ABSTRACT

Approximately 600 m of calcareous siltstone and fine sandstone of the Toad Formation (Montney and Doig equivalent strata) were measured in a section immediately south of Halfway River, within the northwestern part of the Mount Laurier map area (NTS 094B/14). Spectral gamma-ray measurements were obtained every metre throughout the section. In addition, semicontinuous chip samples were collected every 5 m for Rock-Eval analysis together with 11 representative samples across the section for thermal maturation determination via reflective microscopy.

The basal part of the Toad Formation is not exposed in this area. The Toad Formation comprises a coarsening-upward succession of distal turbidites, which become more proximal in the uppermost part of the succession. The lower 140 m of the measured section is dominated by uniform dark, calcareous to dolomitic carbonaceous siltstone, which locally displays faint laminar bedforms. This sequence is followed by a repetitive section some 200 m thick, containing metre-thick beds of slightly coarser and cleaner dolomitic siltstone displaying laminar and graded bedding. The upper 250 m of the section records a greater influx of coarser siltstone with a corresponding decrease in carbonaceous content. Thinly laminated and graded sequences of coarse siltstone to very fine sandstone are common, together with thicker metre-thick successions of cleaner fine sandstone containing current ripples and soft sediment deformation. These increase in abundance up-section until the base of the Liard Formation, designated by continuous thinly to thickly bedded fine-medium sandstone. The base of the Liard Formation also corresponds to the first appearance of bioturbation.

Thin-section examination of representative samples indicates that the darker siltstone samples are rich in carbonate, containing on average 30% carbonate. Siltstone and fine sandstone are dominated by angular to semirounded quartz with up to 20% feldspar (potassium feldspar and plagioclase) followed by mica, chert and minor mafic minerals (hornblende).

Comparisons of gamma-ray patterns obtained from the measured section with subsurface sections immediately to the east suggest correlation of these rocks with the Montney and Doig formations. This is based primarily on the presence of a relatively more radioactive section some 150 m thick, which is correlated with the Doig phosphate zone. The succeeding section displays a pattern consistent with the upper Doig Formation.

Ferri, F., Golding, M.L., Mortensen, J.K., Zonneveld, J-P. and Orchard, M.J. (2010): Toad Formation (*Montney and Doig equivalent*) in the northwestern Halfway River map area, British Columbia (NTS 094B/14); in *Geoscience Reports 2010*, BC Ministry of Energy, Mines and Petroleum Resources, pages 21–34.

<sup>1</sup>BC Ministry of Energy, Mines and Petroleum Resources, Victoria, BC

<sup>2</sup>Department of Earth and Ocean Sciences, The University of British Columbia, Vancouver, BC

<sup>3</sup>Department of Earth and Atmospheric Sciences, University of Alberta, Edmonton, AB

<sup>4</sup>Geological Survey of Canada, Vancouver, BC

**Key Words:** British Columbia, Foothills, Halfway River, 094B/14, Triassic, Toad Formation, Liard Formation, Montney Formation, Doig Formation, stratigraphy, measured section, spectral gamma ray, Rock-Eval, hydrocarbons, correlation.

---

## INTRODUCTION

The Montney Formation shale gas play has been described as one of the most significant unconventional gas resource plays in North America (Canadian Discovery Digest, 2008). Total petroleum and natural gas tenure sales in

the Montney play area totalled \$1.74 billion for 2008 and 2009, and daily gas production from this play in 2009 averaged  $8.5 \times 10^6$  m<sup>3</sup>/day (300 mm cf/d). In addition, 2009 tenure sales show interest in the play area extending to the northwest and into the outer foothills.

In light of this high level of interest, the Resource Development and Geoscience Branch of the BC Ministry of Energy, Mines and Petroleum Resources (BCMEMP), in cooperation with the Geological Survey of Canada, the University of British Columbia and the University of Alberta, undertook a detailed examination of Montney and Doig formation equivalent strata (Toad Formation) within the western foothills of the northern Halfway River map area (NTS 094B/14) with the goal of better understanding this sequence and assisting with its regional characterization. This work builds on recent mapping by the senior author within the Foothills of the Halfway River map area (Ferri, 2009a, b) and on regional thematic studies of Triassic rocks by the University of Alberta and the Geological Survey of Canada (see Zonneveld and Moslow, 2005; Orchard and Zonneveld, 2009). In addition, this new data will form part of a PhD thesis recently started at the University of British Columbia that will examine provenance of clastic detritus within Early and Middle Triassic rocks of the Western Canada Sedimentary Basin (Golding et al., 2010).

The measured section was previously described by Gibson (1975) and was chosen because it affords one of the most complete sequences of the Toad Formation in this area. In addition to a detailed lithological description, samples were taken to determinate organic carbon content (using Rock-Eval), level of thermal maturation (reflectance microscopy), biostratigraphy (micro- and macrofossils) and detrital zircon geochronology (provenance studies). In addition, several thin sections were made for a more detailed examination of clast compositions.

This report summarizes the preliminary findings from the 2009 field season. A more detailed lithological log, together with full descriptions and analytical data (Rock-Eval, thermal maturity, gamma ray) will be available as a BCMEMP open file later in 2010. Detrital zircon geochronology, biostratigraphy and micropaleontology are described in more detail by Golding et al. (2010), as they form the basis of the ongoing PhD thesis.

## LOCATION

The measured section is located within the northern part of NTS map area 094B/14 and a few kilometres south of the Halfway River, near McQue Flats (Figure 1). It is found along a gully, incised on the west-facing side of a north-trending ridge. Access to the section was provided through the establishment of a helicopter fly camp within a cirque approximately 1 km to the east.

## GENERAL GEOLOGY

The section lies along the western margin of the Foothills subprovince of the Foreland Belt (Wheeler and

McFeely, 1991), approximately 7 km west of the northern tip of the Carbon Fault (Figures 2, 3). Strata in this area dip moderately to steeply eastward and comprise the western limb of Fiddes Syncline, which is a tight, northwest-trending chevron to box-like fold structure. Units exposed on this limb encompass the Early Carboniferous Prophet Formation to the Early Cretaceous Gething Formation and include Triassic strata over 1700 m thick. The entire Triassic sequence is represented in this section and belongs to the Early Triassic Grayling Formation, the Early–Middle Triassic Toad Formation, the Middle–Late Triassic Liard Formation and the Late Triassic Charlie Lake, Baldonnel and Pardonet formations (Figures 4, 5). A more detailed description of these units and structures can be found in Thompson (1989) and Ferri (2009a).

Due to its thinness (~35 m) and recessive rock types (shale and siltstone), the Grayling Formation is typically poorly exposed and commonly grouped with the Toad Formation. The lower 200 m of the Toad Formation (including the Grayling Formation) within the study area is covered by scree. Structural sections suggest that there is upward of 850 m of the Toad and Grayling formations along the western limb of the Fiddes syncline.

The Toad and Grayling formations are equivalent to the Montney Formation and lower parts of the Doig Formation in the subsurface (Figure 6), and correlations indicate a westward-thickening wedge. West of the study area, across the large fold cored by Carboniferous strata, only a few hundreds of metres of the Toad and Grayling formations are present below the Ludington Formation, the latter of which represents the westward deeper-water equivalents of the Charlie Lake and Baldonnel formations (Gibson, 1975; Zonneveld, 2008). This implies either the nondeposition or removal of the Liard Formation some 10 km west of the study area. Alternatively, Gibson (1991) suggests that the Ludington Formation also transitions into the Liard Formation, although fossil and depositional relationships are inconclusive.

## DETAILED SECTION

Approximately 609 m of siltstone and fine sandstone were measured as part of the Toad Formation (Figures 5, 7). The base of the unit was not observed and structural sections suggest that there is another 200–250 m of the Toad Formation to the top of the Carboniferous. The base of the overlying Liard Formation was placed where moderately to thickly bedded, very fine sandstone comprised more than 90% of the section and corresponded to the start of a section of resistive, relatively clean sandstone some 100 m thick (Figures 8, 9). This is followed by a horizon of siltstone and very fine sandstone similar to Toad Formation rock types approximately 50 m thick, which is abruptly followed by Liard Formation sandstone several hundreds of metres

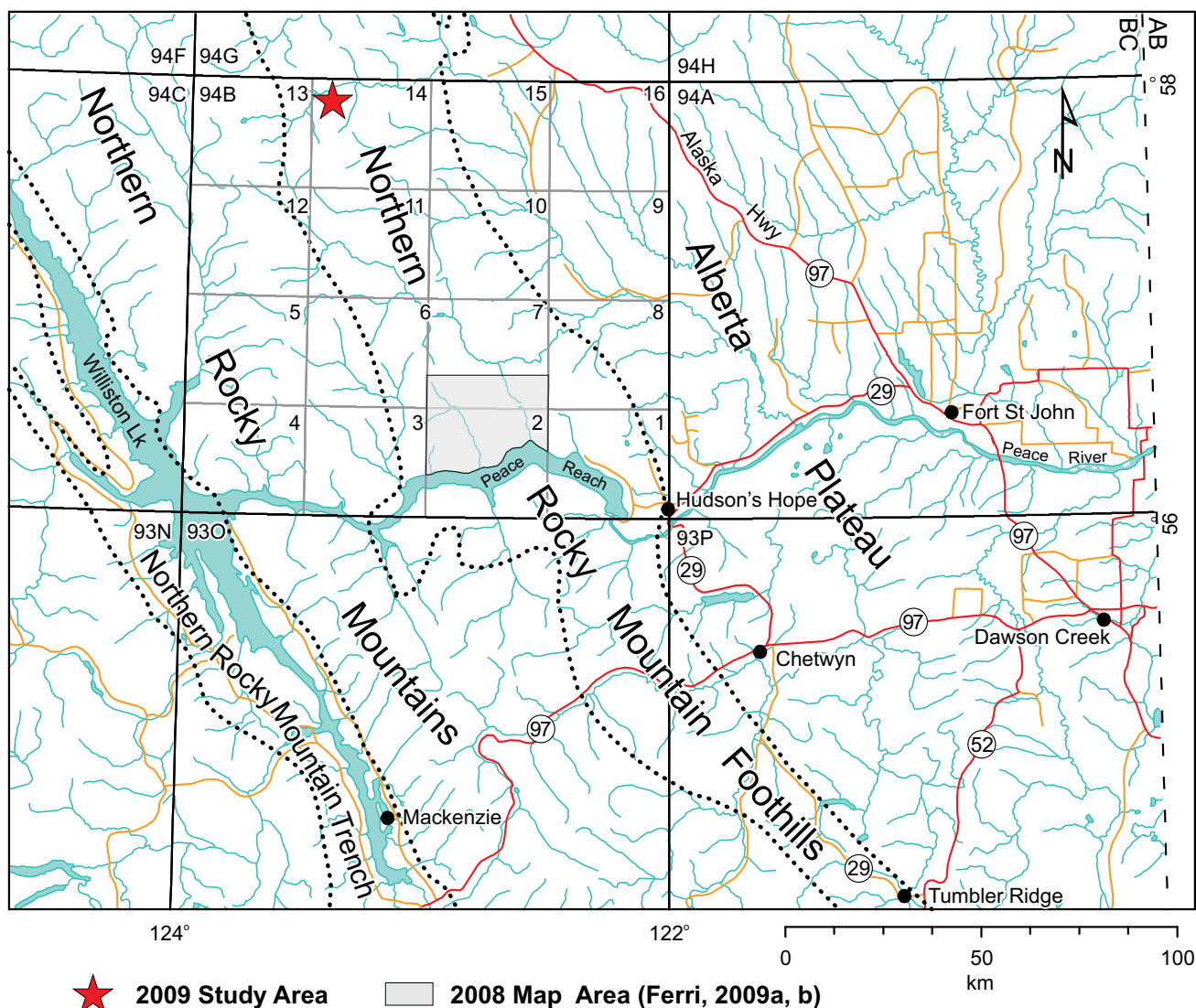


Figure 1. Location of the study area in northeast British Columbia.

thick. Abundant bioclastic debris dominated by terebratulid brachiopods (*Aulacothyroides liardensis*) and lesser spiriferid brachiopods (*Spiriferina borealis*) and ammonoids were found in scree at the foot of the Liard section. These may be sourced from a biostrome developed at the top of the first Liard sandstone section or within the Toad Formation-like siltstone at the base of the Liard Formation. This assumption is based on the presence of a similar build-up observed to the north along this horizon by previous workers (Zonneveld, 2001). The Toad-Liard formation contact defined here is similar to that used by Ferri (2009a, b) in the southern Halfway River area. Thompson (1989), following the work of Gibson (1975), places the Toad-Liard formation contact at the base of the second sandstone section.

The Toad Formation displays a general coarsening-upward succession, which can be subdivided into three broad packages: 1) a lower section, approximately 140 m thick, composed of nondescript, dark grey to grey, calcareous

to dolomitic carbonaceous siltstone; 2) a middle section containing similar dark grey siltstone but also containing beige weathering, more resistive ribs of cleaner and coarser dolomitic to calcareous siltstone to very fine sandstone and forming a section up to 160 m thick; and 3) an upper section where thin, graded laminar bedding is common within the siltstone together with resistive sections of coarse siltstone to very fine or fine sandstone locally displaying higher-energy bedforms such as current ripples. All sedimentary features seen within the succession (see below) are consistent with the deposition of the sediments as turbidites (density flows). This general threefold subdivision (described above) is also evident within the gamma-ray pattern obtained from the outcrops.

The lower part of the Toad section consists of uniform to faintly laminated dark grey calcareous to weakly dolomitic siltstone (Figure 10). These recessive rocks are typically grey to pale buff weathering, are platy to blocky

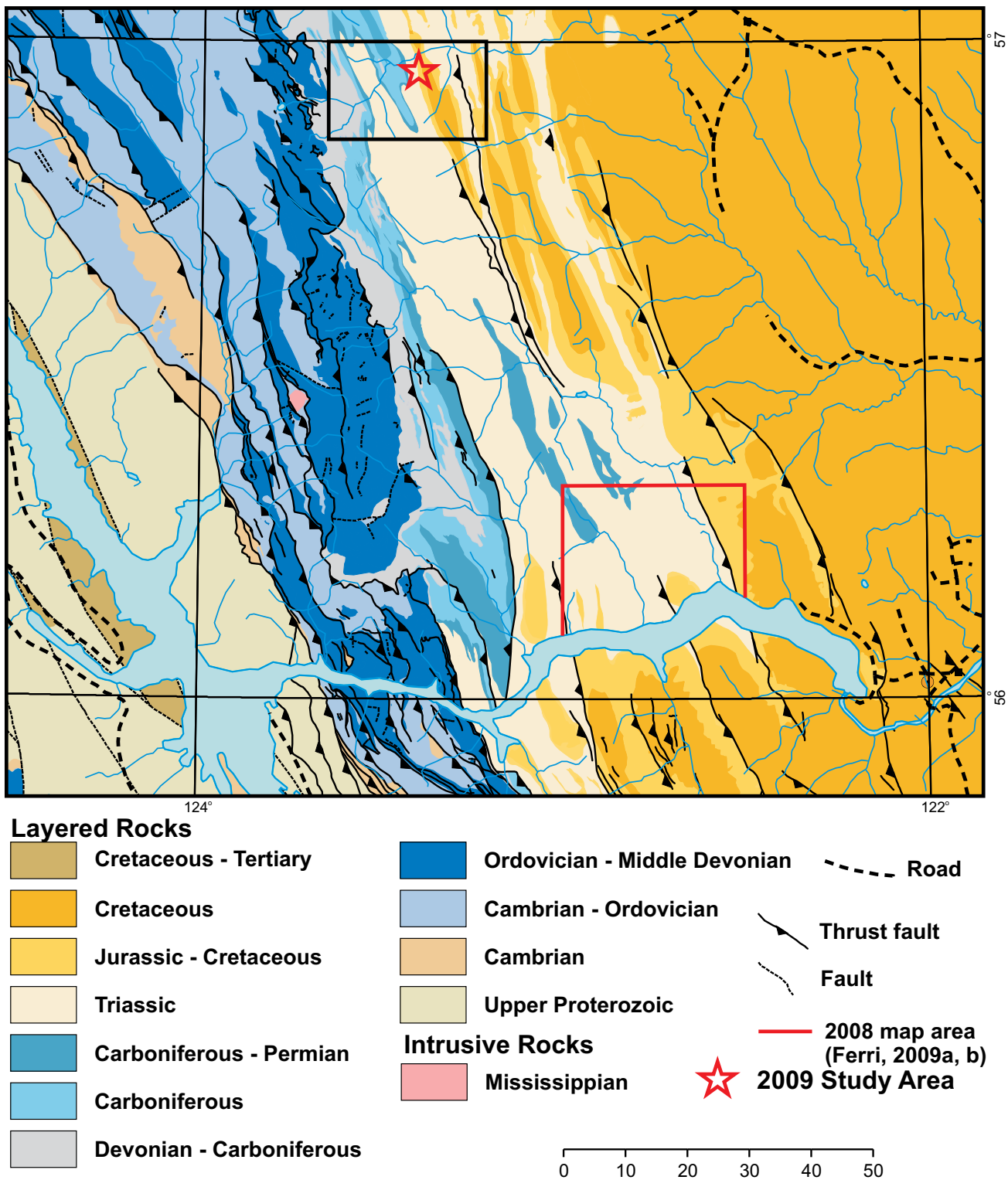


Figure 2. Regional geology of the Halfway River map area (NTS 094B/14). The black box outlines the area shown in Figure 3.

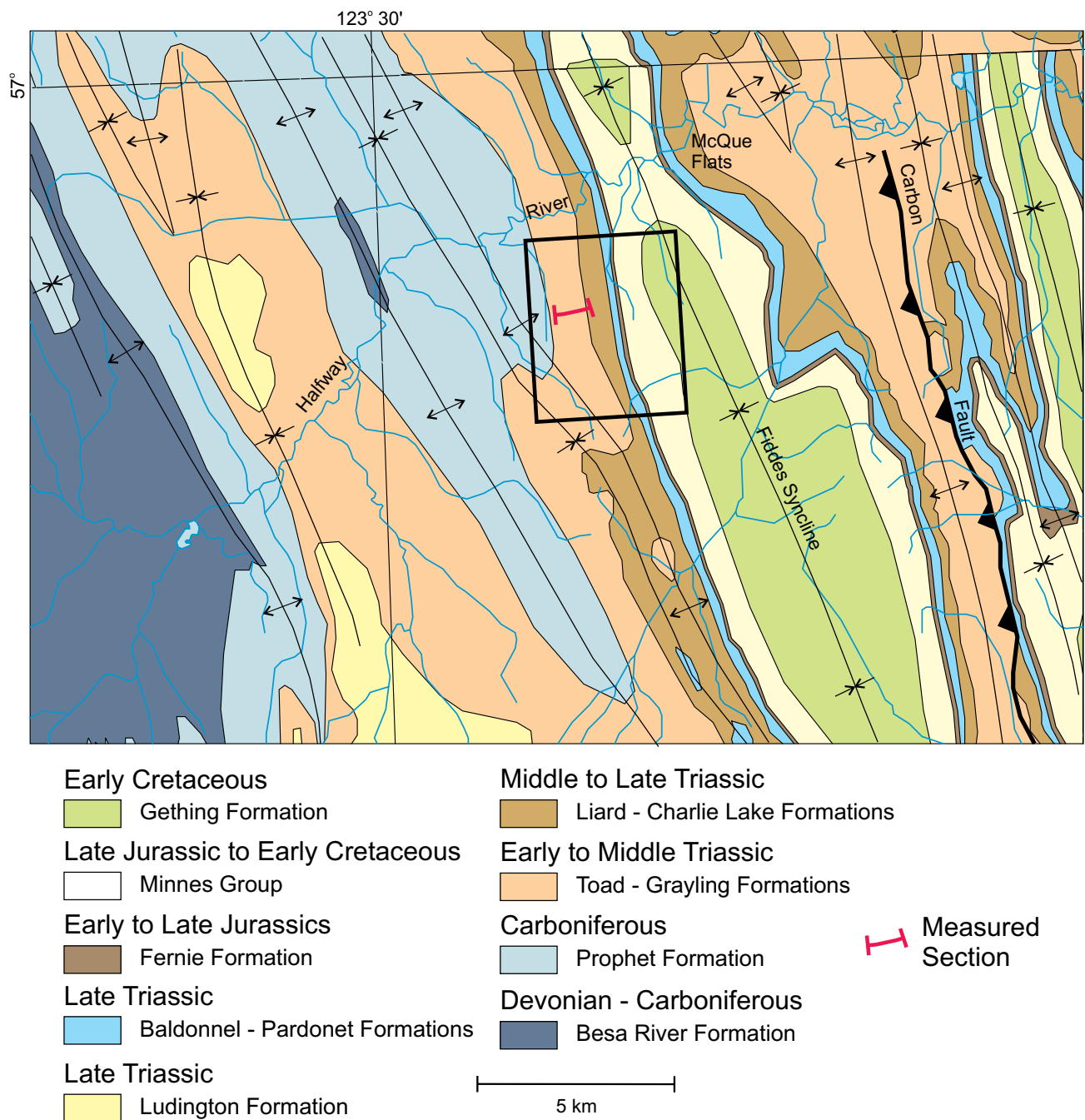


Figure 3. Geology in the vicinity of the measured section. The box outlines the area shown in Figure 5.

or crumbly and are slightly fetid on breakage. This rock type comprises the 'background' rock type throughout the section and becomes less abundant upwards as the amount of coarser clastic material increases.

The middle part of the Toad section is characterized by more resistive ribs of beige to buff weathering, cleaner and coarser dolomitic siltstone to very fine sandstone (Figures 11–13). These beds range in thickness from 0.1 to 4 m in thickness and average 1 m. They are commonly internally uniform, although in the upper part of this sequence they display laminar bedding and graded bedding. Lower and

upper contacts can be sharp to gradational with surrounding dark grey calcareous siltstone. Intervening dark grey siltstone can be quite carbonaceous and crumbly (Figure 14) within specific horizons and correspond to some of the highest gamma-ray counts within the outcrop. Overall, these more prominent ribs comprise up to 60% of the section.

Locally, there is a rhythm to the pattern of the more resistive beds whereby the thickest beds are followed immediately by a thicker section of dark grey siltstone (Figure 12). Above these beds, the amount and thickness of the resistive

| Stratigraphic Age | Foothills - Halfway to Pine Rivers | Peace River Subsurface | Foothills - Sukunka River |                     |
|-------------------|------------------------------------|------------------------|---------------------------|---------------------|
| Jurassic          |                                    |                        |                           |                     |
| Ferne Formation   |                                    |                        |                           |                     |
| Triassic          | Rhaetian                           | Bocock Fm              |                           |                     |
|                   | Norian                             | Pardonet Fm            | Pardonet Fm               |                     |
|                   | Carnian                            | Baldonnel Fm           | Baldonnel Fm              | Winnifred           |
|                   |                                    | Charlie Lk Fm          | Charlie Lk Fm             | Brewster            |
|                   | Ladinian                           | Liard Fm               | Halfway Fm                | Starlight Evaporite |
|                   | Anisian                            | Toad Fm                | Doig Fm                   | Llama               |
| Lower             | Grayling Fm                        | Montney Fm             | Whistler                  |                     |
| Permian           |                                    |                        |                           |                     |
| Fantasque/Ishbel  |                                    |                        |                           |                     |

Figure 4. Stratigraphic nomenclature used in the surface and subsurface areas of northeastern British Columbia.

beds increase until a very thick resistive bed is encountered and the pattern repeats (Figure 12). The significance of this is not known but it may possibly reflect episodic shallowing within the basin, or increased sediment influx.

These prominent ribs continue into the upper part of the section, becoming thicker and coarser grained, although not as abundant as in the middle section. The intervening dark grey siltstone begins to contain coarser, thin laminar bedding, which commonly displays grading (Figure 15, 16). A prominent 8 m thick section of very fine to fine-grained sandstone begins at the 476 m mark of the section. This thick sandstone horizon is characterized by current ripples, load casts and tool marks. In addition, there are horizons displaying convoluted bedding due to soft sediment deformation (Figures 17–20). These features become more common above this level, within thinner sandstone ribs and thinly interlayered coarse siltstone and fine sandstone beds. At several horizons in the upper part of the Toad section, convoluted bedding is associated with low-angle erosional cutoffs where conglomeratic lag occurs at the erosional base (Figure 20). These features are consistent with derivation from high-energy turbid flows.

Compositionally, siltstone in the lower part of the Toad section contains approximately 30–40% carbonate (and locally up to 60%), 10–20% feldspar (potassium and plagioclase), 40–60% quartz and several per cent muscovite. Clasts are angular to subangular. Less argillaceous and coarser siltstone and very fine sandstone contain less carbonate (20–30%) and higher concentrations of subrounded to subangular clastic rocks. Although quartz dominates coarse clastic rocks (70–80%), feldspar can comprise up to 20% and muscovite, chert and rare hornblende are minor constituents. Lower Liard Formation sandstone is very similar in composition to sandstone horizons in the Toad Formation. Coarser, clean (less argillaceous and radioac-

tive) Liard Formation sandstone at ~635 m is subrounded to rounded and dominated by quartz (80%), feldspar (10%), chert (up to 5%) and rare hornblende, with the remainder being carbonate cement.

Several current flow directions were measured, which, upon rotation of bed inclinations, give original flow directions of 200°–219° and an average of 219°. Pelletier (1960, 1961, 1965) recorded similar southwesterly flow directions from the Toad and Grayling formations north of Halfway River.

The lower 25 m of the Liard Formation consist of tan to beige weathering, very fine to medium-grained, massive to crossbedded calcareous sandstone. Bedding is thin to thick or very thick and typically massive. Low-angle crossbeds are locally developed. Several metres of pale grey to grey, medium-grained, thick-bedded sandstone were observed near the top of the section. This section appears consistently less argillaceous and coarser grained than other parts of the Liard section.

The lower part of the Liard Formation, near its contact with the Toad Formation, contains large burrows assigned to *Cruziana* and *Thalassinoides* (Figure 21). Large *Cruziana* are locally common in the Upper Toad–Lower Liard formation interval (Zonneveld et al., 2002). No other bioturbation was observed below the Toad–Liard formation contact. Macrofossils were found at various horizons throughout the Toad section and consist of brachiopod, pelecypod, ammonoid and possibly vertebrate remains. Brachiopods were observed in the lowermost part and are smooth-shelled terebratulids. Pelecypod remains typically consist of individual flat-clam (daonellids) imprints, although ‘crinkly’ beds a few millimetres thick at the 275 m mark are composed almost entirely of flat-clam remains. Ammonoids, up to a few centimetres in diameter were also observed at various horizons.

Fifteen conodont samples were obtained throughout the section in hopes of better defining the age range of the sequence so as to help with regional correlations and the interpretation of geochemistry and detrital zircon samples.

## ROCK-EVAL

A total of 114 samples were obtained from the Toad Formation and analyzed by programmed pyrolysis via a Rock-Eval 6 apparatus at the organic geochemistry laboratories of the Geological Survey of Canada, in Calgary, Alberta. Each sample consists of representative material taken across 5 m intervals. A profile of total organic carbon (TOC) content across the section is shown in Figure 7.

Generally, TOC decreases up-section, reflecting the overall upward-coarsening of the sequence. Total organic carbon levels fall below 1% at approximately the 450 m level. Although the zone containing the highest gamma-

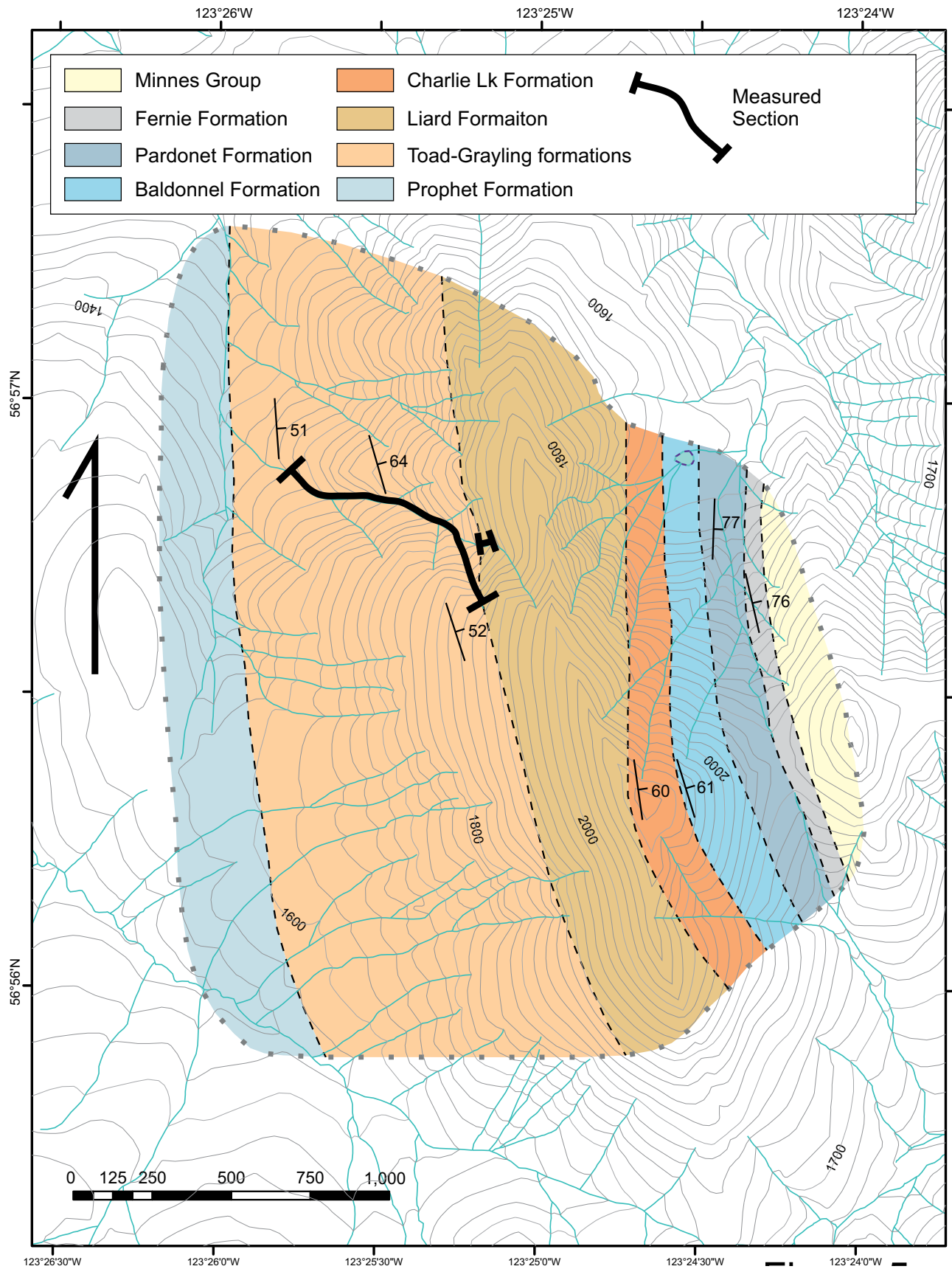


Figure 5. Geology mapped in the vicinity of the measured section.

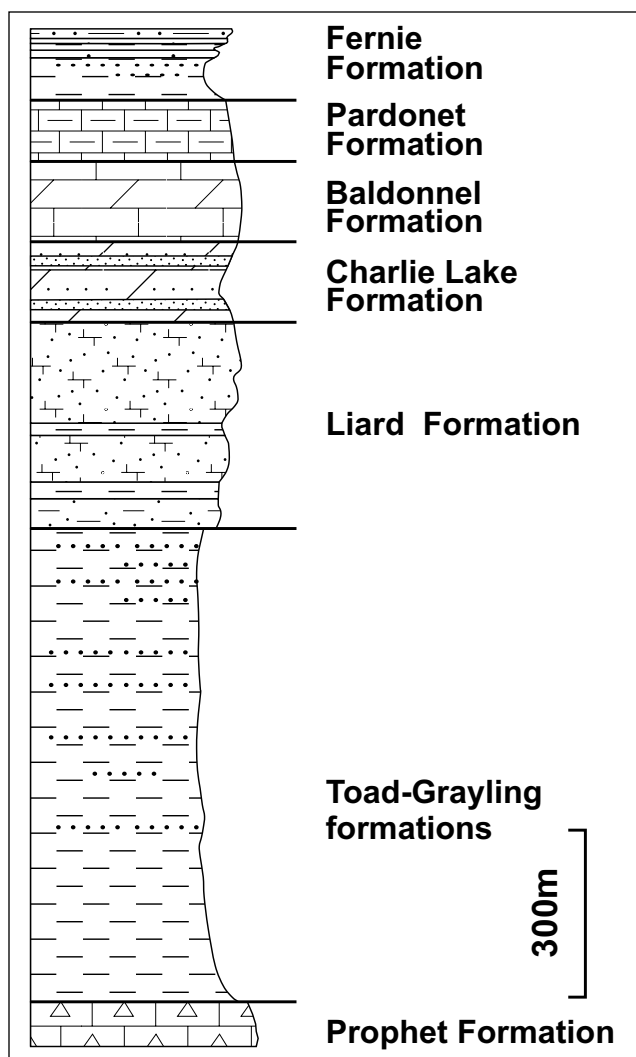


Figure 6. Generalized stratigraphy in the vicinity of the measured section; modified from Davies (1997).

ray readings (140–300 m) has high TOC concentrations (1–4%), the highest levels were found in the lower 140 m (up to 5%). Little generative capacity remains in these thermally mature rocks as shown by HI (hydrogen index) levels of less than 10 mg of hydrocarbons per gram of TOC. Assuming that much of the hydrocarbons have been expelled from the organic matter, then TOC levels originally were most likely at least two times higher (Jarvie, 1991).

## THERMAL MATURITY

Eleven samples were collected during the 2010 field season for reflected-light microscopy determination of thermal maturity. Seven samples were obtained from the measured section and the remainder originated from units higher in the Triassic. Gradients measured within the southern Halfway River area suggest that Toad Formation rock types should occupy the middle–upper dry gas zone ( $R_o$  values of 2–3; Ferri, 2009a).

## GAMMA-RAY MEASUREMENTS

A handheld spectrometer (RS-125 by Radiation Solutions Inc.) was used to acquire a gamma-ray profile across the section to facilitate the correlation of these rocks with subsurface gamma-ray traces acquired across age-equivalent strata to the east. In addition to total counts per second, concentrations of K (%), Th (ppm) and U (ppm), and total dose (nGy/h) were acquired. Elemental concentrations and total dose were acquired every 1 m during a 30 s time period. A total count rate per second was determined through the averaging of maximum and minimum count rates at each sample site. Counts per second and total dose both measure the total level of radioactivity from the section and the respective profiles should mimic each other (Figure 7). The raw data acquired during the 2009 field season will be included with the upcoming open file report.

The trace of total gamma-ray counts per second (dose) shows a zone of higher total counts beginning at approximately 140 m. This zone continues up to about 300 m, at which point the general baseline level decreases up-section until the lowest counts per second were encountered within the coarser sandstone of the Liard Formation. The zone of higher radioactivity (140–300 m) roughly corresponds to the middle part of the lithological section containing the prominent siltstone ribs separated by organic-rich siltstone. The upward decrease in gamma-ray levels reflects the general upward-coarsening and decrease in argillaceous content up the section.

Interestingly, there is no significant decrease in radioactivity at the Toad-Liard formation contact as the gamma-ray trace crosses into fine-grained sandstone of the Liard Formation. The lowest gamma-ray counts are only recorded within the coarser, thicker-bedded sandstone at approximately the 637 m level. The higher radioactivity levels within the Lower Liard Formation sandstone are probably a reflection of the potassium feldspar and mica in this finer sandstone. This is borne out of thin section examinations. Feldspar and mica are probably mechanically removed in the coarser sandstone as they most likely represent higher-energy shoreface environments typical of the Liard Formation (i.e. more akin to Halfway Formation sandstones).

## CORRELATIONS

Although there is a direct correlation of exposed carbonate-dominated Triassic stratigraphy with similar subsurface units (as shown by similar terminology; i.e., Pardonet, Baldonnel, Charlie Lake), direct correlation of formations in the underlying clastic succession is not as straightforward. Though the Halfway, Doig and Montney formations are the combined subsurface equivalents to the Liard, Toad and Grayling formations, defined contacts between each unit are not correlatable. An exercise of tracing the Halfway

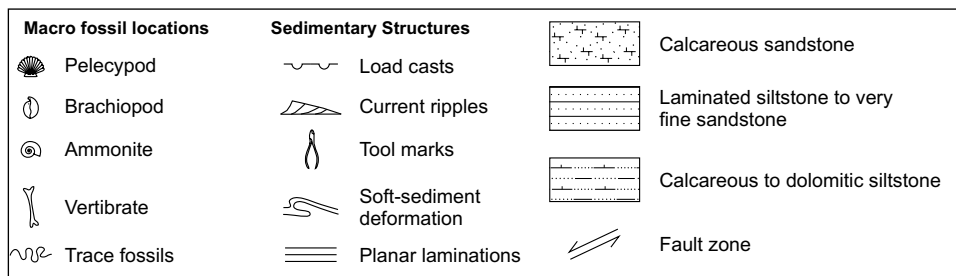
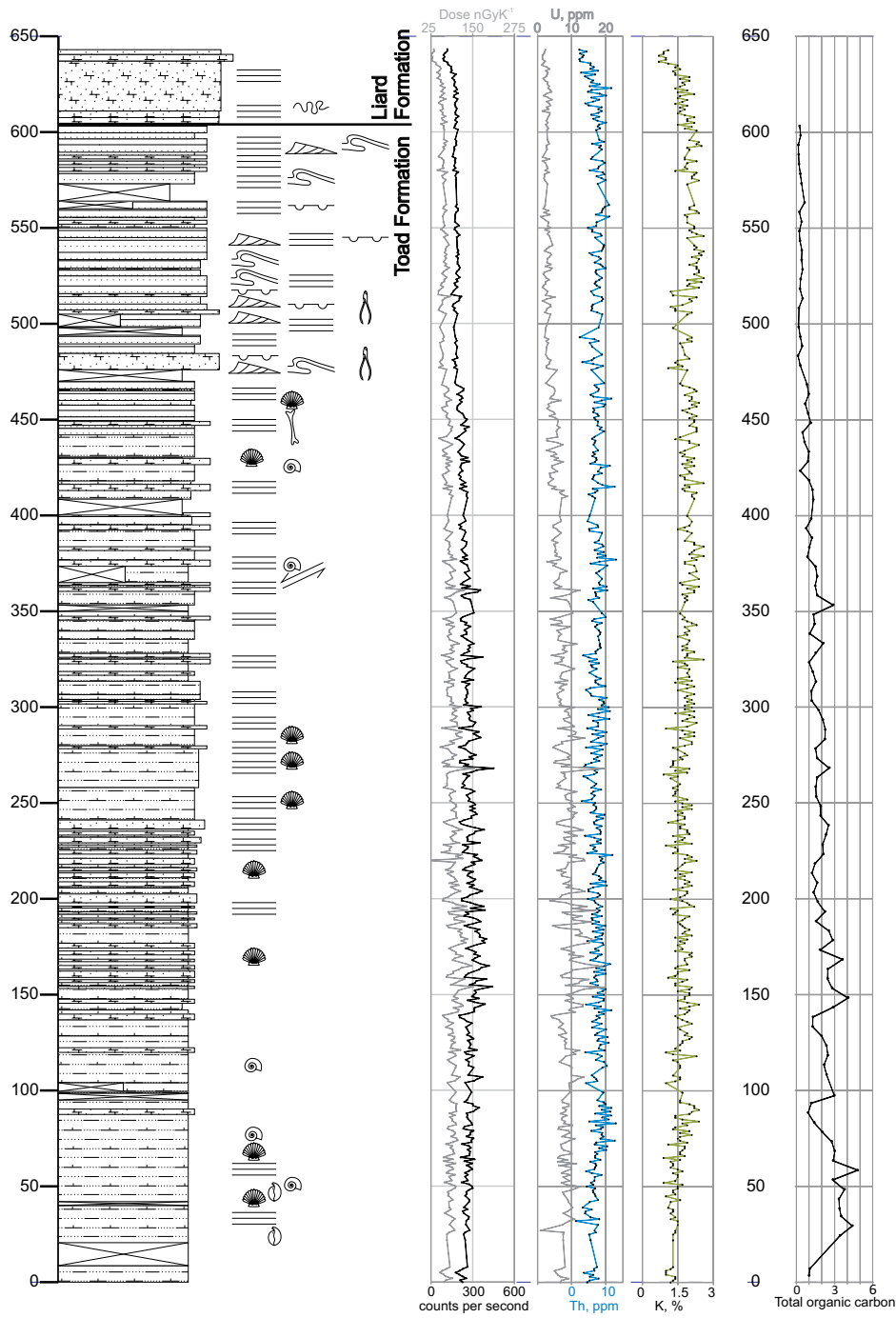


Figure 7. Generalized representation of measured section of Toad and lower Liard formations rock types. Accompanying this are traces of total dose, counts per second and concentrations of U, Th and K.

Formation sandstone westward within the ever-thickening Triassic clastic wedge suggests that these would occupy the upper part of the Liard Formation, and that the Doig Formation correlates with parts of the Liard Formation. Furthermore, the relative thinness of the Grayling Formation (~50 m) suggests that the Toad Formation is equivalent to the Montney Formation and perhaps parts of the Doig Formation.

It is hoped that the gamma-ray trace, together with lithological descriptions from the study area, will shed some light on the correlation of these units. The ability to integrate the detailed lithological descriptions from the described section is a powerful tool in the regional correlation and depositional understanding of these sequences.

Correlation of the gamma-ray trace with nearby wells indicates that the higher zone of radioactivity displayed between the 140 m and the 300 m marks is most likely equivalent to the Doig Formation phosphate (Figure 22). This is based on the overall thickness of the Triassic section together with the relative position of the gamma-ray trace within the section. One of the closest wells to the measured section, c-54-G/94-G-3, contains a Triassic sequence of equal thickness to that in the study area. Although Lower Triassic thicknesses in this well could be structurally related, they are similar to those seen in other wells along strike (e.g., a-4-L/94-B-1) and follow an overall westward thickening of the Triassic sequence shown in Figure 22 (see also Edwards et al., 1994).

The thickness and gamma-ray character of the lower Doig Formation phosphatic zone in the c-54-G well is roughly the same as that in the measured section. Furthermore, the thickness of the underlying Montney Formation in this well is similar to values obtained for the underlying Toad Formation based on the measured and structural sections in the study area.

It appears that the lower Doig Formation phosphatic zone thickens to the west and becomes more diffuse within the western part of the foothills. In Figure 22, the sharp gamma-ray spike at the base of the Doig Formation phosphatic zone shown in wells east of c-54-G is lacking within this well and the study area. No phosphatic horizons or nodules were noted within the measured section. The highest gamma-ray readings in the study area correspond to the most carbonaceous horizons.

These correlations would also suggest that the Liard Formation as described here is probably correlative to parts of the Charlie Lake, Halfway and upper Doig formations in the subsurface and that the Toad Formation is equivalent to the Montney and Doig formations in the subsurface (see also Orchard and Tozer, 1997).



Figure 8. View looking south at the gully where the section of Toad and Liard formations was measured. The Toad-Liard formation contact is shown by the dashed white line. The sandstone section in lower Liard Formation is approximately 50 m thick.



Figure 9. View looking south at the Toad-Liard Formation contact and the lower part of the Liard Formation. The latter contains a tongue of Toad Formation-like siltstone and fine sandstone approximately 75 m thick above a section of equally thick Liard Formation sandstone. The lower part of this siltstone tongue contains a horizon that supplies the abundant bioclastic debris found in the upper part of the gully. The sandstone section in lower Liard Formation is approximately 50 m thick.



Figure 10. Typical grey to dark grey calcareous to dolomitic siltstone within the lower part of the Toad section.



Figure 11. Characteristic ribbing within the lower-middle part of the section (~140–300 m). Here, resistive, buff-weathering, dolomitic siltstone is interlayered with dark grey calcareous siltstone. These buff-weathering horizons (approximately 1 m thick) are cleaner and somewhat coarser than the recessive units.



Figure 12. Close-up view of part of the section seen in Figure 11. Note that the buff-weathering horizons show an overall coarsening or cleaning upwards (to the left in the photo). Also note (along with Figure 11) that the section shows a rhythm, whereby there is an increase in development of the buff-weathering horizons towards the next-thickest resistive rib. Thick, buff-weathering beds are approximately 1 m thick.



Figure 13. Less weathering is seen in the ribbed zone shown in Figures 11 and 12 where erosion has exposed a section.



Figure 14. Contact between carbonaceous siltstone and buff-weathering siltstone. These carbonaceous horizons produced some of the highest readings on the scintillometer.



Figure 15. Laminated and graded fine- to coarse-grained siltstone of the middle part of the section. These rock types become more abundant in the upper half of the section (>300 m).



Figure 16. View looking north at the 450 m level of the section. Here, coarser grained siltstone horizons exist between more recessive, laminated siltstone. The resistive bed on the left side of photo is approximately 2 m thick.



Figure 17. Soft sediment deformation in a fine-grained sandstone to coarse-grained siltstone horizon at the 480 m level.



Figure 18. Current ripples in very fine sandstone, 480 m level.



Figure 19. Graded, finely laminated fine sandstone to coarse siltstone also displaying load casts (lowest part of slab), 506 m level.



Figure 20. Low-angle, angular unconformity. Lower beds are at an angle to the uppermost horizons with the contact between the two at the midway point of the mechanical pencil. Note that the contact is uneven and marked by coarse lag material; 522 m level.



Figure 21. Bedding-parallel burrows (*Cruziana*?) within the very fine sandstone of the Lower Liard Formation, 611 m level. Burrows are 3–5 cm in width.

## SUMMARY

- Over 600 m of the Toad Formation were measured within the western Foothills of northern Halfway River map area (NTS 094B/14). A further 200 m of the lower part of this formation was not exposed.
- Sedimentary structures indicate deposition through low-density flows (turbidites).
- Current indicators suggest south-southwesterly to southwesterly directions.
- A gamma-ray trace across the measured section suggests that the Toad Formation is equivalent to the Montney and Doig formations.

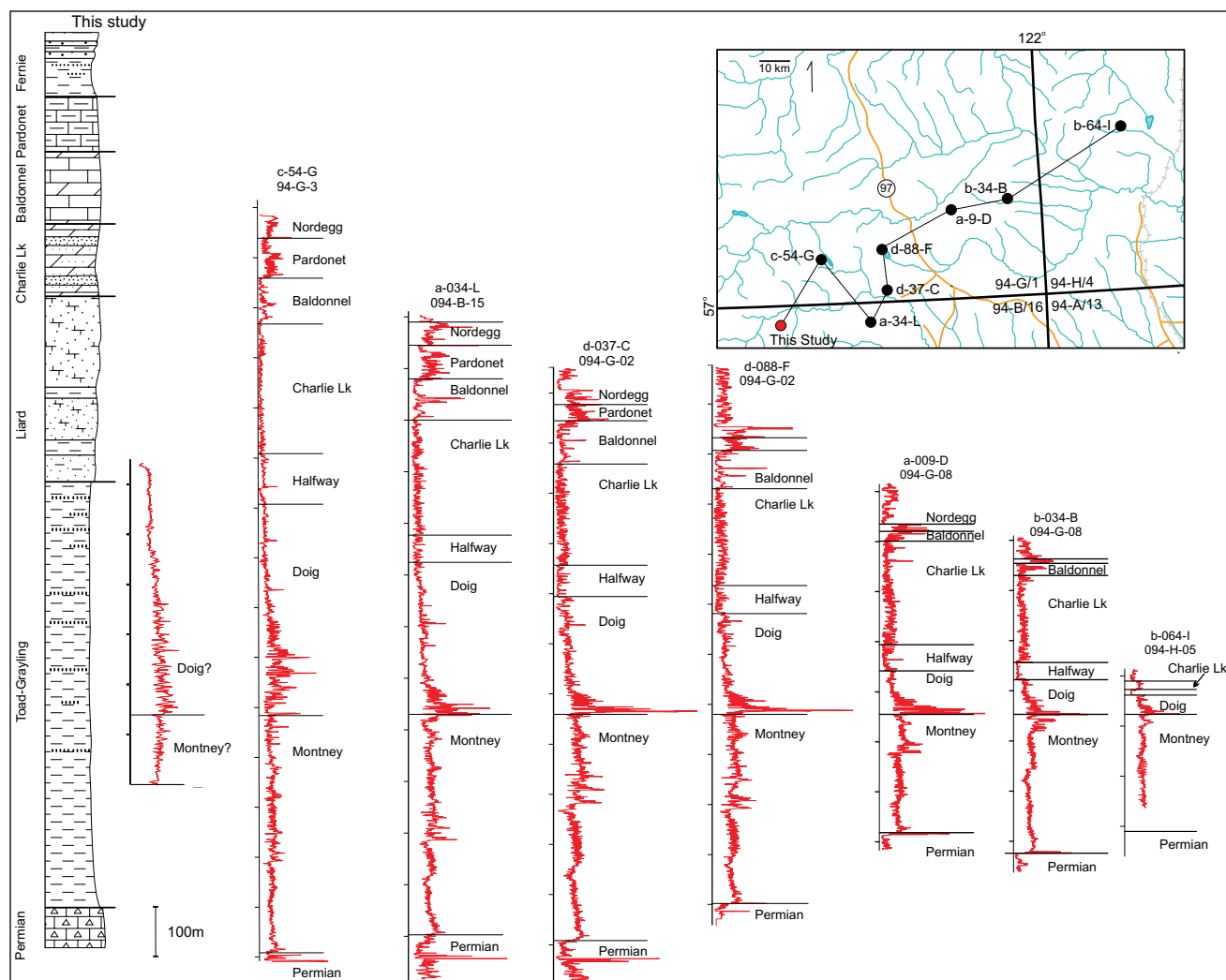


Figure 22. Correlation of lithological section and gamma-ray count trace from the study area (stratigraphic column and gamma-ray trace at the left-hand side of the diagram), with gamma-ray traces from selected wells to the east. Note that the trace of the gamma-ray count from the study area, together with the relative position within the lithological section, suggests that the zone of highest readings in the study area probably corresponds to the phosphatic part of the Doig Formation seen to the east. The correlation is most convincing with the trace from the nearest well (c-54-G). Inset shows location of the sections with respect to the study area.

## ACKNOWLEDGEMENTS

The authors would like to thank Bob Batchelor of Whitney Helicopters for excellent service and making our stay in the mountains much more enjoyable. We would also like to thank Alf Hartling for reviewing early versions of this manuscript. I would like to thank Larry Lane, Jenny Wong and Krista Boyce of the Geological Survey of Canada for assisting with the processing of Rock-Eval samples.

## REFERENCES

- Canadian Discovery Digest (2008): Resource play fever in British Columbia; Exploration Review, Volume 2, pages B1–33.
- Davies, G.R. (1997): The Triassic of the Western Canada Sedimentary Basin: tectonic and stratigraphic framework; *Bulletin of Canadian Petroleum Geology*, Volume 45, pages 434–460.
- Edwards, D.E., Barclay, J.E., Gibson, D.W., Kville, G.E. and Halton, E. (1994): Triassic strata of the Western Canada Sedimentary Basin; in Geological Atlas of the Western Canada Sedimentary Basin, Mossop, G.D. and Shetsen, I., Compilers, *Canadian Society of Petroleum Geologists and Alberta Research Council*, Special Report 4, URL <[http://www.ags.gov.ab.ca/publications/wcsb\\_atlas/atlas.html](http://www.ags.gov.ab.ca/publications/wcsb_atlas/atlas.html)> [January 2010].
- Ferri, F. (2009a): Preliminary geology of the Jones Peak area (NTS 94B/2 and 7), Halfway River map sheet (94B); in Geoscience Reports 2009, *BC Ministry of Energy, Mines and Petroleum Resources*, pages 5–23.

- Ferri, F. (2009b): Preliminary geology of the Jones Peak area (NTS 94B/2 and 7); *BC Ministry of Energy, Mines and Petroleum Resources*, Petroleum Geology Open File 2009-4.
- Gibson, D.W. (1975): Triassic rocks of the Rocky Mountain Foothills and Front Ranges of northeastern British Columbia and west-central Alberta; *Geological Survey of Canada Bulletin* 247, 61 pages.
- Gibson, D.W. (1991): Triassic strata of the Foreland Belt; in Chapter 8, Upper Devonian to Middle Jurassic Assemblages; Gabrielse, H. and Yorath, C.J., Editors, *Geological Survey of Canada Geology of Canada*, Number 4, pages 265–276.
- Golding, M.L., Ferri, F., Mortensen, J.K., Zonneveld, J-P. and Orchard, M.J. (2010): Biostratigraphic and sedimentological studies of natural gas-bearing Triassic strata in the Halfway River map area (NTS 094/B), northeastern British Columbia: progress report; in *Geoscience BC Summary of Activities 2009*, *Geoscience BC*, Report 2010-1, pages 249–258.
- Jarvie, D.M. (1991): Total organic carbon (TOC) analysis; in *Source Migration Processes and Evaluation Techniques*, Merrill, R.K., Editor, *American Association of Petroleum Geologists*, Treatise of Petroleum Geology, Handbook of Petroleum Geology, pages 113–118.
- Orchard, M.J. and Tozer, E.T. (1997): Triassic conodont biochronology, its calibration with the ammonoid standard, and a biostratigraphic summary for the Western Canada Sedimentary Basin; in *Triassic of Western Canada Basin*, Moslow, T. and Wittenberg, J., Editors; *Canadian Society of Petroleum Geologists*, Bulletin 45, pages 675–692.
- Orchard, M.J. and Zonneveld, J.P. (2009): The Lower Triassic Sulphur Mountain Formation in the Wapiti Lake area: lithostratigraphy, conodont biostratigraphy, and a new biozonation for the lower Olenekian (Smithian); *Canadian Journal of Earth Sciences*, Volume 46, pages 757–790.
- Pelletier, B.R. (1960): Triassic stratigraphy, Rocky Mountain Foothills northeastern British Columbia; *Geological Survey of Canada*, Paper 60-2, 32 pages.
- Pelletier, B.R. (1961): Triassic stratigraphy of the Rocky Mountain and Foothills northeastern British Columbia; *Geological Survey of Canada*, Paper 61-8, 32 pages.
- Pelletier, B.R. (1965): Paleocurrents in the Triassic of northeastern British Columbia; in *Primary sedimentary structures and their hydrodynamic interpretation – a symposium*, Special Publication, *Society of Economic Paleontologists and Mineralogists*, pages 233–245.
- Thompson, R.I. (1989): Stratigraphy, tectonic evolution and structural analysis of the Halfway River map area (94B), northern Rocky Mountains, British Columbia; *Geological Survey of Canada*, Memoir 425, 119 pages.
- Wheeler, J.O. and McFeely, P. (1991): Tectonic Assemblage Map of the Canadian Cordillera and Adjacent Parts of the United States of America; *Geological Survey of Canada*, Map 1712A.
- Zonneveld, J-P. (2001): Middle Triassic biostromes from the Liard Formation, British Columbia, Canada: oldest examples from the Mesozoic of North American Pangea; *Sedimentary Geology*, Volume 145, pages 317–341.
- Zonneveld, J-P. (2008): Triassic sedimentary framework and sequence stratigraphy, Williston Lake, British Columbia; *Canadian Society of Petroleum Geologists*, Field Trip Guidebook.
- Zonneveld, J-P. and Moslow, T.F. (2005): Reservoir architecture of a fine-grained turbidite system from outcrop exposures of the Triassic Montney Formation, Western Canada Sedimentary Basin; *American Association of Petroleum Geologists*, Annual Convention, Calgary, Alberta.
- Zonneveld, J-P., Pemberton, S.G., Saunders, T.D.A. and Pickerill, R.K. (2002): Large robust Cruziana from the Middle Triassic of northeastern British Columbia: ethologic, biostratigraphic and paleobiologic significance; *Palaaios*, Volume 17, pages 435–448.

# PRELIMINARY ASSESSMENT OF POTENTIAL HYDRAULIC FRACTURE SAND SOURCES AND THEIR DEPOSITIONAL ORIGIN, NORTHEAST BRITISH COLUMBIA

Adrian S. Hickin<sup>1</sup>, Fil Ferri<sup>1</sup>, Travis Ferbey<sup>1</sup> and I. Rod Smith<sup>2</sup>

---

## ABSTRACT

*The demand for hydraulic fracture proppant ('frac sand') in northeast British Columbia has increased because of the enormous volume of frac sand required to develop unconventional shale gas resources. The increased North American demand on existing frac sand sources and the tremendous cost of transporting the product to northeast British Columbia means that local sand sources once deemed marginal or unsatisfactory may be economic despite the expense of processing.*

*A preliminary assessment of 7 bedrock samples and 17 unconsolidated sand samples from northeast British Columbia is presented. For bedrock samples, thin sections and a distribution map of prospective units in the Rocky Mountain Foothills are provided. For unconsolidated samples, thin sections, grain photographs (binocular, plane light and crossed nicols), major oxide geochemistry and grain-size distribution are provided.*

*Results suggest that the Liard and Charlie Lake formations (Triassic) and the Monteith and Monach formations of the Minnes Group (Late Jurassic to Cretaceous) are the most prospective bedrock units of those assessed. The Liard Formation is mainly a quartz arenite and the Charlie Lake Formation is a feldspathic arenite, both with carbonate cement. The Monteith and Monach formations are quartz arenites.*

*The unconsolidated deposits that are most prospective originate from three depositional environments: glaciodeltaic, aeolian and glaciofluvial. The Komie area is a priority target, located near the intersection of Geetla and Komie roads on the western edge of the Horn River Basin. It is a glaciofluvial delta (~8 km<sup>2</sup>) comprising mainly well-rounded, medium-grained quartz-rich sand. The Redwillow glaciofluvial delta is a large (2 km<sup>2</sup>) sand deposit south of Dawson Creek with abundant quartz grains mixed with lithic grains. Aeolian deposits of the Fontas Dune Field (Wolfe et al., 2007) contain monocrystalline, fine-grained quartz sand and are an excellent target. Other potential dune sources include the Kiskatinaw and Pine River dune fields, but abundant lithic grains make these fields less prospective than those of the Fontas Dune Field. Eskers associated with the Laurentide Ice Sheet, including the Courvoisier Esker Complex, eskers of the Horn River Basin and those found near the northern part of the Sierra-Yoyo-Desan Road may also be viable exploration targets. Despite common lithic fragments, they also contain abundant, well-rounded quartz grains.*

Hickin, A.S., Ferri, F., Ferbey, T. and Smith, I.R. (2010): Preliminary assessment of potential hydraulic fracture sand sources and their depositional origin, northeast British Columbia; Geoscience Reports 2010, BC Ministry of Energy, Mines and Petroleum Resources, pages 35–91.

<sup>1</sup>British Columbia Ministry of Energy, Mines and Petroleum Resources, Victoria, British Columbia

<sup>2</sup>Geological Survey of Canada, Calgary, Alberta

**Key Words:** hydraulic fracturing, frac sand, proppants, shale gas, oil and gas, stimulation, well completion, unconventional gas

---

## INTRODUCTION

The excessive cost associated with transporting hydraulic fracture proppants ('frac sand') from established sources to northeastern British Columbia, and the anticipated demand that will result from increased development of this ar-

ea's unconventional shale gas resources, has prompted the British Columbia Ministry of Energy, Mines and Petroleum Resources (BCMEMP) to compile an initial inventory of promising local frac sand sources. This paper examines the location, nature and origin of naturally occurring quartz-rich unconsolidated sand deposits and bedrock outcrop in northeast British Columbia. The deposits were documented

during bedrock and surficial geology mapping activities by the BCMEMPR in partnership with the Geological Survey of Canada. Some of the samples collected during these mapping programs are evaluated here for frac sand potential.

Northeast British Columbia has become a focus for the development of unconventional shale gas resources. Over the last few years, this interest has resulted in a significant increase in the amount of land sold as well as the price per hectare of petroleum and natural gas rights (Adams et al., 2008). Recent exploration activity has been focused in the Fort St John, Dawson Creek (Montney) and Fort Nelson (Horn River, Cordova Embayment and Liard River) areas, where shale gas is the target. The production of natural gas from organic-rich shale, a rock previously considered as a gas source or reservoir seal, is possible because of advances in directional drilling and production stimulation. To liberate gas from relatively impermeable shale, long horizontal sections are drilled into the formation of interest and the rock fractured, thereby providing conduits (through increased permeability) for gas to move from the rock to the well bore. Fracturing ('frac'ing) is achieved by pumping water at high pressure into the horizontal section and out into the rock. Fractures in the rock are prevented from closing by forcing proppants such as frac sand into the fractures (Figure 1).

A simulation by Kerr (2009) predicts that over the next 20 years, the demand for frac sand in the Horn River Basin, under pessimistic and optimistic drilling scenarios, to be approximately 8.8–19.7 million tons, respectively. At

a cost of \$100–\$200 per ton, the expense associated with this component of well-completion costs could range from \$880 million to \$3.4 billion. As the number of fracs per well increases, along with a shift to higher-tonnage fracs, this demand and the associated cost will also increase.

There are three major sources of frac sand in North America (Dumont, 2007; Zdunczyk, 2007): 1) Middle–Late Ordovician St. Peter sandstone of the Ancell Group (commercially referred to as 'Ottawa' or 'White' sand) from the northeast United States; 2) the Cambrian Hickory Member of the Riley Formation ('Brown' or 'Brady' sand) from Texas; and 3) the Middle Ordovician Black Island Member of the Winnipeg Formation around Hanson Lake, Saskatchewan. There are also a number of smaller frac sand producers in Canada, of which the closest to northeast British Columbia is the Cretaceous Paddy Member sandstone of the Peace River Formation (Fort St John Group) in Peace River, Alberta (Alberta Geological Survey, 1989).

Sand, used as a frac proppant, has rigid engineering standards, as outlined in American Petroleum Institute (API) report numbers API RP 56 (American Petroleum Institute, 1995a), API RP 60 (American Petroleum Institute, 1995b) and International Organization for Standards (ISO) report number ISO 13503-2 (International Organization for Standards, 2006). Critical characteristics include grain-size distribution, average particle sphericity and rounding, acid solubility, crush resistance and particle mineralogy. Most northeast British Columbian quartzite, sandstone and unconsolidated sand deposits, in raw form, fail to meet these

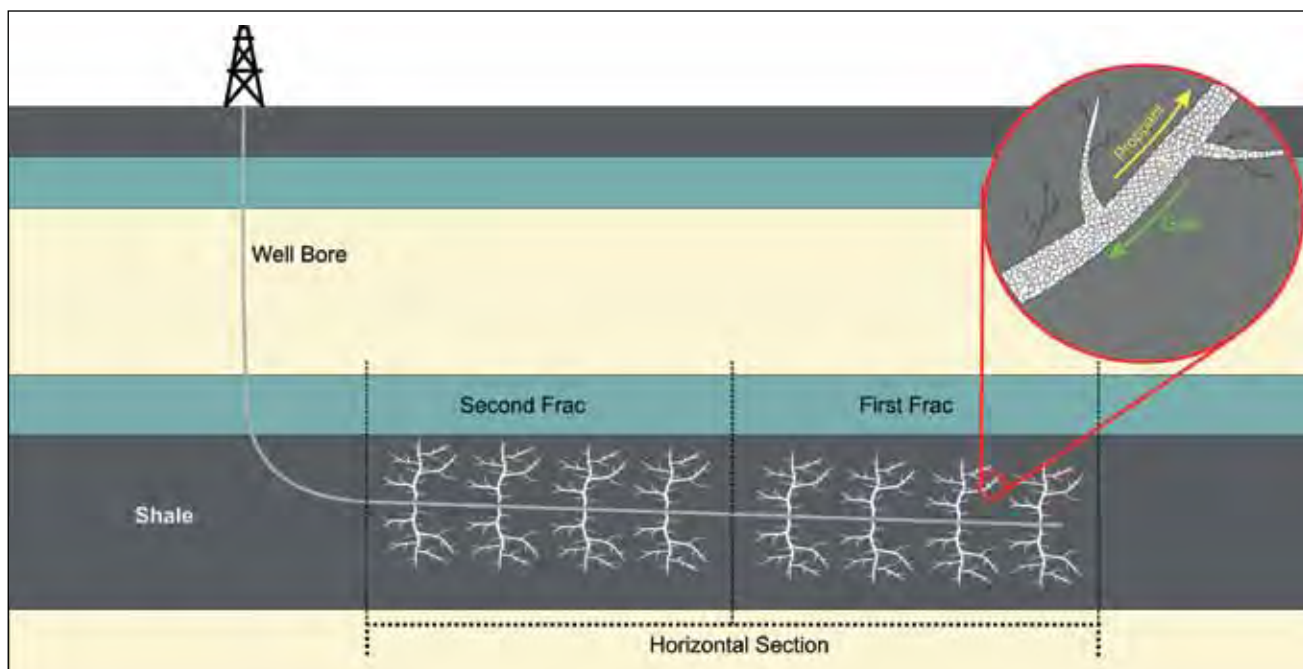


Figure 1. Simplified example of a typical frac'ing operation in northeast British Columbia. Frac'ing is performed on the horizontal section of production wells. Water is pumped into the well bore at high pressure and forced into the rock, causing it to fracture. Proppant is introduced into the fractures to keep them from closing, thereby permitting the gas to travel from the shale back to the well bore.

requirements. However, given that the transportation of frac sand to northeast British Columbia represents a significant cost, it may be economically beneficial to process local sources to meet these stringent frac sand guidelines.

## METHODS

### *Sample Collection*

### BEDROCK

Bedrock samples are from the Rocky Mountain Foot-hills physiographic region (Holland, 1976) and are part of a representative suite of samples from outcrop documented during a regional 1:50 000 scale bedrock mapping program in the Halfway River map area (094B/02 and 07; Ferri, 2009). This area encompasses clastic rocks of Carboniferous to Cretaceous age and includes the Carboniferous to Permian Stoddart Group; Triassic rocks of the Toad, Liard and Charlie Lake formations; and Jurassic to Cretaceous rocks of the Fernie, Minnes and Bullhead groups. Results presented are limited to units with >80% quartz grains, which include only the Cretaceous Monach and Monteith formations of the Minnes Group and the Triassic Charlie Lake and Liard formations.

### UNCONSOLIDATED

Sand samples collected from known and recently discovered sand deposits identified during surficial geology and aggregate potential mapping programs were evaluated for their frac sand potential. Samples are from a variety of genetic deposits including aeolian dunes, subglacial glaciofluvial (eskers) and proglacial glaciofluvial deposits, and deltaic glaciofluvial deposits.

### *Laboratory*

### BEDROCK

Thin sections were prepared and qualitatively evaluated to estimate proportions of matrix to grains and the quantity of quartz, feldspar and lithic grains for use within the classification scheme of Dott (1964) and Williams et al. (1982; Figure 2).

### UNCONSOLIDATED

Grain-size distribution was established by wet sieving raw samples using the Wentworth grain-size classification (Wentworth, 1922). The weight proportion of the sample retained in >2.0 mm, >1.0 mm, >0.5 mm, >0.25 mm,

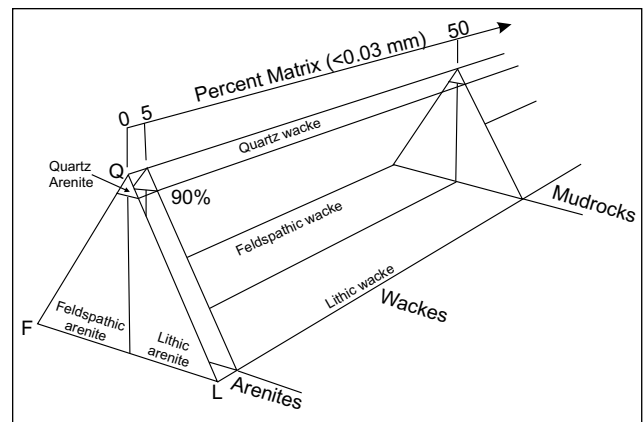


Figure 2. Classification diagram for sandstones used in this report, modified from Dott (1964) and Williams et al. (1982).

>0.125 mm and >0.063 mm sieves, and the proportion <0.063 mm is plotted both as histograms and cumulative percent charts. A split of the sand-sized fraction (<2.0 mm to >0.063 mm) was washed and separated from each raw sample for imaging and analysis. A photomicrograph was taken of the grains using a binocular microscope. Thin sections were made and imaged under plane light and cross nicols. Part of the sand split was milled to <0.063 mm and then analyzed for major oxide geochemistry by inductively coupled plasma–emission spectroscopy (ICP-ES) following a lithium metaborate/tetraborate fusion and dilute nitric digestion.

## RESULTS

### *Bedrock*

Forty-four samples were collected and evaluated; seven promising samples are presented in Table 1 and Appendix 1. The high-potential samples are from the Liard and Charlie Lake formations and the Minnes Group (Monteith and Monach formations) (Figure 3). Liard and Charlie Lake rocks record marine environments, although the latter also documents sabkha environments. The Minnes Group represents a westward-thickening foreland wedge, with the Monteith and Monach formations deposited in deltaic settings.

### *Unconsolidated*

Seventeen unconsolidated sand samples were collected from eleven distinct areas (Table 2; Appendix 2). These areas are shown in Figure 4 and include Bear Lake (aeolian; area 1), Lower Pine River (aeolian; area 2), Kiskatinaw Dune Field (aeolian; area 3), Redwillow River (deltaic; area 4), Fort Nelson Airport (glaciofluvial; area 5), Fontas Dune Field (aeolian; area 6), KM 176 — SYD (esker; area 7),

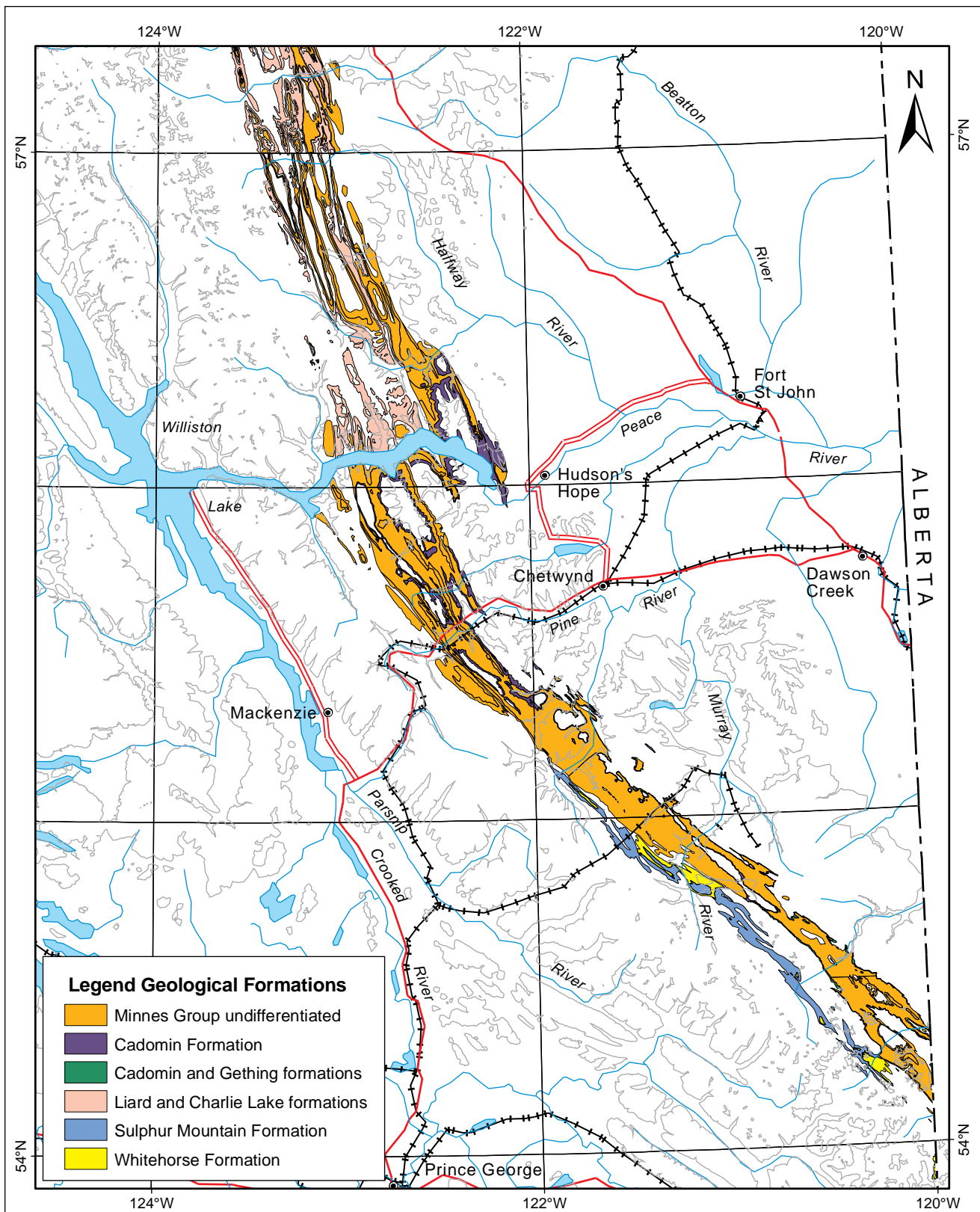


Figure 3a. Distribution within the Rocky Mountain Foothills of outcropping bedrock units discussed in this report: a) Fort St John area; b) Fort Nelson area; Modified from Massey et al., 2005.

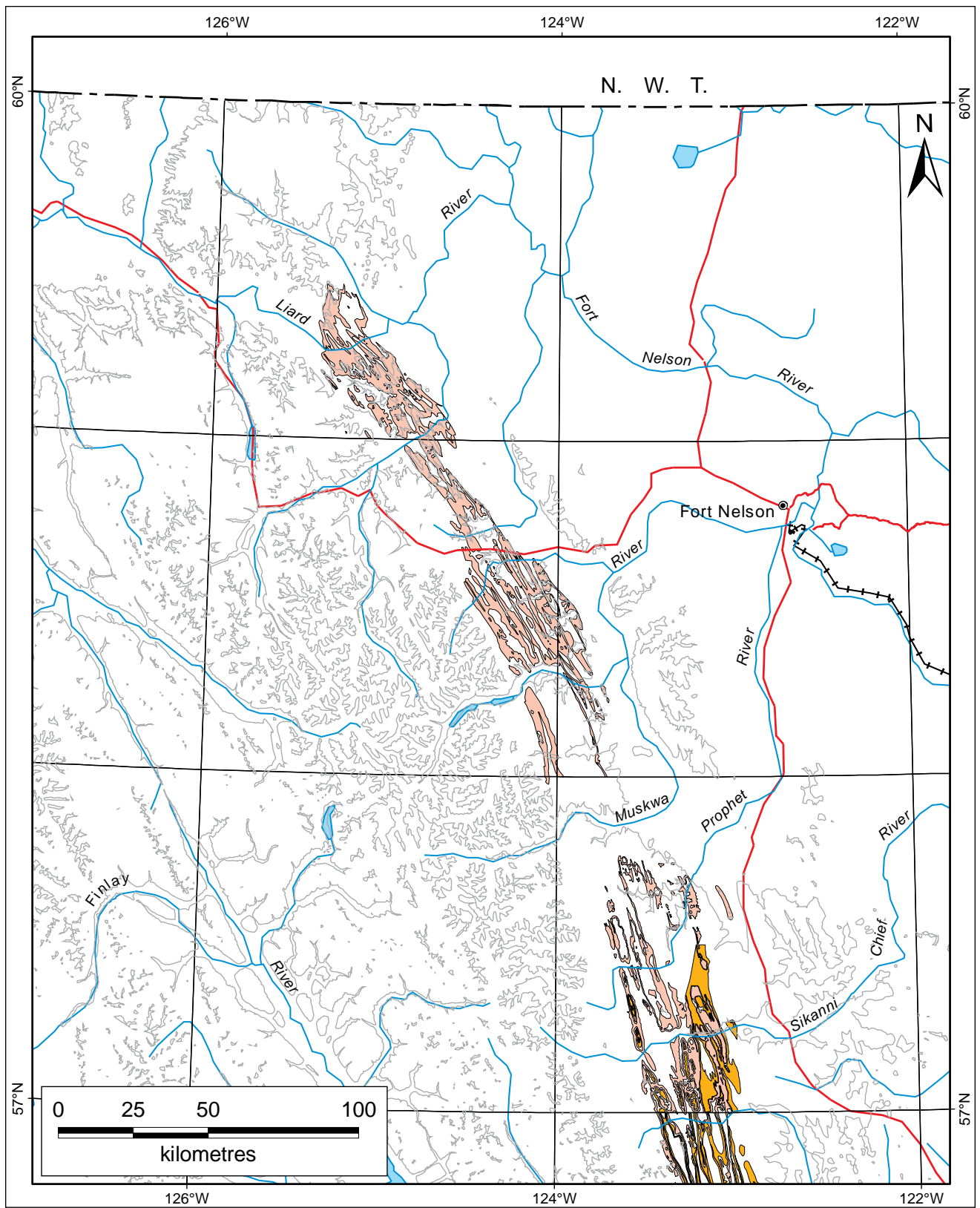


Figure 3b. Distribution within the Rocky Mountain Foothills of outcropping bedrock units discussed in this report: a) Fort St John area; b) Fort Nelson area; Modified from Massey et al., 2005.

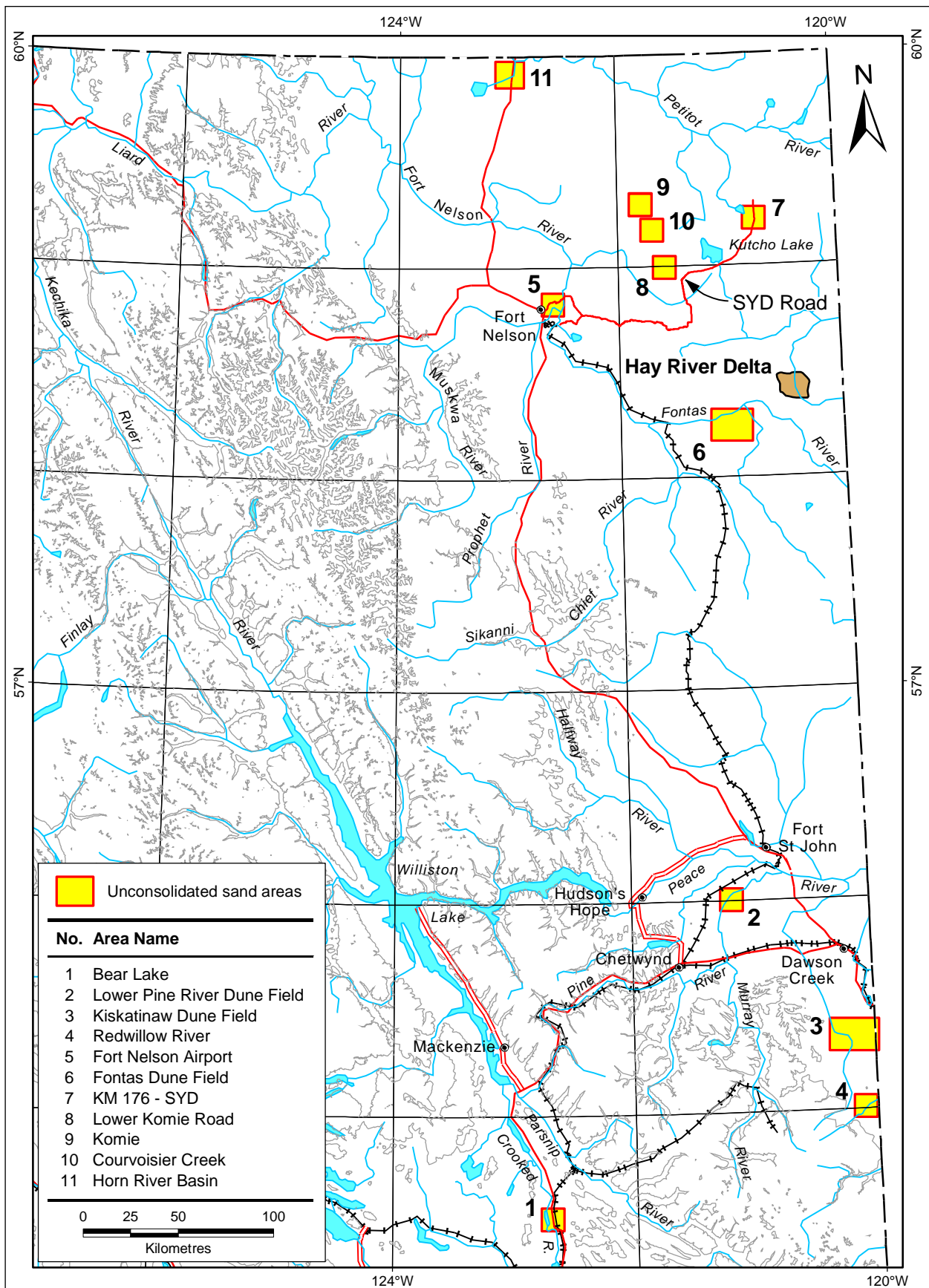


Figure 4. Location of the areas where preliminary evaluation of unconsolidated deposits indicates potential to host a frac sand source.

TABLE 1. SUMMARY OF BEDROCK FRAC SAND SAMPLES.

| Sample    | Easting | Northing | Classification      | Formation    | % Quartz | % Feldspar | % Lithic |
|-----------|---------|----------|---------------------|--------------|----------|------------|----------|
| 08DFM063  | 519797  | 6222783  | Quartz Arenite      | Monteith     | 95       | 0          | 5        |
| 08FFE125  | 521738  | 6224224  | Quartz Arenite      | Monteith     | 95       | 0          | 5        |
| 08FFE220A | 527687  | 6231355  | Quartz Arenite      | Monach       | 95       | 0          | 5        |
| 08FFE205A | 526315  | 6236536  | Quartz Arenite      | Monach       | 95       | 0          | 5        |
| 08FFE021B | 510894  | 6217773  | Feldspathic Arenite | Charlie Lake | 80       | 15         | 5        |
| 08FFE309  | 522190  | 6235343  | Quartz Arenite      | Liard        | 90       | 5          | 5        |
| 08FFE114  | 507488  | 6221073  | Quartz Arenite      | Liard        | 90       | 2          | 8        |

Lower Komie Road (esker; area 8), Komie (deltaic; area 9), Courvoisier Creek (esker; area 10) and Horn River Basin (esker; area 11).

## DISCUSSION

Several deposits are excellent candidates for further evaluation, as processing may upgrade the deposits to a usable frac sand product (i.e., meeting API and ISO standards). The following is a discussion of the most promising of these deposits.

Bedrock units that show the most potential for use as frac sand are the Liard, Charlie Lake, Monteith and Monach formations. Outcrops of the Liard and Charlie Lake formations (and their southern equivalents, the Sulphur Mountain and Whitehorse formations) can be traced throughout the entire length of the inner and western parts of the Rocky Mountain Foothills and therefore represent an extensive target (Figure 3; Gibson, 1975). Although these sandstones can be high in carbonate cement (up to 15%), they are medium to coarse grained and rich in well-rounded quartz (>80%). The carbonate cement in these rocks would make the disassociation of these rocks easier than the disassociation of quartz-cemented sandstone. Charlie Lake rocks record sabkha environments indicating arid conditions in northeast British Columbia for much of the Triassic. The well-rounded nature of the grains in these rocks is probably, in part, a reflection of aeolian transport. Aeolian deposits are considered highly prospective because abrasion due to wind can be 100–1000 times more effective at rounding grains than transport by water (Kuenen, 1959, 1960). A coastal aeolian environment has been suggested for the St Peter sandstone (Mazzullo and Ehrlich, 1983), which is a major source of frac sand in the United States.

Rocks of the Minnes Group can be traced along the entire length of the outer Rocky Mountain Foothills of British Columbia. These fluvial-deltaic rocks form a westward-thickening package formed as a result of Jura-Cretaceous mountain building, which occurred in response to terrane accretion. The two thickest coarse clastic sequences within the Minnes Group belong to the Monteith and Monach formations (Figure 5). Both units are rich in medium- to coarse-grained quartz sand (>90%) and are typically quartz

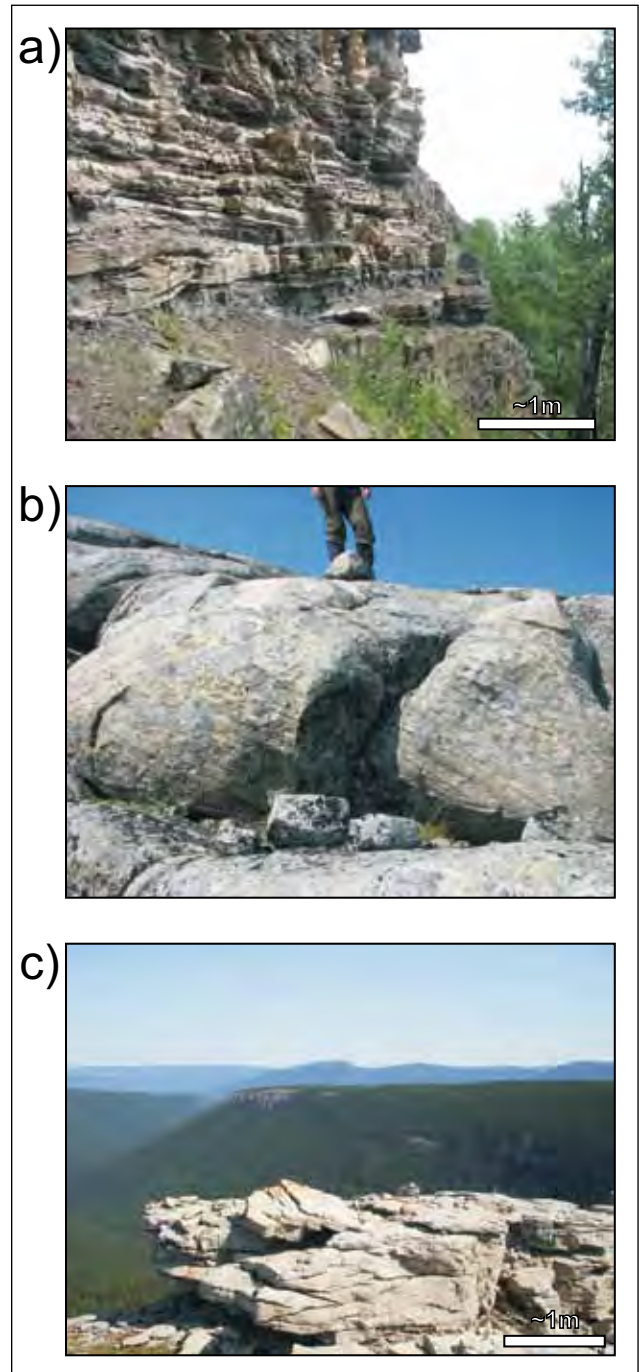


Figure 5. Photographs of the a) Monteith, b) Monach and c) Liard formations from the Halfway River map area (NTS 094B).

TABLE 2. SUMMARY OF PRELIMINARY UNCONSOLIDATED FRAC SAND TARGETS IN NORTHEAST BRITISH COLUMBIA.

| Sample        | General Area                | Areas (Figure 4) | Easting | Northing | NTS Map Sheets | Depositional Origin | Dominant Grain Size | % Silica |
|---------------|-----------------------------|------------------|---------|----------|----------------|---------------------|---------------------|----------|
| ASH080616-01  | Bear Lake                   | 1                | 519588  | 6040819  | 093J/10        | Aeolian             | Fine/Medium Sand    | 85.55    |
| ASH080623-02  | Lower Pine River Dune Field | 2                | 614822  | 6207694  | 094A/03        | Aeolian             | Fine Sand           | 88.49    |
| ASH080711-03  | Kiskatinaw Dune Field       |                  | 686542  | 6140750  | 093P/08        | Aeolian             | Very Fine Sand      | 89.43    |
| ASH080711-01A | Kiskatinaw Dune Field       | 3                | 671684  | 6134020  | 093P/08        | Aeolian             | Fine Sand           | 90.15    |
| ASH080710-03  | Kiskatinaw Dune Field       |                  | 670194  | 6133138  | 093P/08        | Aeolian             | Fine Sand           | 86.34    |
| ASH080923-01  | Redwillow River             | 4                | 685093  | 6099906  | 093P/01        | Glaciofluvial       | Fine Sand           | 88.44    |
| TPAP03-32     | Fort Nelson                 | 5                | 522972  | 6520875  | 094J/15        | Glaciofluvial       | Fine Sand           | 81.10    |
| SUV05302      | Fontas Dune Field           |                  | 621520  | 6456212  | 094I/02        | Aeolian             | Fine Sand           | 91.42    |
| SUV05303      | Fontas Dune Field           | 6                | 621098  | 6456288  | 094I/02        | Aeolian             | Fine Sand           | 90.96    |
| SUV05309      | Fontas Dune Field           |                  | 611404  | 6460199  | 094I/06        | Aeolian             | Fine Sand           | 90.62    |
| TFE0704-01    | KM 176 - SYD                | 7                | 628362  | 6566463  | 094P/02        | Glaciofluvial       | Medium Sand         | 85.01    |
| TFE0704-02    | Lower Komie Road            | 8                | 581274  | 6540078  | 094I/13        | Glaciofluvial       | Medium Sand         | 83.89    |
| TFE0704-03    | Komie                       | 9                | 569040  | 6573180  | 094P/05        | Glaciofluvial       | Medium Sand         | 89.99    |
| TFE0704-04    | Courvoisier Creek           |                  | 574987  | 6560341  | 094P/04        | Glaciofluvial       | Medium Sand         | 87.01    |
| TDE05-04      | Courvoisier Creek           | 10               | 575001  | 6559192  | 094P/04        | Glaciofluvial       | Medium Sand         | 85.97    |
| TFE0711-08    | Horn River                  |                  | 501341  | 6641887  | 094O/15        | Glaciofluvial       | Very Fine Sand/Silt | 80.57    |
| TFE0711-06    | Horn River                  | 11               | 500943  | 6642203  | 094O/15        | Glaciofluvial       | Fine Sand           | 80.41    |

cemented or show compactional welding of grain contacts. The stratigraphically higher Monach Formation tends to contain coarser-grained sandstone with well-rounded grains. Sandstone in this unit also displays higher porosity in surface exposures (up to 15%), which may make mechanical disaggregation easier than Monteith sandstone. The Minnes Group is absent in the north because these units have been eroded at the sub-Cretaceous unconformity. A more thorough description of the Minnes Group and its distribution is given by Stott (1998).

Geologically young deposits are not traditionally considered good sources of frac sand (Zdunczyk, 2007); however, some of the unconsolidated deposits sampled in this study show potential. These are Quaternary deposits that were emplaced during, or shortly after, the glaciation of northeast British Columbia in the Late Wisconsinan (ca. 22 000–10 000 years ago; Mathews 1978, 1980; Clague, 1989; Liverman et al., 1989; Catto et al., 1996; Dyke et al., 2003; Wolfe et al., 2004; Bednarski and Smith, 2007; Bednarski, 2008). The area was affected by three glacial systems: 1) local montane glaciers, 2) the Cordilleran Ice Sheet (CIS) and 3) the continental Laurentide Ice Sheet (LIS). Preliminary evaluation of unconsolidated samples suggests that those associated with the LIS are more likely to host material with favourable properties for use as frac sand than those derived from the CIS or montane glacial deposits.

One of the most prospective landforms is a glaciofluvial delta located in the Komie area (area 9; Figures 4, 6). This feature formed in a shallow proglacial lake (T. Demchuk, pers comm 2009) and has been extensively mapped and evaluated for aggregate potential (Blyth et al., 2003; Dewar and Polysou, 2003; Levson et al., 2004; Demchuk et al., 2005; Ferbey et al., 2005). Although originally targeted as part of gravel resource investigations, volumetrically, much of the granular material encountered is sand. A sample (TFE0704-03) collected from a sandy portion of this feature consists of 89.99% SiO<sub>2</sub>, with 79.38% of the grains falling within the medium-sand-sized fraction. A large proportion of the quartz grains are rounded to well-rounded and have

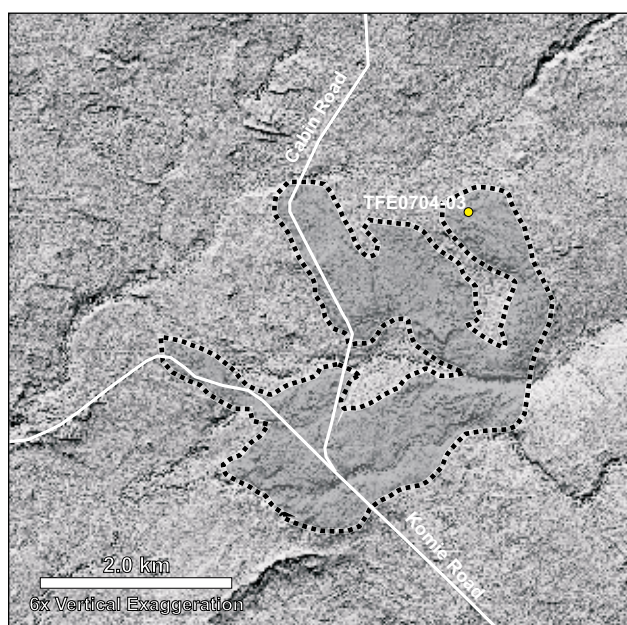


Figure 6. The Komie delta, shown in a high-resolution LiDAR image, consists of a series of incised lobes. Several of the lobes host active gravel mines, while others consist of up to 14 m of sand (location 9 in Figure 4).

moderate to well-developed sphericity. The maturity of the sand in this deposit suggests that despite the glacial origin of the deposit, the sand fraction may have been transported a significant distance or is recycled from older sediments. The deposit is well situated to service the mounting demand for frac sand in the emerging Horn River Basin shale gas play. The feature is located near the intersection of Geetla and Komie roads, providing year-round access to the area.

Another glaciofluvial delta evaluated in this study is situated in the Redwillow River area south of Dawson Creek (area 4; Figure 7). This feature forms a well-defined sand plain that is interpreted to be a delta, subaqueous fan or subaqueous sand plain. The delta was deposited in glacial Lake Peace from sand-laden water flowing from the melt of westerly derived ice (montane or CIS). Sample

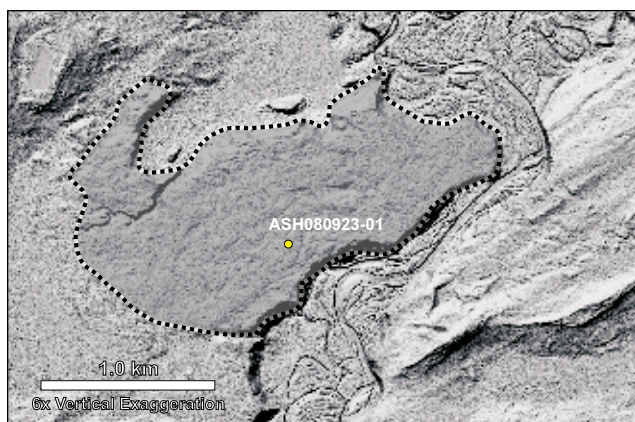


Figure 7. The Redwillow River delta, shown in a high-resolution LiDAR image, forms an extensive plain and consists of up to 10 m of uniform sand (location 4 in Figure 4).

ASH080923-01 is dominated by fine- to medium-grained sand with  $\text{SiO}_2$  content over 88%. A thin section of the sand grains shows that although quartz grains are common, there are abundant polycrystalline quartz grains that are likely chert and fine-grained mudstone with high quartz content. Although the high proportion of lithic fragments reduces the potential of this deposit, the large volume of sand associated with it and the abundance of quartz grains in the smaller size fraction (see Appendix 2) suggest that this deposit may be prospective.

As mentioned earlier, aeolian deposits are considered highly prospective because of grain attrition (which causes the reduction of unstable grains, such as lithic fragments) and enhanced grain rounding (Kuenen, 1959, 1960). The types of grains in an aeolian deposit will be inherited from the types of grains in the source sediments, but will become more mature with distance travelled from the source area. Deposits derived from compositionally mature sediments (high proportion of stable framework grains) will be more prospective, as will deposits that have travelled farther from the source sediment. Four dune fields were sampled in this study, including the Fontas Dune Field (area 6), the Kiskatinaw Dune Field (area 3), the Lower Pine River Dune Field (area 2) and the Bear Lake Dune Field (area 1).

Three samples (SUV05302, SUV05303 and SUV05309) were collected from the Fontas Dune Field near Dazo Creek (area 6; Figures 4, 8–10). Dunes in this field are compound parabolic forms and have been described by Wolfe et al. (2007) and mapped by Trommelen and Smith (2007) and Smith (2009). These dunes formed from glacial outwash and glaciolacustrine sediments associated with distal deposits of the large Hay River fan-delta (Figure 4) described by Levson et al. (2004) and Smith (2009). The delta formed where subglacial drainage and water from glacial Lake Peace incised a spillway channel across the divide north of the Clear Hills in Alberta and emptied into glacial Lake Hay, a proglacial lake of the LIS. It is speculated that the fan-delta sands are derived directly from glacial com-

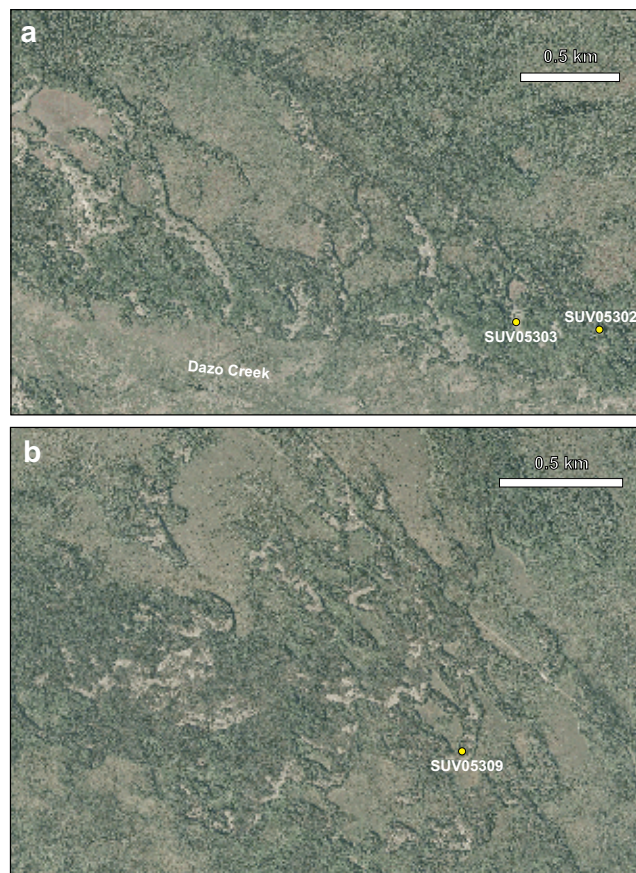


Figure 8. The Fontas Dune Field, shown in a 1:20 000 scale colour orthophoto, consists of several related fields including the north section of the main dune field a) straddling Dazo Creek and b) the northwestern dune field. The dunes are compound parabolic sand dunes derived from sandy glaciolacustrine and glacial outwash sediments (location 6 in Figure 4).

minution and subglacial erosion of Dunvegan Formation sandstone, which may account for its relative maturity. The Hay River fan-delta itself represents an uninvestigated sand source of immense size (~181 km<sup>2</sup>, up to 30 m thick at its apex; Smith, 2009). The dunes are excellent targets for frac sand evaluation because they represent an additional cycle of transport and deposition, thereby extending their maturity. All three samples from the Fontas Dune Field contain over 90%  $\text{SiO}_2$  and the majority of the sand grains fall within the fine-sand-sized fraction. The grains are angular to well-rounded with poor to well-developed sphericity. There is currently no all-season road access to these deposits; however, there is an abundance of seismic cut lines intersecting the deposits and a winter road that crosses the northwesternmost portion of the dune field.

Another aeolian dune field is located south of Dawson Creek in the Kiskatinaw River area (Figure 9). These dunes are highly elongated parabolic dunes that are similar in morphology to the so-called ‘Cree Lake-type’ dunes described by David (1981). The dunes formed from winds blowing from the west to east, transporting sediment from sandy glaciolacustrine deposits associated with an early

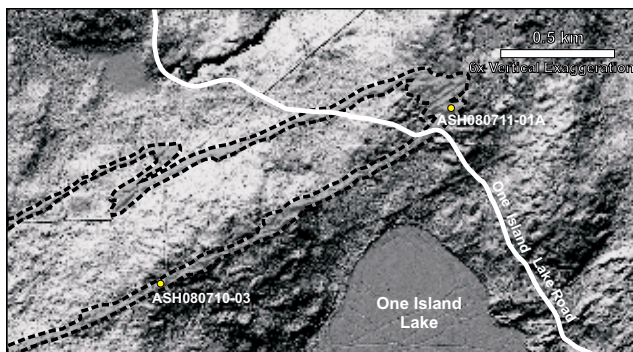


Figure 9. A high-resolution LiDAR image of one of the elongated sand dunes of the Kiskatinaw Dune Field (location 3 in Figure 4).

stage of glacial Lake Peace (Mathews, 1980). Much of the glaciolacustrine sediments are associated with sediments derived from the Rocky Mountains. Samples ASH080710-03, ASH080711-01A and ASH080711-03 contained  $\text{SiO}_2$  proportions of 86.34%, 89.43% and 90.15%, respectively. There is a high proportion of well-rounded monocrystalline quartz in these samples, which indicates that there is potential for these dunes to serve as a frac sand source. Unfortunately, thin sections show that there is an abundance of quartz-rich mudstone fragments and some chert, making these dunes less prospective than those in the Fontas Dune Field. Three other samples from dunes on the proximal side of the field (west; upwind) are not included in this report because their  $\text{SiO}_2$  content is below 80%. This suggests that the distal dunes (east; downwind) have a higher proportion of quartz grains and are therefore more prospective. Regardless, the abundance of lithic fragments in all samples would necessitate extensive processing before this sand could be considered for use as a proppant.

Two other dune fields that were sampled returned relatively poor results. The Lower Pine River Dune Field is approximately 6 km long and consists of well-developed parabolic dunes (Figure 10). These dunes are likely derived from glaciofluvial and glacial diamict (till) sediments associated with the CIS. The dunes formed from valley-parallel winds blowing from southwest to northeast. Despite high  $\text{SiO}_2$  content in sample ASH080623-02 (88.49%), the thin section reveals a large proportion of angular grains, of which quartz-rich mudstone grains make up a significant portion. This deposit, therefore, has only limited prospectivity. The sample was, however, collected from the proximal end of the dune field in a relatively poorly developed dune; therefore, additional sampling downwind of this sample may show more promising results. The dune field at Bear Lake (area 1; Figure 4) also has a relatively high  $\text{SiO}_2$  content (85.55%), but an abundance of lithic fragments and poor rounding and sphericity render this deposit marginal.

Several eskers associated with the LIS show promising results. This is very encouraging as depositional environments associated with glaciofluvial deposits are not generally well suited for frac sands. Eskers form in or under



Figure 10. The Pine River Dune Field, shown in a 1:20 000 scale colour orthophoto, consists of well-developed parabolic dunes (location 2 in Figure 4).

ice where closed-channel hydraulics result in sediments that are typically poorly sorted. Nonetheless, results from samples TFE0704-04 and TDE05-04 (area 10; Figures 4, 11) collected from a sandy portion of an extensive esker complex near the Courvoisier Creek area (the Courvoisier Esker Complex; Ferbey et al., 2005; T. Demchuk, pers comm 2009), indicate well-sorted sand with  $\text{SiO}_2$  values of 87.01% and 85.97%, respectively. Furthermore, despite an abundance of lithic fragments, there is a substantial population of well-rounded, moderately spherical, monocrystalline quartz grains that would be excellent for frac sand. As mentioned earlier, the ability to process out the undesirable grains will be critical in determining the suitability and economics of these deposits. Other eskers were sampled (TFE0704-01, area 7; TFE0704-02, area 8; and TFE0711-06 and TFE0711-08, area 11). All of these glaciofluvial features have a high proportion of well-rounded grains with moderate to well-developed sphericity, and warrant additional evaluation. Ongoing aggregate mapping in northeast British Columbia is showing that sediments associated with subglacial deposits (e.g., eskers) are more likely to host sand-sized material than gravel-sized material. Given the promising results discussed here and the abundance of eskers near the Horn River Basin, these features may represent a local frac sand exploration target.

Sample TPAP03-32 is from a sand-dominated glaciofluvial deposit (likely subglacial) located at the Fort Nelson Airport. The deposit was tested during a detailed granular aggregate assessment conducted by BCMEMPR for the Northern Rockies Regional District (Ferbey et al.,

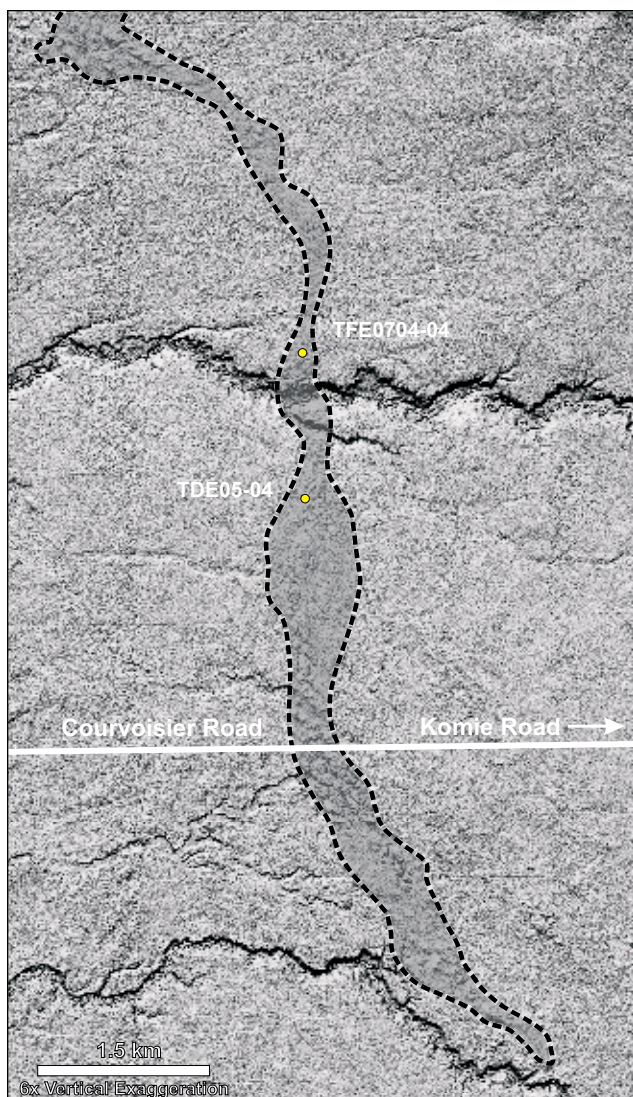


Figure 11. Courvoisier Ridge, a long esker complex that hosts sand and gravel, is outlined from high-resolution LiDAR imagery (location 10 in Figure 4).

2004; Johnsen et al., 2004). This deposit consists entirely of moderately sorted fine-grained sand that contains 81.1%  $\text{SiO}_2$ . There are abundant lithic grains, but a population of well-rounded, monocrystalline quartz grains dominates. With processing, this deposit may also have the potential to be a frac sand source.

## CONCLUSION

Preliminary evaluation of bedrock units suggests the Liard and Charlie Lake formations (Triassic) and the Monteith and Monach formations of the Minnes Group (Late Jurassic to Cretaceous) are the most encouraging bedrock units for a potential frac sand source in northeast British Columbia. The Liard Formation is a quartz arenite that contains 90% quartz grains in carbonate cement. The Charlie Lake Formation is a feldspathic arenite with well-rounded grains, also in carbonate cement. These units are present throughout the Rocky Mountain Foothills from Williston Lake north to the Liard River. The Monteith and Monach formations of the Minnes Group are classified as quartz arenite and consist of more than 95% quartz grains. The Minnes Group is present in the foothills south of the Profit River on the eastern edge of the deformed belt.

The unconsolidated deposits that are most prospective are associated with three depositional environments: deltaic, aeolian and glaciofluvial. In the Komie area, a glaciofluvial delta consists of sand and gravel. A sample from this feature mainly consists of well-rounded, well-sorted, medium-grained quartz sand. The deposit is located on the western rim of the Horn River Basin and is an excellent target for further evaluation. Another deltaic feature of interest occurs in the Redwillow River valley. This large sandy glaciofluvial delta has a significant proportion of lithic fragments, but does contain an abundance of quartz grains in the finer sand-sized fraction; therefore, is a potential frac sand exploration target.

Another highly prospective target is the Fontas Dune Field near Dazo Creek. This dune field includes three distinct subfields consisting of either parabolic or compound parabolic sand dunes. Three samples from different dunes contain mostly monocrystalline fine-sand quartz grains. Other dunes were investigated from the Kiskatinaw and Pine River dune fields, but abundant lithic grains make these fields less prospective.

Several eskers associated with the LIS are prospective. The Courvoisier Esker Complex consists of sand and gravel, with portions hosting well-sorted, medium-grained sand with a population of well-rounded, moderately spherical quartz grains. Several other eskers in the Horn River Basin and around KM 176 – SYD Road also show encouraging results. Although lithic fragments are common in these deposits, abundant, well-rounded quartz grains make LIS eskers a target for evaluation.

## ACKNOWLEDGMENTS

We acknowledge the excellent work of the many geologists, field assistants and students that have participated in the Surficial Geology and Aggregate Mapping Program and the bedrock mapping program. We thank EnCana Corporation, ConocoPhillips and EOG Resources for providing LiDAR data and field logistics. Acme Laboratories (Vancouver, British Columbia) conducted the major oxide geochemical analyses and Vancouver Petrographics produced the thin sections. This project has benefitted from the excellent collaborative relationship established between the Geological Survey of Canada and BCMEMPR. The authors would like to thank Tania Demchuk for providing samples from the Komie and Courvoisier deposits and data from her M.Sc. research currently in progress.

## REFERENCES

- Adams, C., McPhail, S. and Walsh, W. (2008): Summary of shale gas activity in northeast British Columbia 2007; *BC Ministry of Energy, Mines and Petroleum Resources*, Petroleum Geology Open File 2007-1, 10 pages.
- Alberta Geological Survey (1989): Frac sand evaluation Peace River silica sand deposit final report; *Alberta Research Council*, Open File Report 1998-08, 105 pages.
- American Petroleum Institute (1995a): Recommended practices for testing sand used in hydraulic fracturing operations; *American Petroleum Institute*, API RP 56, 12 pages.
- American Petroleum Institute (1995b): Recommended practices for testing high-strength proppants used in hydraulic fracturing operations; *American Petroleum Institute*, API RP 60, 14 pages.
- Bednarski, J.M. (2008): Landform assemblages produced by the Laurentide Ice Sheet in northeastern British Columbia and adjacent Northwest Territories – constraints on glacial lakes and patterns of ice retreat; *Canadian Journal of Earth Sciences*, Volume 45, Number 5, pages 593–610.
- Bednarski, J.M. and Smith, I.R. (2007): Laurentide and montane glaciation along the Rocky Mountain Foothills of northeastern British Columbia; *Canadian Journal of Earth Sciences*, Volume 44, Number 4, pages 445–457.
- Blyth, H., Levson, V.M. and Savinkoff, P. (2003): Sierra-Yoyo-Desan aggregate potential mapping; *BC Ministry of Energy, Mines and Petroleum Resources*, 14 maps at 1:50 000 scale.
- Catto, N., Liverman, D.G.E., Bobrowsky, P.T. and Rutter, N. (1996): Laurentide, Cordilleran, and montane glaciations in the western Peace River – Grande Prairie region, Alberta and British Columbia, Canada; *Quaternary International*, Volume 32, pages 21–32.
- Clague, J.J. (1989): Quaternary geology of the Canadian Cordillera, Chapter 1; in *Quaternary Geology of Canada and Greenland*, Fulton, R.J., Editor, *Geological Survey of Canada*, pages 17–96.
- David, D.P. (1981): Stabilized dune ridges in northern Saskatchewan; *Canadian Journal of Earth Sciences*, Volume 18, pages 286–310.
- Demchuk, T.E., Ferbey, T., Kerr, B.J. and Levson, V.M. (2005): Surficial geology and aggregate potential mapping in northeast British Columbia using LiDAR imagery; in *Summary of Activities 2005, BC Ministry of Energy, Mines and Petroleum Resources*, pages 51–59.
- Dewer, D. and Polysou, N. (2003): Area 10 (Kotcho East) gravel investigation — Sierra-Yoyo-Desan Road area, north eastern British Columbia; *AMEC Earth and Environmental Limited*, Report Number KX04335, 13 pages.
- Dott, R.H., Jr. (1964) Wacke, graywacke, and matrix: what approach to immature sandstone classification; *Journal of Sedimentary Petrology*, Volume 34, pages 625–632.
- Dumont, M. (2007): Silica/quartz; in *Canadian Mineral Yearbook*, Godin, E., Editor, *Natural Resources Canada*, pages 47.1–47.12.
- Dyke, A.S., Moore, A. and Robertson, L. (2003): Deglaciation of North America; *Geological Survey of Canada*, Open File 1574, CD-ROM.
- Ferbey, T., Hickin, A.S., Demchuk, T.E. and Levson, V.M. (2005): Northeast British Columbia aggregate mapping program: a summary of selected aggregate occurrences northeast of Fort Nelson; in *Summary of Activities 2005, BC Ministry of Energy, Mines and Petroleum Resources*, pages 65–74.
- Ferbey, T., Levson, V.M. and Johnsen, T. (2004): Preliminary report on aggregate potential investigation of Fort Nelson airport area, Fort Nelson, British Columbia; *BC Ministry of Energy, Mines, and Petroleum Resources*, 41 pages.
- Ferri, F. (2009): Geology of the Jones Peak area (NTS 94B/02 and 07), Halfway River map sheet (94B); in *Geoscience Reports 2009, BC Ministry of Energy, Mines and Petroleum Resources*, pages 5–23.
- Gibson, D.W. (1975): Triassic rocks of the Rocky Mountain foothills and front ranges of northeastern British Columbia and west-central Alberta; *Geological Survey of Canada*, Bulletin 247, 61 pages.
- Holland, S.S. (1976): Landforms of British Columbia, a physiographic outline; *BC Department of Mines and Petroleum Resources*, Bulletin 48, 138 pages.
- International Organization for Standards (2006): Petroleum and natural gas industries – completion fluids and materials – part 2: measurement of properties of proppants used in hydraulic fracturing and gravel-packing operations; *International Organization for Standards*, Report Number ISO 13503-2, 28 pages.
- Johnsen, T., Ferbey, T., Levson, V.M. and Kerr, B. (2004): Quaternary geology and aggregate potential of the Fort Nelson airport area; in *Summary of Activities 2004, BC Ministry of Energy, Mines and Petroleum Resources*, pages 19–27.
- Kerr, B. (2009): Looking to the future: development in the Horn River Basin; in *Unconventional Gas Technical Forum 2009 presentations*; *BC Ministry of Energy, Mines and Petroleum Resources*, Petroleum Geology Information Circular 2009-02.
- Kuenen, P.H. (1959): Experimental abrasion, part 3: fluvialite action on sand; *American Journal of Science*, Volume 257, pages 172–190.

- Kuenen, P.H. (1960): Experimental abrasion, part 4: eolian action; *Journal of Geology*, Volume 68, pages 427–449.
- Levson, V.M., Ferbey, T., Kerr, B., Johnsen, T., Bednarski, J., Smith, I.R., Blackwell, J. and Jonnes, S. (2004): Quaternary geology and aggregate mapping in northeast British Columbia: applications for oil and gas exploration and development; in Summary of Activities 2004, *BC Ministry of Energy, Mines and Petroleum Resources*; pages 29–40.
- Liverman, D.G.E., Catto, N.R. and Rutter, N.W. (1989): Laurentide glaciation in west-central Alberta: a single (Late Wisconsinan) event; *Canadian Journal of Earth Sciences*, Volume 26, Number 2, pages 266–274.
- Massey, N.W.D., MacIntyre, D.G., Desjardins, P.J. and Cooney, R.T., (2005): Digital geology map of British Columbia, *BC Ministry of Energy, Mines and Petroleum Resources*, Open File 2005-2, DVD.
- Mathews, W.H. (1978): Quaternary stratigraphy and geomorphology of Charlie Lake (94A) map-area, British Columbia; *Geological Survey of Canada*, Paper 76-20, 25 pages.
- Mathews, W.H. (1980): Retreat of the last ice sheets in northern British Columbia and adjacent Alberta; *Geological Survey of Canada*, Bulletin 331, 33 pages.
- Mazzullo, J.M. and Ehrlich, R. (1983): Grain shape variations in the St. Peter sandstone: a record of eolian and fluvial sedimentation of early Paleozoic cratonic sheet sand; *Journal of Sedimentary Research*, Volume 53, pages 105–119.
- Smith, I.R. (2009): Surficial geology, Kahntah River, British Columbia; Geological Survey of Canada, Open File 5540, *BC Ministry of Energy, Mines and Petroleum Resources*, Surficial Geology Map 2009-5, scale 1:100 000.
- Stott, D.F. (1998): Fernie Formation and Minnes Group (Jurassic and lowermost Cretaceous), northern Rocky Mountain Foothills, Alberta and British Columbia; *Geological Survey of Canada*, Bulletin 516, 516 pages.
- Trommelen, M. and Smith, I.R. (2007): Surficial geology, Dazo Creek, British Columbia; *Geological Survey of Canada*, Open File 5527 and *BC Ministry of Energy, Mines and Petroleum Resources*, Surficial Geology Map 2007-1, scale 1:100 000.
- Wentworth, C.K. (1922): A scale of grade and class terms for clastic sediments; *Journal of Geology*, Volume 30, pages 377–392.
- Williams, D.F., Turner, F.J. and Gilbert, C.M. (1982): Petrography, 2nd Edition; *W.H. Freeman*, San Francisco, 626 pages.
- Wolfe, S.A., Huntley, D.J. and Ollerhead, J. (2004): Relict Late Wisconsinan Dune Fields of the northern Great Plains, Canada; *Géographie physique et Quaternaire*, Volume 58, Number 2–3, pages 9019–9032.
- Wolfe, S.A., Paulen, R.C., Smith, I.R. and Lamothe, M. (2007): Age and paleoenvironmental significance of Late Wisconsinan Dune Fields in the Mount Watt and Fontas River map areas, northern Alberta and British Columbia; *Geological Survey of Canada*, Current Research 2007-B4, 10 pages.
- Zdunczyk, M. (2007): The facts of frac; *Industrial Minerals*, January 2007, pages 58–61.



**APPENDIX ONE - BEDROCK SAMPLES**

|                 |          |
|-----------------|----------|
| <b>Sample</b>   | 08DFM063 |
| <b>Easting</b>  | 519797   |
| <b>Northing</b> | 6222783  |

|                  |                    |
|------------------|--------------------|
| <b>Group</b>     | Minnes Group       |
| <b>Formation</b> | Monteith Formation |
| <b>Age</b>       | Early Cretaceous   |

|                 |     |
|-----------------|-----|
| <b>% Matrix</b> | <5  |
| <b>% Grains</b> | >95 |

|                       |
|-----------------------|
| <b>Classification</b> |
| Quartz Arenite        |

**Comment:**  
Medium to coarse grained sandstone.  
Sub-angular.  
Quartz cement.  
Lithics consist of chert, polycrystalline quartz and hornblende.

|                   |    |
|-------------------|----|
| <b>% Quartz</b>   | 95 |
| <b>% Feldspar</b> | 0  |
| <b>% Lithic</b>   | 5  |

|               |
|---------------|
| <b>Origin</b> |
| Deltaic       |



Plane Light



Crossed Nicols

|                 |          |
|-----------------|----------|
| <b>Sample</b>   | 08FFE125 |
| <b>Easting</b>  | 521738   |
| <b>Northing</b> | 6224224  |

|                  |                                   |
|------------------|-----------------------------------|
| <b>Group</b>     | Minnes Group                      |
| <b>Formation</b> | Monteith Formation                |
| <b>Age</b>       | Late Jurassic to Early Cretaceous |

|                 |    |
|-----------------|----|
| <b>% Matrix</b> | 5  |
| <b>% Grains</b> | 95 |

|                       |
|-----------------------|
| <b>Classification</b> |
| Quartz Arenite        |

**Comment:**

Fine grained sandstone. Relatively uniform grain size distribution.  
 Sub-angular to sub-rounded grains.  
 Lithics are chert, siltstone, carbonate and polycrystalline quartz.  
 Matrix consists of quartz overgrowths and fine opaques.

|                   |    |
|-------------------|----|
| <b>% Quartz</b>   | 95 |
| <b>% Feldspar</b> | 0  |
| <b>% Lithic</b>   | 5  |

|               |
|---------------|
| <b>Origin</b> |
| Deltaic       |



Plane Light



Crossed Nicols

|                 |           |
|-----------------|-----------|
| <b>Sample</b>   | 08FFE220A |
| <b>Easting</b>  | 527687    |
| <b>Northing</b> | 6231355   |

|                  |                  |
|------------------|------------------|
| <b>Group</b>     | Minnes Group     |
| <b>Formation</b> | Monach Formation |
| <b>Age</b>       | Early Cretaceous |

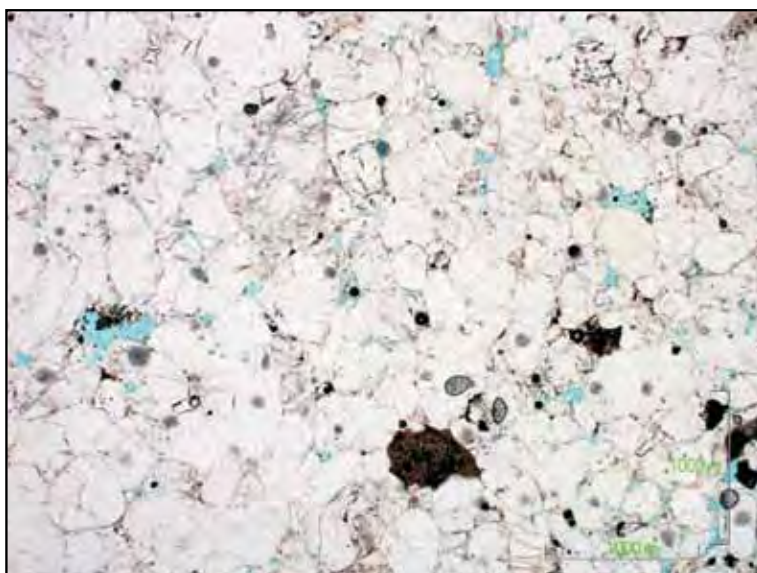
|                 |    |
|-----------------|----|
| <b>% Matrix</b> | <2 |
| <b>% Grains</b> | 98 |

|                       |
|-----------------------|
| <b>Classification</b> |
| Quartz Arenite        |

**Comment:**  
 Medium to coarse grained sandstone.  
 Spherical, sub-rounded to rounded.  
 Very little matrix, quartz plus opaques.  
 Lithics consist of chert and polycrystalline quartz.

|                   |    |
|-------------------|----|
| <b>% Quartz</b>   | 95 |
| <b>% Feldspar</b> | 0  |
| <b>% Lithic</b>   | 5  |

|               |
|---------------|
| <b>Origin</b> |
| Deltaic       |



Plane Light



Crossed Nicols

|                 |           |
|-----------------|-----------|
| <b>Sample</b>   | 08FFE205A |
| <b>Easting</b>  | 526315    |
| <b>Northing</b> | 6236536   |

|                  |                  |
|------------------|------------------|
| <b>Group</b>     | Minnes Group     |
| <b>Formation</b> | Monach Formation |
| <b>Age</b>       | Early Cretaceous |

|                 |    |
|-----------------|----|
| <b>% Matrix</b> | <2 |
| <b>% Grains</b> | 98 |

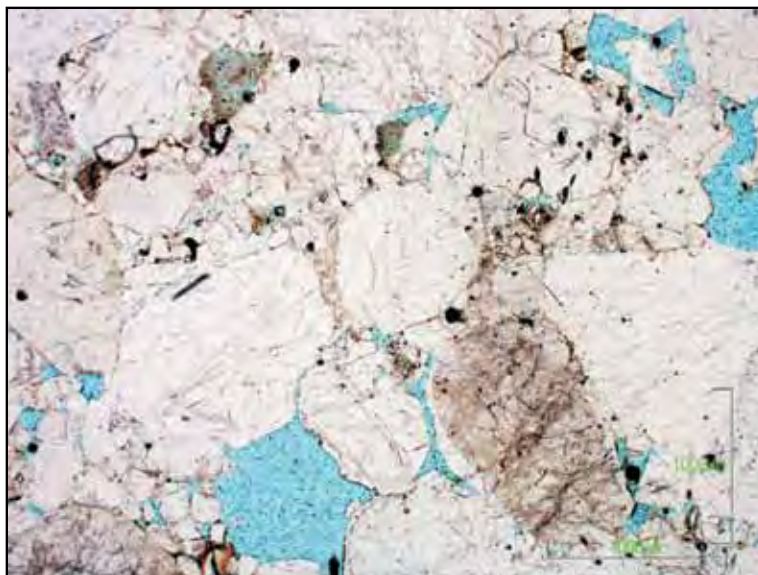
|                       |                |
|-----------------------|----------------|
| <b>Classification</b> | Quartz Arenite |
|-----------------------|----------------|

|                   |    |
|-------------------|----|
| <b>% Quartz</b>   | 95 |
| <b>% Feldspar</b> | 0  |
| <b>% Lithic</b>   | 5  |

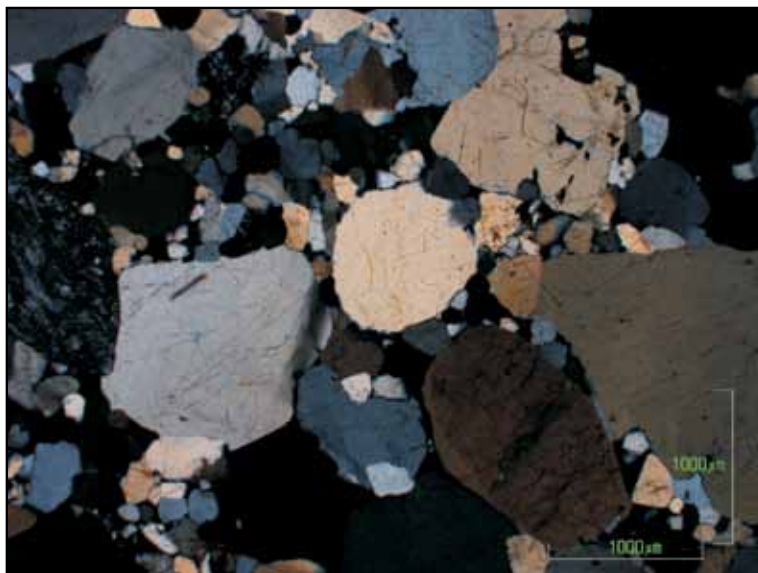
|               |         |
|---------------|---------|
| <b>Origin</b> | Deltaic |
|---------------|---------|

**Comment:**

Bimodal size distribution consisting of coarse to granule conglomerate with matrix of fine to coarse sandstone. Spherical and rounded grains (60 to 70%) with sub-rounded matrix (30-40%). Lithics are chert and polycrystalline quartz. 5-10% porosity.



Plane Light



Crossed Nicols

|                 |           |                  |                        |
|-----------------|-----------|------------------|------------------------|
| <b>Sample</b>   | 08FFE021B | <b>Group</b>     |                        |
| <b>Easting</b>  | 510894    | <b>Formation</b> | Charlie Lake Formation |
| <b>Northing</b> | 6217773   | <b>Age</b>       | Late Triassic          |

|                 |    |
|-----------------|----|
| <b>% Matrix</b> | <1 |
| <b>% Grains</b> | 99 |

|                       |
|-----------------------|
| <b>Classification</b> |
| Feldspathic Arenite   |

**Comment:**

Fine to medium sandstone. Relatively good grain size distribution. Clasts are oblate to spherical, well- to sub-rounded. Lithic fragments include chert, siltstone and calcite. Cement is calcite.

|                   |    |
|-------------------|----|
| <b>% Quartz</b>   | 80 |
| <b>% Feldspar</b> | 15 |
| <b>% Lithic</b>   | 5  |

|                     |
|---------------------|
| <b>Origin</b>       |
| Intertidal (Marine) |



Plane Light



Crossed Nicols

|                 |          |
|-----------------|----------|
| <b>Sample</b>   | 08FFE309 |
| <b>Easting</b>  | 522190   |
| <b>Northing</b> | 6235343  |

|                  |                         |
|------------------|-------------------------|
| <b>Group</b>     |                         |
| <b>Formation</b> | Liard Formation         |
| <b>Age</b>       | Middle to Late Triassic |

|                 |    |
|-----------------|----|
| <b>% Matrix</b> | <1 |
| <b>% Grains</b> | 99 |

|                       |
|-----------------------|
| <b>Classification</b> |
| Quartz Arenite        |

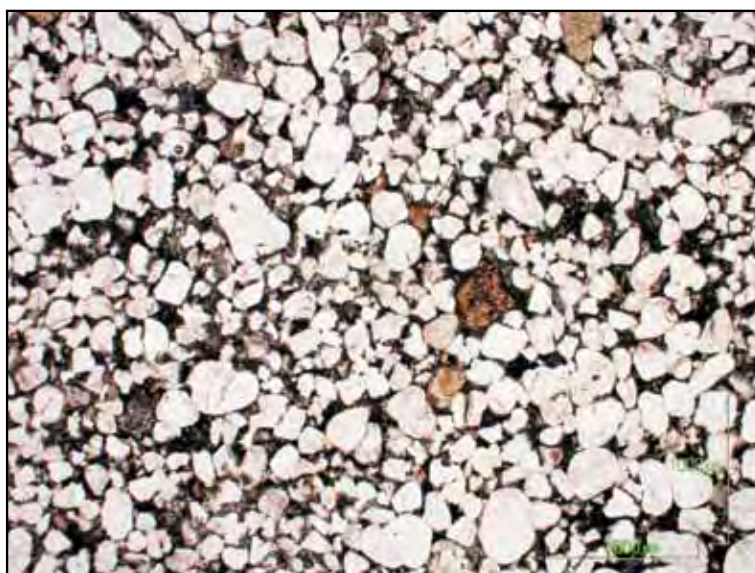
**Comment:**

Fine to medium grained sandstone. Larger grains are well rounded and spherical whereas smaller grains tend to blade or tabular shapes and are sub-rounded to sub-angular.

|                   |    |
|-------------------|----|
| <b>% Quartz</b>   | 90 |
| <b>% Feldspar</b> | 5  |
| <b>% Lithic</b>   | 5  |

|               |
|---------------|
| <b>Origin</b> |
| Shoreface     |

Grains size can range down to silt size within matrix areas and these grains are quite angular. Lithics are chert (brown and clear), platy poly crystalline quartz, hornblende, calcite. Cement is calcite



Plane Light



Crossed Nicols

|                 |          |                  |                         |
|-----------------|----------|------------------|-------------------------|
| <b>Sample</b>   | 08FFE114 | <b>Group</b>     |                         |
| <b>Easting</b>  | 507488   | <b>Formation</b> | Liard Formation         |
| <b>Northing</b> | 6221073  | <b>Age</b>       | Middle to Late Triassic |

|                 |    |
|-----------------|----|
| <b>% Matrix</b> | <1 |
| <b>% Grains</b> | 99 |

|                       |
|-----------------------|
| <b>Classification</b> |
| Quartz Arenite        |

**Comment:**

Fine to medium grained sandstone. Fairly uniform grain size distribution. Some coarser grains. Sub-rounded to sub-angular and spherical grains, larger grains tend to be well rounded. Lithics include chert, siltstone, hornblende, calcite and fossil material. Cement is calcite.

|                   |    |
|-------------------|----|
| <b>% Quartz</b>   | 90 |
| <b>% Feldspar</b> | 2  |
| <b>% Lithic</b>   | 8  |

|               |
|---------------|
| <b>Origin</b> |
| Shoreface     |



Plane Light



Crossed Nicols

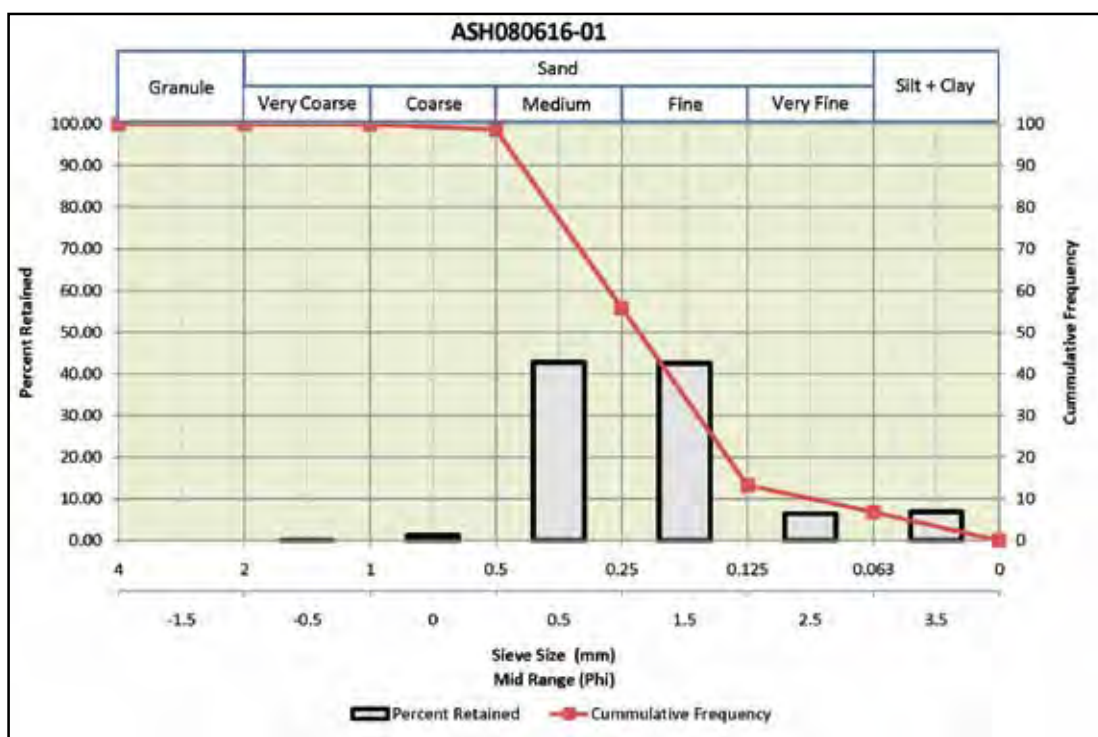
**APPENDIX TWO - UNCONSOLIDATED SAMPLES**

|                       |              |
|-----------------------|--------------|
| <b>Sample</b>         | ASH080616-01 |
| <b>Easting</b>        | 519588       |
| <b>Northing</b>       | 6040819      |
| <b>Genetic Origin</b> | Aeolian Dune |



**Comment:**

This sample was collected from an excavation in an aeolian sand dune along Highway 97 near Bear Lake, British Columbia, west of the Rocky Mountains.

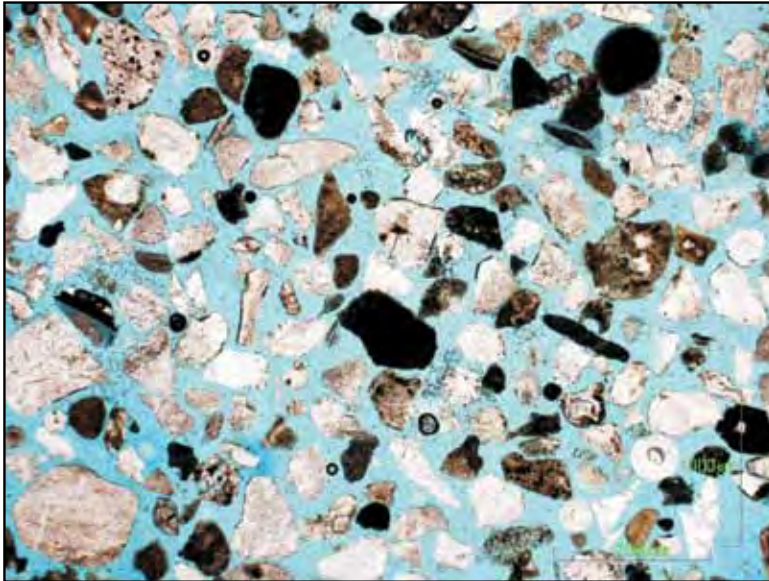


| Sieve Size | Mass  | Percent Retained | Cumulative Frequency |
|------------|-------|------------------|----------------------|
| 4.0        | 0.0   | 0.00             | 100.00               |
| 2.0        | 0.0   | 0.00             | 100.00               |
| 1.0        | 0.4   | 0.08             | 99.92                |
| 0.500      | 6.4   | 1.23             | 98.69                |
| 0.250      | 222.2 | 42.84            | 55.85                |
| 0.125      | 220.8 | 42.57            | 13.28                |
| 0.063      | 33.4  | 6.44             | 6.84                 |
| <0.063     | 35.5  | 6.84             | 0.00                 |

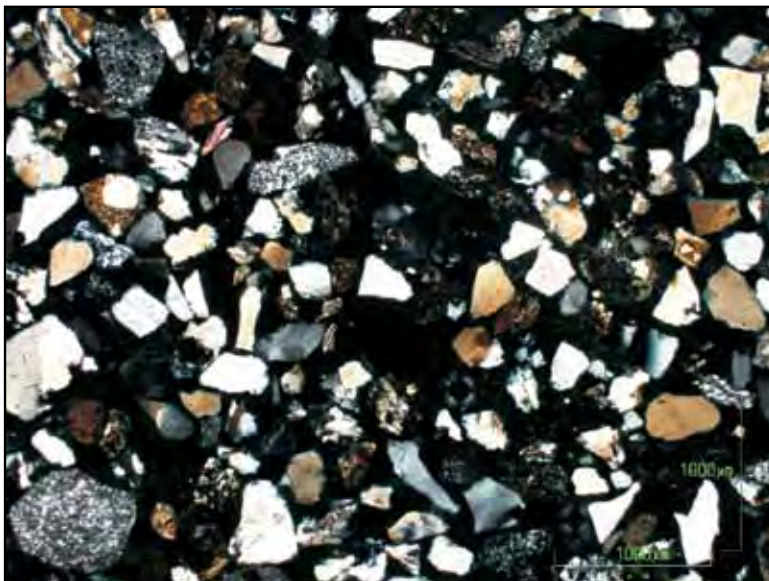
| Element                        | Percent |
|--------------------------------|---------|
| SiO <sub>2</sub>               | 85.55   |
| Al <sub>2</sub> O <sub>3</sub> | 6.02    |
| Fe <sub>2</sub> O <sub>3</sub> | 2.66    |
| MgO                            | 0.77    |
| CaO                            | 0.77    |
| Na <sub>2</sub> O              | 1.17    |
| K <sub>2</sub> O               | 1.17    |
| TiO <sub>2</sub>               | 0.34    |
| P <sub>2</sub> O <sub>5</sub>  | 0.09    |
| MnO                            | 0.04    |
| Cr <sub>2</sub> O <sub>3</sub> | 0.013   |
| LOI                            | 1.3     |



Binocular Microscope



Plane Light



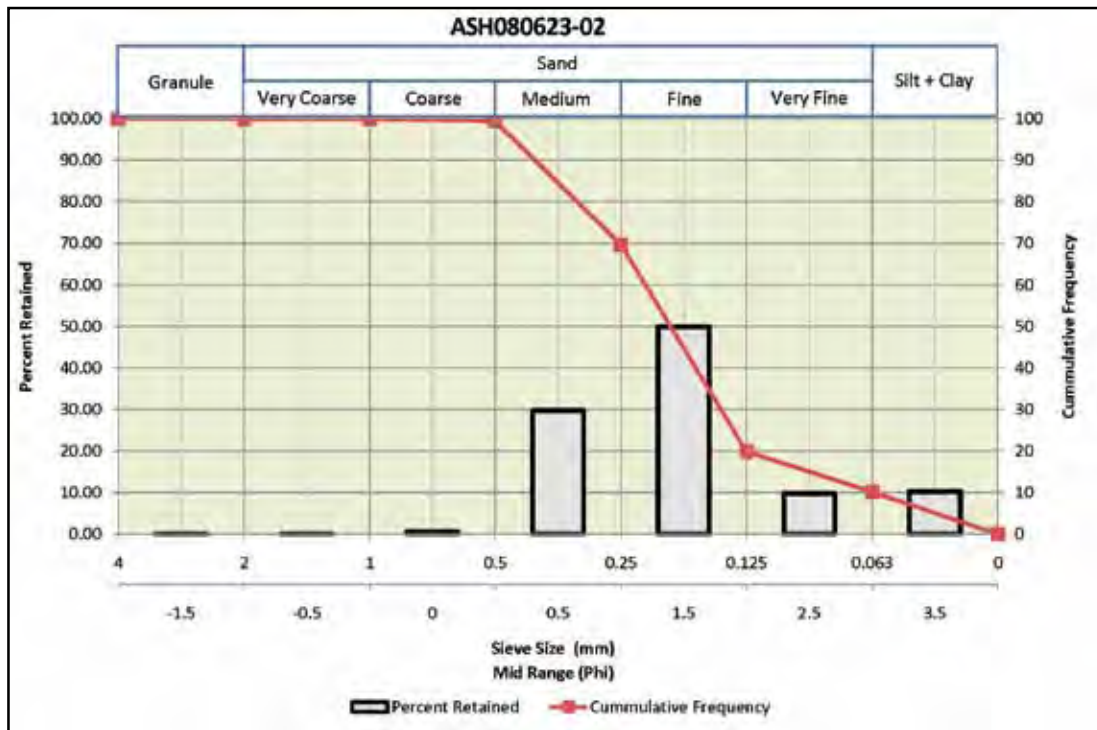
Crossed Nicols

|                       |               |
|-----------------------|---------------|
| <b>Sample</b>         | ASH080623-02  |
| <b>Easting</b>        | 614822        |
| <b>Northing</b>       | 6207694       |
| <b>Genetic Origin</b> | Aeolian Dunes |



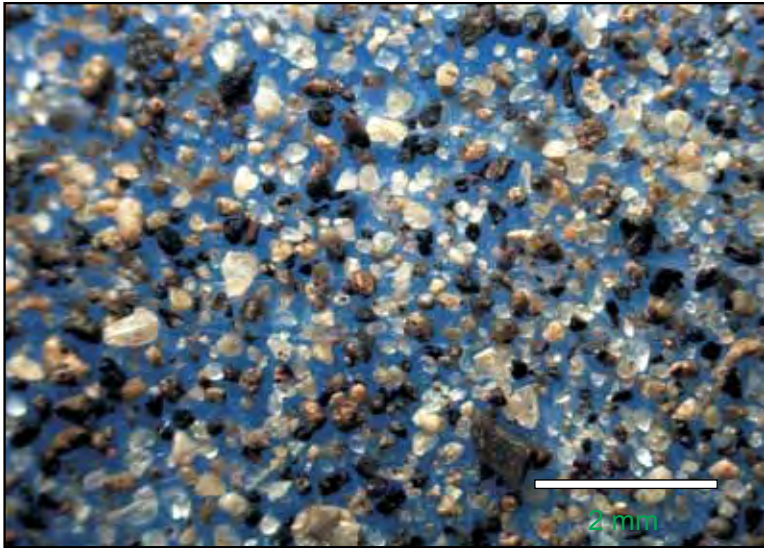
**Comment:**

Sample was collected from well-developed parabolic sand dunes on a terrace of the lower Pine River. Dunes are up to 10 metres high, several hundred metres long, and are derived from glaciofluvial outwash and glacial Lake Peace sediments.

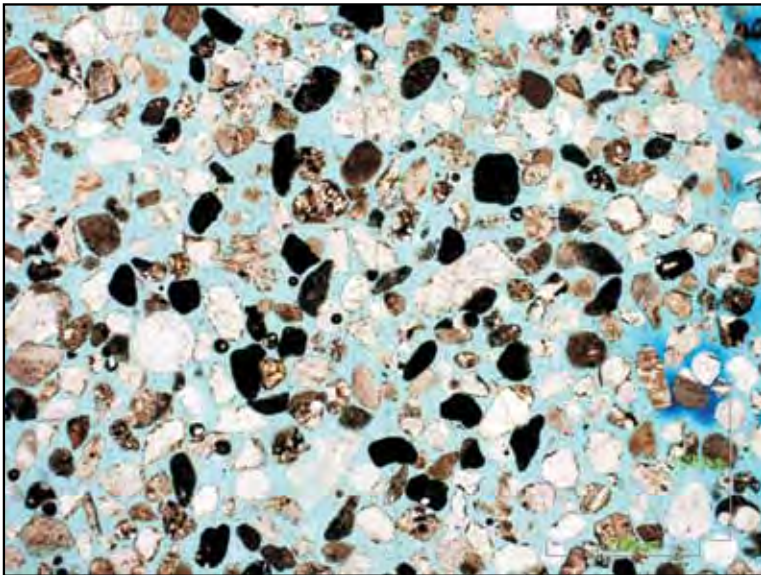


| Sieve Size | Mass  | Percent Retained | Cumulative Frequency |
|------------|-------|------------------|----------------------|
| 4.0        | 0.0   | 0.00             | 100.00               |
| 2.0        | 0.1   | 0.02             | 99.98                |
| 1.0        | 0.2   | 0.04             | 99.94                |
| 0.500      | 2.4   | 0.51             | 99.43                |
| 0.250      | 139.4 | 29.68            | 69.74                |
| 0.125      | 234.0 | 49.83            | 19.91                |
| 0.063      | 45.7  | 9.73             | 10.18                |
| <0.063     | 47.8  | 10.18            | 0.00                 |

| Element                        | Percent |
|--------------------------------|---------|
| SiO <sub>2</sub>               | 88.49   |
| Al <sub>2</sub> O <sub>3</sub> | 3.61    |
| Fe <sub>2</sub> O <sub>3</sub> | 3.18    |
| MgO                            | 0.33    |
| CaO                            | 0.67    |
| Na <sub>2</sub> O              | 0.17    |
| K <sub>2</sub> O               | 0.74    |
| TiO <sub>2</sub>               | 0.20    |
| P <sub>2</sub> O <sub>5</sub>  | 0.19    |
| MnO                            | 0.03    |
| Cr <sub>2</sub> O <sub>3</sub> | 0.005   |
| LOI                            | 2.3     |



Binocular Microscope



Plane Light



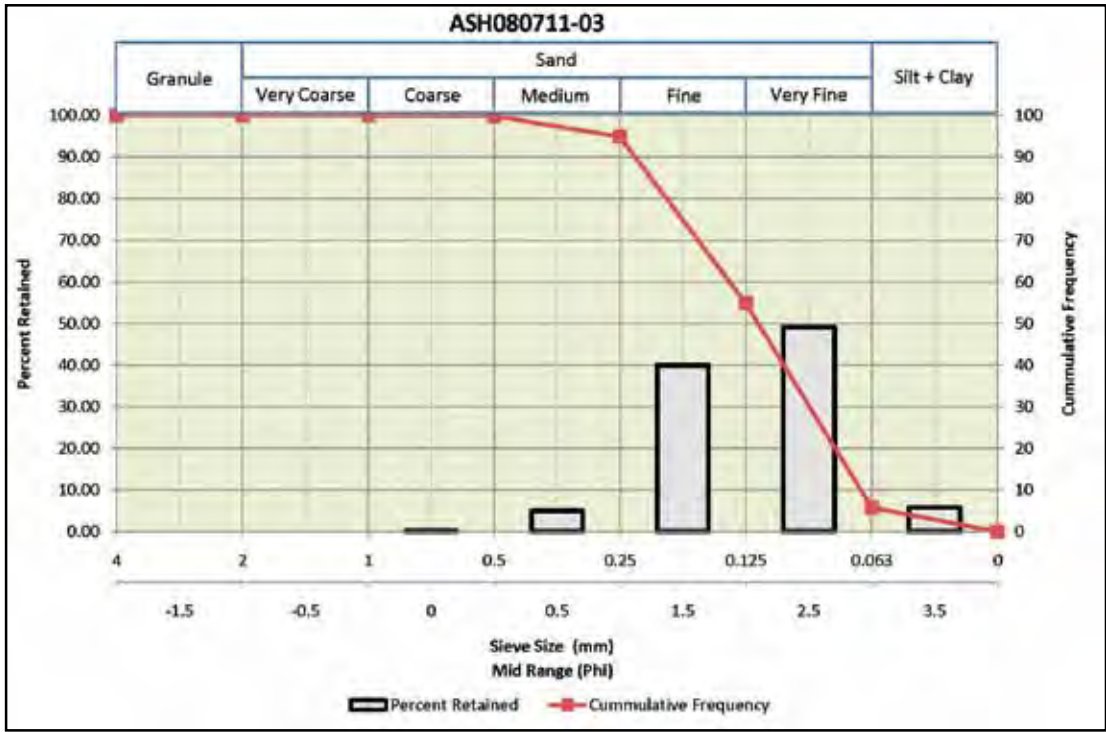
Crossed Nicols

|                       |              |
|-----------------------|--------------|
| <b>Sample</b>         | ASH080711-03 |
| <b>Easting</b>        | 686542       |
| <b>Northing</b>       | 6140750      |
| <b>Genetic Origin</b> | Aeolian Dune |



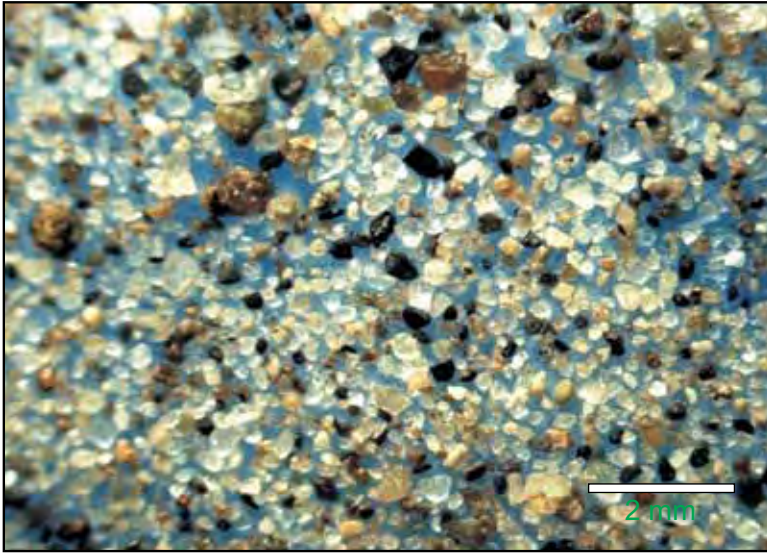
**Comment:**

Sample was taken from the arm of a elongate parabolic sand dune on the distal side (east; downwind) of the Kiskatinaw Dune Field south of Dawson Creek.

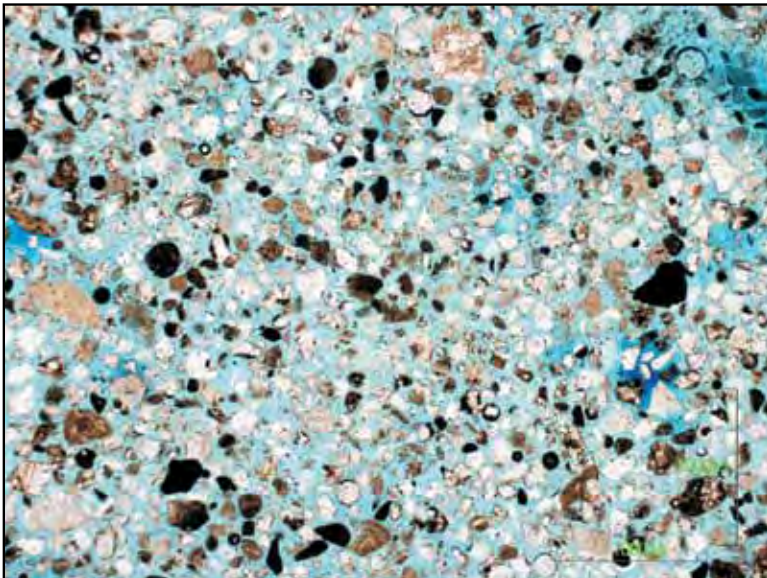


| Sieve Size | Mass  | Percent Retained | Cummulative Frequency |
|------------|-------|------------------|-----------------------|
| 4.0        | 0.0   | 0.00             | 100.00                |
| 2.0        | 0.0   | 0.00             | 100.00                |
| 1.0        | 0.0   | 0.00             | 100.00                |
| 0.500      | 0.6   | 0.14             | 99.86                 |
| 0.250      | 20.9  | 4.97             | 94.89                 |
| 0.125      | 168.2 | 39.96            | 54.93                 |
| 0.063      | 206.8 | 49.13            | 5.80                  |
| <0.063     | 24.4  | 5.80             | 0.00                  |

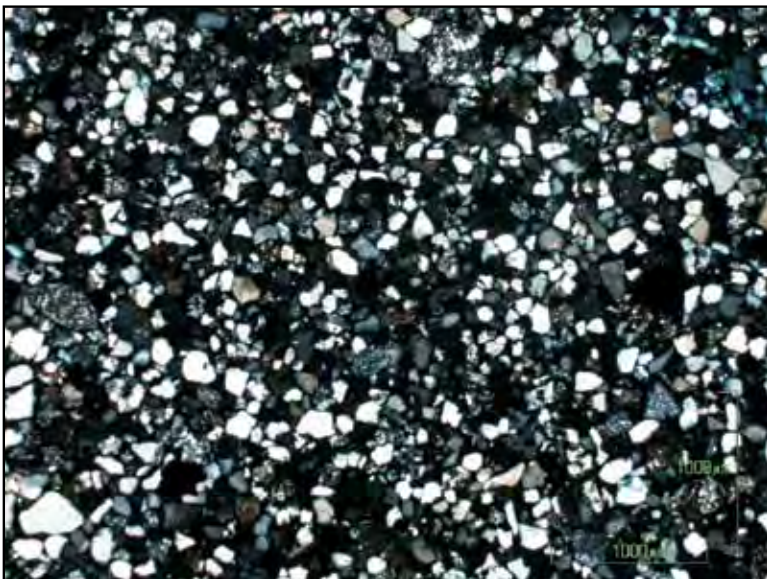
| Element                        | Percent |
|--------------------------------|---------|
| SiO <sub>2</sub>               | 89.43   |
| Al <sub>2</sub> O <sub>3</sub> | 4.23    |
| Fe <sub>2</sub> O <sub>3</sub> | 2.22    |
| MgO                            | 0.28    |
| CaO                            | 0.35    |
| Na <sub>2</sub> O              | 0.59    |
| K <sub>2</sub> O               | 0.90    |
| TiO <sub>2</sub>               | 0.19    |
| P <sub>2</sub> O <sub>5</sub>  | 0.14    |
| MnO                            | 0.02    |
| Cr <sub>2</sub> O <sub>3</sub> | 0.005   |
| LOI                            | 1.5     |



Binocular Microscope



Plane Light



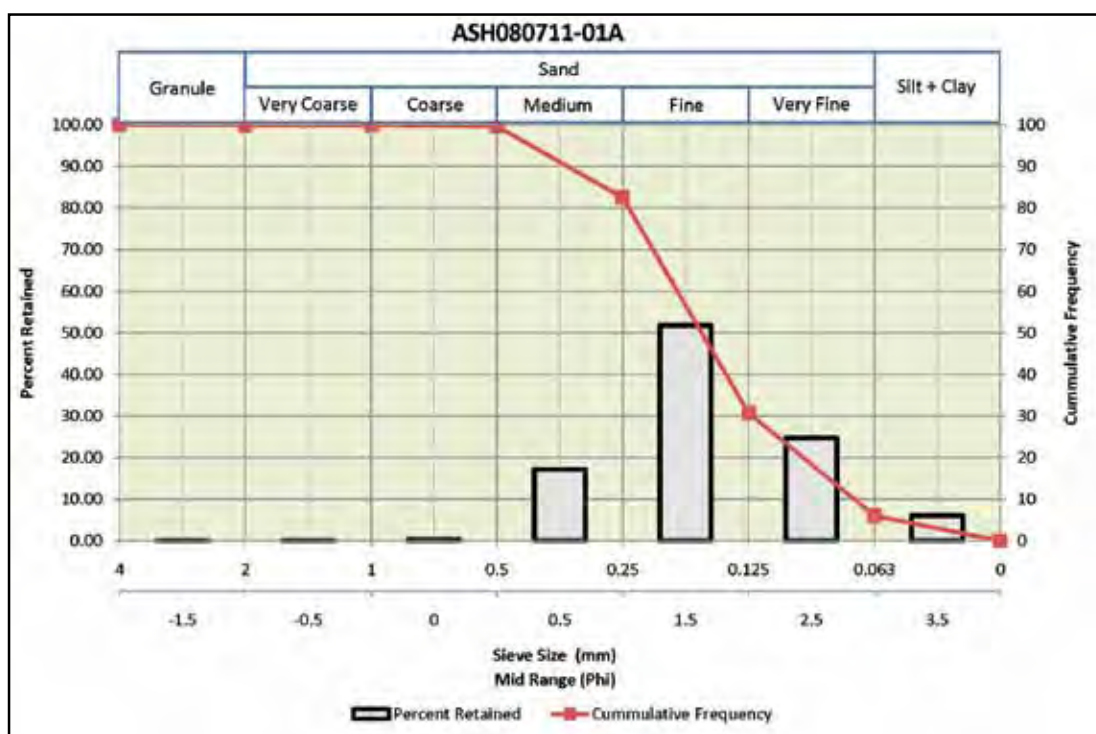
Crossed Nicols

|                       |               |
|-----------------------|---------------|
| <b>Sample</b>         | ASH080711-01A |
| <b>Easting</b>        | 671684        |
| <b>Northing</b>       | 6134020       |
| <b>Genetic Origin</b> | Aeolian Dune  |



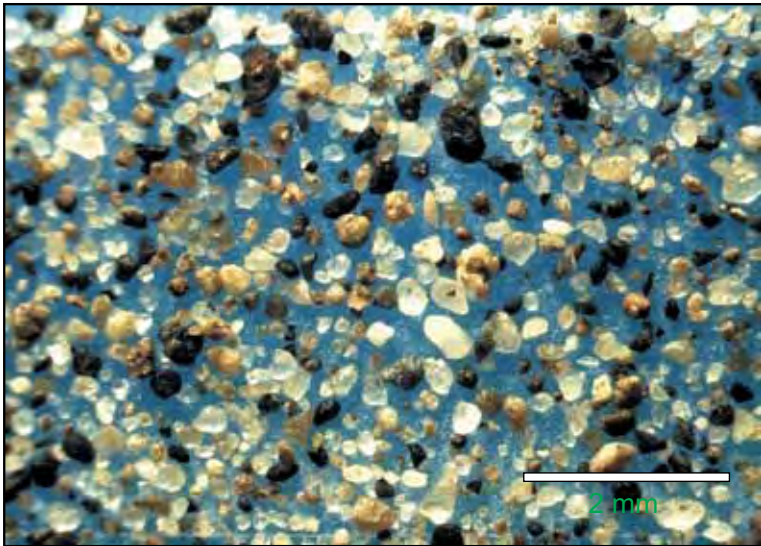
**Comment:**

This samples was collected from the head of a sand dune in the Kiskatinaw Dune Field south of Dawson Creek. These dunes are more distal from source and appear to have a higher proportion of silica than more proximal dunes.

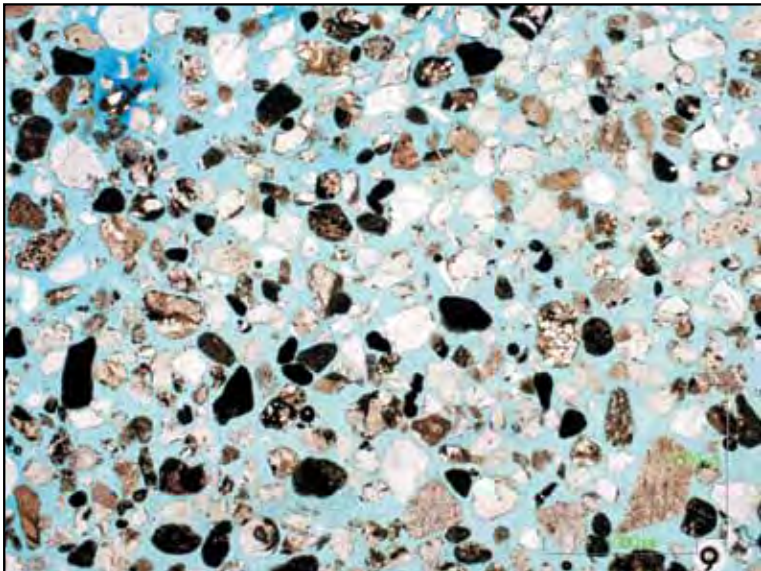


| Sieve Size | Mass  | Percent Retained | Cummulative Frequency |
|------------|-------|------------------|-----------------------|
| 4.0        | 0.0   | 0.00             | 100.00                |
| 2.0        | 0.1   | 0.02             | 99.98                 |
| 1.0        | 0.1   | 0.02             | 99.96                 |
| 0.500      | 1.4   | 0.30             | 99.66                 |
| 0.250      | 81.0  | 17.14            | 82.52                 |
| 0.125      | 244.7 | 51.78            | 30.74                 |
| 0.063      | 116.6 | 24.67            | 6.07                  |
| <0.063     | 28.7  | 6.07             | 0.00                  |

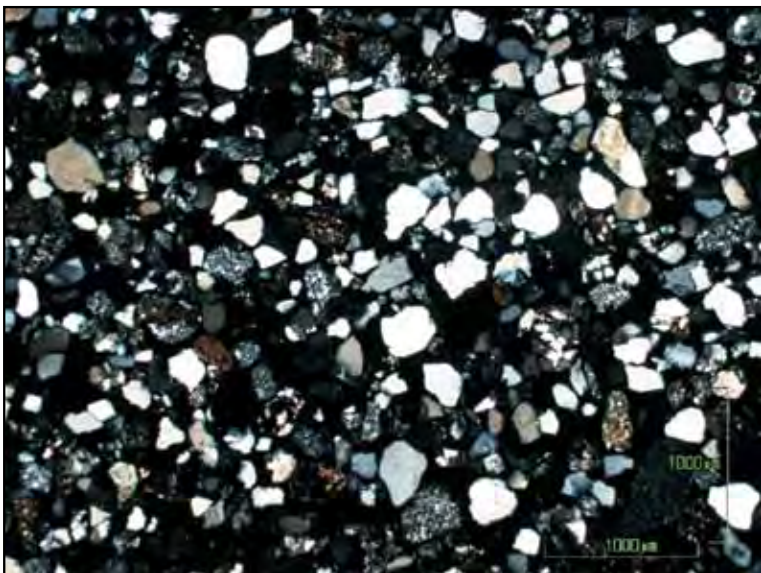
| Element                        | Percent |
|--------------------------------|---------|
| SiO <sub>2</sub>               | 90.15   |
| Al <sub>2</sub> O <sub>3</sub> | 3.62    |
| Fe <sub>2</sub> O <sub>3</sub> | 2.33    |
| MgO                            | 0.31    |
| CaO                            | 0.31    |
| Na <sub>2</sub> O              | 0.28    |
| K <sub>2</sub> O               | 0.77    |
| TiO <sub>2</sub>               | 0.22    |
| P <sub>2</sub> O <sub>5</sub>  | 0.17    |
| MnO                            | 0.02    |
| Cr <sub>2</sub> O <sub>3</sub> | 0.004   |
| LOI                            | 1.7     |



Binocular Microscope



Plane Light



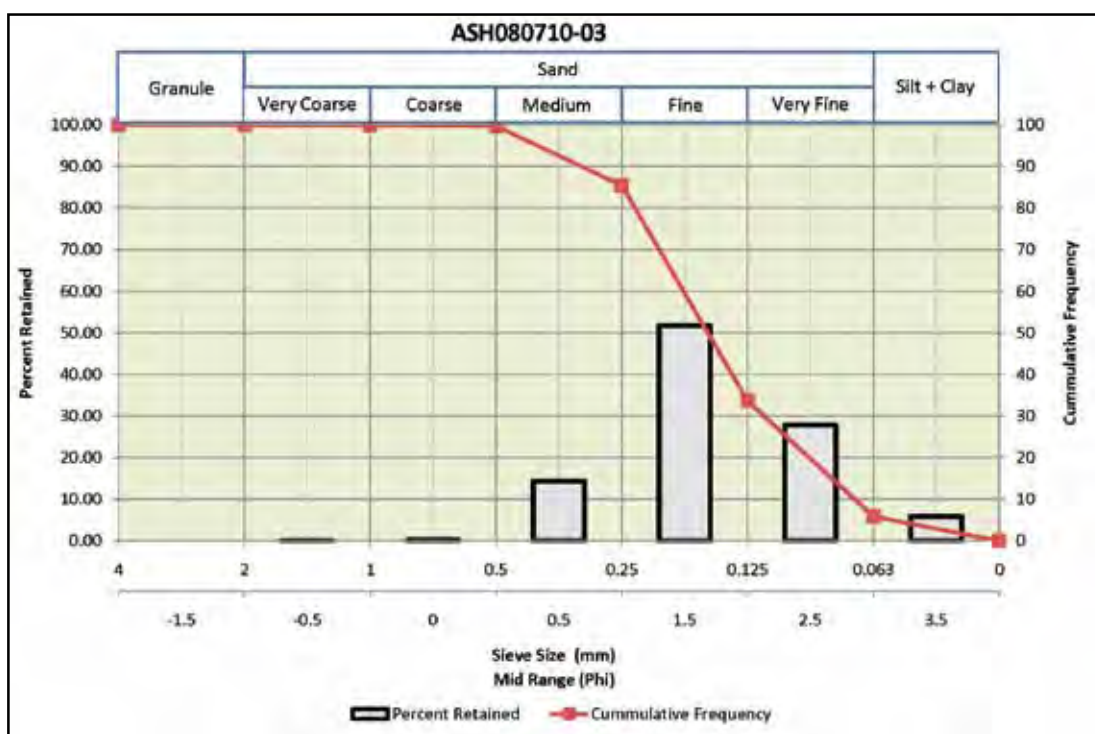
Crossed Nicols

|                       |              |
|-----------------------|--------------|
| <b>Sample</b>         | ASH080710-03 |
| <b>Easting</b>        | 670194       |
| <b>Northing</b>       | 6133138      |
| <b>Genetic Origin</b> | Aeolian Dune |



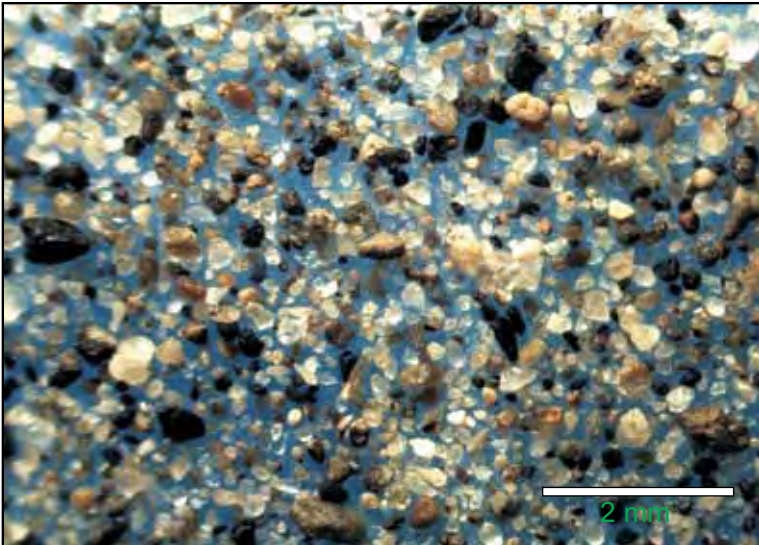
**Comment:**

This sample was collected from an elongate parabolic dune in the Kiskatinaw Dune Field south of Dawson Creek. The dunes are 3 to 20 metres high, can extend for over a kilometre, and may be several hundred metres across at the dune head.

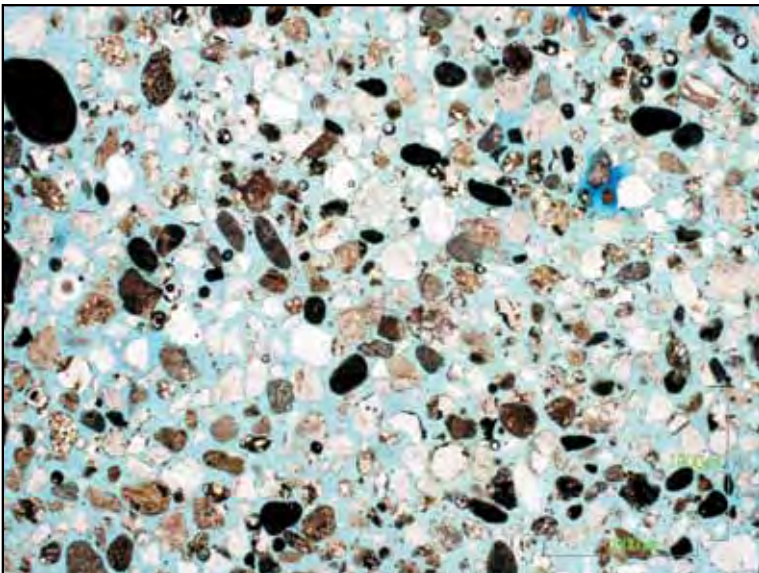


| Sieve Size | Mass  | Percent Retained | Cumulative Frequency |
|------------|-------|------------------|----------------------|
| 4.0        | 0.0   | 0.00             | 100.00               |
| 2.0        | 0.0   | 0.00             | 100.00               |
| 1.0        | 0.2   | 0.04             | 99.96                |
| 0.500      | 1.2   | 0.23             | 99.73                |
| 0.250      | 74.5  | 14.25            | 85.48                |
| 0.125      | 270.6 | 51.77            | 33.71                |
| 0.063      | 145.6 | 27.86            | 5.85                 |
| <0.063     | 30.6  | 5.85             | 0.00                 |

| Element                        | Percent |
|--------------------------------|---------|
| SiO <sub>2</sub>               | 86.34   |
| Al <sub>2</sub> O <sub>3</sub> | 3.47    |
| Fe <sub>2</sub> O <sub>3</sub> | 2.33    |
| MgO                            | 0.59    |
| CaO                            | 2.32    |
| Na <sub>2</sub> O              | 0.27    |
| K <sub>2</sub> O               | 0.76    |
| TiO <sub>2</sub>               | 0.21    |
| P <sub>2</sub> O <sub>5</sub>  | 0.19    |
| MnO                            | 0.02    |
| Cr <sub>2</sub> O <sub>3</sub> | 0.005   |
| LOI                            | 3.4     |



Binocular Microscope



Plane Light



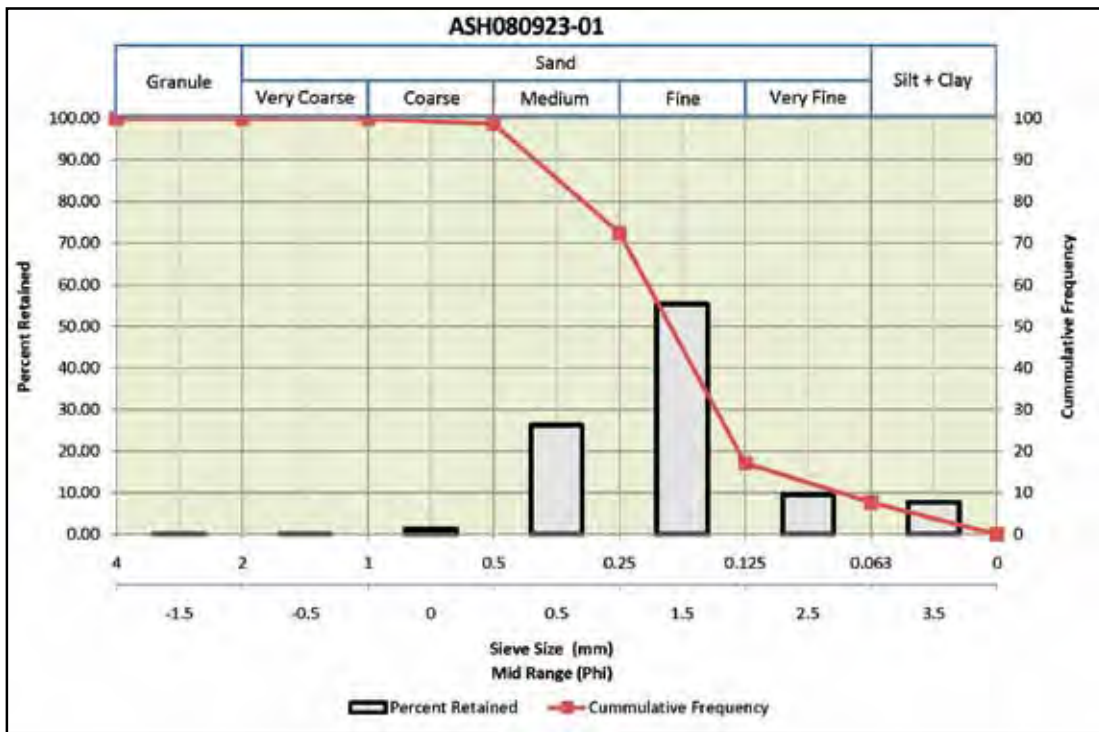
Crossed Nicols

|                       |                        |
|-----------------------|------------------------|
| <b>Sample</b>         | ASH080923-011          |
| <b>Easting</b>        | 685093                 |
| <b>Northing</b>       | 6099906                |
| <b>Genetic Origin</b> | Glaciofluvial (Delta?) |



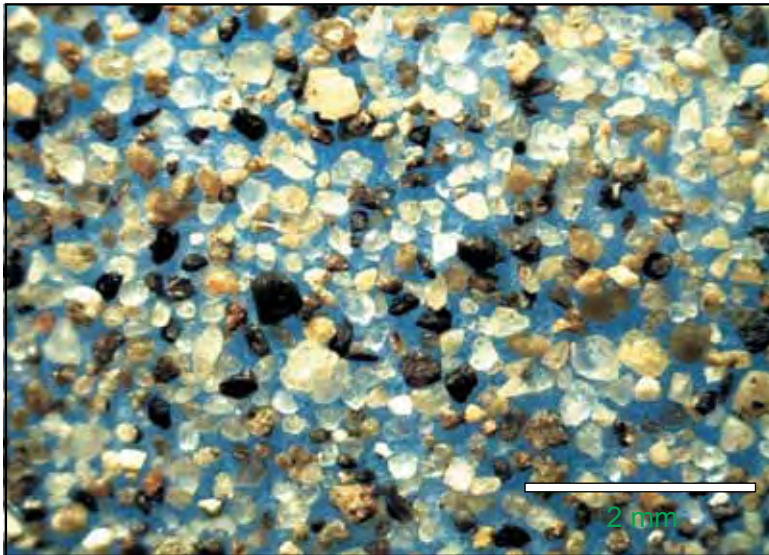
**Comment:**

This sample was collected from a large sandy terrace near the Redwillow River. The material is up to 5 metres thick and consists of uniform medium sand. The feature may be a delta associates with glacial Lake Peace.

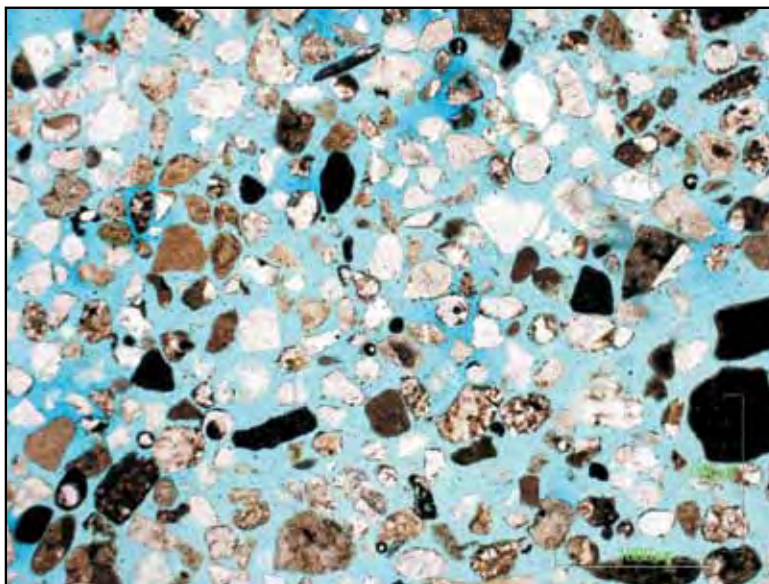


| Sieve Size | Mass  | Percent Retained | Cumulative Frequency |
|------------|-------|------------------|----------------------|
| 4.0        | 0.3   | 0.00             | 100.00               |
| 2.0        | 0.2   | 0.04             | 99.96                |
| 1.0        | 0.3   | 0.06             | 99.89                |
| 0.500      | 5.7   | 1.21             | 98.69                |
| 0.250      | 123.7 | 26.23            | 72.46                |
| 0.125      | 260.8 | 55.30            | 17.15                |
| 0.063      | 44.6  | 9.46             | 7.70                 |
| <0.063     | 36.3  | 7.70             | 0.00                 |

| Element                        | Percent |
|--------------------------------|---------|
| SiO <sub>2</sub>               | 88.44   |
| Al <sub>2</sub> O <sub>3</sub> | 4.59    |
| Fe <sub>2</sub> O <sub>3</sub> | 2.41    |
| MgO                            | 0.35    |
| CaO                            | 0.28    |
| Na <sub>2</sub> O              | 0.54    |
| K <sub>2</sub> O               | 0.95    |
| TiO <sub>2</sub>               | 0.24    |
| P <sub>2</sub> O <sub>5</sub>  | 0.12    |
| MnO                            | 0.03    |
| Cr <sub>2</sub> O <sub>3</sub> | 0.005   |
| LOI                            | 2.0     |



Binocular Microscope



Plane Light



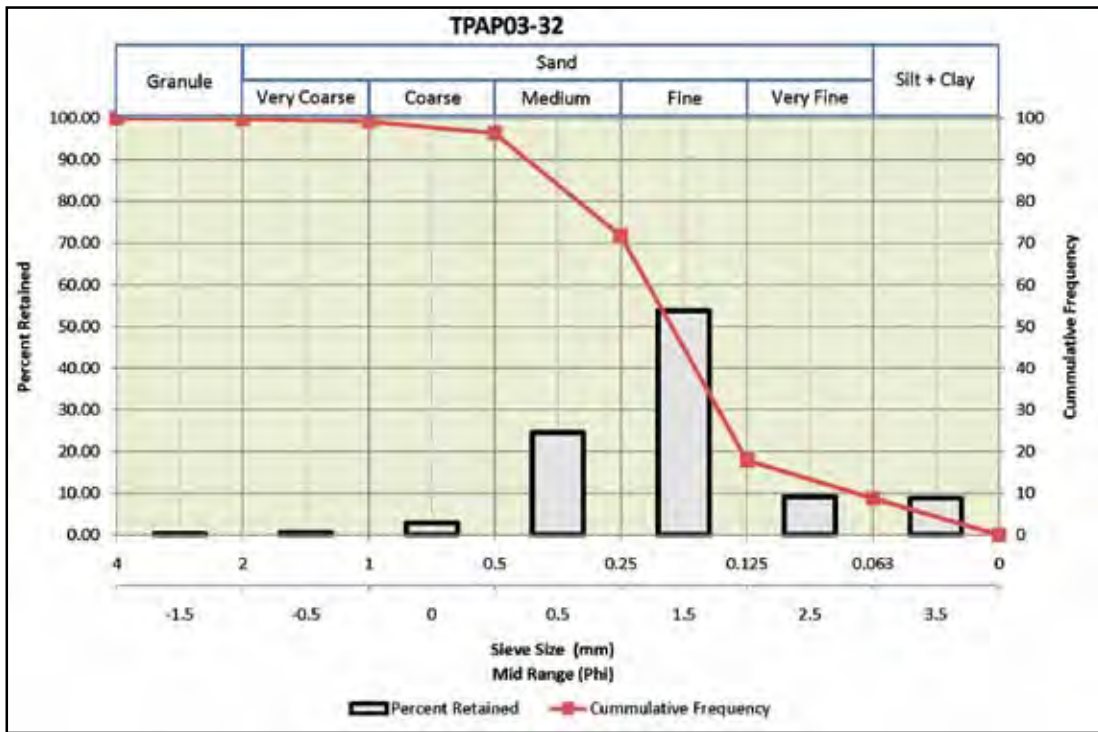
Crossed Nicols

|                       |               |
|-----------------------|---------------|
| <b>Sample</b>         | TPAP03-32     |
| <b>Easting</b>        | 522972        |
| <b>Northing</b>       | 6520875       |
| <b>Genetic Origin</b> | Glaciofluvial |



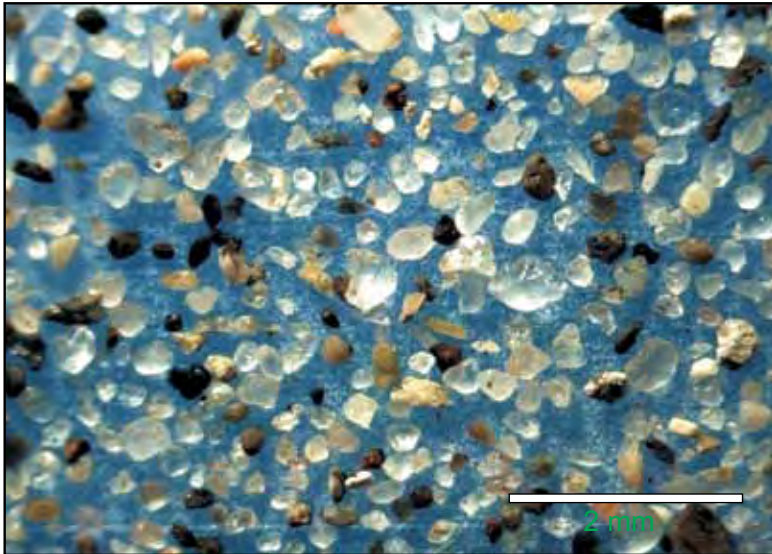
**Comment:**

This sample was collected from a 5 metre deep test pit on a sandy hill near the Fort Nelson Airport.

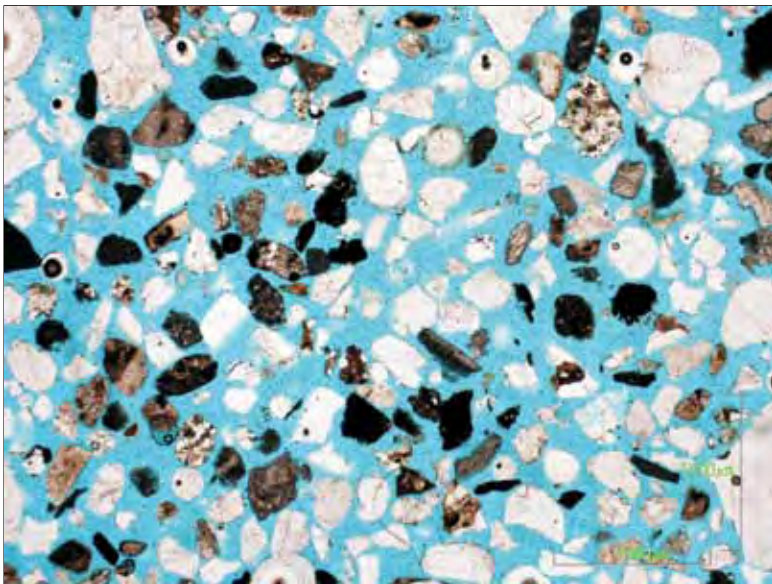


| Sieve Size | Mass  | Percent Retained | Cumulative Frequency |
|------------|-------|------------------|----------------------|
| 4.0        | 0.7   | 0.00             | 100.00               |
| 2.0        | 1.1   | 0.25             | 99.75                |
| 1.0        | 2.5   | 0.58             | 99.17                |
| 0.500      | 12.1  | 2.80             | 96.37                |
| 0.250      | 106.5 | 24.62            | 71.75                |
| 0.125      | 232.8 | 53.81            | 17.94                |
| 0.063      | 39.5  | 9.13             | 8.81                 |
| <0.063     | 38.1  | 8.81             | 0.00                 |

| Element                        | Percent |
|--------------------------------|---------|
| SiO <sub>2</sub>               | 81.1    |
| Al <sub>2</sub> O <sub>3</sub> | 4.58    |
| Fe <sub>2</sub> O <sub>3</sub> | 2.04    |
| MgO                            | 0.84    |
| CaO                            | 4.38    |
| Na <sub>2</sub> O              | 0.89    |
| K <sub>2</sub> O               | 1.23    |
| TiO <sub>2</sub>               | 0.15    |
| P <sub>2</sub> O <sub>5</sub>  | 0.11    |
| MnO                            | 0.03    |
| Cr <sub>2</sub> O <sub>3</sub> | <0.002  |
| LOI                            | 4.5     |



Binocular Microscope



Plane Light



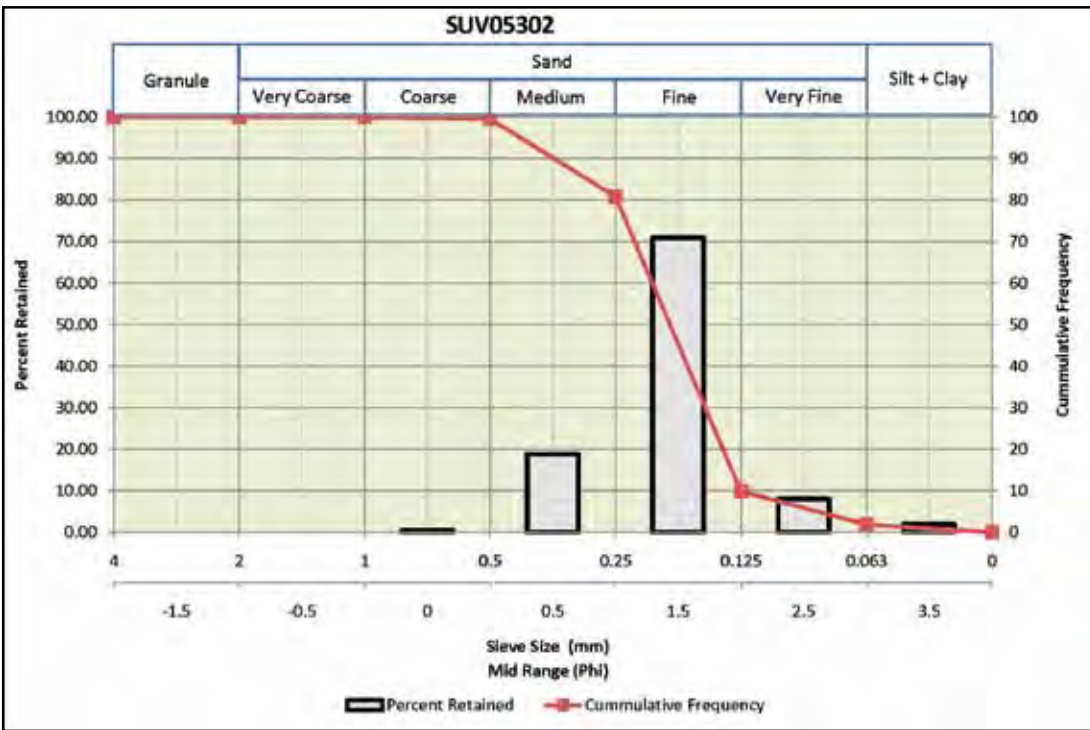
Crossed Nicols

|                       |               |
|-----------------------|---------------|
| <b>Sample</b>         | SUV05302      |
| <b>Easting</b>        | 621520        |
| <b>Northing</b>       | 6456212       |
| <b>Genetic Origin</b> | Aeolian Dunes |



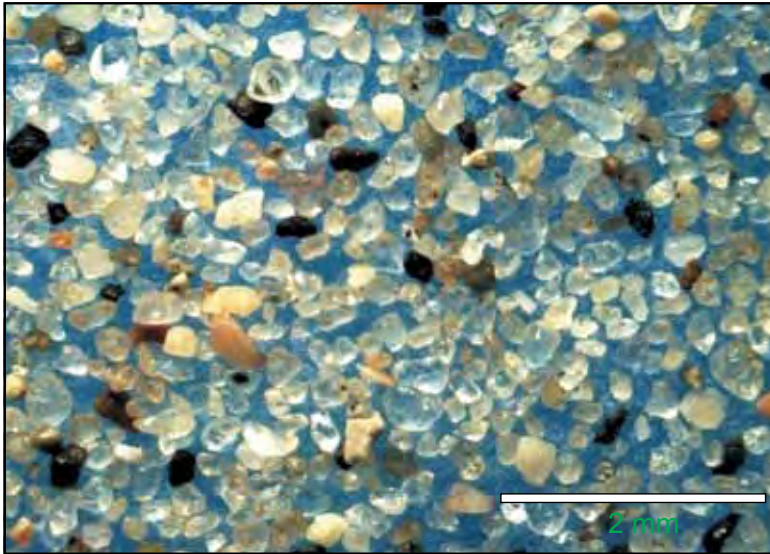
**Comment:**

This samples was collected from a compound parabolic dune from the main dune field north of Dazo Creek in the Fontas River Dune Field, east of Fort Nelson. Dune crests are up to 7 m high, with average sand thicknesses across the field estimated to be 10 m.

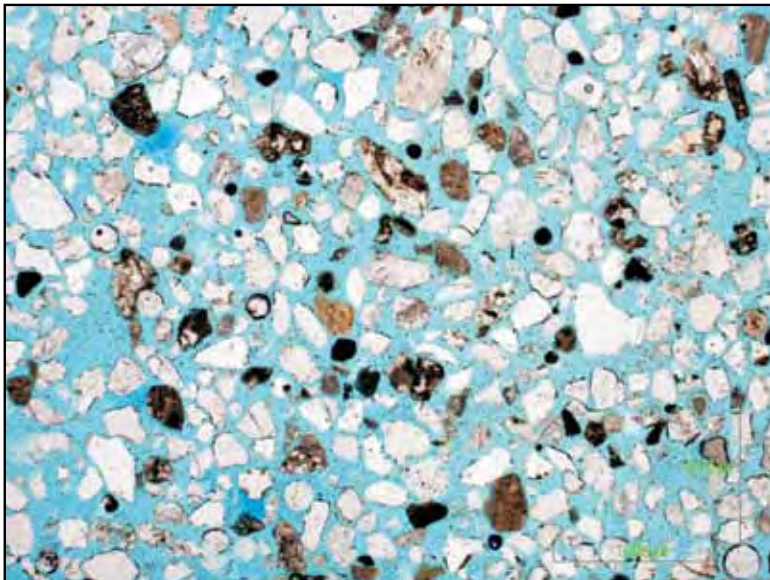


| Sieve Size | Mass | Percent Retained | Cummulative Frequency |
|------------|------|------------------|-----------------------|
| 4.0        | 0.0  | 0.00             | 100.00                |
| 2.0        | 0.0  | 0.00             | 100.00                |
| 1.0        | 0.0  | 0.00             | 100.00                |
| 0.500      | 0.5  | 0.37             | 99.63                 |
| 0.250      | 25.1 | 18.80            | 80.82                 |
| 0.125      | 94.7 | 70.94            | 9.89                  |
| 0.063      | 10.7 | 8.01             | 1.87                  |
| <0.063     | 2.5  | 1.87             | 0.00                  |

| Element                        | Percent |
|--------------------------------|---------|
| SiO <sub>2</sub>               | 91.42   |
| Al <sub>2</sub> O <sub>3</sub> | 3.58    |
| Fe <sub>2</sub> O <sub>3</sub> | 2.22    |
| MgO                            | 0.18    |
| CaO                            | 0.44    |
| Na <sub>2</sub> O              | 0.74    |
| K <sub>2</sub> O               | 0.93    |
| TiO <sub>2</sub>               | 0.11    |
| P <sub>2</sub> O <sub>5</sub>  | 0.07    |
| MnO                            | 0.03    |
| Cr <sub>2</sub> O <sub>3</sub> | 0.002   |
| LOI                            | 0.2     |



Binocular Microscope



Plane Light



Crossed Nicols

|                       |              |
|-----------------------|--------------|
| <b>Sample</b>         | SUV05303     |
| <b>Easting</b>        | 621098       |
| <b>Northing</b>       | 6456288      |
| <b>Genetic Origin</b> | Aeolian Dune |



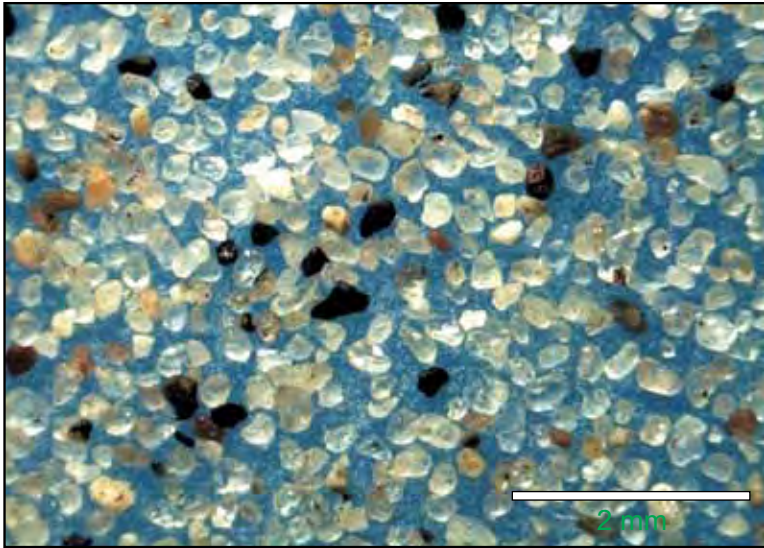
**Comment:**

This samples was collected from a compound parabolic dune from the main dune field north of Dazo Creek in the main Fontas River Dune Field, east of Fort Nelson. Dune crests are up to 7 m high, with average sand thicknesses across the field estimated to be 10 m.

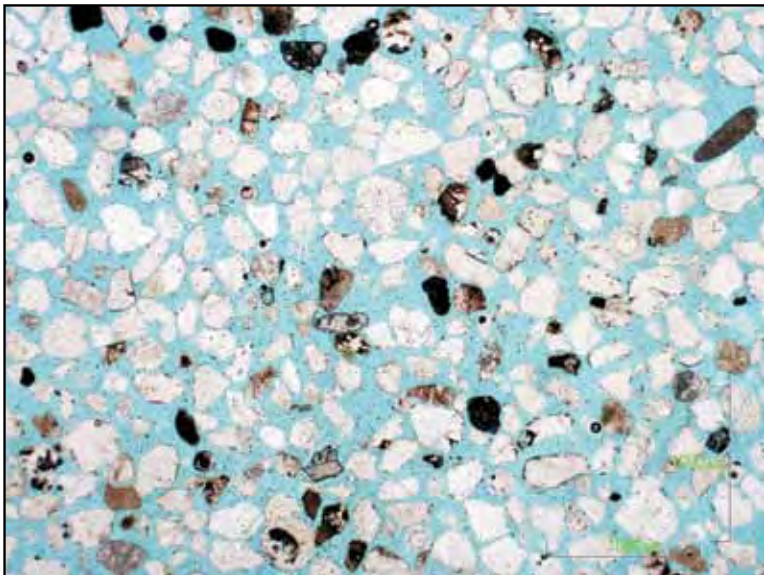


| Sieve Size | Mass | Percent Retained | Cummulative Frequency |
|------------|------|------------------|-----------------------|
| 4.0        | 0.0  | 0.00             | 100.00                |
| 2.0        | 0.0  | 0.00             | 100.00                |
| 1.0        | 0.0  | 0.00             | 100.00                |
| 0.500      | 0.8  | 0.57             | 99.43                 |
| 0.250      | 41.9 | 29.76            | 69.67                 |
| 0.125      | 88.7 | 63.00            | 6.68                  |
| 0.063      | 7.8  | 5.54             | 1.14                  |
| <0.063     | 1.6  | 1.14             | 0.00                  |

| Element                        | Percent |
|--------------------------------|---------|
| SiO <sub>2</sub>               | 90.96   |
| Al <sub>2</sub> O <sub>3</sub> | 3.51    |
| Fe <sub>2</sub> O <sub>3</sub> | 2.49    |
| MgO                            | 0.22    |
| CaO                            | 0.48    |
| Na <sub>2</sub> O              | 0.74    |
| K <sub>2</sub> O               | 0.85    |
| TiO <sub>2</sub>               | 0.16    |
| P <sub>2</sub> O <sub>5</sub>  | 0.08    |
| MnO                            | 0.03    |
| Cr <sub>2</sub> O <sub>3</sub> | 0.003   |
| LOI                            | 0.4     |



Binocular Microscope



Plane Light



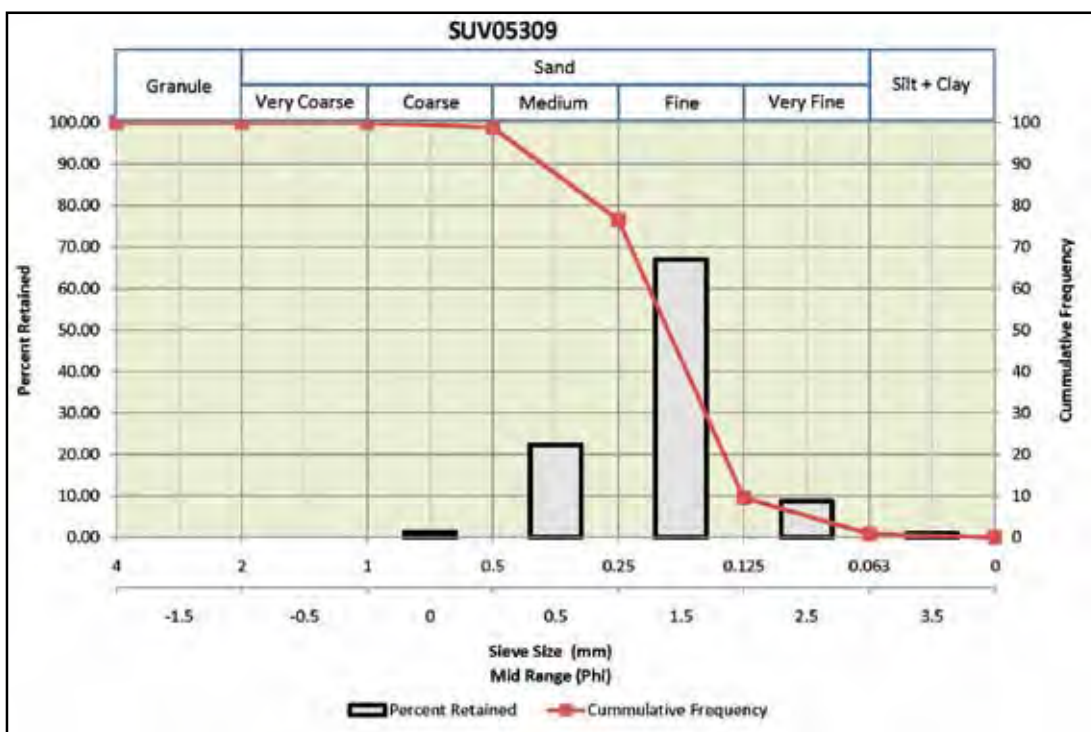
Crossed Nicols

|                       |              |
|-----------------------|--------------|
| <b>Sample</b>         | SUV05309     |
| <b>Easting</b>        | 611404       |
| <b>Northing</b>       | 6460199      |
| <b>Genetic Origin</b> | Aeolian Dune |



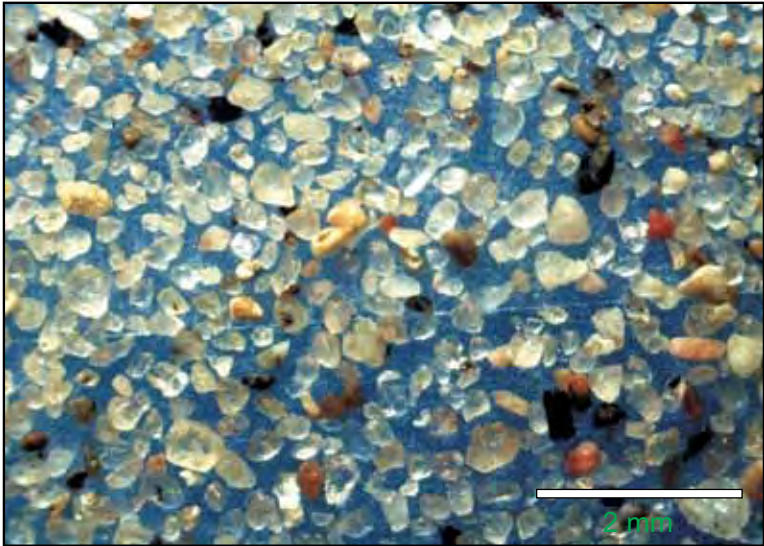
**Comment:**

This sample was collected from a parabolic sand dune in the northwestern sub-field of the Fontas Dune Field. Dunes are up to 4 m high large parabolic forms several hundreds of metres in length, with only thin sand cover in the inter-dune regions.

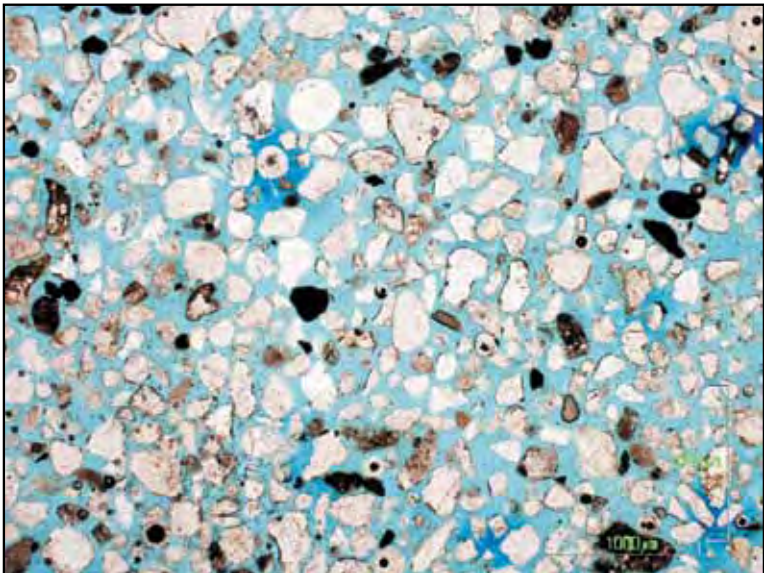


| Sieve Size | Mass | Percent Retained | Cummulative Frequency |
|------------|------|------------------|-----------------------|
| 4.0        | 0.0  | 0.00             | 100.00                |
| 2.0        | 0.0  | 0.00             | 100.00                |
| 1.0        | 0.0  | 0.00             | 100.00                |
| 0.500      | 1.5  | 1.19             | 98.81                 |
| 0.250      | 28.0 | 22.28            | 76.53                 |
| 0.125      | 84.2 | 66.98            | 9.55                  |
| 0.063      | 10.9 | 8.67             | 0.88                  |
| <0.063     | 1.1  | 0.88             | 0.00                  |

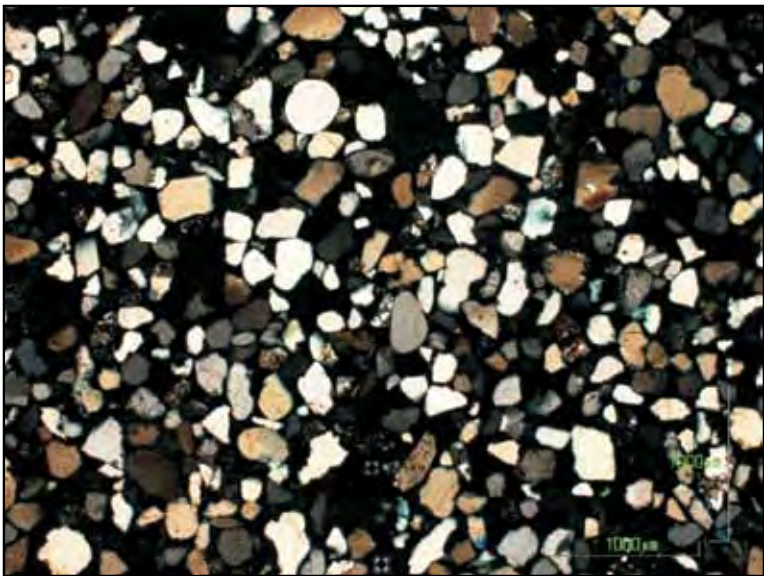
| Element                        | Percent |
|--------------------------------|---------|
| SiO <sub>2</sub>               | 90.62   |
| Al <sub>2</sub> O <sub>3</sub> | 3.83    |
| Fe <sub>2</sub> O <sub>3</sub> | 2.36    |
| MgO                            | 0.19    |
| CaO                            | 0.45    |
| Na <sub>2</sub> O              | 0.78    |
| K <sub>2</sub> O               | 0.99    |
| TiO <sub>2</sub>               | 0.13    |
| P <sub>2</sub> O <sub>5</sub>  | 0.08    |
| MnO                            | 0.03    |
| Cr <sub>2</sub> O <sub>3</sub> | 0.002   |
| LOI                            | 0.5     |



Binocular Microscope



Plane Light



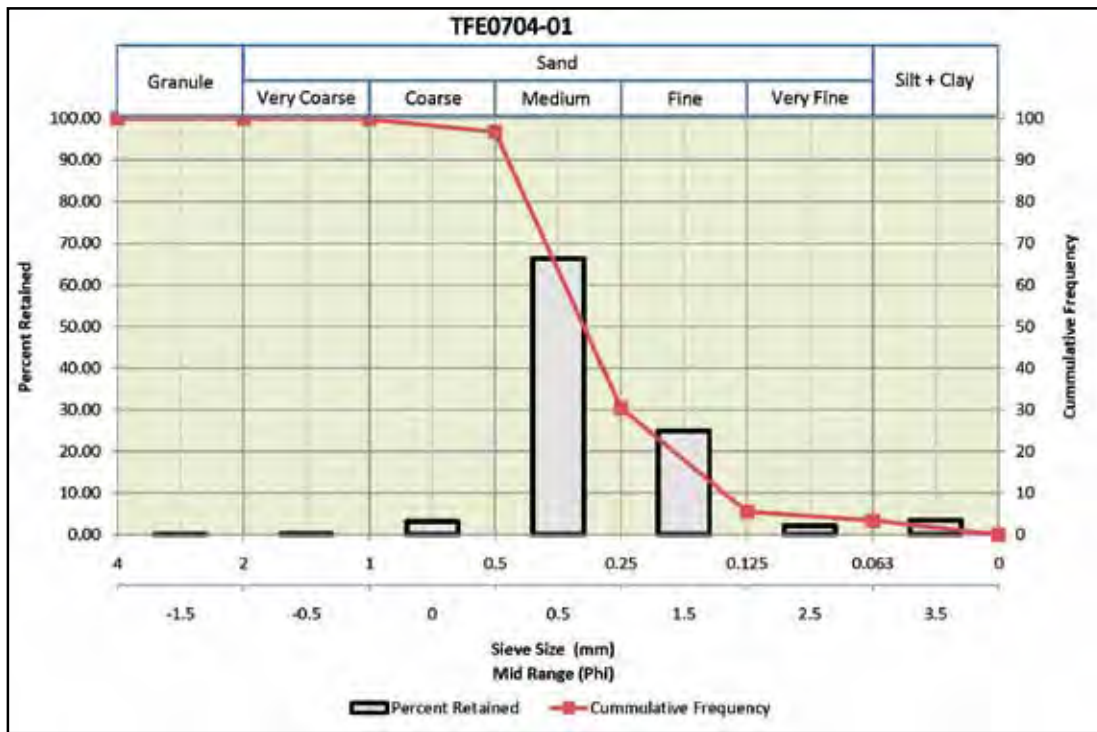
Crossed Nicols

|                       |                       |
|-----------------------|-----------------------|
| <b>Sample</b>         | TFE0704-01            |
| <b>Easting</b>        | 628362                |
| <b>Northing</b>       | 6566463               |
| <b>Genetic Origin</b> | Glaciofluvial (Esker) |



**Comment:**

The sample was collected from an esker that crosses Sierra-Yoyo\_Desan road at kilometre 176. The sample was taken approximately 2 metres below the surface where an excavation has exposed the interior of the esker.

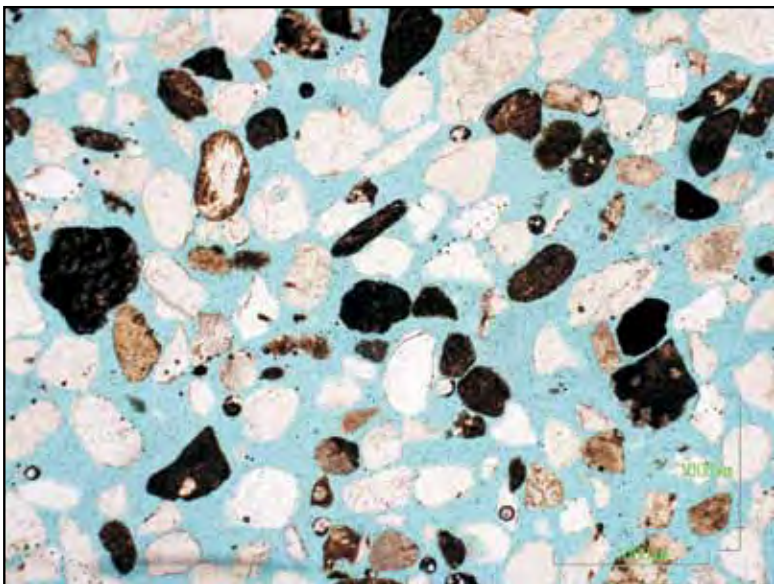


| Sieve Size | Mass   | Percent Retained | Cummulative Frequency |
|------------|--------|------------------|-----------------------|
| 4.0        | 0.0    | 0.00             | 100.00                |
| 2.0        | 1.1    | 0.04             | 99.96                 |
| 1.0        | 3.4    | 0.12             | 99.84                 |
| 0.500      | 87.7   | 3.08             | 96.76                 |
| 0.250      | 1886.6 | 66.32            | 30.43                 |
| 0.125      | 707.6  | 24.88            | 5.56                  |
| 0.063      | 60.5   | 2.13             | 3.43                  |
| <0.063     | 97.6   | 3.43             | 0.00                  |

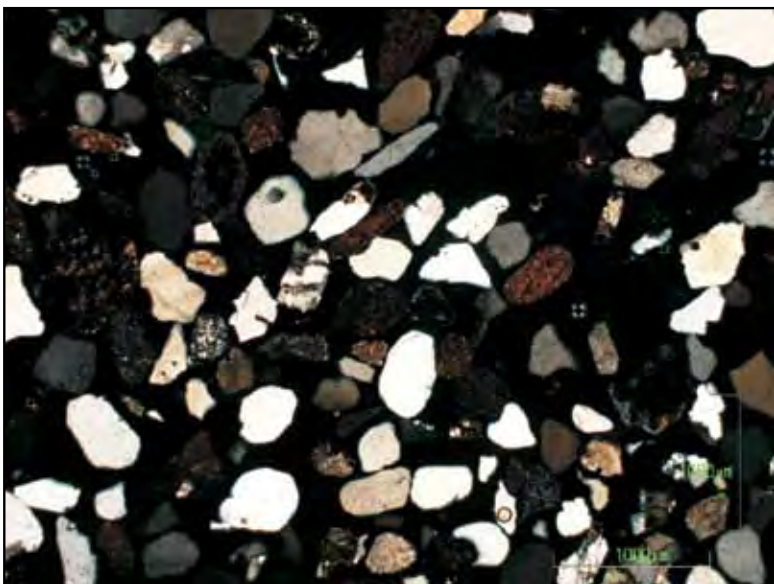
| Element                        | Percent |
|--------------------------------|---------|
| SiO <sub>2</sub>               | 85.01   |
| Al <sub>2</sub> O <sub>3</sub> | 4.86    |
| Fe <sub>2</sub> O <sub>3</sub> | 1.70    |
| MgO                            | 0.60    |
| CaO                            | 2.30    |
| Na <sub>2</sub> O              | 0.85    |
| K <sub>2</sub> O               | 1.35    |
| TiO <sub>2</sub>               | 0.13    |
| P <sub>2</sub> O <sub>5</sub>  | 0.10    |
| MnO                            | 0.02    |
| Cr <sub>2</sub> O <sub>3</sub> | <0.002  |
| LOI                            | 3.0     |



Binocular Microscope



Plane Light



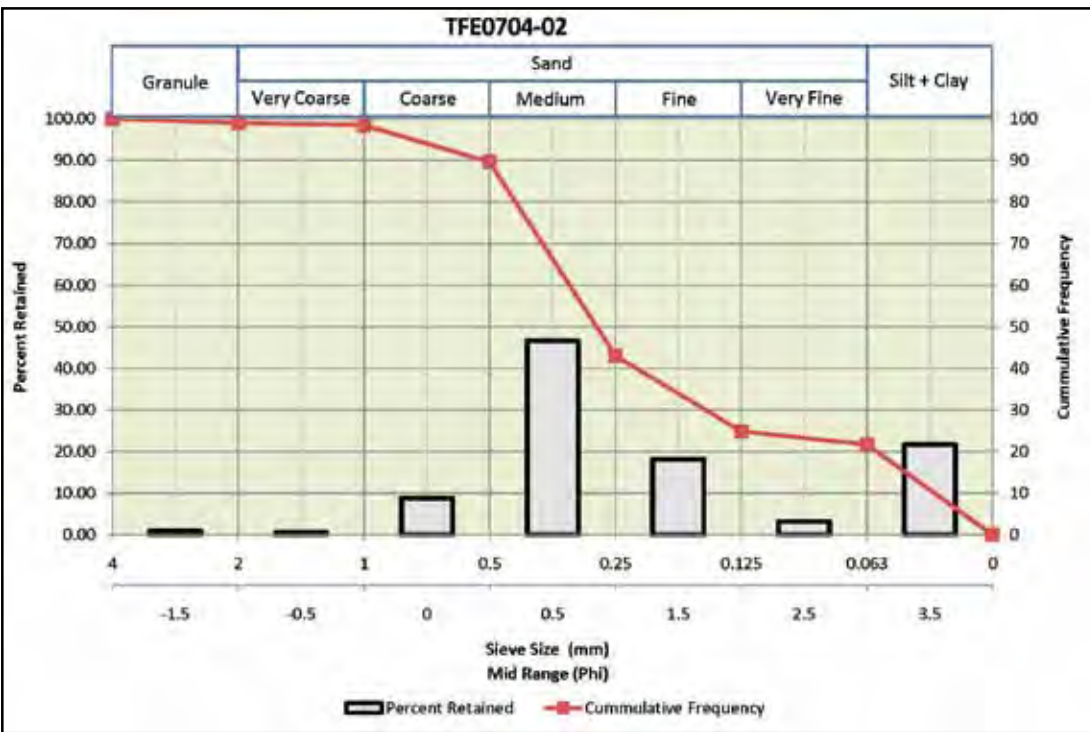
Crossed Nicols

|                       |                       |
|-----------------------|-----------------------|
| <b>Sample</b>         | TFE0704-02            |
| <b>Easting</b>        | 581274                |
| <b>Northing</b>       | 6540078               |
| <b>Genetic Origin</b> | Glaciofluvial (Esker) |



**Comment:**

This sample was collected from the top of an esker (ridge) located west of the Komie Road. The esker is approximately 10 metres high, consisting mainly of sand with a thin 20 centimetre gravel lag at the surface.

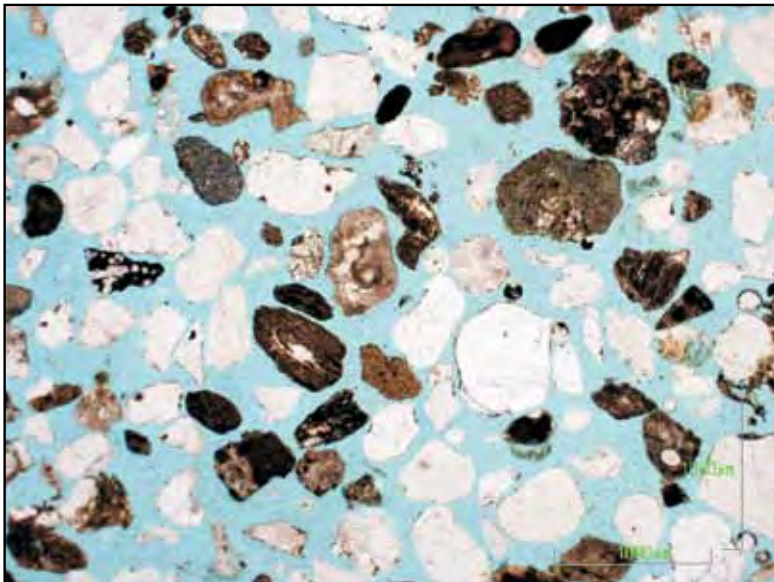


| Sieve Size | Mass  | Percent Retained | Cumulative Frequency |
|------------|-------|------------------|----------------------|
| 4.0        | 0.0   | 0.00             | 100.00               |
| 2.0        | 18.2  | 0.94             | 100.00               |
| 1.0        | 11.2  | 0.58             | 99.06                |
| 0.500      | 171.5 | 8.82             | 98.49                |
| 0.250      | 906.4 | 46.61            | 89.67                |
| 0.125      | 352.7 | 18.14            | 43.05                |
| 0.063      | 62.3  | 3.20             | 24.92                |
| <0.063     | 422.2 | 21.71            | 21.71                |

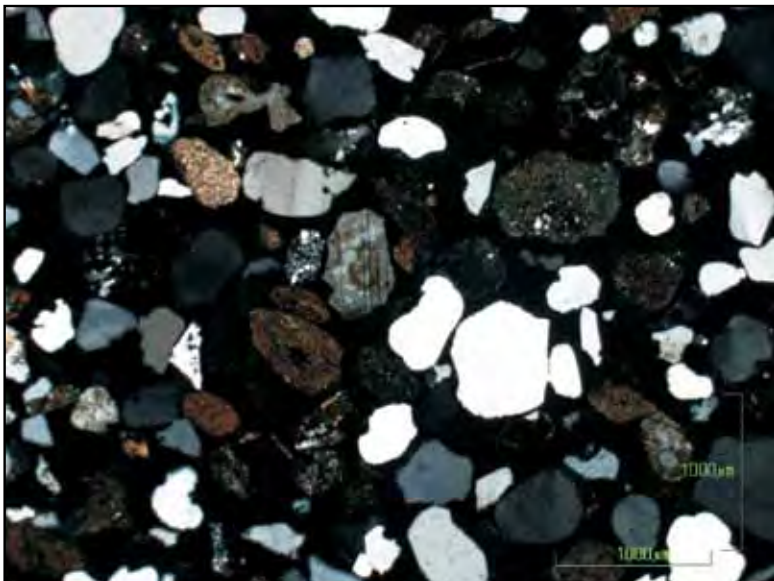
| Element                        | Percent |
|--------------------------------|---------|
| SiO <sub>2</sub>               | 83.89   |
| Al <sub>2</sub> O <sub>3</sub> | 6.08    |
| Fe <sub>2</sub> O <sub>3</sub> | 2.45    |
| MgO                            | 0.53    |
| CaO                            | 1.35    |
| Na <sub>2</sub> O              | 0.96    |
| K <sub>2</sub> O               | 1.51    |
| TiO <sub>2</sub>               | 0.17    |
| P <sub>2</sub> O <sub>5</sub>  | 0.08    |
| MnO                            | 0.03    |
| Cr <sub>2</sub> O <sub>3</sub> | 0.003   |
| LOI                            | 2.9     |



Binocular Microscope



Plane Light



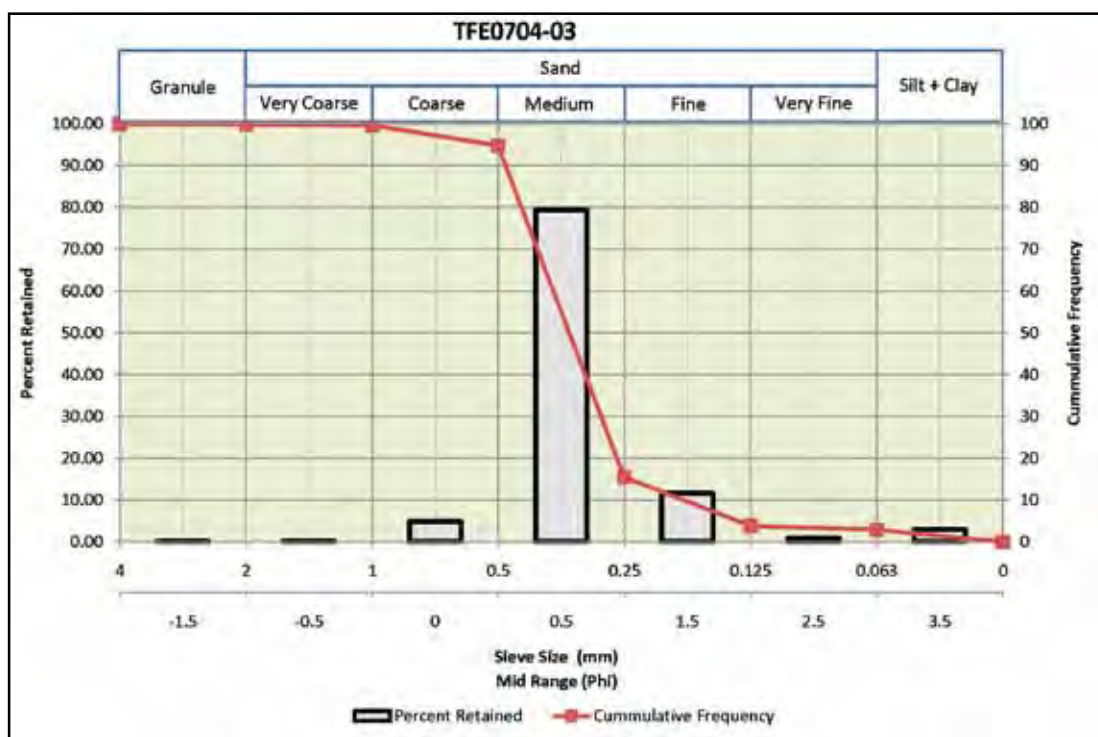
Crossed Nicols

|                       |               |
|-----------------------|---------------|
| <b>Sample</b>         | TFE0704-03    |
| <b>Easting</b>        | 569040        |
| <b>Northing</b>       | 6573180       |
| <b>Genetic Origin</b> | Glaciofluvial |



**Comment:**

The sample was taken from a borrow pit in the Komie area east of the Geetlah Road. This is interpreted as a glaciofluvial delta that formed in a shallow glacial lake. There are several active and past producing sand and gravel pits in the area.

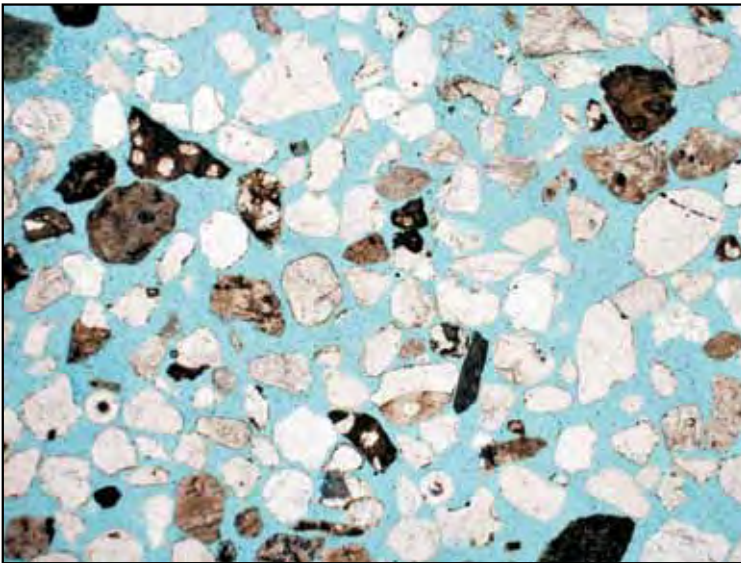


| Sieve Size | Mass   | Percent Retained | Cumulative Frequency |
|------------|--------|------------------|----------------------|
| 4.0        | 0.0    | 0.00             | 100.00               |
| 2.0        | 1.3    | 0.10             | 99.90                |
| 1.0        | 2.6    | 0.19             | 99.71                |
| 0.500      | 65.3   | 4.87             | 94.84                |
| 0.250      | 1065.1 | 79.38            | 15.46                |
| 0.125      | 156.0  | 11.63            | 3.83                 |
| 0.063      | 12.0   | 0.89             | 2.94                 |
| <0.063     | 39.4   | 2.94             | 0.00                 |

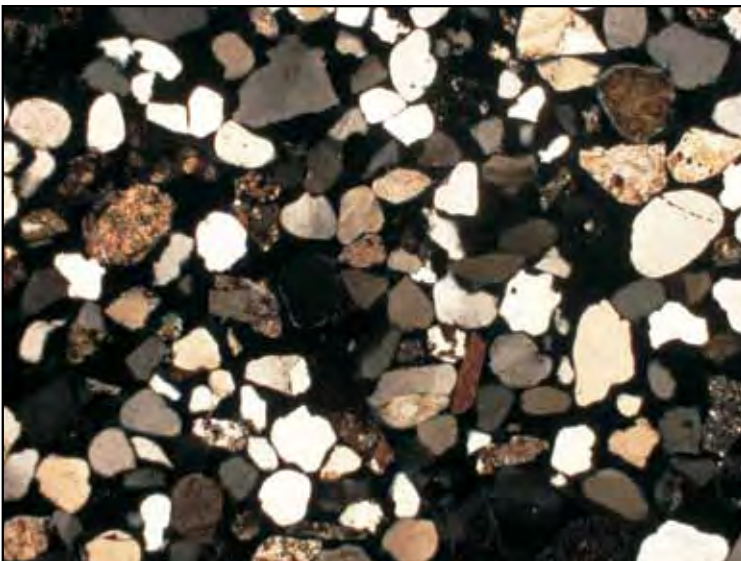
| Element                        | Percent |
|--------------------------------|---------|
| SiO <sub>2</sub>               | 89.99   |
| Al <sub>2</sub> O <sub>3</sub> | 4.26    |
| Fe <sub>2</sub> O <sub>3</sub> | 2.00    |
| MgO                            | 0.23    |
| CaO                            | 0.43    |
| Na <sub>2</sub> O              | 0.90    |
| K <sub>2</sub> O               | 1.25    |
| TiO <sub>2</sub>               | 0.10    |
| P <sub>2</sub> O <sub>5</sub>  | 0.06    |
| MnO                            | 0.02    |
| Cr <sub>2</sub> O <sub>3</sub> | <0.002  |
| LOI                            | 0.7     |



Binocular Microscope



Plane Light



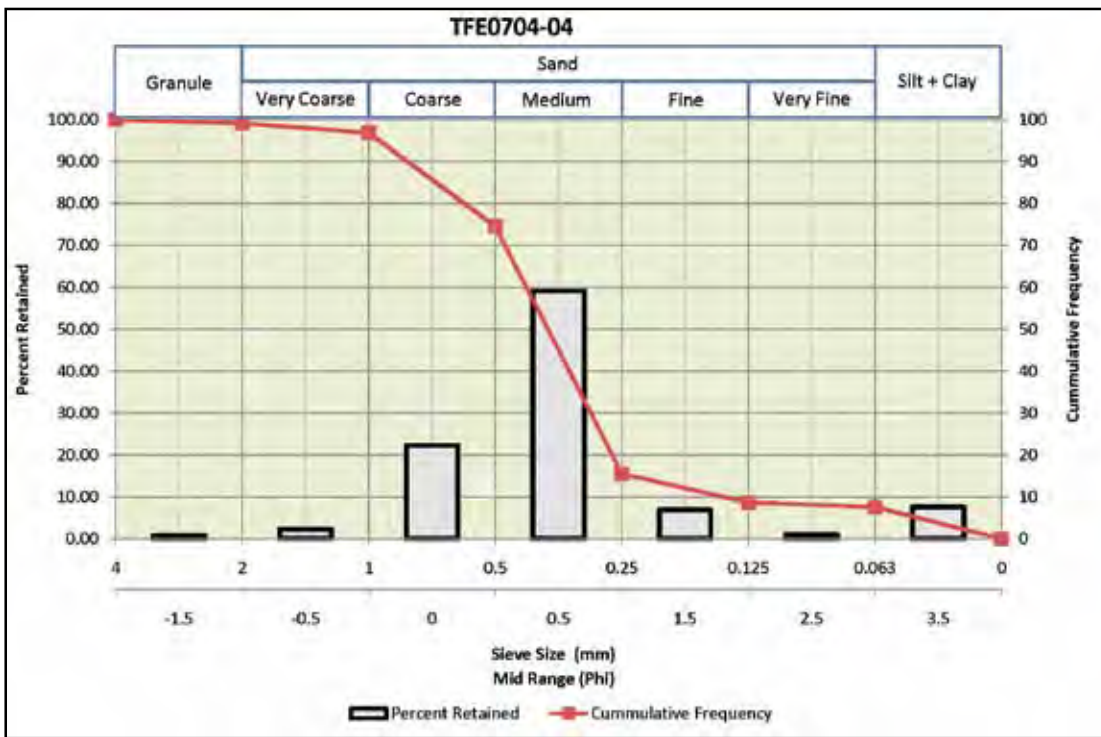
Crossed Nicols

|                       |                       |
|-----------------------|-----------------------|
| <b>Sample</b>         | TFE0704-04            |
| <b>Easting</b>        | 574987                |
| <b>Northing</b>       | 6560341               |
| <b>Genetic Origin</b> | Glaciofluvial (Esker) |



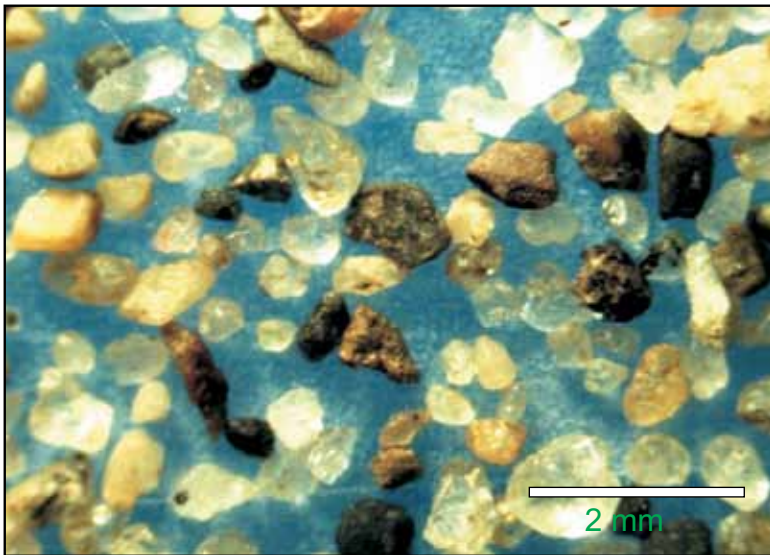
**Comment:**

Sample was collected from a recontoured borrow pit north of Courvoisier Creek, west of the Komie Road. The feature that hosts this deposit is an esker complex.

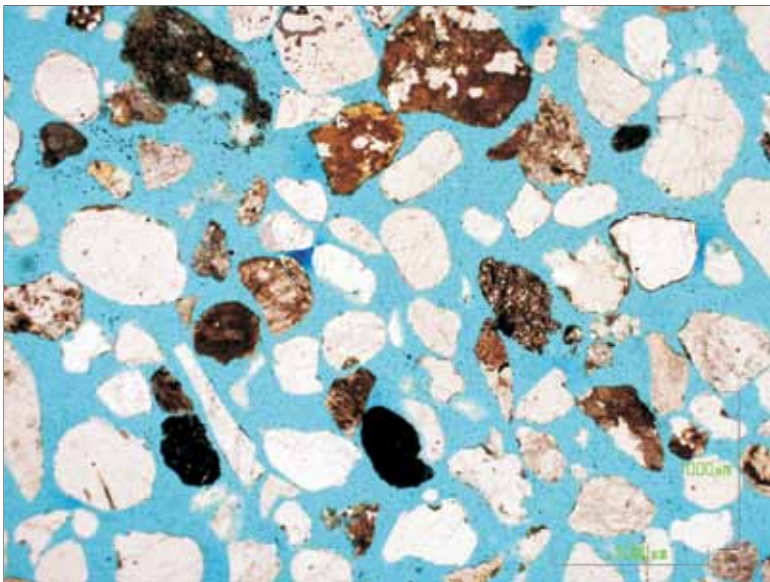


| Sieve Size | Mass   | Percent Retained | Cumulative Frequency |
|------------|--------|------------------|----------------------|
| 4.0        | 0.0    | 0.00             | 100.00               |
| 2.0        | 25.6   | 0.78             | 99.22                |
| 1.0        | 75.8   | 2.32             | 96.89                |
| 0.500      | 727.5  | 22.28            | 74.61                |
| 0.250      | 1929.0 | 59.08            | 15.53                |
| 0.125      | 224.0  | 6.86             | 8.67                 |
| 0.063      | 35.0   | 1.07             | 7.59                 |
| <0.063     | 247.9  | 7.59             | 0.00                 |

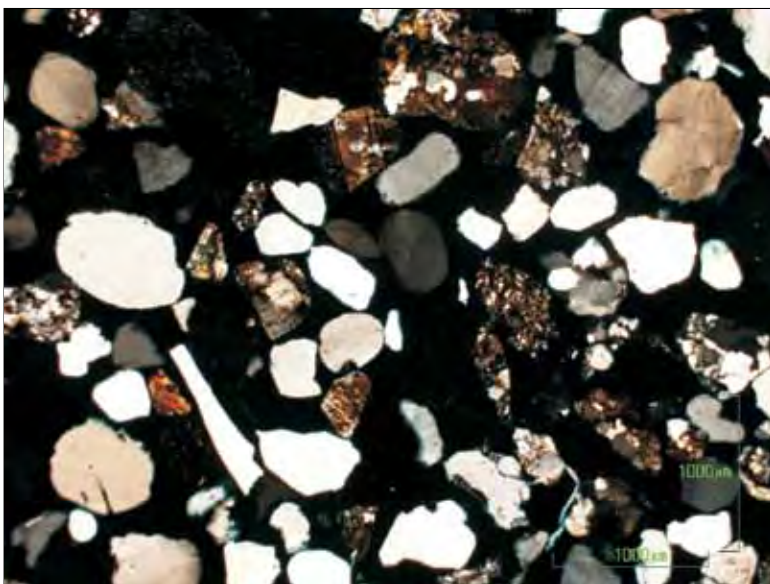
| Element                        | Percent |
|--------------------------------|---------|
| SiO <sub>2</sub>               | 87.01   |
| Al <sub>2</sub> O <sub>3</sub> | 5.70    |
| Fe <sub>2</sub> O <sub>3</sub> | 2.28    |
| MgO                            | 0.31    |
| CaO                            | 0.52    |
| Na <sub>2</sub> O              | 1.14    |
| K <sub>2</sub> O               | 1.65    |
| TiO <sub>2</sub>               | 0.13    |
| P <sub>2</sub> O <sub>5</sub>  | 0.08    |
| MnO                            | 0.03    |
| Cr <sub>2</sub> O <sub>3</sub> | <0.002  |
| LOI                            | 1.1     |



Binocular Microscope



Plane Light



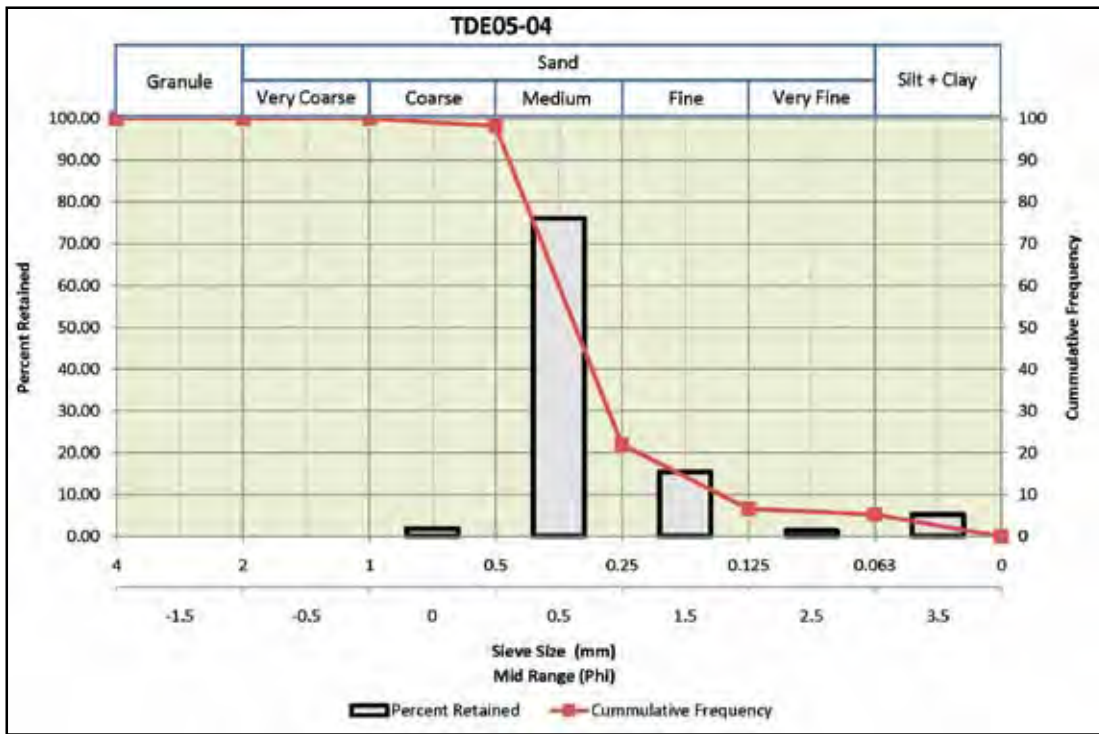
Crossed Nicols

|                       |                       |
|-----------------------|-----------------------|
| <b>Sample</b>         | TDE05-04              |
| <b>Easting</b>        | 575001                |
| <b>Northing</b>       | 6559192               |
| <b>Genetic Origin</b> | Glaciofluvial (esker) |



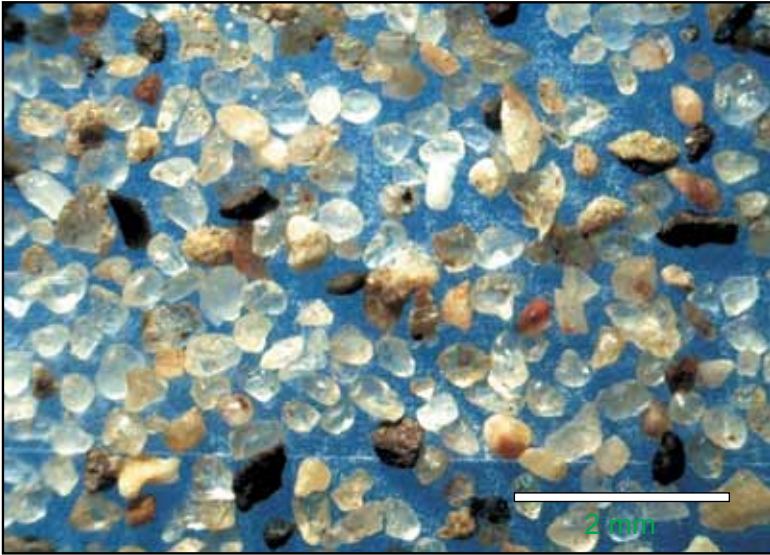
**Comment:**

This sample was collected from a borrow pit near Courvoisier Creek. The pit is in an esker complex that contains sand and gravel.



| Sieve Size | Mass  | Percent Retained | Cumulative Frequency |
|------------|-------|------------------|----------------------|
| 4.0        | 0.0   | 0.00             | 100.00               |
| 2.0        | 0.0   | 0.00             | 100.00               |
| 1.0        | 0.0   | 0.00             | 100.00               |
| 0.500      | 8.2   | 1.84             | 98.16                |
| 0.250      | 339.2 | 76.11            | 22.06                |
| 0.125      | 68.7  | 15.41            | 6.64                 |
| 0.063      | 6.1   | 1.37             | 5.27                 |
| <0.063     | 23.5  | 5.27             | 0.00                 |

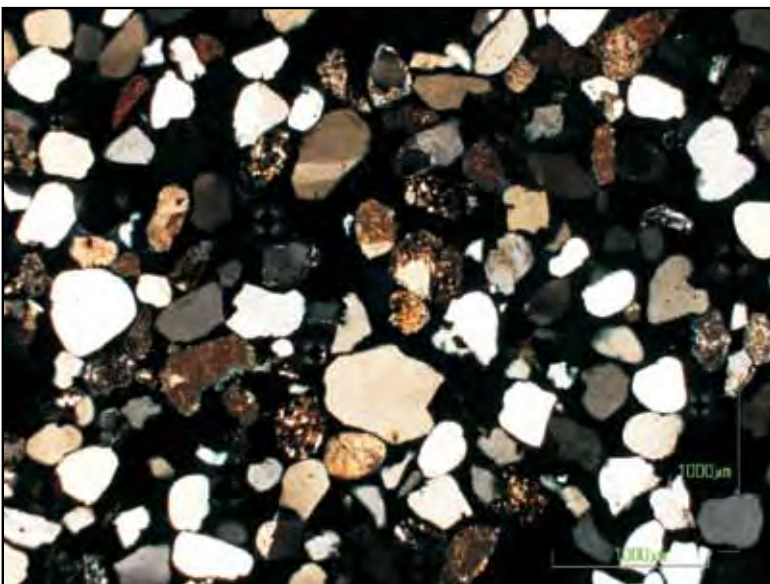
| Element                        | Percent |
|--------------------------------|---------|
| SiO <sub>2</sub>               | 85.97   |
| Al <sub>2</sub> O <sub>3</sub> | 4.16    |
| Fe <sub>2</sub> O <sub>3</sub> | 2.84    |
| MgO                            | 0.51    |
| CaO                            | 2.05    |
| Na <sub>2</sub> O              | 0.84    |
| K <sub>2</sub> O               | 1.16    |
| TiO <sub>2</sub>               | 0.13    |
| P <sub>2</sub> O <sub>5</sub>  | 0.09    |
| MnO                            | 0.02    |
| Cr <sub>2</sub> O <sub>3</sub> | 0.002   |
| LOI                            | 2.1     |



Binocular Microscope



Plane Light



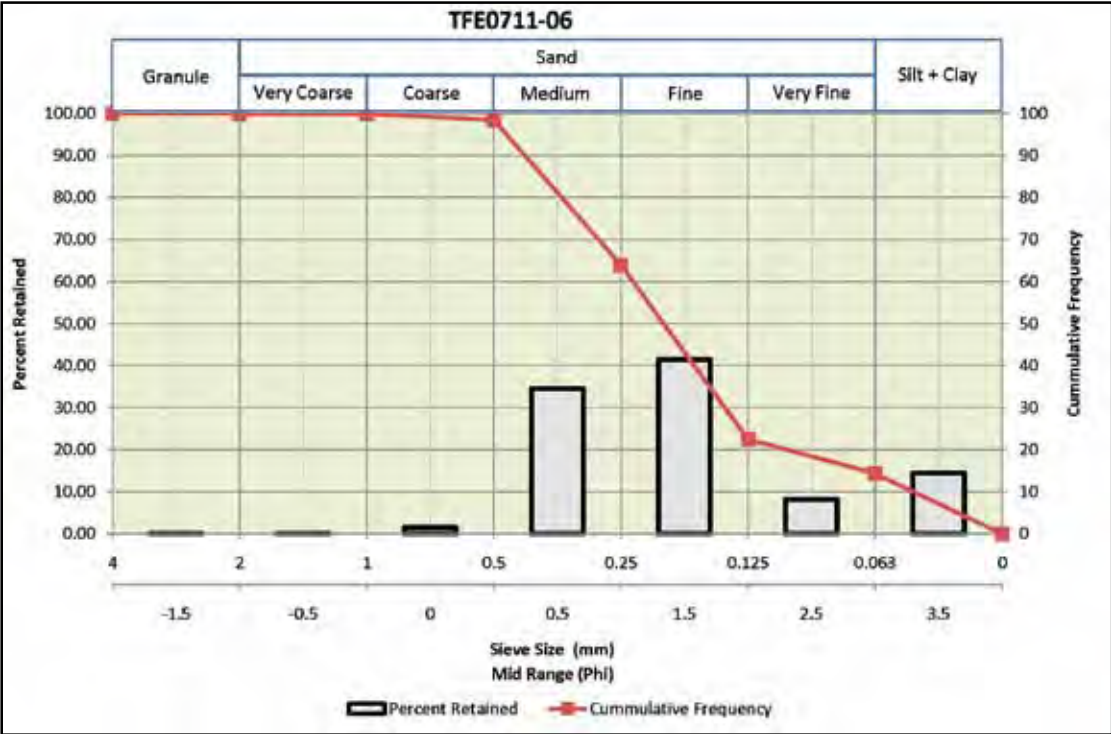
Crossed Nicols

|                       |                       |
|-----------------------|-----------------------|
| <b>Sample</b>         | TFE0711-06            |
| <b>Easting</b>        | 500943                |
| <b>Northing</b>       | 6642203               |
| <b>Genetic Origin</b> | Glaciofluvial (Esker) |



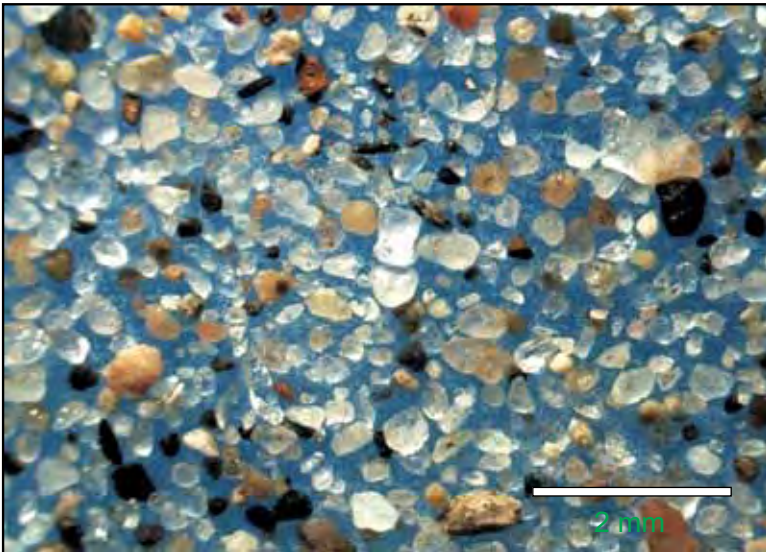
**Comment:**

The sample was collected from a 4 metres high esker west of the Liard Highway (Highway 77). The material in this deposit consist of a range of grain sizes ranging from pebble gravel to fine sand.

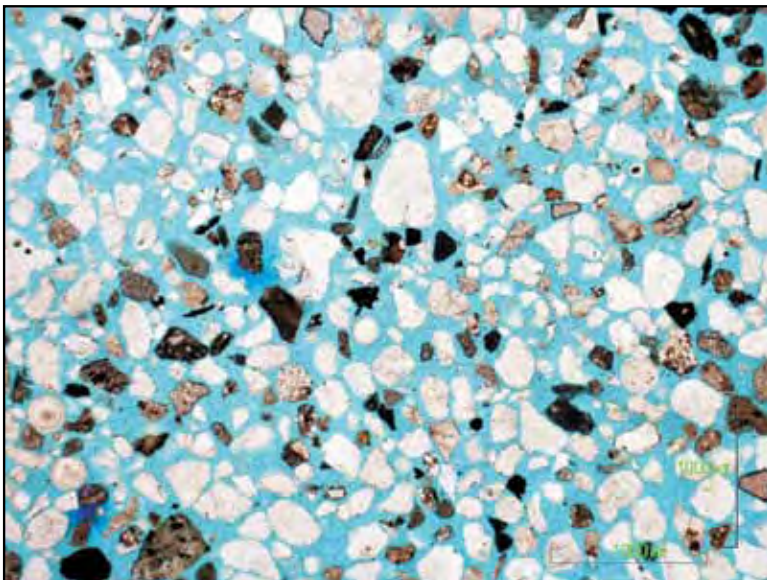


| Sieve Size | Mass   | Percent Retained | Cummulative Frequency |
|------------|--------|------------------|-----------------------|
| 4.0        | 0.0    | 0.00             | 100.00                |
| 2.0        | 1.3    | 0.10             | 99.90                 |
| 1.0        | 2.6    | 0.19             | 99.71                 |
| 0.500      | 65.3   | 4.87             | 94.84                 |
| 0.250      | 1065.1 | 79.38            | 15.46                 |
| 0.125      | 156.0  | 11.63            | 3.83                  |
| 0.063      | 12.0   | 0.89             | 2.94                  |
| <0.063     | 39.4   | 2.94             | 0.00                  |

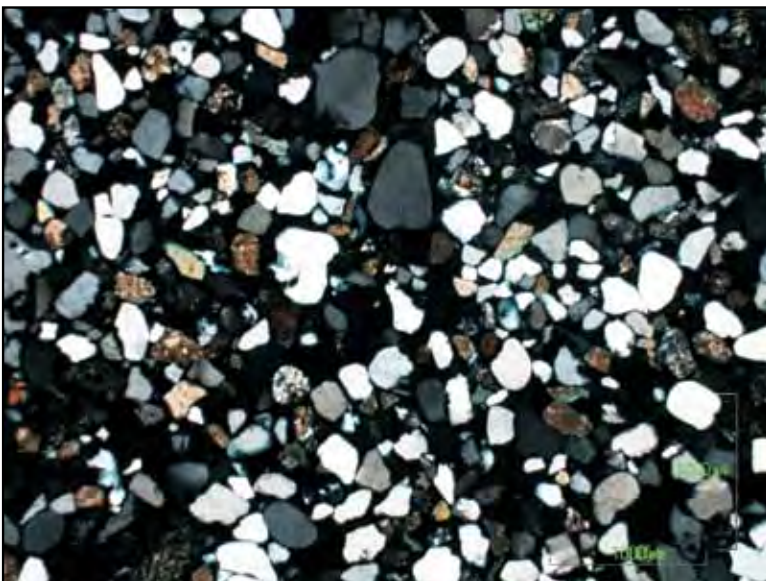
| Element                        | Percent |
|--------------------------------|---------|
| SiO <sub>2</sub>               | 80.41   |
| Al <sub>2</sub> O <sub>3</sub> | 4.51    |
| Fe <sub>2</sub> O <sub>3</sub> | 1.66    |
| MgO                            | 0.97    |
| CaO                            | 5.00    |
| Na <sub>2</sub> O              | 0.97    |
| K <sub>2</sub> O               | 1.26    |
| TiO <sub>2</sub>               | 0.12    |
| P <sub>2</sub> O <sub>5</sub>  | 0.08    |
| MnO                            | 0.02    |
| Cr <sub>2</sub> O <sub>3</sub> | <0.002  |
| LOI                            | 4.9     |



Binocular Microscope



Plane Light



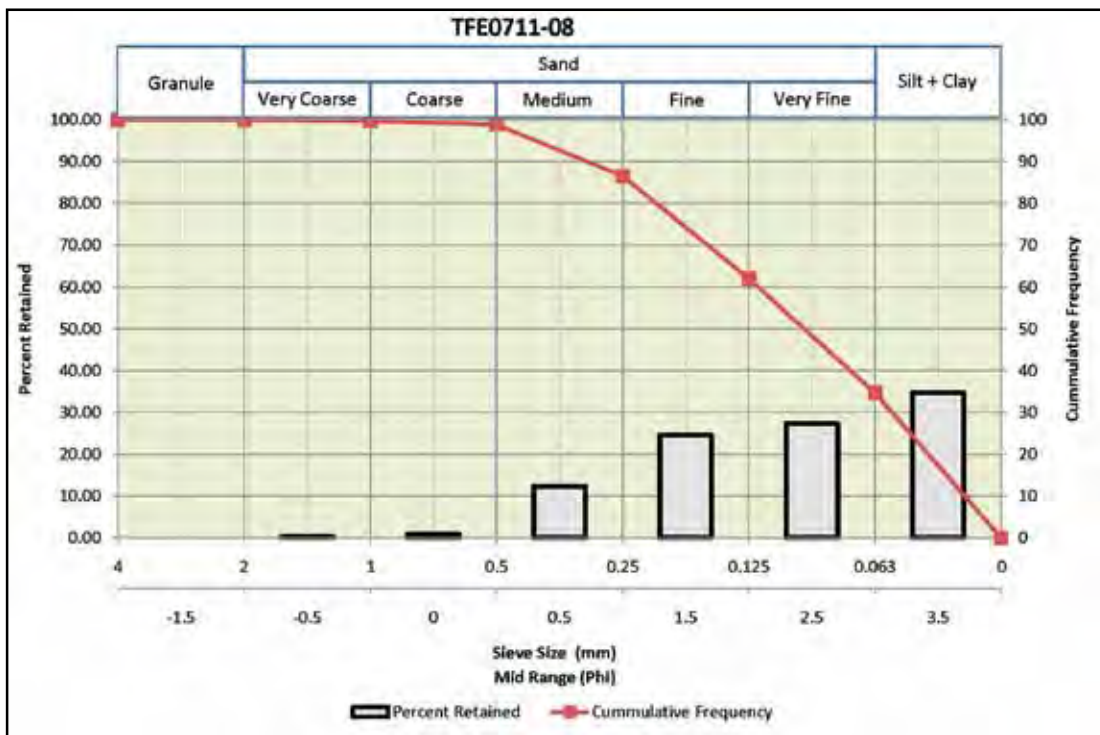
Crossed Nicols

|                       |                       |
|-----------------------|-----------------------|
| <b>Sample</b>         | TFE0711-08            |
| <b>Easting</b>        | 501341                |
| <b>Northing</b>       | 6641887               |
| <b>Genetic Origin</b> | Glaciofluvial (Esker) |



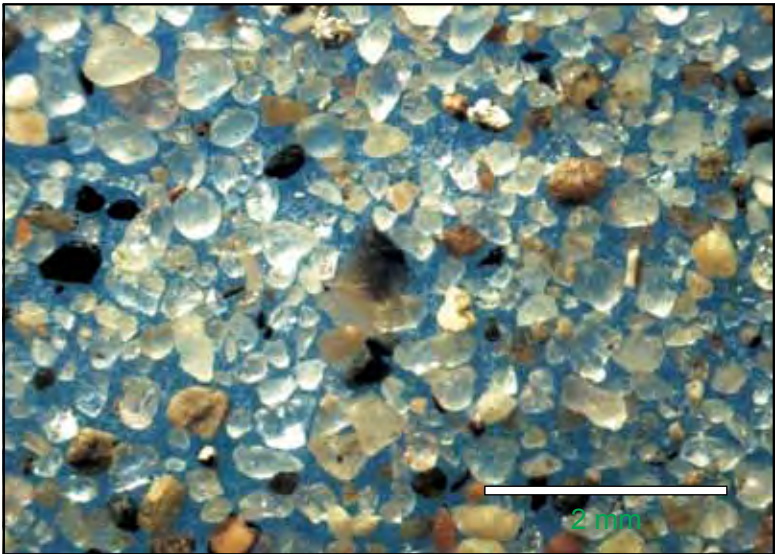
**Comment:**

Sample was collected one metre below surface in a small esker west of the Highway 77.

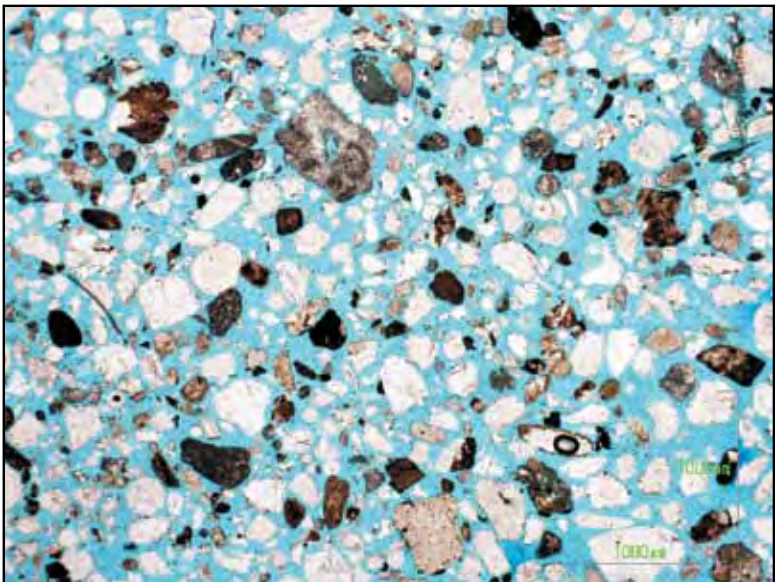


| Sieve Size | Mass  | Percent Retained | Cummulative Frequency |
|------------|-------|------------------|-----------------------|
| 4.0        | 0.0   | 0.00             | 100.00                |
| 2.0        | 0.0   | 0.00             | 100.00                |
| 1.0        | 5.6   | 0.25             | 99.75                 |
| 0.500      | 18.9  | 0.85             | 98.89                 |
| 0.250      | 272.6 | 12.30            | 86.60                 |
| 0.125      | 544.6 | 24.57            | 62.02                 |
| 0.063      | 605.5 | 27.32            | 34.70                 |
| <0.063     | 769.2 | 34.70            | 0.00                  |

| Element                        | Percent |
|--------------------------------|---------|
| SiO <sub>2</sub>               | 80.57   |
| Al <sub>2</sub> O <sub>3</sub> | 5.00    |
| Fe <sub>2</sub> O <sub>3</sub> | 1.72    |
| MgO                            | 1.03    |
| CaO                            | 4.19    |
| Na <sub>2</sub> O              | 1.03    |
| K <sub>2</sub> O               | 1.42    |
| TiO <sub>2</sub>               | 0.15    |
| P <sub>2</sub> O <sub>5</sub>  | 0.10    |
| MnO                            | 0.03    |
| Cr <sub>2</sub> O <sub>3</sub> | 0.002   |
| LOI                            | 4.7     |



Binocular Microscope



Plane Light



Crossed Nicols



# TRIASSIC POROSITY TRENDS IN NORTHEASTERN BRITISH COLUMBIA UPDATE FEBRUARY 2009

*E. Janicki<sup>1</sup>*

---

## ABSTRACT

*This report updates Triassic porosity-trend mapping from 2008 to identify possible sites for carbon storage and sequestration (CCS). Wireline logs from an additional 200 wells were added to the initial study of 600 wells to improve data density and extend the study area. A strong southeast Halfway Formation porosity trend, roughly adjacent to the edge of the deformed belt, was reaffirmed. The best prospects for CCS are likely to be found in thick, porous sections of the Halfway and Baldonnel formations near the southern end of the map area. Secure locations for CCS might also be located in several more isolated, lightly drilled areas around the edge of existing Triassic oil and gas production.*

Janicki, E. (2010): Triassic porosity trends in northeastern British Columbia — update February 2009; in Geoscience Reports 2010, BC Ministry of Energy, Mines and Petroleum Resources, pages 93–97.

<sup>1</sup>British Columbia Ministry of Energy, Mines and Petroleum Resources, Victoria, British Columbia

**Key Words:** Triassic, porosity, Halfway Formation, Baldonnel Formation, Carbon Capture and Storage (CCS), water disposal

---

## INTRODUCTION

After reviewing an initial set of Triassic porosity-trend maps published in 2008 (Janicki, 2008), additional data was collected from the central portion and around the edges of the map (Figure 1). In this subsequent phase of mapping, 213 well locations were added to the 600 wells selected in 2008 to enhance the overall result. Approximately one extra location per township or NTS block was added, employing the same set of well-log quality criteria used for the initial phase (e.g., newer wells and Compensated Neutron/Formation Density (CNFD) preferred). Attention was paid to finding suitable locations around the map edges to the north and west while the southern edge was extended by roughly one township. The same log criteria for porosity cut-offs (10% porosity for the Halfway Formation and 6% for the Baldonnel Formation) were used as in 2008.

Only the Halfway and Baldonnel formation maps were revised because they seem to hold the greatest promise for CCS among Triassic formations in this area. Both of these formations have long been used for the analogous activity of water disposal, and more recently for limited disposal of acid gas. Good Doig Formation porosity is scattered and of limited areal extent. Porosity in the various Charlie Lake Formation members tends to be thin and inconsistent.

## FINDINGS

### *Halfway Formation porosity*

The updated porosity mapping (Figure 1) of the Halfway Formation shows essentially the same southeast trend displayed in the previous version. Several thick accumulations are centred along the edge of the deformed belt, which may suggest that deep-seated structures played a role in influencing porosity distribution (the Laramide orogeny having occurred after the deposition of the Halfway Formation). A separate northeast data trend, which has been made a little more apparent with additional data, also appears to be related to deep-seated structural influences — in this case, the Great Slave Shear Zone.

Thick and wet (water-saturated) Halfway Formation porosity (Figure 1) might represent the best possible situation for CCS because good reservoir capacity can be inferred and there is no offsetting hydrocarbon production. The best area displaying these characteristics occurs at the southern edge of the map area, and to a lesser degree scattered throughout the central portion of the map, north of Fort St John.

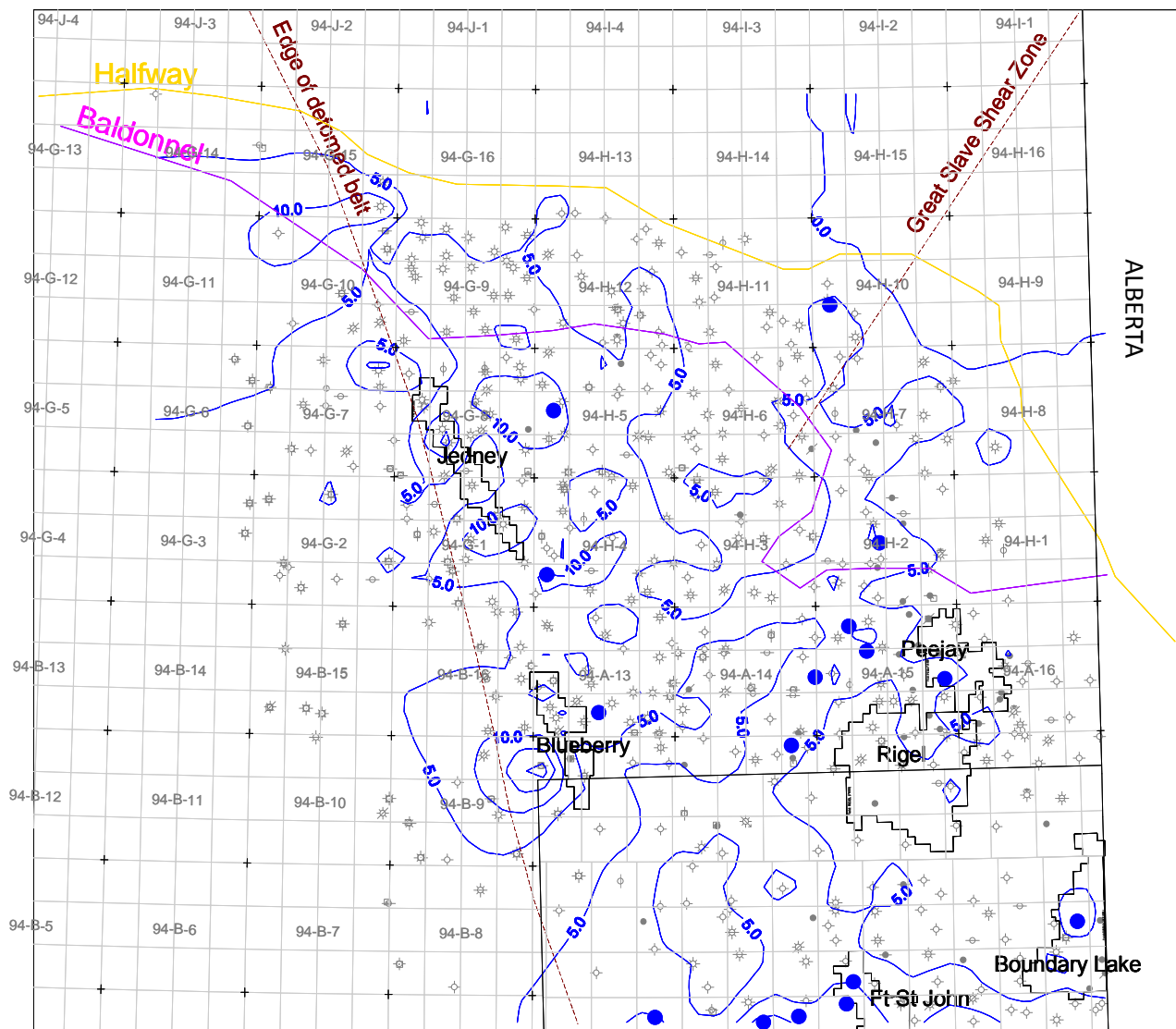


Figure 1. Halfway Formation porosity; contour interval 5 m. Blue dots represent wells where porosity in the Halfway Formation is thick, wet and possibly well suited for CCS. Selected oil and gas fields with production in the Halfway Formation are outlined in black. The Baldonnel Formation subcrop edge is indicated by magenta; the Halfway Formation depositional edge is in yellow. Wells included in this study are shown in grey. Petroleum and Natural Gas grid groups are indicated by 94-B-6, 94-B-7, etc. (Petroleum and Natural Gas Act, 1996). The Peace River Block is outlined in the southeast corner.

### ***Baldonnel Formation porosity***

Porosity trends are more difficult to distinguish for the Baldonnel Formation (Figure 2) than for the Halfway Formation because they are segregated into a few relatively thick areas isolated by intervening areas of low porosity. The single region of wet Baldonnel Formation porosity identified presents an interesting prospect for CCS because it is discretely concentrated into one small area at the southern end of the map (Figure 2), surrounded by relatively nonporous rock.

### **CARBON CAPTURE AND STORAGE**

Figure 3 shows some possible prospects for CCS in the map area. These are locations with greater than 10 m in the Halfway Formation, where the injection of carbon dioxide would likely occur sufficiently far from the existing boreholes to minimize the possibility of upward migration.

For the purpose of carbon capture and storage (CCS) and/or deep waste disposal, an ideal location should meet the following criteria, at least in part (Texas World Operations, 2008):

- It should have a thick and continuous porous section.
- It should have good matrix permeability.
- It should not be highly fractured.

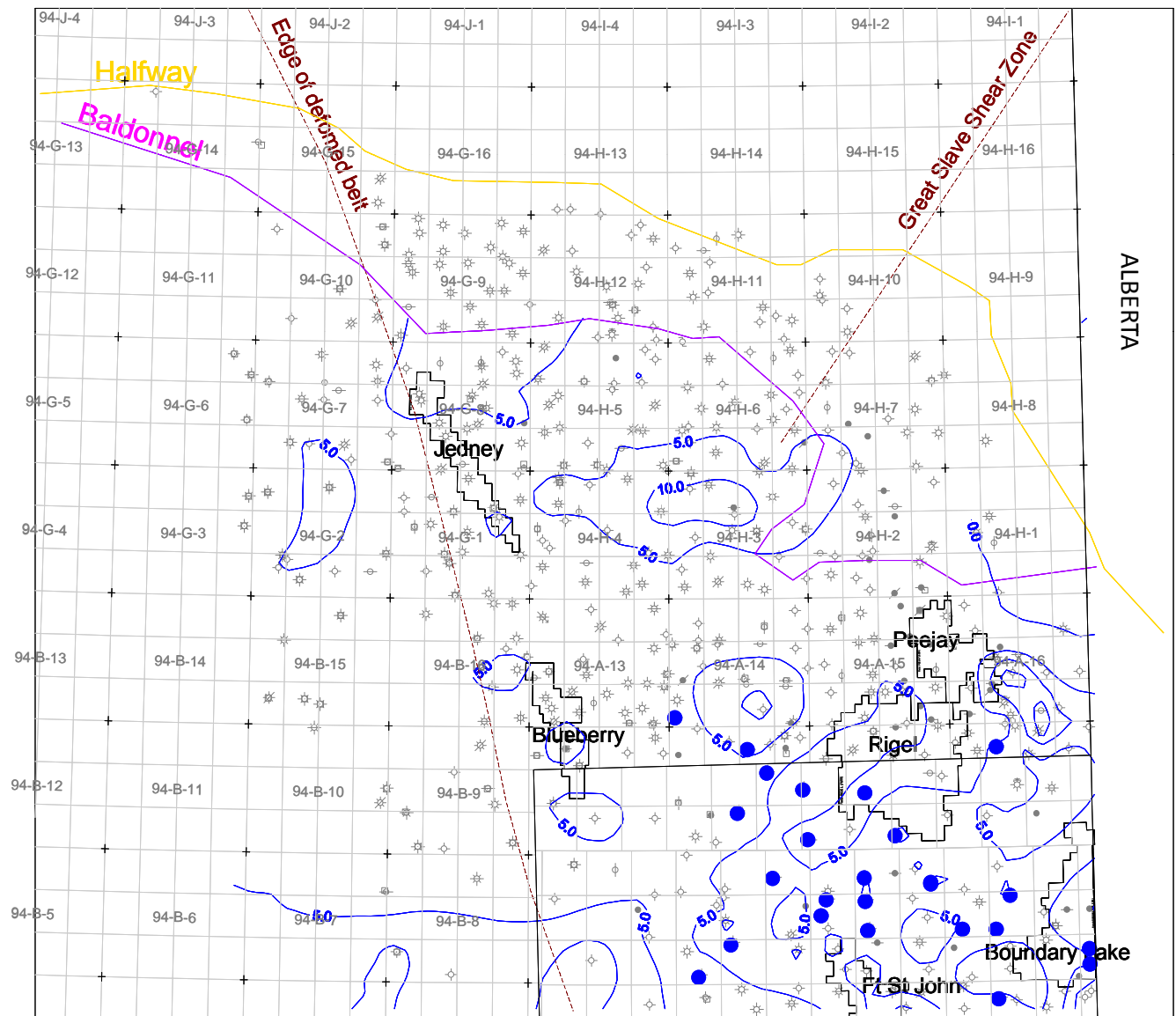


Figure 2. Baldonnell Formation porosity; contour interval 5 m. Trends may not be apparent, but the central part of the map area appears to be relatively less favourable for Baldonnell Formation porosity. Locations with wet Baldonnell Formation porosity are shown with blue dots.

- It should be isolated from other wells, producing or abandoned.
- It should have a good seal; the trap should be secure.
- It should be within a reservoir with readily defined boundaries, or within a large, slow-moving aquifer.
- It should be in a stable, unfaulted structure.
- It should preferably not be offset by hydrocarbon producers from the same reservoir to avoid potential conflicts.

Based on these criteria, the Halfway Formation appears to be more favourable than the Baldonnell Formation for CCS. Porosity in the Halfway Formation is usually in one thick, continuous zone, whereas Baldonnell Formation porosity is often divided into thin irregular streaks. Perme-

ability in the Halfway Formation is usually intergranular, whereas the Baldonnell Formation depends to a greater extent on natural fracturing to provide pathways for fluids or gas to flow. Porosity is also generally higher in the Halfway Formation, which would provide more storage capacity for CCS. The Halfway Formation has served as a water disposal zone at a number of wells in northeastern British Columbia (Janicki, unpublished work, 2008), so that gives reason to expect it to be appropriate for CCS as well. The Baldonnell Formation could also be acceptable for CCS because it is also used for water disposal with no reported incidents, but its tendency to fracture and the shallower depth are cause for further investigation.

A difficult, but important, criterion to satisfy in this study area is the preference for isolation from other wells.

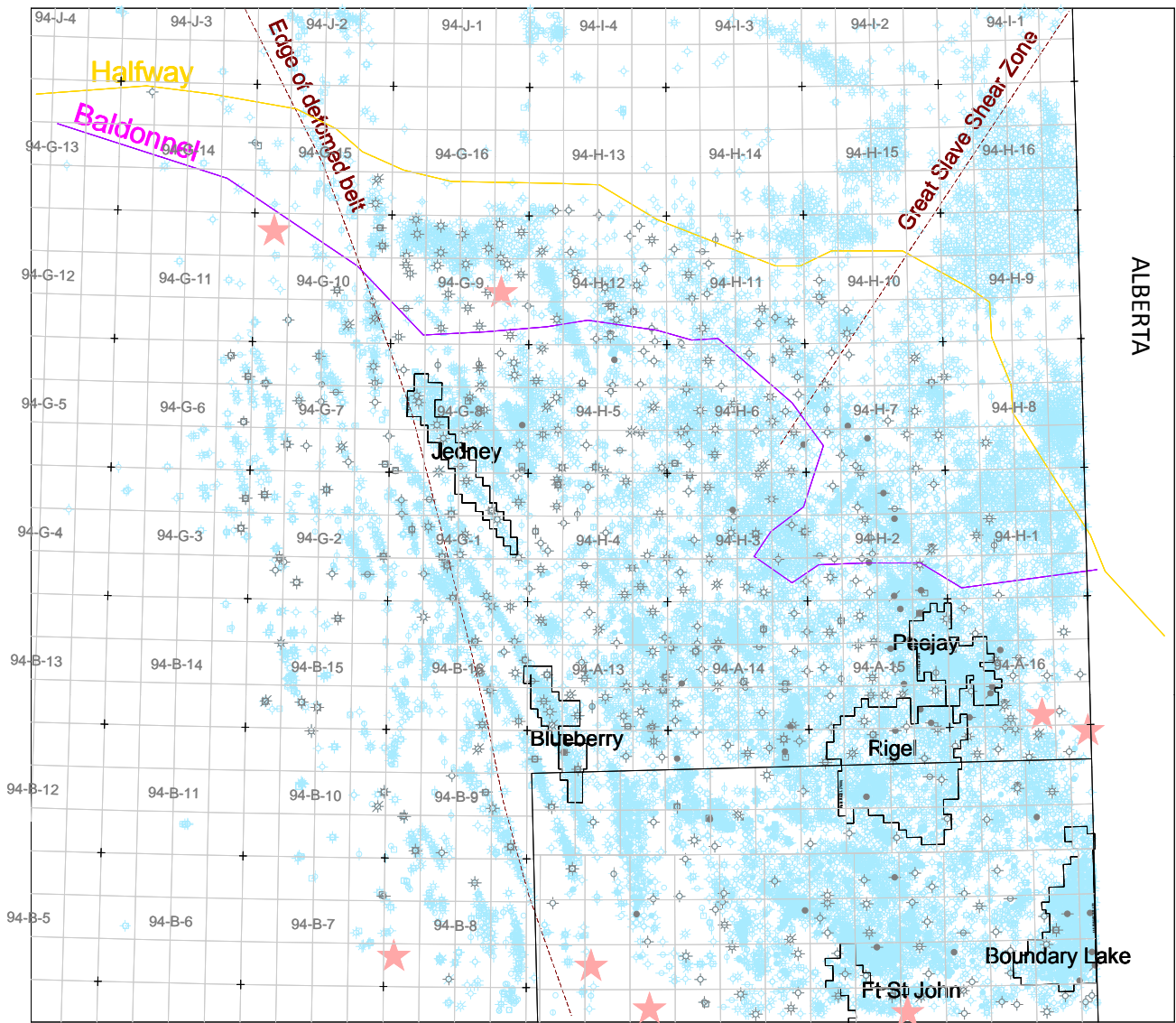


Figure 3. Suggested CCS locations in the Halfway Formation. Favourable locations for CCS are identified with pink stars. They may be sufficiently isolated from other boreholes to avoid uphole migration, and they have at least 10 m of rock with porosity greater than 10%. Wells selected for inclusion in this study are indicated by black well symbols; the balance of wells in the study area is indicated in light blue.

At the scale of mapping presented here, the density of drilling illustrates the difficulty of placing a CCS facility. Most of the areas mapped with thick Halfway or Baldonnell formation porosity rocks are surrounded by many existing wells. The use of these locations for CCS would require a stringent review of the integrity of the surrounding boreholes to ensure no leakage up improperly completed or abandoned boreholes. The locations suggested in Figure 3 could be drilled far enough from existing wells that it would likely take many years for CO<sub>2</sub> to reach the closest well. Further work would be required to ensure the suitability of site-specific CCS locations.

## CONCLUSIONS

Two hundred additional well data points were added to the Triassic porosity mapping originally done in 2008. Greater data density in the central regions of the map area was achieved along with greater control along the edges.

The Halfway Formation appears to be the most promising Triassic strata within the map area for the purpose of CCS, due to the more continuous nature of the porosity, deeper burial within the subsurface and proven storage capacity for water disposal. To avoid possible leakage up other boreholes, isolated areas with thick Halfway Formation porosity should initially be considered.

The Baldonnel Formation has generally less favourable characteristics for CCS due to its shallower depth of burial, lower porosity and the greater degree of fracturing. However, of note, the Baldonnel Formation has a long history of use for water disposal with no reported leakage or contamination issues.

The data used for this mapping have been compiled and are available upon request.

## REFERENCES

- Janicki, E.P. (2008): Triassic porosity trends in northeastern British Columbia; in Geoscience Reports 2008, *BC Ministry of Energy, Mines and Petroleum Resources*, pages 59–66.
- Petroleum and Natural Gas Act (1996): Chapter 361: petroleum and natural gas grid regulation, Regulation 536/2004; *BC Oil and Gas Commission, Queen's Printer*, Victoria, British Columbia, Revised Statutes British Columbia (RSBC), 79 p.
- Texas World Operations (2008): Class I UIC operator training; *Ground Water Protection Council* – January 2008, New Orleans, Louisiana.



# CONCEPTUAL WATER MODEL FOR THE HORN RIVER BASIN, NORTHEAST BRITISH COLUMBIA (PARTS OF NTS 094I, J, O, P)

*Elizabeth Johnson<sup>1</sup>*

---

## ABSTRACT

*Work was undertaken to develop a conceptual water model for the Horn River Basin (HRB). Water models are needed for resource management because of a rapidly growing water demand associated with shale gas development in northeast British Columbia. Lumped-parameter models are easier to generate, but for the scale of watersheds in the HRB, distributed-parameter models are more appropriate. A representative distributed-parameter model already exists for the Liard Basin. Modeling the spatial distribution and interrelationship between evapotranspiration, permafrost and muskeg is challenging in this relatively flat-lying region of forests, fens, bogs, numerous small and shallow lakes and discontinuous permafrost. Groundwater represents the mechanism by which peatlands retain water, lakes and uplands exchange water, and streamwater quality and quantity is maintained. Information gaps were also identified.*

Johnson, E. (2010): Conceptual water model for the Horn River Basin, northeast British Columbia (NTS 094O, parts of 094P, J); in Geoscience Reports 2010, *BC Ministry of Energy, Mines and Petroleum Resources*, pages 99–121

<sup>1</sup>British Columbia Ministry of Energy, Mines and Petroleum Resources, Victoria, British Columbia

**Key Words:** Horn River Basin, surface water, climate, peatland, muskeg, permafrost

---

## INTRODUCTION

Recent shale gas exploration and development in the Horn River Basin (HRB) region of northeastern British Columbia has created a demand for large amounts of water to hydraulically fracture shale and release trapped gas. To sustainably<sup>1</sup> develop surface-water resources to meet this growing demand, sound water models are required. This paper generates a conceptual model that summarizes the current understanding of the key catchment processes, dependencies and impacts on the water resource. It also highlights public information resources for the Horn River Basin.

Developing models in the Horn River Basin region is challenging. The region has low relief with patchy to widespread wetland. The wetland, predominantly sphagnum moss and black spruce forest, is universally referred to as muskeg, but is more properly classified as fens and bogs. Fens have a surface water–groundwater connection and network with lakes and streams to channel water off the landscape, while bogs function as reservoirs in isolation from groundwater and are interconnected only when the water table is sufficiently high. Another challenge to modeling is discontinuous permafrost and heavy seasonal ground frost in the region. Infiltration and overland flow are impacted by the depth to ice and the thickness of ground frost.

The goal of this paper is to outline important information sources for the HRB and identify features that will affect hydrological predictions in the HRB. This paper is divided into three sections: first, a discussion of water model types and regional models in existence for the HRB; second, a review of publicly available data and hydrogeological implications of important complexities particular to the HRB (including climate, permafrost, lakes and streams and muskeg); and third, a discussion of information gaps.

---

<sup>1</sup>Sustainability is defined by the Council of Canadian Academies (2009) as the following:

- (1) Protection of groundwater supplies from depletion: Sustainability requires that withdrawals can be maintained indefinitely without creating significant long-term declines in regional water levels.
- (2) Protection of groundwater quality from contamination: Sustainability requires that groundwater quality is not compromised by significant degradation of its chemical or biological character.
- (3) Protection of ecosystem viability: Sustainability requires that withdrawals do not significantly impinge on the contribution of groundwater to surface water supplies and the support of ecosystems. Human users will inevitably have some impact on pristine ecosystems.
- (4) Achievement of economic and social well-being: Sustainability requires that allocation of groundwater maximizes its potential contribution to social well-being (interpreted to reflect both economic and noneconomic values).
- (5) Application of good governance: Sustainability requires that decisions as to groundwater use are made transparently through informed public participation and with full account taken of ecosystem needs, intergenerational equity and the precautionary principle.

## BACKGROUND

### *Horn River Basin Location and Geography*

The Horn River Basin (Figure 1) is located in north-eastern British Columbia between Fort Nelson and the Northwest Territories border (mostly in NTS map area 094O eastward into 094P and southward to 094J). Located in the Fort Nelson Lowland of the Alberta Plateau, the area has very low relief (300–730 m above sea level), with the Etsho Plateau forming a minor upland, oriented southeast in the central region (Holland, 1976). The Muskwa Uplands of the Rocky Mountains can just be seen along the southwestern map edge. Two major drainage systems are incised up to 150 m below the general level of the lowland: the Fort Nelson River and the Petitot River, which are tributaries of the Liard River system. In total, the Horn River Basin contains portions of three major watersheds (Figure 2), which drain into the Mackenzie River system. The Fort Nelson and Petitot rivers flow into the Liard River, whereas the Hay River drains into Great Slave Lake. Table 1 gives the overall area of the watersheds and the catchment area within the Horn River Basin (HRB) calculated on the basis of the subwatersheds. Subwatersheds are considered part of the HRB if any portion of the watershed is within the boundary.

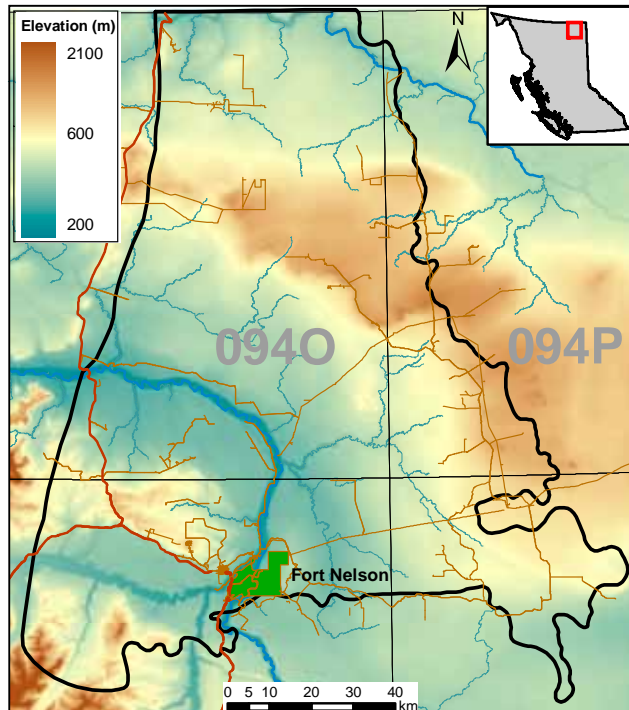


Figure 1. Topography of the Horn River Basin.

The broader HRB area is characterized by muskeg and a black spruce forest. Black spruce bogs are prevalent, especially in the northeast. In drier areas of the HRB, there are stands of white spruce and trembling aspen. Overall, forest productivity is generally low due to long, cold winters and short growing seasons. Winter temperatures average  $-18^{\circ}\text{C}$  between November and February. There is discontinuous permafrost throughout the region. The region is relatively dry (annual average precipitation of approximately 450 mm; Environment Canada, 2009). Because of the low relief and muskeg-dominated headwaters, river flows tend to be stable and laminar in highly incised channels and waters have a tannic character. In the summer, flow volumes are low and water temperatures are high (Anderson et al., 2009).



Figure 2. Watersheds of the Horn River Basin. Large colour groupings identify the three major watersheds (i.e., Petitot, Fort Nelson and Hay). Heavy green outlines define the watersheds. Subwatersheds are defined in light grey. The outline of the Horn River Basin is in red.

### *Demand for water in the HRB*

The increased demand for water is primarily owed to hydraulic fracturing, the stimulation technique necessary for the economic development of tight and shale gas. To develop shale gas plays, hydraulic fracturing (herein referred to as ‘frac’ or ‘fracing’) is used to create fractures in the shale that increase borehole access to the gas trapped in the rock. Fracing requires high pressures and injection rates to create fractures around the borehole. A proppant such as sand is added to the water to prevent the fractures from closing again. In the HRB, these fracs are generated with substantial volumes of water with estimates ranging from 1 200 m<sup>3</sup> to over 4 000 m<sup>3</sup> of water per frac depending on

TABLE 1. WATERSHEDS IN THE HORN RIVER BASIN.

| Major watershed          | Watershed                | Total Area (km <sup>2</sup> ) | Area in HRB (km <sup>2</sup> ) |
|--------------------------|--------------------------|-------------------------------|--------------------------------|
| <b>Fort Nelson River</b> | Lower Fort Nelson River  | 4 905                         | 2 980                          |
|                          | Lower Muskwa River       | 3 345                         | 2 258                          |
|                          | Lower Prophet River      | 1 589                         | 612                            |
|                          | Middle Fort Nelson River | 3 051                         | 3 001                          |
|                          | Sahtaneh River           | 4 114                         | 3 780                          |
|                          | Upper Fort Nelson River  | 3 737                         | 349                            |
|                          | <b>TOTAL</b>             | <b>53 891</b>                 | <b>12 981</b>                  |
| <b>Hay River</b>         | Kotcho Lake              | 4 163                         | 2 812                          |
|                          | <b>TOTAL</b>             | <b>8 098</b>                  | <b>2 813</b>                   |
| <b>Petitot River</b>     | Lower Petitot River      | 4 169                         | 3 447                          |
|                          | Tsea River               | 3 597                         | 1 095                          |
|                          | <b>TOTAL</b>             | <b>12 083</b>                 | <b>4 542</b>                   |

geology and engineering (Johnson, 2009; Hayes, 2010). An average well may contain six to eighteen fracs, so the water requirement for one well could be as low as 7 000 m<sup>3</sup> or more than 60 000 m<sup>3</sup>. The density of water demand depends partly on the well configuration. The HRB is expected to have three to eight wells per gas spacing unit (approximately 240 ha; R. Stefik, pers comm, 2008).

The amount of water used in multistage fracturing of a well varies widely. Unlike vertical wells, whose length is constrained by the thickness of the formation, horizontal well laterals can be extended as far as technology allows. A better metric for water use in horizontal wells is water use ‘intensity,’ or water volume per unit lateral length. This metric is more informative and is easily scalable to future work (Bene et al., 2007). Early data indicates water use in the Horn River Basin is similar to that in the Barnett shale in Texas, where volumes range from 25 to 40 m<sup>3</sup> per lateral metre drilled.

Permission to use surface water for oil and gas-related activities is either licensed by the British Columbia Ministry of Environment or temporarily granted by the Oil and Gas Commission under Section 8 of the Water Act (Water Act, 2010). There is currently one active water license in the HRB. Temporary water permits are issued for a volume per diem or total volume per permit. As of October 2009, there were 210 active Section 8 permits in northeast BC.

### **Watershed Modeling**

The most reliable decision support tool for water allocation decisions and water resource management is a water balance with supporting water model(s). Watershed models are necessary in the HRB to: 1) characterize and develop an understanding of groundwater and surface-water processes in the watershed and 2) provide spatial and temporal

hydrological datasets for use by water-resource managers in decision-making concerning stream habitat, land use and water use.

The province encourages the use of water models in water-management plans. Recently, the Township of Langley, under Part 4 of the Water Act, collaborated with the province to develop British Columbia’s first water-management plan. At its core were a conceptual model and a numerical hydrogeological model. The conceptual model is a descriptive model of the system based upon qualitative assumptions about its elements, interrelationships and system boundaries.

Water models are based on a water balance where the amount of water incoming to a region balances with the amount outgoing plus changes in groundwater storage. For example, a lake has a given volume of water that is maintained (balanced) by inputs (precipitation, inflowing streams and groundwater flow into the lake) and outputs (discharge from the lake, evaporation and transpiration and groundwater flow out of the lake). The goal is to generate an accurate and efficient simulation of water-system mechanics within the watershed.

To develop appropriate watershed models, information is required about

- precipitation and drainage area (to determine input volume of water);
- land use, soil types and permafrost (to determine how much water infiltrates to the water table);
- slope (to determine the rate water reaches the drainage outlet);
- land cover of vegetation and lake abundance and size (to determine rates of evapotranspiration);
- climate data (to determine seasonality, snow-water equivalent and runoff); and

- streamflow data and water-level data (to understand discharge and storage diversion data).

Water models can range from simple to very complex. There are two styles of watershed models: spatially lumped (low-resolution) models using basin-averaged input data and spatially distributed (high-resolution) models. Watershed models are strengthened if they can account for heterogeneity of vegetation, soils and land-use characteristics in the watershed; however, each additional component increases the complexity of the model. For the size of watersheds in the HRB, a spatially distributed model would be most appropriate because distributed models have resolutions on the order of 150 m. The most commonly used distributed hydrological models, in order of decreasing popularity, are HBV, HEC-HMS, UBCWM, TOPMODEL, HSPF, SWAT, SHE, SAC-SMA, VIC, DHSVM and WATFLOOD (Beckers et al., 2009).

A ‘conceptual model’ defines the base assumptions employed to make the model simulate reality. The assumptions used when modeling can dramatically affect the results. Table 2 exemplifies the sensitivity of a single predicted variable, evapotranspiration, to different assumptions in a low-relief northern boreal forest (northern study site for BOREAS; Soulis and Seglenieks, 2005). For three land-cover types, evapotranspiration was calculated three ways: 1) a simple model with no subsurface water transport and no permafrost, 2) a model allowing for subsurface lateral transport of water and no permafrost and 3) a model allowing for subsurface lateral transport of water and ice in the soil. The resulting estimates of evapotranspiration vary substantially across the three models. Differences are not consistent; they change with the season (summer versus

fall) and the saturation of the soil (wet versus dry forest). The conceptual model dictates whether permafrost or lateral flow is important.

### Modeling Complexities of the HRB

Water modeling in the HRB is complicated by several considerations, including low topography, peatland, discontinuous permafrost and lack of independent data from monitoring stations.

The HRB is an area of low relief. In high-relief areas, drainage pathways are clearly delineated, rivers respond quickly to rainfall events and infiltration periods are limited. In low-relief areas, total discharge is low because snow water is retained on the landscape and stored in soils above frost and in wetlands through spring. Drainage is slow, water infiltration can occur across broad areas and streams can be difficult to identify (Figure 3). The drainage characteristics are typified in the following account:

*“Few of the reaches sampled were found to be streams (17%). The remainder of the reaches assessed were wetlands, unchannelized drainage areas, or areas where no visible channel was found... Watercourses identified as intermittent on TRIM maps (as indicated by discontinuous lines) were often found to be swamps or to have no visible channel...”*

*(Golder Associates Ltd., 1998)*

TABLE 2. EVAPOTRANSPIRATION FOR THE BOREAS STUDY AREA USING DIFFERENT WATCLASS MODELS (SOULIS AND SEGLENIEKS, 2005).

| Modeled Evaporation  |        | No lateral flow, no permafrost |     | Lateral flow, no permafrost |     | Lateral flow, permafrost |  |
|----------------------|--------|--------------------------------|-----|-----------------------------|-----|--------------------------|--|
|                      |        | mm                             | mm  | % change                    | mm  | % change                 |  |
| <b>a) Dry Forest</b> | Spring | 77                             | 92  | <b>19</b>                   | 169 | <b>119</b>               |  |
|                      | Summer | 156                            | 134 | <b>14</b>                   | 203 | <b>30</b>                |  |
|                      | Fall   | 10                             | 3   | <b>75</b>                   | 24  | <b>137</b>               |  |
|                      | Annual | 243                            | 229 | <b>6</b>                    | 400 | <b>65</b>                |  |
| <b>b) Wet Forest</b> | Spring | 115                            | 102 | <b>11</b>                   | 149 | <b>30</b>                |  |
|                      | Summer | 148                            | 124 | <b>17</b>                   | 156 | <b>5</b>                 |  |
|                      | Fall   | 9                              | 3   | <b>130</b>                  | 13  | <b>45</b>                |  |
|                      | Annual | 274                            | 224 | <b>19</b>                   | 321 | <b>17</b>                |  |
| <b>c) Wetland</b>    | Spring | 118                            | 105 | <b>11</b>                   | 159 | <b>35</b>                |  |
|                      | Summer | 155                            | 126 | <b>19</b>                   | 166 | <b>7</b>                 |  |
|                      | Fall   | 10                             | 1   | <b>108</b>                  | 13  | <b>31</b>                |  |
|                      | Annual | 285                            | 232 | <b>19</b>                   | 341 | <b>20</b>                |  |



Figure 3. Unchanneled drainage in wetland. Photo by Elizabeth Johnson.

The presence and type of wetland is very important to hydrological modeling. For most land-cover types, infiltration allows the downward flux of precipitation to the water table. In peatland, however, subsurface shallow flow is mainly horizontal and there is virtually no downward conductivity of water. Rainfall runoff is routed through bogs and fens. Fens promote lateral flow, whereas bogs efficiently store water. The quantity of fen coverage on the landscape is directly related to runoff, whereas the prevalence of bogs is inversely related to runoff. Lack of topographic relief, absence of well-defined channels and shallow groundwater tables all combine to make peatlands behave hydrologically like unregulated shallow reservoirs. Beyond wetlands themselves, the depth and texture of surficial deposits influence the extent, ephemeral nature and type of flowpath connecting slopes to streams, wetlands and lakes (Devito et al., 2005).

The HRB lies in an area of discontinuous permafrost. The distribution of permafrost is important to hydrological modeling as the presence of ice impedes the downward infiltration of surface water and limits water storage to a thin surficial layer. The discontinuous nature of permafrost makes it difficult to assess soil as a lumped parameter or to define similar hydrological response units.

Finally, modeling of the hydrological systems in the HRB is limited by the lack of ground-based monitoring for calibration. River gauge stations tend to be developed in densely populated areas and on large water systems. The Horn River Basin is a remote region with mostly smaller, slow-moving water systems (other than the Fort Nelson and Petitot rivers). The most pertinent active station for the HRB is on the Liard River at Fort Liard in the Northwest Territories. There are discontinued stations on the Fort Nelson and Petitot rivers. Weather data is monitored hourly at Fort Nelson, BC and Fort Liard, Northwest Territories dating back to 1953 and 1973, respectively. Groundwater data from shallow-water wells is located near Fort Nelson.

## AVAILABLE DATA

Water availability can be estimated from models that incorporate climate (precipitation, temperature, evapotranspiration, wind, radiation, pressure, etc.), land cover, soil type, topography and stream discharge. The remainder of this paper details available data useful for structuring and parameterizing models. Much of this information is available indirectly. One source of information widely available but generally not considered by resource managers are large-scale hydrological models. These models provide coarse-resolution information and constrain unknown variables for the region. There are several models available for cross reference and the input data and results are often available without fee.

### *Hydrogeological modeling*

Acquiring the necessary data can be difficult. There are many global and regional databases that provide data and hydrological models on major drainage systems of the world. The Water Systems Analysis Group at the University of New Hampshire provides a comprehensive listing of global hydrological consortiums that provide data (Water Systems Analysis Group, 2010). In particular, ArcticRIMS (2000; Rapid Integrated Monitoring System) combines several well-established datasets to produce time-varying, region-wide land surface water budgets across the pan-Arctic drainage region (including the Mackenzie Basin). Algorithms include vapour flux convergence, a satellite-derived snow product, a permafrost water-balance model, a water transport model and simulated river networks. Products include components of the water cycle (atmospheric convergence, precipitation, evapotranspiration, change in soil, snowpack, shallow groundwater, runoff and river discharge) and estimates of potential error. Nominal resolution is 25 km with daily time steps.

Researchers within the Mackenzie GEWEX (Global Energy and Water Cycle Experiment) Study (MAGS) developed distributed hydrological models for larger basins with the Mackenzie River drainage (e.g., Liard River, Peace River, Athabasca River) using WATFLOOD and WATCLASS hydrological models (Burn et al., 2004; Soulis and Burn, 2004). The model was constructed at 20 km resolution. Notice the excellent agreement between observed discharge and modeled discharge for the Liard River at Fort Liard in Figure 4. The Nash goodness-of-fit coefficient is 0.77 (where values less than 0 indicate the observed value is a better predictor and 1 represents a perfect fit; Soulis and Seglenieks, 2005). This station is just downstream of the confluence of the Fort Nelson River and the Liard River.

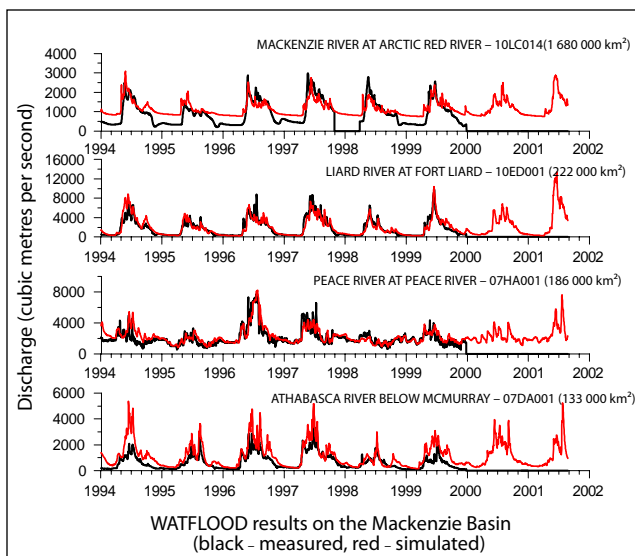


Figure 4. Observed and simulated discharge in the Mackenzie Basin using the WATFLOOD distributed hydrological model (Souliis and Burn, 2004).

A separate independent method for validating the WATFLOOD hydrological model of the Liard Basin involved a comparison of estimated and observed water storage. Remotely sensed data from GRACE (the Gravity Recovery and Climate Experiment) produces integrated geopotential anomalies that relate directly to stored water. In 2002, the GRACE satellite observations showed a gain in storage of 10 mm compared to 7 mm for the WATFLOOD model. In 2003, the GRACE satellite estimated a loss of  $-1.3$  mm, whereas WATFLOOD averages were  $-3.1$  mm (Souliis and Seglenieks, 2005). Recent work by Yirdaw et al. (2009) indicates 70% correlation in the Liard Basin between GRACE total water storage and storage calculated from an atmospherically based water balance model between 2002 and 2005 (Figure 5).

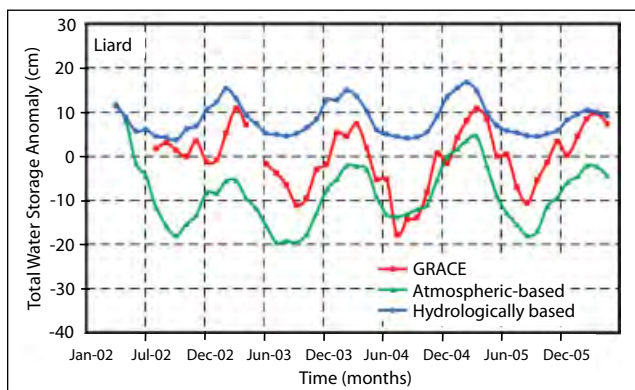


Figure 5. Total water storage anomalies derived from GRACE, atmospheric-based water balance techniques and WATCLASS for the Liard sub-basin (Yirdaw et al., 2009).

The Dartmouth Flood Observatory (DFO) provides another independent means of validating estimated discharge. River discharge is estimated using a surface wetness method that relates changes in river width to changes in river volume. The DFO's River Watch tool uses satellite-based brightness temperatures to estimate river discharge at over 2500 selected river measurement sites globally. The Liard River at Fort Liard (coordinates 61.3703,  $-121.8324$ ) is one of those sites. They have collected data from 2002 to 2009 (Figure 6).

Models for watersheds in the 10–50 km<sup>2</sup> range should be consistent with models for the larger Liard River watershed. They require finer resolution on spatial input parameters like vegetation and climate and are much more sensitive to the effects of muskeg, soil, water-table elevation and local topography.

### Climate Data

Climate data are available from several sources. Climate data from the Fort Nelson weather station (Fort Nelson A at 58.84°N, 122.6°W) are available from Environment Canada. Daily data exists from 1937 to present. Ground snow data collection began in 1955. The British Columbia Ministry of Environment provides Fort Nelson snow pillow data from 1966 to present. Meteorological researchers have used climate observations from across Canada to create gridded data at roughly 50 km spacing. A widely available 30 year set of temperature and precipitation has been created for the interval of 1961 to 1990 (Hopkinson, 2000; IPCC, 2008; Girardin et al., 2006). Agriculture Canada has recently released 10 km gridded climatic data from across Canada for 2004–2008, which may be useful for finer-resolution watershed models. Additionally, there are many gridded regional and global datasets where climate is estimated from models including the National Centers for Environmental Prediction — Global Reanalysis 2 (NCEP-R2), the European Centre for Medium-Range Weather Forecasts 40 year Global Reanalysis (ERA-40) and the Canadian Meteorological Centre (CMC) Global Environmental Multiscale model (GEM) Regional Analysis, to name a few. These models incorporate multiple parameters of observed and remotely sensed data to estimate climate variables. This modeled data is commonly available at coarse resolution (2.5°) but modeled climate is a rapidly advancing field of study and finer-resolution models (0.5°) are becoming available.

### Spatial Analysis

Gridded data are useful for understanding the spatial variability of climate across the Horn River Basin. The Meteorological Service of Canada interpolated data from 1961

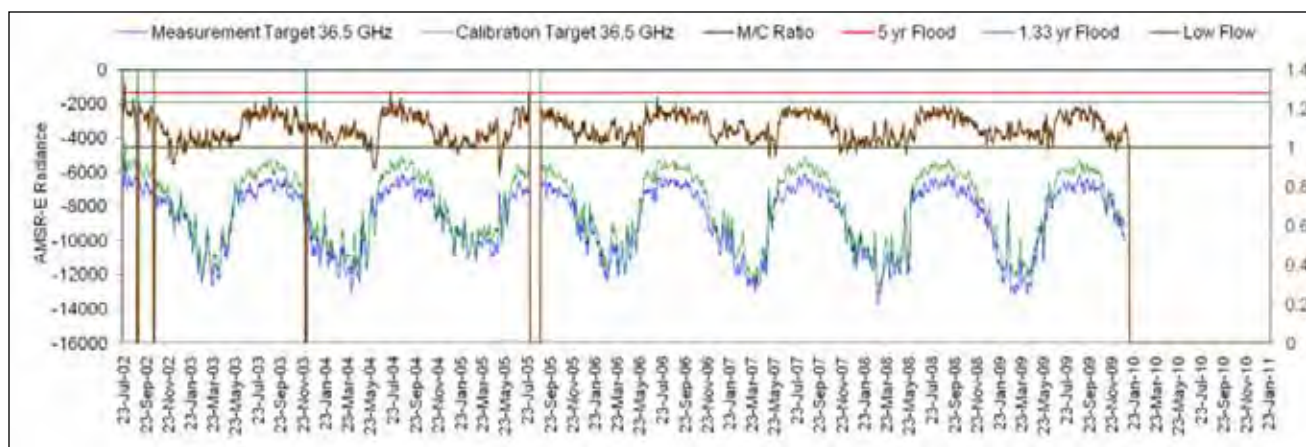


Figure 6. Discharge from the Liard River at Fort Liard as measured by 36 GHz brightness temperature. Discharge is estimated directly via a rating equation from the remote-sensing data (M/C ratio) shown below. The green line records an upwelling microwave emission from a land parcel (~10 km × 10 km) near the river and the blue line from a parcel centred over the river. The brown line is their ratio (M/C; scale on right) and is used to estimate river discharge via a rating equation (Dartmouth Flood Observatory, 2009).

to 1990 from climate observation stations across Canada. Monthly mean temperature and total precipitation data were interpolated to a 50 km grid on polar stereographic secant projection true at 60°N aligned north along 111°W (Hopkinson, 2000; IPCC, 2008). The size of the Horn River Basin (over 150 km long and from 50 to 140 km wide) is large enough to include more than ten cells.

Mean monthly temperature and precipitation data were averaged for three-month seasons (December-January-February, DJF; March-April-May, MAM; June-July-August, JJA; and September-October-November, SON). Figures 7 and 8 show the spatial variation in surface air temperature and precipitation, respectively, across the Horn River Basin for all four seasons.

In this northern region of low topographic relief, temperature varies mostly with latitude as a function of solar radiation: colder in the north, warmer in the south. The temperature is moderated by the Muskwa Ranges of the Rocky Mountains to the west of the HRB (see Figure 1). The air is warmer proximal to the base of the mountains in the winter.

Precipitation is governed by the Rocky Mountains. Precipitation patterns run parallel to the mountains with regions proximal to the mountains having heavier snow accumulation in winter and greater rainfall in summer. Annual precipitation (Figure 9) varies widely between 420 and 510 mm per year with the driest areas along the eastern edge of the HRB. The spatial distribution of wetland and lakes does not correlate with precipitation abundance. For example, land cover over the Petitot Plain is dense wetland, yet that region receives far less precipitation than in the southwest.

Evapotranspiration (ET) is the dominant means of water loss in the area, yet it is very difficult to quantify precisely. Studies in the Liard River Basin from just north of the HRB indicate that evapotranspiration accounts for two-thirds to

three-quarters of the annual precipitation input (Quinton and Hayashi, 2005). Quinton and Hayashi (2005) estimated annual ET rates of 241, 245, 271 and 297 mm in the nearby Birch, Blackstone, Jean-Marie and Scotty watersheds, respectively. They confirmed this estimate using a chloride mass-balance approach in Scotty Creek (282 mm/yr). There is more than 5% error between different ET measurement styles for Scotty Creek, but this is an excellent correlation given the uncertainties inherent in ET measurement.

## TIME SERIES ANALYSIS

Data were reorganized and analyzed to generate a mean, maximum, minimum and standard deviation for each calendar day (Julian day) for up to 61 years of data. Melting degree days (the temperature difference above 0°C over time) were calculated from temperature data. Snow on the ground measurements were converted to snow water equivalent (SWE) using mean snow density measurements from the British Columbia Ministry of Environment's Fort Nelson snow pillow data (1966–present) (BC Ministry of Environment, 2009). The Canadian Drought Code (CDC) was calculated using temperature and potential evapotranspiration.

### Seasonal Breaks

Seasonal breaks were evaluated using melting degree days, snow on the ground and mean temperature and precipitation type. Figure 10 shows the changing volume of snow throughout the year with accumulation beginning in September and loss (melting) beginning in March and continuing until no snow exists in May. Rainfall begins in April and continues through November.

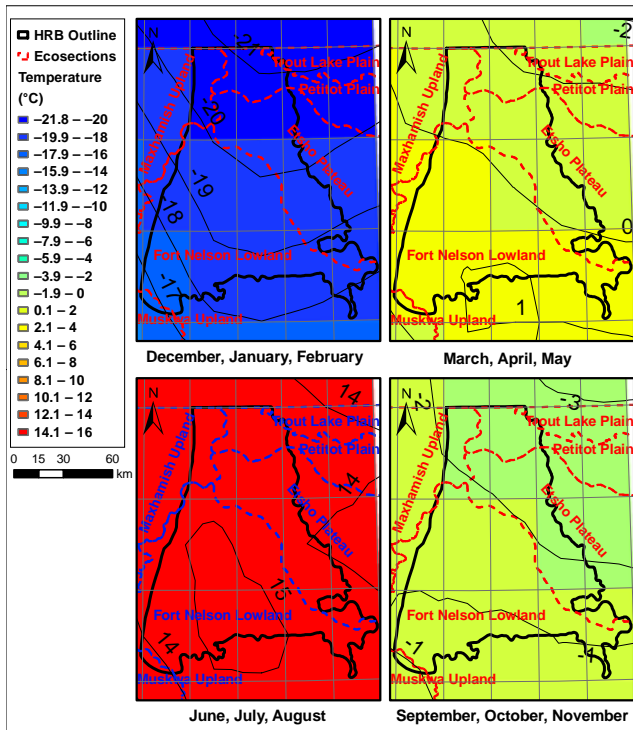


Figure 7. Seasonal surface air temperature in the HRB.

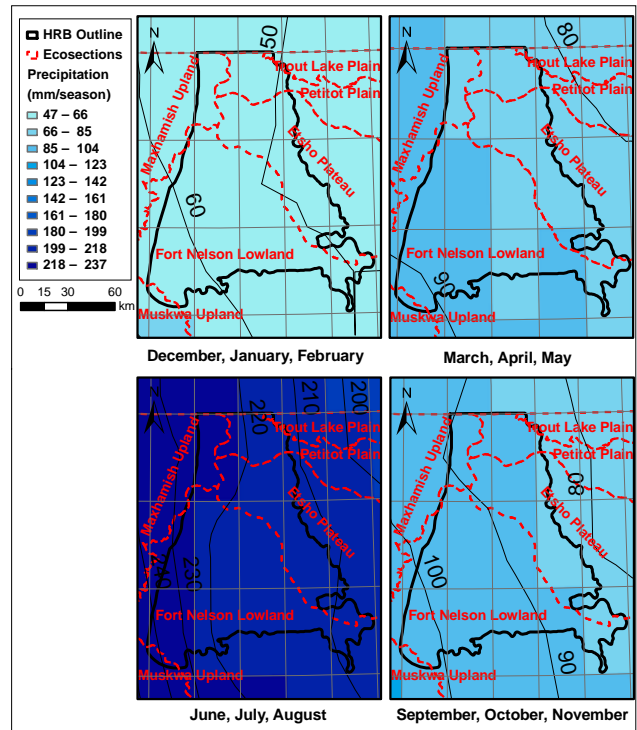


Figure 8. Seasonal precipitation as the sum of three months.

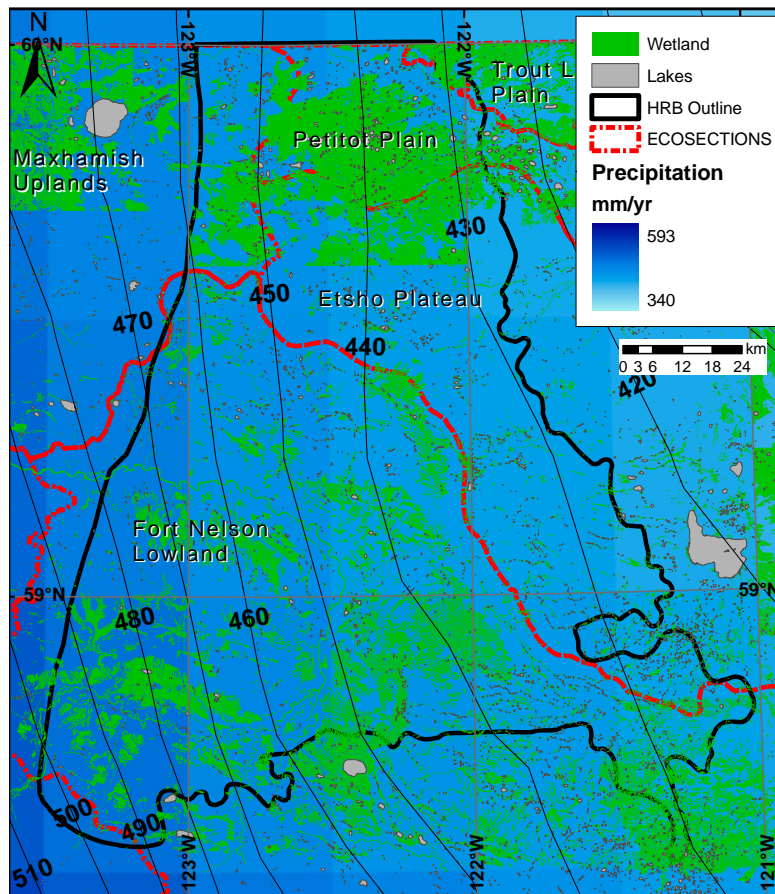


Figure 9. Annual precipitation in the HRB. Precipitation decreases to the east. Wetland and lake distribution is unrelated to regional precipitation patterns.

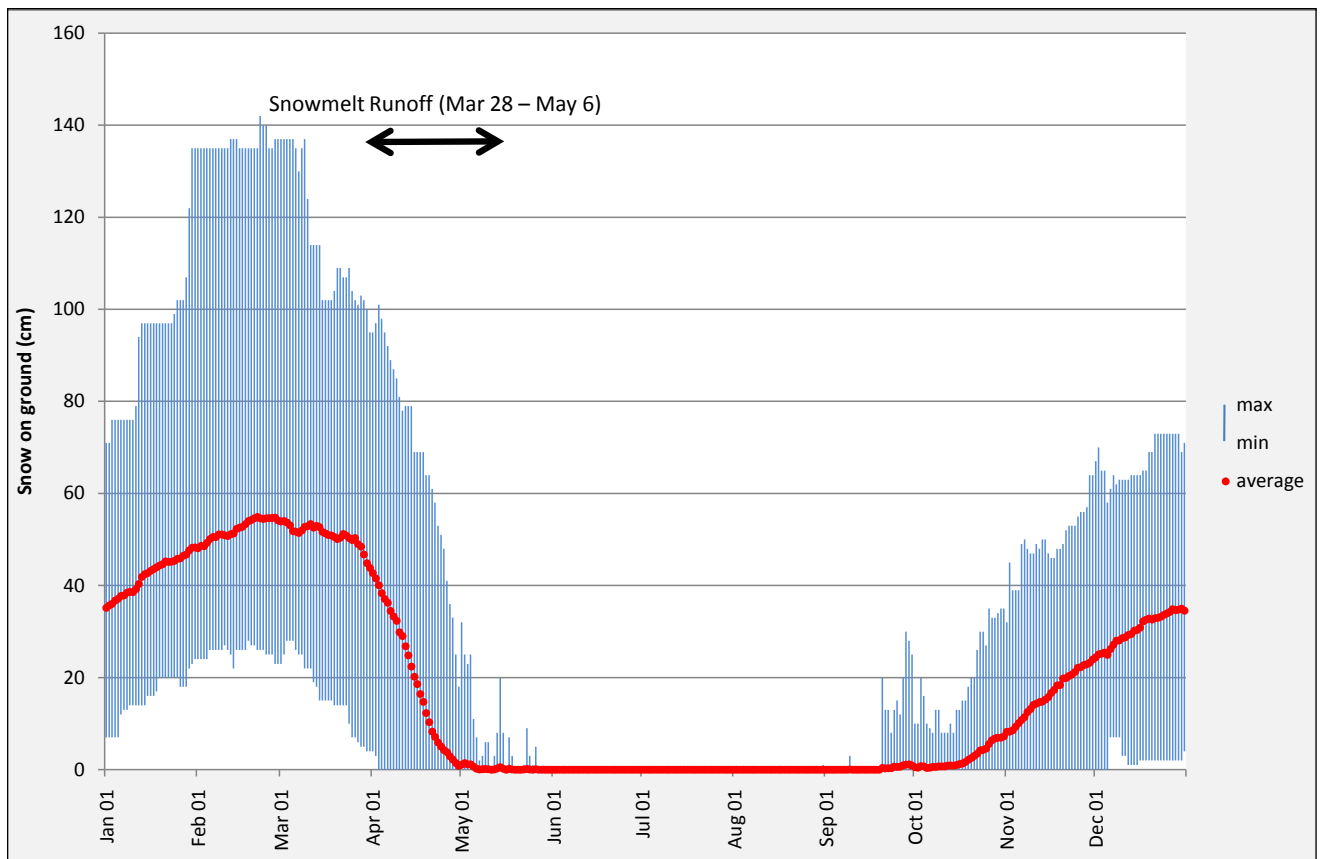


Figure 10. Snowpack volume changes throughout the year based on 54 years of data from the Fort Nelson weather station. Values in snow-water equivalent.

For hydrogeological modeling purposes, the change in season from winter to spring begins is when snowmelt runoff begins. The change in season is marked by a precipitous decrease in the snow on the ground or SWE after ambient daily temperatures rise. Melting degree days is a metric that represents the degrees centigrade above melting over the time causing melting. In Fort Nelson, SWE drops after an average of 2.5 melting degree days (Figure 11).

The snowmelt was charted against degree days to determine the distribution across a calendar year. Figure 12 shows a traditionally shaped curve of snowmelt relative to melting degree days. The historical averages were cross referenced with the melting degree day to determine the calendar date for the change of season. Because there is noise at the beginning and end of the warm season, a normalized curve was used to cross reference 2.5 melting degree days with March 28. Snowmelt runoff declines after eight melting degree days (Figure 11), which approximately corresponds to May 6 (Figure 12).

If climate change was not a factor, then March 28 would be the fixed date for the start of snowmelt. Figure 13 charts the number of melting degree days between February 1 and April 1 over time. In 1948, there was an average of three melting degree days before April 30, but there are currently five melting degree days. Regression analysis shows an increase of one melting degree day for every 27.4 years.

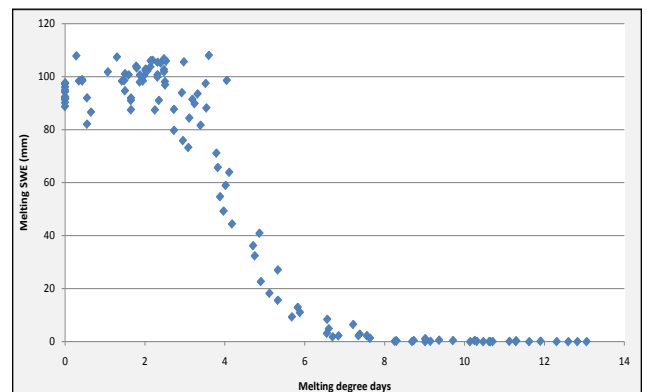


Figure 11. Snowmelt as a function of melting degree days. The graph demonstrates the rate at which the snowpack decreases with increasing numbers of days at temperatures above 0°C.

Fort Nelson is becoming progressively warmer earlier in the season and runoff is occurring earlier.

The final seasonal break occurs when rainfall diminishes and snowfall is retained on the landscape. Figure 14 shows the three runoff phases of the year with predominantly snowmelt-based runoff from March 28 to May 6, mainly rainfall runoff from May 7 to October 15 and winter low flow from October 16 to March 27.

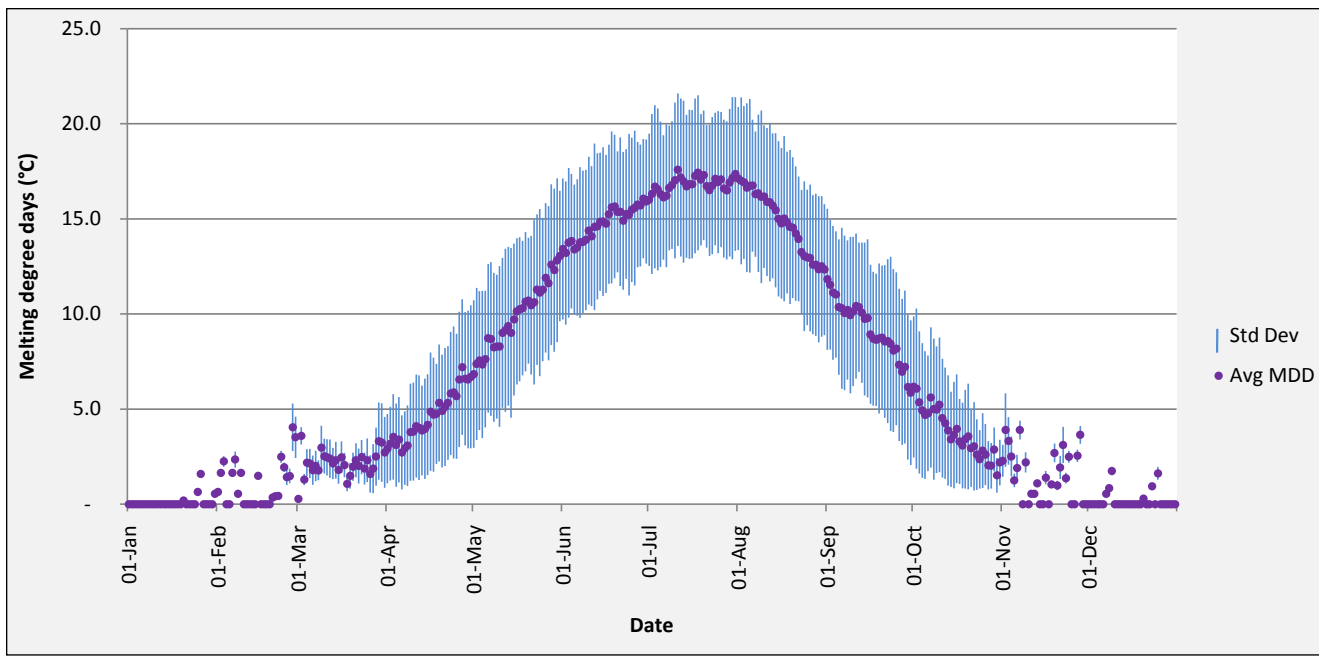


Figure 12. Melting degree days in the Horn River Basin indicate the portion of the year when melting will occur.

### Drought

The Canadian Drought Code (CDC) is a meteorological estimate that uses evapotranspiration and precipitation to model water stored in the soil. It estimates soil dryness at an average depth of 20 cm and serves to warn when lower layers of deep partly decomposed organic material may be drier than the upper layers (Girardin et al., 2006). It was designed to indicate slow drying in Canadian boreal forests as a part of the Canadian Forest Weather Index system. The CDC calculation makes no allowance for seasonal changes in vegetation but does account for daylight length. The index accounts for the effect of snowmelt and provides an indicator of water-table depth (Girardin et al., 2004). Figure 15 shows variation in CDC across 61 years. A minimum CDC value of zero represents soil saturation, whereas

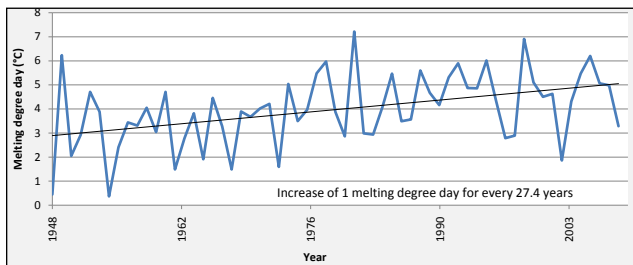


Figure 13. Average annual number of melting degree days each spring between February 1 and April 30. Regression analysis shows an increase of one melting degree day for every 27.4 years. a rating of 200 indicates high drought and a rating of over 300 indicates severe drought. Each year, CDC values begin low and climb as the cumulative effects of heat and lack of precipitation reduce soil moisture. The month during which maximum drought severity is attained is September (Figure 16).

Using Fort Nelson climate data, there is no significant trend to drought severity over time except for a slight decrease in drought severity. There is a cyclical pattern to dryness severity with a periodicity of approximately 10 years. This cyclicity does not align with El Niño or La Niña weather events. The wettest years are 1948, 1957, 1962, 1977, 1984, 1988, 1997 and 2007. Currently the climate is in a wetter phase. This should be taken into consideration when collecting new baseline data in the HRB. Lake and river levels measured now are significantly higher than during drought years. Current and accepted water withdrawal volumes may not be tenable during a drought period.

Dry spells have a direct effect on runoff. Soil moisture deficits during dry years can have a significant impact on the magnitude of the subsequent spring runoff. The length of the dry periods may control minimum runoff more than the actual values of rainfall or evapotranspiration (Metcalf and Buttle, 1999).

### Permafrost

The entire HRB lies in a region of discontinuous permafrost. Systematic observations of the distribution and thickness of the permafrost were made in the HRB along a traverse extending northeastward from Fort Nelson across the southwest-facing Etsho Escarpment and to the boundary of the Northwest Territories (Figure 17; Crampton, 1977). The thickness and hardness of permafrost increases with increasing latitude, but decreases in areas with increased insulation (e.g., southwest-facing slopes). In general, permafrost throughout the HRB exists at 51 cm (20 in.) below the surface and varies from 38 to 102 cm (15–40 in.).

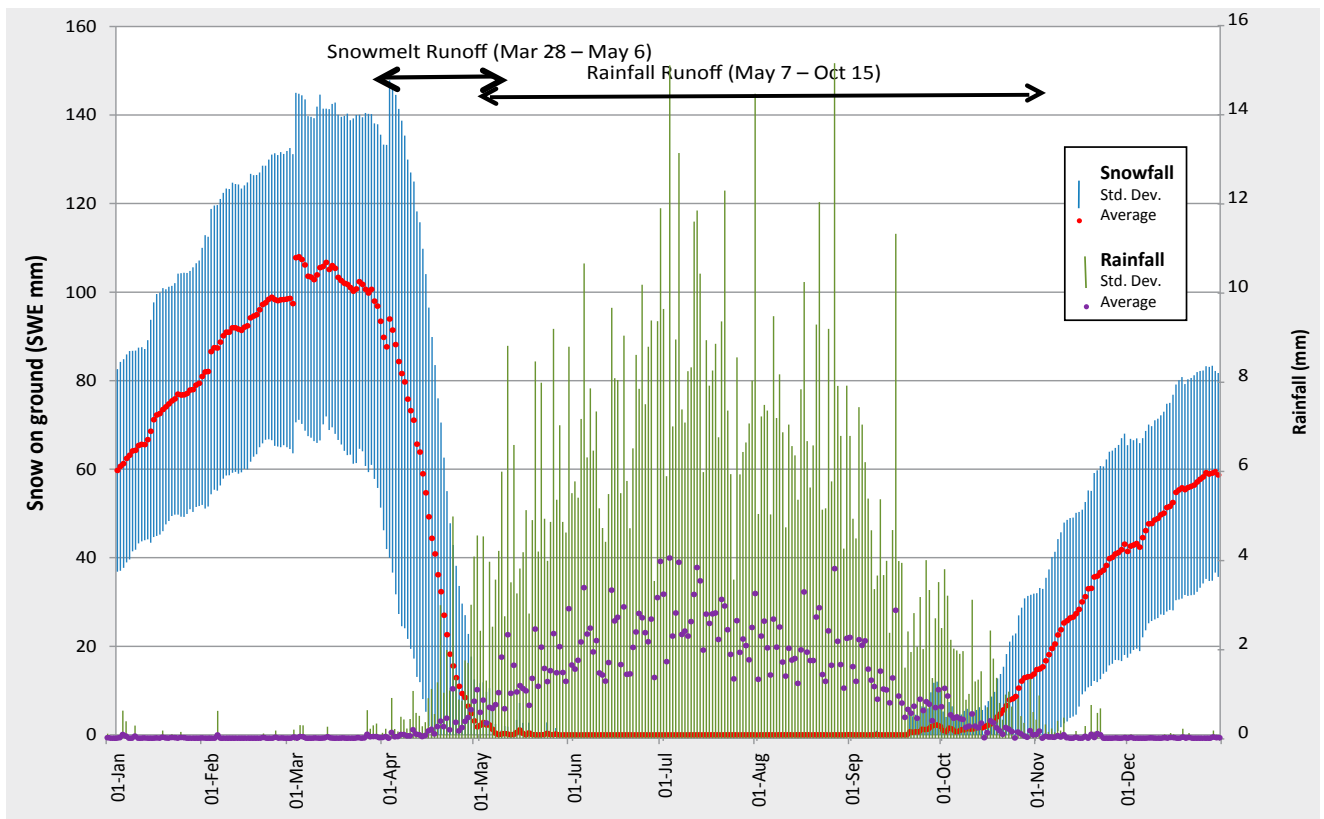


Figure 14. Precipitation in Fort Nelson as three runoff phases of the year with mainly snowmelt runoff from March 28 to May 6, mainly rainfall runoff from May 7 to October 15 and winter low flow from October 16 to March 27.

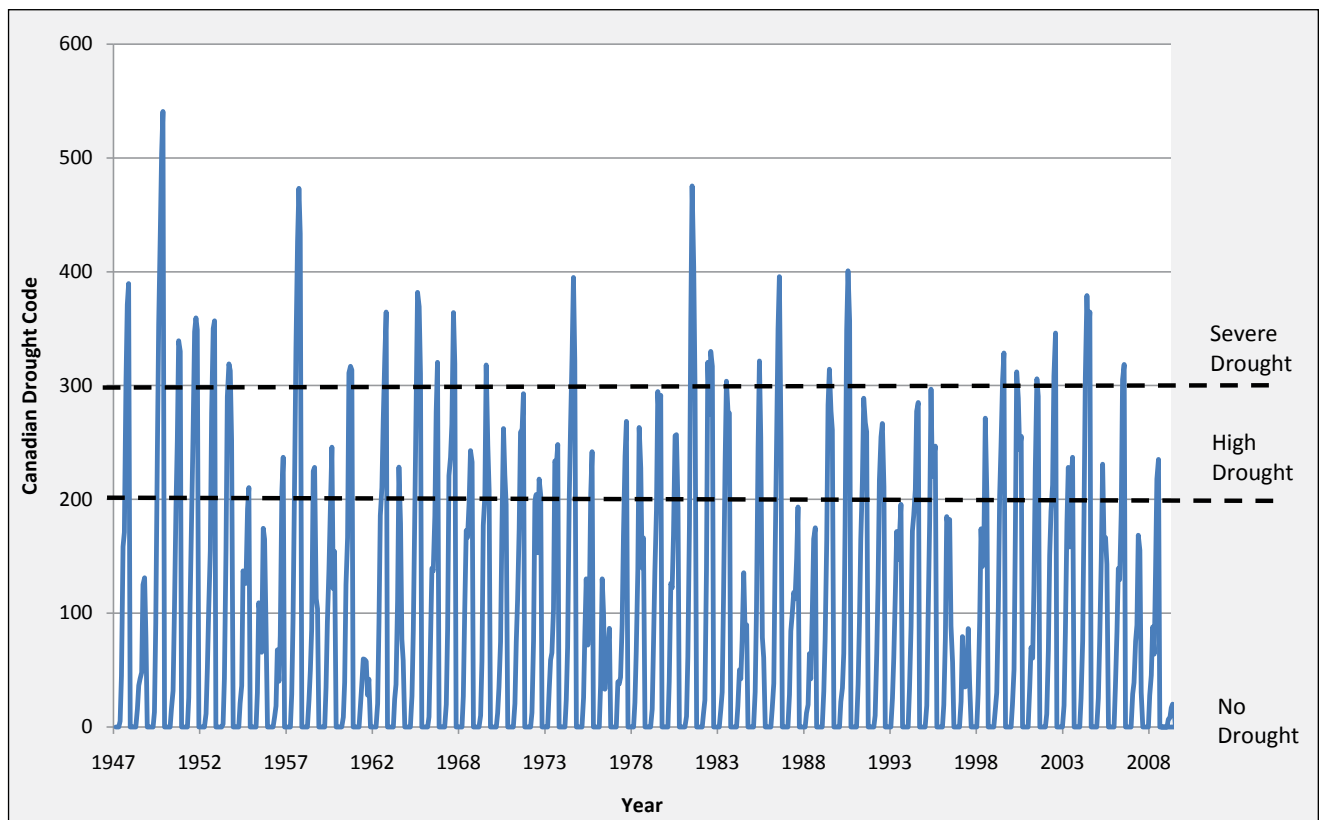


Figure 15. Canadian Drought Code averages for each month from 1948 to 2009.

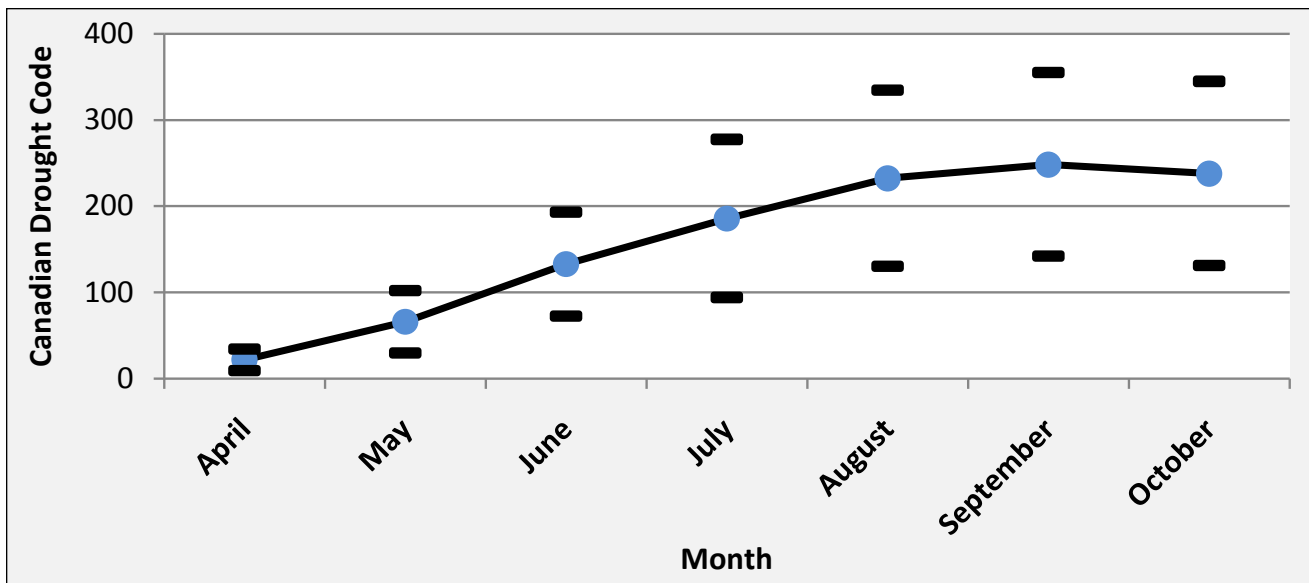


Figure 16. Average (with error bars) of the mean monthly drought index value (April–October) for the period of 1948 to 2009.

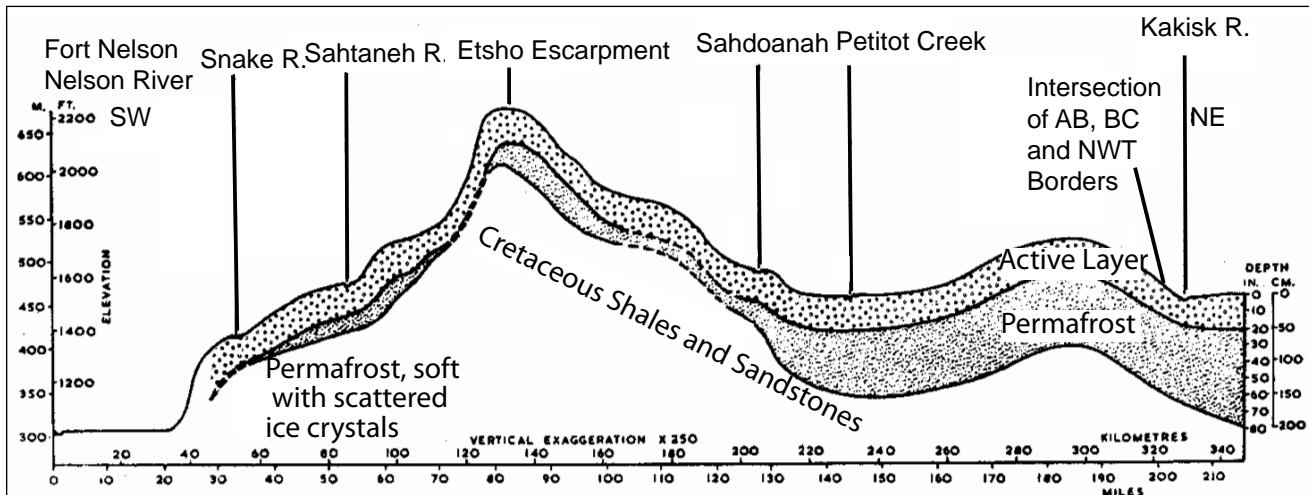


Figure 17. Longitudinal profile of the terrain across the Etsho Escarpment showing the distribution of permafrost. Vertical scale is 1:250 (Crampton, 1977).

Thermal conductivity associated with increased wetness decreases permafrost locally. However, in areas of discontinuous or isolated permafrost, ice can be found under bogs with raised sphagnum-covered mounds (M. Geertsema, pers comm, 2010). A rise in the water table (flooding) can cause permafrost degradation and the development of thermokarst terrain in areas of black spruce bog (Rennie, 1978). Areas where permafrost has melted may be marked by the development of thermokarst lakes and a transition to fen conditions (Figure 18). Permafrost will melt in areas of road development because compaction of surface soils reduces the porosity of the overlying soil and its attendant insulating capacity.



Figure 18. Thermokarst lakes in the Horn River Basin. Photo Courtesy of Adrian Hickin.

The presence of permafrost affects watershed discharge. As the temperatures climb in the spring and summer, the depth to the top of the permafrost falls so the thickness of the ice-free soil horizon is increased. The regulation of river flow by the soil horizon is restricted to short periods in the summer while there is an effective storage capacity in the soil horizon, but before the water table is lowered by evaporation.

Modeling subsurface water flow below the top of permafrost is challenging, because ice in the soil horizon affects horizontal and vertical hydraulic conductivity and porosity. The degree of soil saturation needs to be adjusted for ice content. When ice is present, it is considered to be part of the soil matrix that reduces the pore space, thereby increasing effective saturation and reducing pore size and connectivity, which decreases the saturated conductivity (Soulis and Seglenieks, 2005). One hydrogeological modeling strategy for permafrost is to preferentially adjust horizontal and vertical hydraulic conductivity by a modified form of an impedance factor. Horizontal conductivity can be restricted by reducing the thickness of the transmitting layer, which is directly related to the ice fraction. Vertically, hydraulic conductivity is restricted by reducing the width along connected pathways.

## Streams and Lakes

### STREAM DISCHARGE

The HRB lies within the Liard Basin of the Mackenzie River drainage basin. The primary gauging station for the Liard Basin (222 000 km<sup>2</sup>) is located at Fort Liard, Northwest Territories on the Liard River (station number 10ED001). Data can be acquired through the Water Survey of Canada (2010), Environment Canada. Data are also available through GEWEX's Global Runoff Data Centre (2010). Peak flows occur in June, and low flow is from November to April. The greatest percentage of annual stream flow occurs in the spring months due to snow melt. Streamflow is reduced in the summer due to lower precipitation and higher evapotranspiration.

Figure 19 displays gauging stations in the HRB and the surrounding area. The stations are listed in Table 3. There are no hydrostations capturing the outflow of the Fort Nelson River from the HRB prior to its confluence with the Liard River. There was, however, a hydrostation (station number 10DA001) that captured discharge on the Petitot River briefly from 1992 to 1996 in coordination with the MAGS project.

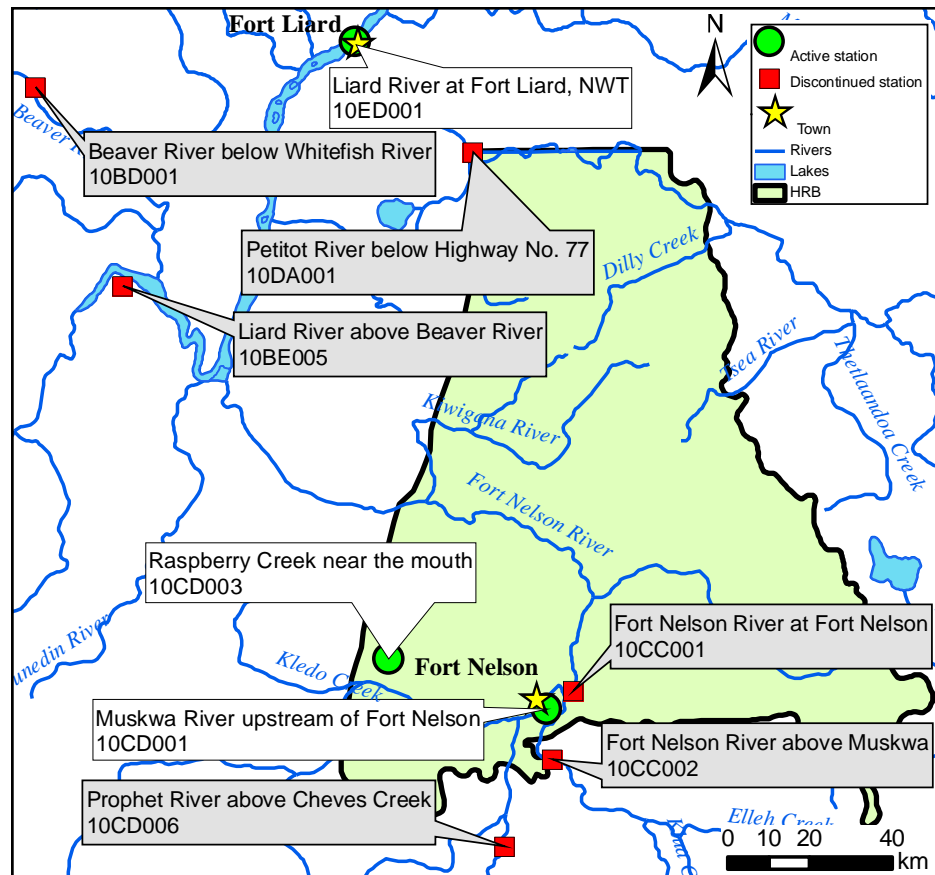


Figure 19. Locations of the streamflow gauging stations near the HRB.

TABLE 3. HYDROSTATIONS NEAR THE HORN RIVER BASIN (ENVIRONMENT CANADA, 2009).

| Location                              | Coordinates        | Station | Data available | Volume (km <sup>2</sup> ) |
|---------------------------------------|--------------------|---------|----------------|---------------------------|
| Liard River above Beaver River        | 59.70°N, 124.48°E  | 10BE005 | 1958–1995      | 119 000                   |
| Fontas River near the mouth           | 52.27°N, 121.46°E  | 10CA001 | 1988–present   | 7400                      |
| Sikanni Chief River near Fort Nelson  | 57.23°N, 122.69°E  | 10CB001 | 1944–2007      | 2160                      |
| Fort Nelson River at Fort Nelson      | 58.82°N, 122.54°E  | 10CC001 | 1960–1978      | 43 500                    |
| Fort Nelson River above Muskwa River  | 58.67°N, 122.63°E  | 10CC002 | 1978–2004      | 22 800                    |
| Muskwa River upstream of Fort Nelson  | 58.78 °N, 122.65°E | 10CD001 | 1944–present   | 20 300                    |
| Parker Creek near the mouth           | 58.24°N, 122.80 °E | 10CD002 | 1979–1982      | 61                        |
| Raspberry Creek near the mouth        | 58.89°N, 123.32°E  | 10CD003 | 1979–present   | 273                       |
| Bougie Creek at Km 368 Alaska Highway | 58.03°N, 122.72°E  | 10CD004 | 1981–2007      | 332                       |
| Prophet River above Cheves Creek      | 58.48°N, 122.83°E  | 10CD006 | 1988–1995      | 7320                      |
| Adsett Creek at Km 386 Alaska Highway | 58.11°N, 122.72°E  | 10CD005 | 1983–present   | 109                       |
| Petitot River below Hwy 77            | 60.00°N, 122.96°E  | 10DA001 | 1992–1996      | 22 400                    |
| Liard River at Fort Liard             | 60.24°N, 123.48°E  | 10ED001 | 1942–present   | 222 000                   |
| Liard River near the mouth            | 61.74°N, 121.22°E  | 10ED002 | 1974 –present  | 275 000                   |
| Rabbit Creek below Hwy 7              | 60.46°N, 123.41°E  | 10ED004 | 1978–1984      | 105                       |
| Rabbit Creek below Hwy 7              | 60.46°N, 123.36°E  | 10ED006 | 1984–1990      | 92.7                      |
| Liard River at Lindberg Landing       | 61.74°N, 121.22°E  | 10ED008 | 1991–1996      | □                         |

## LAKES

Most lakes in the HRB are small (<1 km<sup>2</sup>) and very shallow, rarely measuring more than 2 m deep. The two largest and deepest lakes in the larger HRB region are Maxhamish Lake (12 m deep) and Kotcho Lake (2 m deep). There are publicly available bathymetric surveys on less than five ‘large’ lakes in the HRB and its environs. Of those surveyed, three lakes are steep sided and deep, and two are very shallow.

The British Columbia Ministry of Environment’s GIS data layer of lakes (EAUBC\_LAKES\_SP) was compared with the Base Mapping and Geomatic Services Branch of the Integrated Land Management Bureau’s layer of lakes (TRIM\_EBM\_WATERBODIES). The TRIM layer places a minimum size threshold for a lake at 19 m<sup>2</sup> as opposed to EAUBC’s threshold of 109 m<sup>2</sup> (Table 4), so TRIM has approximately twice as many lakes (7376 TRIM compared to 3732 EAUBC). The statistically determined average diameter of HRB lakes in EAUBC is 150 m (62.5 m TRIM) and the average area is 24 000 m<sup>2</sup> (2 285 m<sup>2</sup> TRIM). The

TRIM layer's inclusion of the smaller lakes lowers the estimated mean lake size. The volume of standing surface water was estimated assuming an average flat-bottomed lake depth of 1 m and vertical sides. The estimated volume is 90 000 000 m<sup>3</sup> (106 000 000 m<sup>3</sup> TRIM).

Figure 20 shows the size distribution for lakes in the HRB. The red line represents the cumulative total. Note that 65% of all lakes are smaller than 0.5 ha, 80% of lakes are smaller than 1 ha and 95% of lakes are smaller than 4 ha. Figure 19 shows that more than a third of the larger lakes are located in the northernmost part of the basin (north of 59.7°N).

In northeast British Columbia, the maximum lake ice thickness is approximately 1 m. Ice duration averages 200 days (October–April; Rouse et al., 2008). Maximum ice-cover thickness shows differences of only about 10–20 cm for lakes of different depths.

### Muskeg

When constructing watershed models for the HRB, it is important to understand that the quantity, location and character of muskeg controls discharge. 'Muskeg' is a traditional Algonquin term for peatland that generally refers to a bog or marsh with thick layers of decaying material. The

Canadian Wetland Classification System and special studies from British Columbia (MacKenzie and Moran, 2004) use the ecological wetland classes of bog, fen, swamp and marsh. The differentiation between bogs and fens is important. To quote Quinton and Hayashi (2005), the

*...contrast between the channel fens and flat bogs suggests that the relative proportion of two these two peatland types should have implications for basin runoff. For example, a basin with a relatively high proportion of flat bogs should generate less runoff than a basin with a lower coverage of flat bogs. [Figure 4] indicates that annual runoff was positively correlated with the percentage cover of channel fens, and negatively correlated with the percentage cover of flat bogs.*

In the Taiga Plains ecoregion of the province, bogs predominate, though fens and swamps occur along the sluggish streams that drain the region. Wetlands have developed in depressions left in thick till by receding glaciers (Vitt et al., 2000). Figure 21 shows wetland distribution throughout the HRB. In detail, ponds tend to be ringed by peat deposits known as 'pond-peatland complexes' (Devito et al., 2005). According to MacKenzie and Moran (2004), a bog is a nutrient-poor, sphagnum moss-dominated peatland ecosystem in which the rooting zone is isolated from mineral-enriched groundwater, soils are acidic and few minerotrophic

TABLE 4. LAKE SIZES FOR THE HORN RIVER BASIN.

| EAUBC Lakes              |         |         |           |
|--------------------------|---------|---------|-----------|
|                          | Average | Minimum | Maximum   |
| Diameter (m)             | 149     | 15      | 2 435     |
| Area (m <sup>2</sup> )   | 24 000  | 109     | 1 740 000 |
| Volume (m <sup>3</sup> ) | 24 000  | 109     | 1 740 000 |
| TRIM Lakes               |         |         |           |
|                          | Average | Minimum | Maximum   |
| Diameter (m)             | 393     | 30      | 9 293     |
| Area (m <sup>2</sup> )   | 14 400  | 19      | 1 750 000 |
| Volume (m <sup>3</sup> ) | 14 400  | 19      | 1 750 000 |

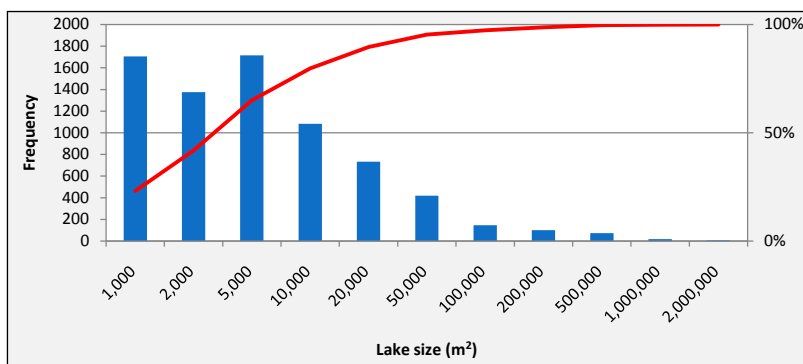


Figure 20. Histogram of lake sizes in the HRB from TRIM data.

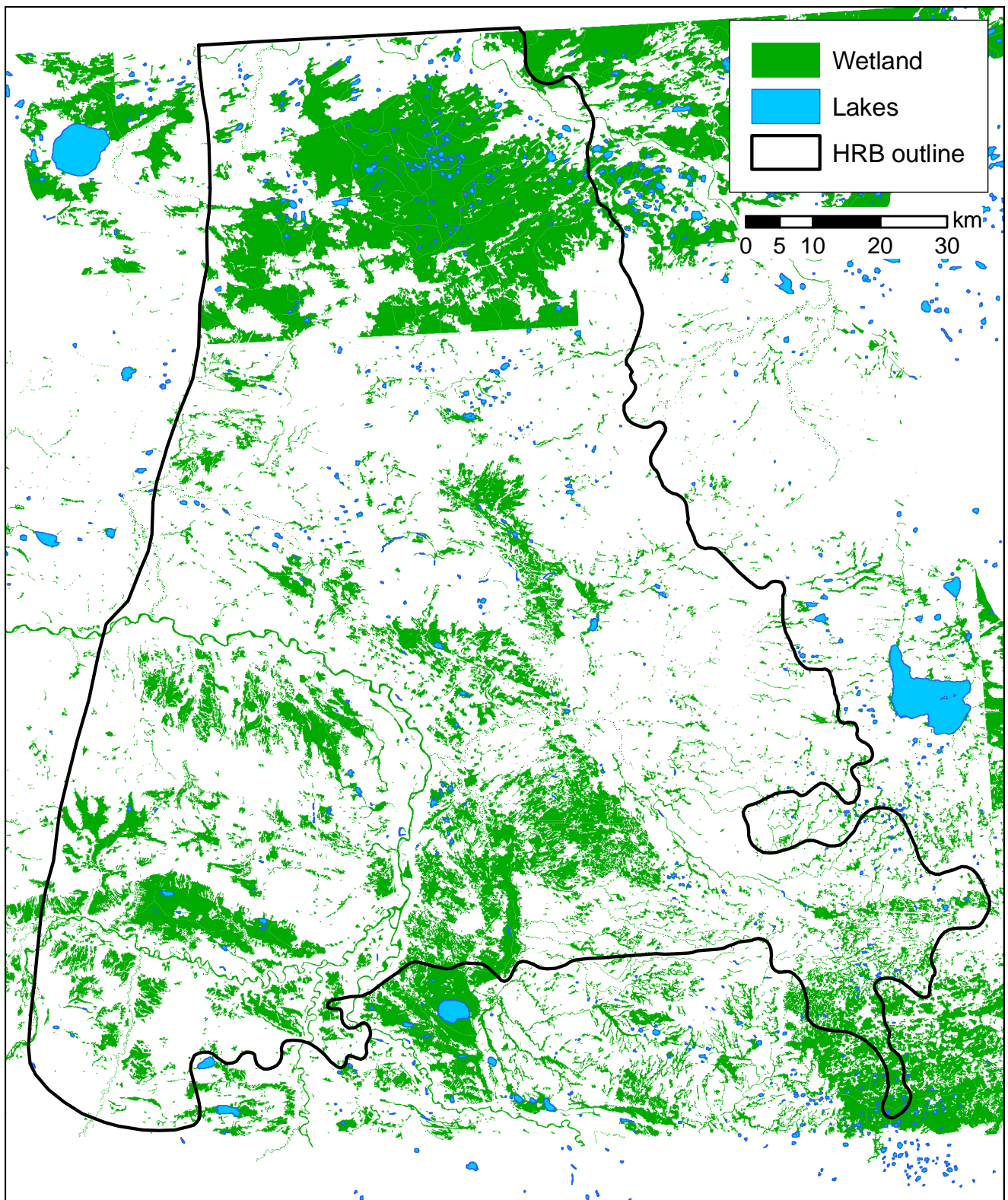


Figure 21. Wetlands and lakes (larger than 4 ha) in the HRB.

plant species occur. A fen is a nutrient-medium peatland ecosystem dominated by sedges and brown mosses, where mineral-bearing groundwater is within the rooting zone and minerotrophic plant species are common (Figure 22).



Figure 22. Bog and fen in the HRB. Photo by Elizabeth Johnson

The region southeast of Fort Simpson, Northwest Territories, is characterized by a mosaic of sphagnum moss and black spruce bogs underlain by permafrost and wet fens without permafrost (Pomeroy, 1985). There is considerable potential for development of thermokarst in the bog terrain (Pomeroy, 1985). The seven categories of muskeg in the lower Liard River valley (Pomeroy, 1985) are shown on the triangle diagram of Figure 23. Vegetation types in the HRB are shown in Figure 24.

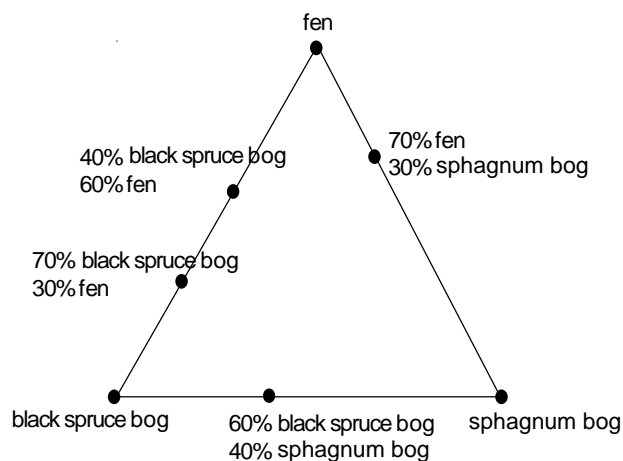


Figure 23. Triangle diagram showing seven categories of muskeg in the lower Liard River valley.

## EVAPOTRANSPIRATION

Evaporation is one of the most important factors in developing a water budget. Potential evapotranspiration is often greater than precipitation in summer months (Petroni et al., 2008). Open-water evaporation accounts for 5–60% of total evapotranspiration, depending on latitude and geography (Gibson and Edwards, 2002). Calculated catchment-weighted evaporation losses typically range from approximately 10–15% in tundra areas draining into the Arctic Ocean to as high as 60% in forested subarctic areas draining into the Mackenzie River (Gibson and Edwards, 2002).

Lakes have the highest evaporation rates of any land-cover type. Evaporation for medium and large lakes is significantly greater than for wetlands and small lakes (Table 5). Small lakes have a longer ice-covered period (six to seven months) than large lakes (four to seven months; Rouse et al., 2008). Shallow lakes warm quickly in spring and have very high evaporation rates. Evaporation during the open-water period is an important water-loss component for a small lake of 4 ha and ranges from 70 to 100% of annual precipitation (Gibson et al., 1996). In peatland, water losses through evapotranspiration are far more directly related to evaporation than transpiration. Fen areas can be expected to have evapotranspiration rates that are 10–20% lower than adjacent upland areas during a growing season. This difference may only be about 0.2 mm/day, a total of 30 mm in 150 days. For large drainage basins on the order of 10 000 km<sup>2</sup>, this difference represents  $3 \times 10^8$  m<sup>3</sup> water annually that is lost to the atmosphere (Barker et al., 2009).

Vegetation type is a large controlling feature in evapotranspiration. Sphagnum moss is prevalent in bogs and widespread in fens. It can hold large amounts of water in its cells and the surrounding area. Evaporation from sphagnum mosses is well below potential evaporation (Campbell and Williamson, 1997) compared to relatively efficient latent heat transfer by (vascular) sedges (Lafleur et al., 1997). Sphagnum can reduce evaporation by changing shape to increase water retention and changing colour to increase the albedo effect. Evaporation from fens is 20–25% greater than sphagnum bogs with dwarf shrubs and 3–10% greater than whole raised bogs.

For modern water-modeling applications, it is important to be aware that evaporative water loss and water-table drawdown can cause groundwater reversals in peatland (Devito et al., 1997). The use of lumped-parameter models for evapotranspiration can result in substantial errors when calculating long-term values for evaporation, particularly for strongly seasonal climates where errors may be as high as 50% for low-throughflow, high-evaporation lakes.

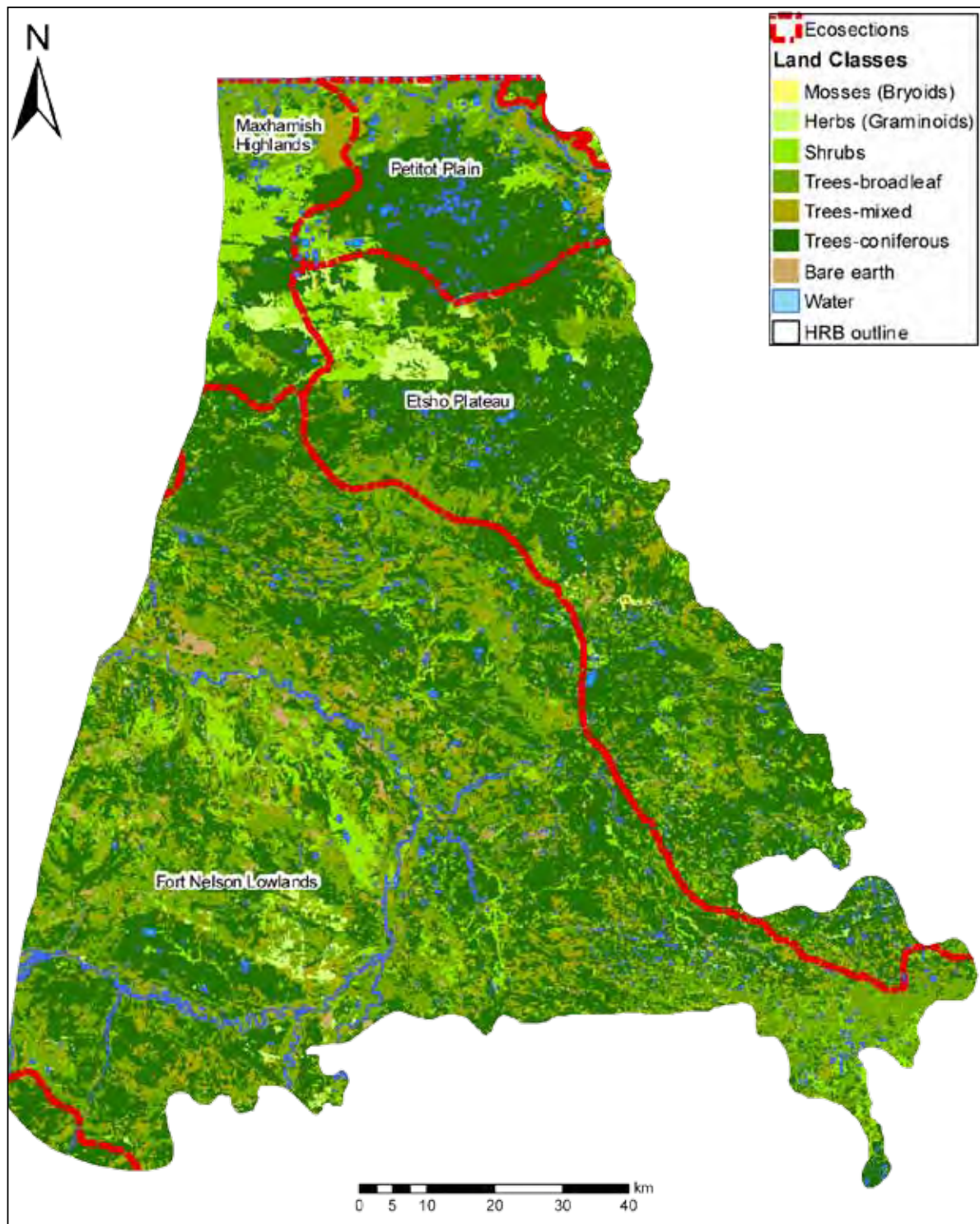


Figure 24. Vegetation map for the HRB.

TABLE 5. EVAPORATION FOR DIFFERENT-SIZED LAKES IN THE MACKENZIE BASIN COMPARED TO UPLANDS AND WETLANDS (AFTER ROUSE ET AL., 2008).

|             | Evaporation<br>(mm) | Days of open<br>water |
|-------------|---------------------|-----------------------|
| Upland      | 227                 |                       |
| Wetland     | 314                 |                       |
| Small lake  | 346                 | 154                   |
| Medium lake | 406                 | 170                   |
| Large lake  | 422                 | 228                   |

## TOPOGRAPHY

Topographic relief is important to modeling drainage in discontinuous permafrost areas. Peatlands occur extensively in the headwaters of many streams and rivers, but those headwaters can be in mountainous regions or low-lying plains. High-relief catchments efficiently drain water while lowland catchments store water (McEachern et al., 2002). Most of the HRB is low relief with less than 5% gradient. The edge of the Etsho Plateau has higher relief, up to 10%. Slope analysis shows that only a few streams appear to exceed that gradient in 094O/08 (A, F, K and L) and 094P/05E.

In high-relief catchments, snowmelt comprises half of the annual discharge. Initially, discharge is predominantly groundwater for the first week melting, but by the second week, discharge comprises mainly precipitation. Overall, discharge is low after snowmelt until mid-summer because lowering of the permafrost layer allows the creation of substantial soil volume for snowmelt infiltration (McEachern et al., 2002).

In lowlands, the depth to the water table governs streamflow response to moisture input and evapotranspiration losses. Peatland operates as a single source area with rapid response for spring runoff when the water table exceeds the depression storage capacity of wetland pools. Bogs are not generally capable of storing all of the annual precipitation because most precipitation occurs in the spring when there is a considerable surplus over storage capacity (Goode, 1977). Following snowmelt, streams in the lowlands follow predictions for saturated catchments with rapid response in streamflow for even small precipitation events. As water levels decline in lowland catchments, stream discharge becomes increasingly dominated by organic sources. Contributions to stream discharge from groundwater tends to remain relatively constant but the majority of runoff is generated from surficial water stored in peatland (McEachern et al., 2002). Relatively slow stream responses occur when

pools become disconnected into separate microcatchments during drier periods (Goode, 1977; Quinton and Roulet, 1998).

## HYDRAULIC CONDUCTIVITY

Peat has a strong ability to retain water by shrinking (compressing) to reduce pore size and increase water retention by matrix forces. The associated changes in internal pore structure can alter hydraulic properties such as bulk density and hydraulic conductivity (Price and Waddington, 2000).

Porosity is so great in peatland that precipitation will cause an immediate change in the water table. Larger-diameter soil pores of the living vegetation and lightly decomposed peat near the surface of the peat offer much less resistance to water motion than the finer-grained peat deeper in the profile (Quinton et al., 2000). Sphagnum-covered peat has macroporosity down to 20 cm depth. The macropores have been found to transport greater than 50% of the flux in a fen (Martini, 2006). In an overall context, however, evapotranspiration and groundwater–surface water interactions are more important to the water balance than changes in peat volume (Petroni et al., 2008).

Subsurface shallow flow is mainly horizontal, while flow in the lower anaerobic layer provides a negligible contribution to streamflow. The hydraulic conductivity close to the surface is often thousands of times greater than at the base of the peat layer. Hydraulic conductivity in the lowermost inert horizons of bogs is lower than that of glacial tills. There is a very marked decrease in lateral subsurface flow as the water table falls toward the base of the active layer. Although interflow can occur in substantial amounts within the active layer, water is unable to move downwards through the relatively large impermeable layers (Goode, 1977).

Subsurface drainage is strongly affected by the position and thickness of the saturated zone within the peat matrix. A first approximation for a model of the flow regime may consider a peat profile with depth-varying resistance properties with respect to subsurface flow (Quinton et al., 2000). Goode (1977) shows that vertical fluctuation is greater within the active layer of ridges than in adjacent pools over the same period of time. It is important to note that knowledge of the ratio of areas occupied by positive and negative relief elements (ridges and pools) together with their storage capacity is essential to the calculation of total runoff.

The water table often does not mirror topography in the boreal plain. Water-table gradients (counterintuitively) slope against topography. Surficial landforms influence the scale of groundwater interactions, water-table configuration and the distribution of discharge and recharge locations (Devito et al., 2005). The blanket bogs are often recharge

zones, while forested wetlands are often discharge zones. The amounts of wetland recharge and discharge can be very small. A study in Alaska found that recharge from wetlands to viable aquifers was less than 1% of the total annual recharge to the aquifer system. The amount of groundwater discharge to streams from wetlands was too small to measure (Siegel, 1989). Although groundwater plays a relatively minor part in the water balance, the mechanisms by which the peatlands retain water and exchange groundwater with adjacent ponds or uplands are important to their maintenance and the quantity of water in the ponds and hill slope soils (Petrone et al., 2008).

Groundwater participates in many peatland water budgets, but its role is difficult to quantify. The quantity of groundwater in a wetland can affect vegetation, water chemistry and biogenic gas production. The presence of permafrost (or thick and persistent ground frost) adds to this complexity. Frost hinders peat shrinkage above the water table until late summer. The ground frost also regulates horizontal and vertical moisture exchanges within the peatland and between the peatland and nearby ponds (Petrone et al., 2008).

#### ANTHROPOGENIC EFFECTS ON PEATLAND

Peatlands are developed and maintained when a positive water balance exists and there is a surplus of peat production over decomposition. In northeast British Columbia, precipitation exceeds evapotranspiration because evapotranspiration is hindered by weak sunlight and shortened growing seasons. There is very little downward loss of water because peat tends to have low vertical permeability and because there are areas of discontinuous impermeable permafrost throughout the HRB. Muskegs in the region will often not include a major outflow of water as they are found on almost completely flat land. The arctic nature of their climate severely limits peat production and the decomposition rate of peat. Little live peat grows each year, so there is that much less that can die off and decompose annually.

Anthropogenic affects on peatland are mostly associated with artificially raising or lowering the water table. When the water table is raised, forests die as they are flooded out, fens develop, CH<sub>4</sub> emissions increase and more CO<sub>2</sub> is sequestered. When the water table drops, CO<sub>2</sub> is released to the atmosphere and stream chemistry is significantly more affected by the acidic, mineral-rich waters of the peatland.

Peatlands are one of the largest terrestrial carbon reservoirs in the world (Whitfield et al., 2009). When the addition of plant material exceeds decomposition, peatlands represent a long-term net transfer site for the removal of carbon from the atmosphere. However, peatlands have the potential to become immense sources of greenhouse gases (Waddington et al., 2009). Plant material does not decompose quickly in waterlogged, airless, acidic conditions in peatlands but when the water table is lowered, significant

amounts of plant material are exposed to the air and the rate of decomposition increases dramatically. During hot dry summers when there is a drop in moisture availability, peatlands can become a net source of atmospheric CO<sub>2</sub> as photosynthesis is decreased and respiration loss enhanced (Price and Waddington, 2000). Drainage of peat also cause increases in summer baseflow, suspended sediments, maximum stream temperature, specific conductivity, pH, and NH<sub>4</sub><sup>+</sup>, NO<sub>3</sub><sup>-</sup>, Ca<sup>2+</sup>, Mg<sup>2+</sup> and Na<sup>+</sup> stream concentrations (Prevost et al., 1999).

In muskegs containing discontinuous permafrost, such as those in the HRB, road development can cause flooding. Flooding will cause permafrost degradation, development of thermokarst terrain in areas of black spruce bog and a rapid transition to fen conditions (Rennie, 1978). For example, along portions of the Liard Highway, the roadbed has acted as a dike. Surficial flows have ponded against the road increasing the area of fen and a decreasing the area of black spruce (Pomeroy, 1985).

#### INFORMATION GAPS

This paper has identified the important features for inclusion in any hydrogeological model(s) in the HRB. However, the transition from this conceptual model to a representative numerical model requires more information in the following areas:

1. Muskeg: The identification of wetland and delineation of fens and bogs. Muskeg in the HRB allows very little downward infiltration of water. Fens channel water laterally towards the basin outlet, whereas bogs retain water within the basin. Some basins in the HRB are identified as having more than 25% wetland. The appropriate characterization of wetland will dramatically affect the accuracy of the model.
2. Permafrost: Location and distribution of discontinuous permafrost. In permafrost areas, water flows in a shallow horizon with little storage capacity, while in nonpermafrost areas water may infiltrate to depth and directly affect the water table. Permafrost dictates regions of surface water-groundwater interaction. Better delineation of fens and bogs will aid in identifying potential permafrost locations.
3. Climate: The spatial distribution of evapotranspiration. Evapotranspiration is one of the largest parameters affecting water balance and is poorly understood across most of the HRB. It varies spatially with the distribution of vegetation type (e.g., upland forest, fen, bog), lakes and water-table depth.
4. Stream discharge: Increased monitoring of stream levels and watershed discharge. Greater ground-based knowledge will help calibrate any numerical model(s).

5. Water table: Increased monitoring of water-table levels basin-wide. Greater ground-based knowledge will help calibrate any numerical model(s). It will also identify spatial sensitivity to seasonal climatic variation. Water-table height dictates evapotranspiration and lateral flow. Lowering of the water-table fragments subsurface channels in fens and causes shallow lakes to disappear.
6. Topography: Delineation of lake depth. Understanding lake bathymetry will clarify the volume of water stored in lakes.
7. Lake-wetland interconnection: Identification of lakes that are connected to wetland via subsurface lateral flow and those that are isolated. Lakes are often identified as ready, replenishable water sources. Identifying isolated lakes will focus water withdrawal toward lakes that can better support the demand.
8. Identification of thermokarst lakes: Thermokarst lakes form where permafrost melts and tend to be associated with a transition to fen.

## CONCLUSIONS AND APPROACH FORWARD

The purpose of this report was to generate a conceptual model for the HRB. Generating a sound numerical water model is challenging for northeast British Columbia because of the complications introduced by discontinuous permafrost, widespread patchy muskeg, low relief and a lack of ground-based observations. Overcoming these challenges requires applying all resources available.

Information sources available relate to international, government and academic studies on global and Canadian climate and surface hydrological process modeling, the Mackenzie Basin, Canadian boreal peatland function and carbon storage modeling for peatland. An extensive international study on the Mackenzie Basin has generated a good regional water model for the Liard Basin and provided much information on surface and subsurface forcing factors that affect hydrological models. Time series and gridded climate data are available from Canadian research institutes. Gridded data are becoming available at increasingly finer resolutions. Water movement in peatland-pond complexes has been the subject of much recent research because it affects the carbon-storing capability Canadian boreal peatlands.

Climate analysis indicates that precipitation is not uniform across the HRB. Evapotranspiration is a very important component in a water balance, at times exceeding precipitation, but it varies with water table, lake distribution and vegetation type. The depth, thickness and duration of ground frost and permafrost control subsurface flow, infiltration and recharge rates. The distinction between fen and

bog is imperative to understanding and predicting stream discharge. Fens indicate interaction with laterally flowing groundwater, whereas bogs represent the storage of water and regions of potential permafrost. Water models should account for groundwater. While the groundwater component in the water balance may be minor, it represents the mechanism by which peatlands retain water, lakes and uplands exchange water, and streamwater quality and quantity is maintained.

## REFERENCES

- Anderson, B., Raabis, T. and Schwarz, C. (2009): Walleye movement and population status in the Petitot River watershed; *BC Ministry of Environment*, Paper 2004-08, 156 pages.
- ArcticRIMS (2010): A regional, integrated hydrological monitoring system for the Pan-Arctic Land Mass; *ArcticRIMS*, URL <<http://rims.unh.edu/index.shtml>> [January 2010].
- Barker, C.A., Amiro, B.D., Kwon, H., Ewers, B.E. and Angstrom, J.L. (2009): Evapotranspiration in intermediate-aged and mature fens and upland Black Spruce boreal forests; *Ecology*, Volume 2, pages 462–471.
- BC Ministry of Environment (2009): Historic snow survey data for British Columbia; *BC Ministry of Environment*, <<http://a100.gov.bc.ca/pub/mss/stationdata.do?station=4C05>> [November 2009]
- Beckers, J., Smerdon, B. and Wilson, M. (2009): Review of hydrologic models for forest management and climate change applications in British Columbia and Alberta; *FORREX Forum for Research and Extension in Natural Resources*, FORREX series 25, 166 pages.
- Bene, J., Harden, B., Griffin, S. and Nicot, J.-P. (2007): Northern Trinity/Woodbine aquifer groundwater availability model: assessment of groundwater use in the Northern Trinity aquifer due to urban growth and Barnett Shale development; *Texas Water Development Board*, Report TWDB 0604830613, pages 109–115.
- Burn, D.H., Cunderlik, J.M. and Pietroniro, A. (2004): Hydrological trends and variability in the Liard River Basin; *Hydrological Sciences Journal*, Volume 49, Number 1, pages 53–67.
- Campbell, D.I. and Williamson, J.L. (1997): Evaporation from a raised peat bog; *Journal of Hydrology*, Volume 193, Number 1–4, pages 142–160.
- Council of Canadian Academies (2009): The sustainable management of groundwater in Canada: report of the expert panel on groundwater; *Council of Canadian Academies*, page 270.
- Crampton, C.B. (1977): Changes in permafrost distribution in northeastern British Columbia; *Arctic*, Volume 30, pages 61–62.
- Dartmouth Flood Observatory (2009): Liard River Station; *Dartmouth Flood Observatory*, URL <<http://www.dartmouth.edu/~floods/AMSR-E%20Gaging%20Reaches/896.htm>> [January 2010].

- Devito, K.J., Creed, I., Gan, T., Mendoza, C., Petrone, R., Silins, U. and Smerdon, B. (2005): A framework for broad scale classification of hydrologic response units on the boreal plain: is topography the last thing to consider?; *Hydrological Processes*, Volume 19, pages 1705–1714.
- Devito, K.J., Waddington, J.M. and Branfireun, B.A. (1997): Flow reversals in peatlands influenced by local groundwater systems; *Hydrological Processes*, Volume 11, Number 1, pages 103–110.
- Environment Canada (2009): Archived hydrometric data; *Environment Canada*, URL <[http://www.wsc.ec.gc.ca/hydat/H2O/index\\_e.cfm?cname=main\\_e.cfm](http://www.wsc.ec.gc.ca/hydat/H2O/index_e.cfm?cname=main_e.cfm)> [December 2009].
- Environment Canada (2009): National climate data and information archive, daily data report; *Environment Canada*, URL <[http://www.climate.weatheroffice.ec.gc.ca/Welcome\\_e.html](http://www.climate.weatheroffice.ec.gc.ca/Welcome_e.html)> [November 2009].
- Fleming, S.W. (2009): An informal survey of watershed model users: preferences, applications, and rationales; *Streamline Watershed Management Bulletin*, Volume 13, Number 1, pages 32–35.
- Gibson, J. J. and Edwards, T.W.D. (2002): Regional water balance trends and evaporation-transpiration partitioning from a stable isotope survey of lakes in northern Canada; *Global Biogeochemical Cycles*, Volume 16, Number 2, page 1026.
- Gibson, J.J., Prowse, T.D. and Edwards, T.W.D. (1996) Evaporation from a small lake in the continental Arctic using multiple methods; *Nordic Hydrology*, Volume 24, pages 1–24.
- Girardin, M.P., Tardif, J., Flannigan, M.D., Wotton, B.M. and Bergeron, Y. (2004): Trends and periodicities in the Canadian Drought Code and their relationships with atmospheric circulation for the southern Canadian boreal forest; *Canadian Journal of Forest Research*, Volume 34, pages 103–119, doi 10.1139/X03-195.
- Girardin, M.P., Tardif, J., Flannigan, M.D. and Bergeron, Y. (2006): Forest fire-conducive drought variability in the southern Canadian boreal forest and associated climatology inferred from tree rings; *Canadian Water Resources Journal*, Volume 31, pages 275–296.
- Global Runoff Data Centre (2010): Home page; *Global Energy and Water Cycle Experiment*, URL <<http://www.gewex.org/grdc.html>> [January 2010].
- Golder Associates Ltd. (1998): Reconnaissance level (1:20,000) fish and fish habitat inventory of Slocan Group Fort Nelson Division operating area “Sahtaneh/Snake River Watershed”–1997; prepared for the Slocan group, Report Number 972-3130.
- Goode, D.A. (1977): Water resources: in Muskeg and the Northern Environment in Canada, Radforth, N.W. and Browner, C.O., Editors, *University of Toronto Press*, pages 299–331.
- Hayes, B.J.R. (2010): Horn River Basin aquifer characterization project, northeastern British Columbia (NTS 094I, J, O, P): progress report; *Geoscience BC Summary of Activities 2009*, Geoscience BC, Report 2010-1, pages 245–248.
- Holland, S.S. (1976): Landforms of British Columbia: a physiographic outline; *BC Ministry of Energy, Mines and Petroleum Resources*, Bulletin 48, 138 pages.
- Hopkinson, R. (2000): Canada gridded climate data 1961 to 1990 documentation; *Canadian Institute for Climate Studies*, URL <<http://www.cics.uvic.ca/climate/CanadaGriddedClimateData/CanadaGriddedClimateDataDocumentation.htm>> [January 2010].
- IPCC (Intergovernmental Panel on Climate Change) (2008): High resolution observational climatologies; *The IPCC Data Distribution Centre*, URL <[http://www.ipcc-data.org/cgi-bin/ddc\\_nav/?%2BVariable=pre&%3Ddisplay\\_mode=xy](http://www.ipcc-data.org/cgi-bin/ddc_nav/?%2BVariable=pre&%3Ddisplay_mode=xy)> [January 2010].
- Johnson, E. (2009): Water potential of the Mississippian Debolt Formation in the Horn River Basin, northeastern British Columbia; in *Geoscience Reports 2009*, *BC Ministry of Energy, Mines and Petroleum Resources*, pages 39–47.
- Lafleur, P.M., McCaughey, J.H., Bartlett, P.A. and Jelinski, D.E. (1997): Seasonal trends in energy, water, and carbon dioxide fluxes at a northern boreal wetland; *Journal of Geophysical Research-Atmospheres*, Volume 102, Issue D24, pages 29 009–29 020.
- MacKenzie, W.H. and Moran, J.R. (2004): Wetlands of British Columbia: a guide to identification; *Research Branch, BC Ministry of Forests*, Land Management Handbook, No. 52, URL <<http://www.for.gov.bc.ca/hfd/pubs/Docs/Lmh/Lmh52.htm>> [December 2009].
- Martini, I.P. (2006): The cold-climate peatlands of the Hudson Bay Lowland, Canada: brief review of recent work; *Peatlands*, Volume 9, Chapter 3, pages 53–84.
- McEachern, P., Prepas, E.E. and Chanasyk, D.S. (2002): Landscape control of water chemistry in northern boreal streams of Alberta; *Journal of Hydrology*, Volume 323, pages 303–324.
- Metcalf, R.A. and Buttle, J.M. (1999): Semi-distributed water balance dynamics in a small boreal forest basin; *Journal of Hydrology*, Volume 226, pages 66–87.
- Petrone, R.M., Devito, K.J., Silins, U., Mendoz, C., Brown, S.C., Kaufman, S.C. and Price, J.S. (2008): Mires and peat; *International Mire Conservation Group and International Peat Society*, Volume 3, Article 05, page 3, URL <<http://www.mires-and-peat.net>> [December 2009].
- Prevost, M., Plamondon, A.P. and Belleau, P. (1999): Effects of drainage of a forested peatland on water quality and quantity; *Journal of Hydrology*, Volume 214, Numbers 1–4, pages 130–143.
- Price, J.S. and Waddington, J.M. (2000): Advances in Canadian wetland hydrology and biogeochemistry; *Hydrological Processes*, Volume 14, pages 1579–1589.
- Pomeroy, J.W. (1985): An identification of environmental disturbances from road developments in subarctic muskeg; *Arctic*, Volume 8, Number 2, pages 104–111
- Quinton, W.L., Gray, D.M. and Marsh, P. (2000): Subsurface drainage from hummock-covered hillslopes in the Arctic tundra; *Journal of Hydrology*, Volume 237, Number 1–2, pages 113–125.

- Quinton, W.L. and Hayashi, M. (2005): Recent advances toward physically-based runoff modelling of the wetland-dominated, central Mackenzie River Basin; Final report of the Mackenzie GEWEX Study (MAGS): Proceedings of the Final (11th) Annual Scientific Meeting, 22–25 November, 2005, Ottawa, pages 565–584, URL <[http://www.usask.ca/geography/MAGS/Events/Workshops/workshop05/Workshop\\_11.pdf](http://www.usask.ca/geography/MAGS/Events/Workshops/workshop05/Workshop_11.pdf)> [December 2009].
- Quinton, W.L. and Roulet, N.T. (1998): Spring and summer runoff hydrology of a subarctic patterned wetland; *Arctic and Alpine Research*, Volume 30, Number 3, pages 285–294.
- Rennie, P.J. (1978): Forests, muskeg and organic terrain in Canada in muskeg and the northern environment in Canada; Radforth N.W. and Browner, C.O., Editors, *University of Toronto Press*, Toronto, Ontario, pages 167–207.
- Rouse, W.R., Blanken, P.D., Duguay, C.R., Oswald, C.J. and Schertzer, W.M. (2008): Climate-lake interactions; Chapter 8 in *Cold Region Atmospheric and Hydrologic Studies: The Mackenzie GEWEX Experience, Volume 2; Hydrologic Processes*, Springer-Verlag, pages 139–160.
- Siegel, D.I. (1989): The recharge-discharge function of wetlands near Juneau, Alaska: Part I. hydrogeological investigations; *Ground Water*, Volume 26, Number 4, pages 427–434.
- Soulis, E.D. and Burn, D. (2004): Integrated modelling of the Mackenzie: bringing the MAGS-I system to the application stage; Proceedings of the 10th Annual Scientific Meeting of the Mackenzie GEWEX Study (MAGS), 3–5 November 2004, Vancouver, pages 227–232, URL <[http://www.usask.ca/geography/MAGS/Events/Workshops/workshop04/Workshop\\_10.pdf](http://www.usask.ca/geography/MAGS/Events/Workshops/workshop04/Workshop_10.pdf)> [December 2009].
- Soulis, E.D. and Seglenieks, F.R. (2005): Integrated Modelling System for MAGS; final report of the Mackenzie GEWEX study (MAGS), Proceedings of the Final (11th) Annual Scientific Meeting, 22–25 November, 2005, Ottawa, pages 64–85, URL <[http://www.usask.ca/geography/MAGS/Events/Workshops/workshop05/Workshop\\_11.pdf](http://www.usask.ca/geography/MAGS/Events/Workshops/workshop05/Workshop_11.pdf)> [December 2009].
- Vitt, D.H., Halsey, L.A., Bauer, I.E. and Campbell, C. (2000): Spatial and temporal trends in carbon storage of peatlands of continental Western Canada through the Holocene; *Canadian Journal of Earth Sciences*, Volume 37, Number 5, pages 683–693.
- Waddington, J.M., Quinton, W.L., Price, J.S. and Lafleur, P.M. (2009): Advances in Canadian peatland hydrology, 2003–2007; *Canadian Water Resources Journal*, Volume 34, Number 2, pages 139–148.
- Water Act (2010): Short term use of water; *BC Ministry of Environment*, Section 8, URL <[http://www.bclaws.ca/Recon/document/freeside/--%20W%20--/Water%20Act%20%20RSBC%201996%20%20c.%20483/00\\_96483\\_01.xml](http://www.bclaws.ca/Recon/document/freeside/--%20W%20--/Water%20Act%20%20RSBC%201996%20%20c.%20483/00_96483_01.xml)> [March 2010].
- Water Survey of Canada (2010): *BC Water Resources Atlas*; Environment Canada, URL <<http://webmaps.gov.bc.ca/imf5/imf.jsp?site=wrbc>> [January 2010].
- Water Systems Analysis Group (2010): Home page; *Water Systems Analysis Group*, URL <<http://www.wsag.unh.edu>> [January 2010].
- Whitfield, P., Van der Kamp, G. and St-Hilaire, A. (2009): Introduction to peatlands special issue: improving hydrological prediction in Canadian peatlands; *Canadian Water Resources Journal*, Volume 34, Number 4, pages 303–310.
- Yirdaw, S.Z., Snelgrove, K.R., Seglenieks, F.R., Agoma, C.O. and Soulis, E.D. (2009): Assessment of the WATCLASS hydrological model result of the Mackenzie River basin using the GRACE satellite total water storage measurement; *Hydrological Processes*, Volume 23, pages 3391–3400.



# SUMMARY OF APATITE FISSION-TRACK ANALYSES AND RADIOMETRIC DATES FROM THE NECHAKO REGION, BRITISH COLUMBIA (NTS 920, N; 93B, C, E, F, G, L) AND IMPLICATIONS FOR OIL AND GAS PROSPECTIVITY

*J.M. Riddell<sup>1</sup>*

---

## ABSTRACT

*The Nechako Geoscience Project of the BC Ministry of Energy, Mines and Petroleum Resources' Oil and Gas Division began in 2004. Fieldwork and sample gathering ended in 2007, and sample analyses are largely complete. Interpretation and publication of data continues. This paper presents a summary of 17 radiometric dates and 69 apatite fission-track analyses completed during the life of the project. New radiometric ages from surface outcrops and wells provide constraints on the distribution of prospective rocks and the locations of important structures. Apatite fission-track (AFT) ages constrain the time limits of a rock's most recent passage through the oil and gas windows. The AFT data for each sample indicate whether it has been heated enough for hydrocarbon generation since trap-forming compressional tectonic events occurred in the central Cordillera.*

Riddell, J.M. (2010): Summary of apatite fission-track analyses and radiometric dates from the Nechako region, British Columbia, and implications for oil and gas prospectivity; in *Geoscience Reports 2010, BC Ministry of Energy, Mines and Petroleum Resources*, pages 123–131.

<sup>1</sup>Resource Development and Geoscience Branch, BC Ministry of Energy, Mines and Petroleum Resources, Victoria, BC

**Key Words:** Nechako Basin, apatite fission-track analyses, thermochronology, U-Pb radiometric dates, hydrocarbon generation, oil and gas window

---

## INTRODUCTION

The Nechako Geoscience Project began in 2004 with the goal of assessing the oil and gas potential of the Nechako region, specifically by evaluating critical factors of a petroleum system: the quality of petroleum source and reservoir rocks, an appropriate thermal history, and timing of potential trap formation and petroleum migration. The project involved fieldwork and sampling, regional stratigraphic correlations, thermal history studies and radiometric and fossil dating. The integration of these results with those of concurrent Nechako geoscience projects led by the Geological Survey of Canada, Geoscience BC and other partners, is ongoing.

Previous publications generated by the project have reported on fieldwork, surface geology, vitrinite reflectance and palynology (Ferri and Riddell, 2006; Riddell et al., 2007; Riddell and Ferri, 2008) and reservoir quality (Brown et al., 2008).

This paper presents a summary of radiometric dates and apatite fission-track analyses completed during the life of the project. Comprehensive analytical datasets from these studies will be released this year as open file publications.

Early Jurassic to Early Eocene formations host potential source and reservoir units in the region, so an understanding of their distribution and structure is important to the assessment of their oil and gas potential. However, in the Nechako region, rocks older than the volcanic and sedimentary rocks of the Early Eocene Ootsa Lake Group are poorly exposed and structures cannot be mapped directly. The radiometric dates and apatite fission-track analyses summarized here provide constraints on the distribution of prospective rocks and the locations of important structures.

We can infer the regional tectonic history of the covered area by assuming continuity with the areas along the strike of the Cordillera to the northwest and southeast. A large-scale compressional-transpressional regime was active from the mid-Cretaceous to the earliest Tertiary during the accretion of outboard terranes to North America. Events associated with this regime are expressed along the Intermontane Belt (in the Bowser Basin to the northwest of Nechako and in the Chilcotin Mountains to the southeast) as thrust faults and folds and by accumulations of synorogenic clastic deposits of locally derived detritus on angular unconformities (Schiarizza et al., 1997; Evenchick et al., 2007). In the Chilcotin Mountains, the main contractional structures predate the Cenomanian and younger Powell Creek formation (Schiarizza et al., 1997, 2003). In

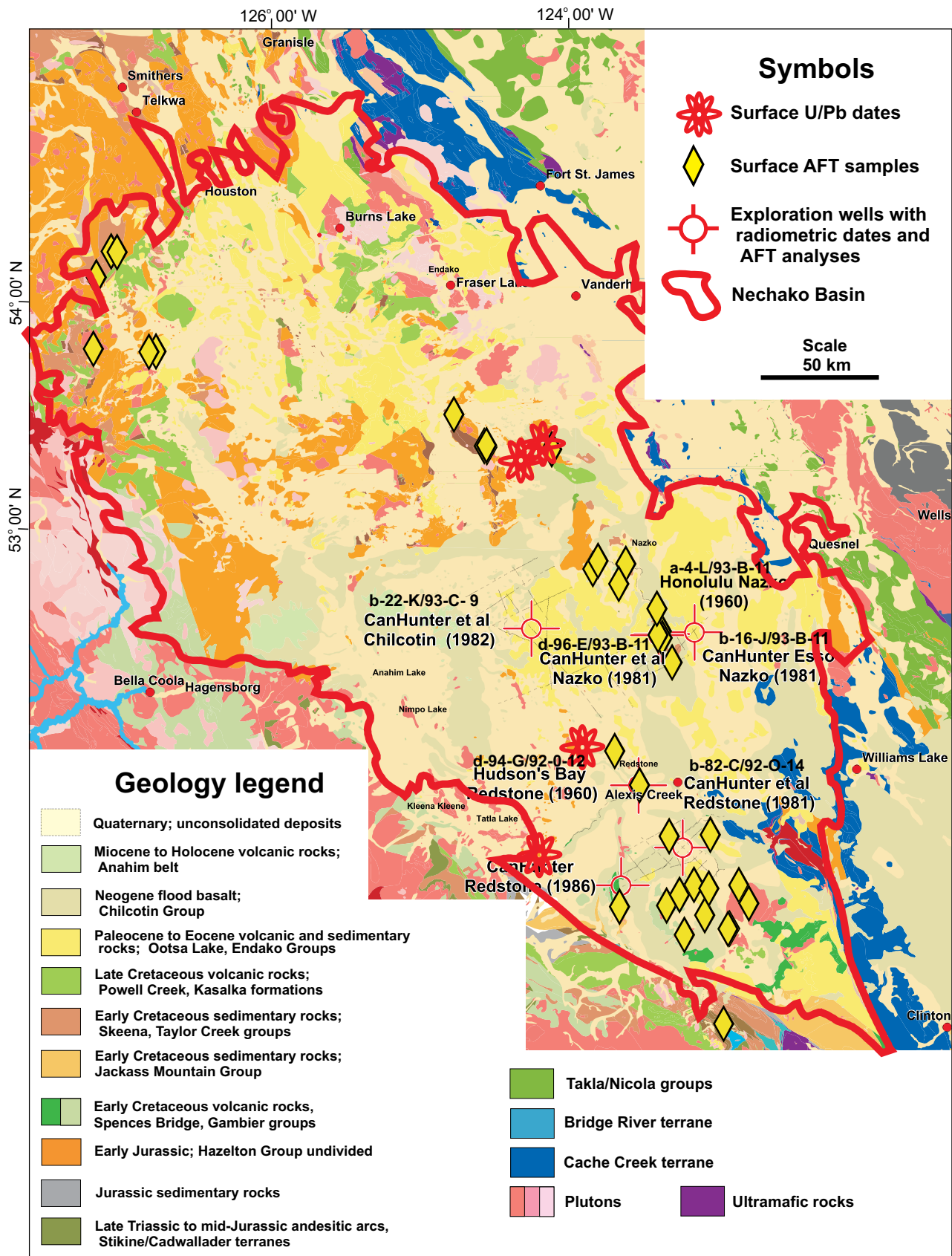


Figure 1. Nechako Basin map with radiometric and AFT sample locations.

the Bowser Basin, evidence of thrust faulting and clastic deposition continued until the Maastrichtian (Evenchick et al., 2007). The shift to Eocene transtensional tectonics is marked along the Intermontane Belt by continued and significant dextral movement along steeply dipping strike-slip structures such as the Pinchi, Fraser–Straight Creek, Yalakom and associated faults, and unroofing of metamorphic core complexes such as the Wolverine (Struik, 1993), Tatla Lake (Friedman and Armstrong, 1988) and Vanderhoof (Grainger et al., 2001) complexes. The initiation of strike-slip movement is documented in the Chilcotin Mountains beginning sometime between 70 and 65 Ma, and continuing until about 35 Ma (Umhoefer and Schiarizza, 1996). Eocene normal faulting is mapped in the south part of the Bowser Basin (O’Sullivan et al., 2009) and is inferred from interpretations of magnetic and paleomagnetic data (Lowe et al., 2001) in the Endako region.

Similar structural patterns are assumed to underlie the covered areas of the Nechako. The loci and timing of these inferred structures have direct implications for oil and gas prospectivity. Favourable conditions for the construction of important components of functioning petroleum systems would have occurred during the compressional regime;

deposition of coarse clastic reservoir units, the formation of fold and thrust-fault traps, and the burial/heating of potential source-rock units. During the Eocene transtensional regime, the deposition of volcanic, volcanoclastic and clastic sedimentary rocks of the Ootsa Lake Group may have buried and heated prospective Mesozoic source-rock units. Clastic rocks in these Eocene sequences represent additional potential reservoir units. However, Eocene movement along steeply dipping strike-slip faults would have a detrimental effect on oil and gas prospectivity by introducing vertical conduits from hydrocarbon traps to the surface, and by fragmenting plays.

## RADIOMETRIC DATES

Table 1 summarizes data from 17 U-Pb radiometric zircon dates from plutonic and volcanic rocks from the Interior Plateau of south-central British Columbia. Four samples are from surface outcrops and 13 are from archived oil and gas exploration well cuttings and core. The samples were analyzed to address stratigraphic questions about the underlying, poorly exposed Mesozoic and early Cenozoic

TABLE 1. SUMMARY OF 17 RADIOMETRIC DATES\*

| Field label                | Report #<br>(A to Z lab #) | Location                                       | Easting<br>UTM NAD 83<br>Zone 10 | Northing<br>UTM NAD 83<br>Zone 10 | Rock type                       | Sample type | U/Pb age<br>(or youngest<br>population) | Geological<br>implications   |
|----------------------------|----------------------------|--|----------------------------------|-----------------------------------|---------------------------------|-------------|---|--|
| <b>Sub-surface samples</b> |                            |  |                                  |                                   |                                 |             |   |  |
| a-4-L 10625-10864 ft       | 965-03                     | Honolulu Nazko well<br>(a-4-L/93-B-11)         | 471599                           | 5835406                           | Diorite                         | igneous     | 170.8 ± 0.8                             | mid-Jurassic pluton, co-eval with Stag Lake Stock and Spike Peak Stock                               |
| b-16-J 1060-1120m          | 738-27 (2-2)               | CanHunter Esso Nazko well<br>(b-16-J/93-B-11)  | 486398                           | 5836290                           | Clastic rocks with tuff and ash | detrital    | 57.0 ± 2.5                              | Paleocene or younger deposition above 1720 m   |
| b-16-J 1640-1720m          | 738-28 (2-3)               |  |                                  |                                   | Clastic rocks with tuff and ash | detrital    | 57.5 ± 1.4                              | Volcanics at well-base are early Cretaceous, correlation unknown                                     |
| b-16-J 2300-2385m          | 738-30 (2-5)               |  |                                  |                                   | Volcanoclastic tuffs and ash    | igneous     | 140.6 ± 1.6                             |  |
| b-22-K 2020-2095m          | 738-45 (5-3)               | Canhunter et al. Chilcotin<br>(b-22-K/93-C-14) | 413936                           | 5837969                           | Ash tuff                        | igneous     | 52.4 ± 1.6                              | Early Tertiary from 2020 to 3745 m<br>Mainly Early Eocene Ootsa Lake volcanics                       |
| b-22-K 2570-2670m          | 738-44 (5-2)               |  |                                  |                                   | Andesite flow                   | igneous     | 54.0 ± 2.1                              |  |
| b-22-K 3119-3124.5m        | 824                        |  |                                  |                                   | Flow or tuff                    | igneous     | 60.3 ± 2.2                              |  |
| b-22-K 3625-3745m          | 738-43 (5-1)               |  |                                  |                                   | Fragmental volcanic             | igneous     | 50.6 ± 1.6                              |  |
| b-82-C 635-730m            | 738-49 (6-3)               | CanHunter et al Redstone<br>(b-82-C/92-O-14)   | 480980                           | 5740701                           | Siltstone                       | detrital    | 101.7 ± 2.2                             | Deposition is Albian or later, dominant source terrane is Albian Granite at well-base is Albian-aged |
| b-82-C 1100-1200m          | 805-01                     |  |                                  |                                   | Siltstone, claystone, sst       | detrital    | 107.3 ± 0.9                             |  |
| b-82-C 1640-1700m          | 738-47 (6-1)               |  |                                  |                                   | Granite                         | igneous     | 101.4 ± 1.9                             |  |
| d-94-G 2050-2160m          | 738-36 (3-6)               | CanHunter Redstone<br>(d-94-G/92-O12)          | 453711                           | 5723900                           | Andesite                        | igneous     | 93.7 ± 3.2                              | Andesite at well-base could be Powell Creek Volcanics, OR Spences Bridge Group                       |
| d-96-E 3180-3320m          | 805-02                     | CanHunter et al. Nazko<br>(d-96-E/93-B-11)     | 470283                           | 5834950                           | Volcanoclastic lithic tuffs     | igneous     | 150.2 ± 3.1                             | Volcanics are Late Jurassic. A possible correlation is Nechako volcanics                             |
| <b>Surface samples</b>     |                            |  |                                  |                                   |                                 |             |   |  |
| FF05-85                    | 857-05                     | Puntzi Lake                                    | 434471                           | 5785920                           | andesite                        | igneous     | 101.1 ± 2.2                             | Probably Spences Bridge Group volcanics  |
| FF06-66                    | 857-04                     | Batnuni Lake                                   | 413345                           | 5917087                           | tuff                            | igneous     | 161.6 ± 2.4                             | Probably Bowser Lake Gp, possibly Hazelton   |
| JR06-28                    | 857-09                     | Batnuni Cone                                   | 422969                           | 5917545                           | rhyolite                        | igneous     | 48.51 ± 0.99                            | Ootsa Lake Group   |
| JR06-112                   | 857-12                     | Choequoit Lake                                 | 422274                           | 5731989                           | andesite                        | igneous     | 101.1 ± 2.8                             | Probably Spences Bridge Group volcanics  |

\*Surface samples were collected in 2005 and 2006; locations on Figure 1. Archived well cuttings were sampled in 2006. Analyses were performed by Apatite to Zircon, Inc. of Viola, Idaho.

stratigraphy, and to constrain timing and location of important structures. In some locations, apatite fission-track samples were collected concurrently. The specific implications of the results of U-Pb zircon dates for individual samples will be discussed in detail in a forthcoming open file publication. Some general implications about regional scale structures can be made:

- Four Paleocene to Early Eocene dates were returned from cuttings from the CanHunter et al. Chilcotin well (b-22-K/93-C-14) at depths between 2020 and 3745 m. This represents an anomalously thick section of early Paleogene and younger deposits, and may represent the location of an Eocene pull-apart basin between two en-echelon strike-slip faults. The same interpretation is made by Hayward and Calvert (in prep) based on observations of Canadian Hunter seismic and gravity surveys of the early 1980s. Bouguer low-gravity anomalies and magnetic lineations show that the well is within a rhomboidal basin.
- Two detrital and one igneous sample from the well cuttings of the CanHunter et al. Redstone well (b-82-C/92-O-14) produced ages between 101 and 108 Ma, putting them in Albian time. Granite at the base of the well is about the same age as the detrital zircons in overlying coarse clastic sediment. This is similar to what is observed during Albian time in the Bowser Basin to the north (Evenchick et al., 2007) and in the Chilcotin Mountains to the south; the peak of compressional tectonics along the Cordillera was accompanied by magmatism, concurrent rapid uplift and shedding of local detritus into adjacent basins. This is an important time in the region for the deposition of Cretaceous reservoir beds, formation of structural traps and maturation of potential source rocks by burial.
- Two surface samples from Puntzi Lake and Choelquoit Lake produced very similar ages of around 101 Ma. Both samples came from outcrops of purple and green andesitic flows and breccia that were originally mapped by Tipper (1959, 1968) as the Jurassic Hazelton Group. The new dates indicate that they are actually part of a broad but poorly exposed belt of mid-Cretaceous volcanic rocks that also crops out in the Taseko Lake map area (92O) to the east-southeast (Hickson and Higman, 1993; Riesterer et al., 2001; Schiarizza et al., 2002), where they have been correlated with the Spences Bridge Group.

## APATITE FISSION-TRACK ANALYSES

Results of 69 surface and subsurface apatite fission-track analyses are summarized in Table 2. Apatite fission-track data are used for oil and gas studies because the temperature range over which track annealing occurs, 60° to 160°C (Ketcham et al., 1999), is about the same as temperatures required for oil and gas generation. Apatite fission-track ages can thereby be used to constrain the time limits of a rock's most recent cooling through the oil and gas windows. Samples with more than one species of apatite, such as detrital samples with mixed source terrains, can contain multiple apatite geothermometers in a single sample, and can provide improved detail of the sample's cooling history.

The implications of AFT analyses for individual samples or sample sets will be discussed in detail in a forthcoming open file publication. Some general implications about regional scale structures can be made:

Figure 2 is a histogram of the oldest apatite dates from samples from the Nechako region. The oldest apatite age of a given sample indicates the earliest period of cooling through the annealing temperature of apatite. The smaller, flatter peak between 75 and 125 Ma shows samples that cooled following compressional events of the mid-Mesozoic and were not reheated again before the present. The larger histogram peak at about 50 Ma represents rocks that either formed or were reheated enough to anneal older apatite fission tracks during magmatic and volcanic events associated with the transtensional regime of the Paleocene and Eocene.

TABLE 2. SUMMARY OF 69 APATITE FISSION-TRACK SAMPLES\*

| Field label | AZZ Sample Number      | Eastings | Northing | Apatite grains observed | Data Quality<br>1=poor<br>10=excellent | Age of Oldest Apatite Fission Track (Ma) | Timing of Initiation of Uplift/Cooling (Ma) | Fission-Track Age (Zircon U/Pb Age) (Ma) | Sample type                |
|-------------|------------------------|----------|----------|-------------------------|--|--|---|--|----------------------------|
| FF05-17     | 738-01                 | 499257   | 5662348  | 1000s                   | 7                                      | Dpar (µm)=1.68: 106 ± 11.4               | Dpar (µm)=1.68: ≥106 ± 11.4                 | 82.5 ± 8.9                               | detrital                   |
| FF05-32     | 738-02                 | 453115   | 5714378  | 1000s                   | 8                                      | Dpar (µm)=1.68: 79.5 ± 3.5               | Dpar (µm)=1.68: ≥79.5 ± 3.5                 | 64.2 ± 2.8                               | detrital                   |
| FF05-38     | 738-03                 | 475060   | 5745563  | 1000s                   | 7                                      | Dpar (µm)=1.60: 51.1 ± 3.5               | Dpar (µm)=1.60: ≥51.1 ± 3.5                 | 52.3 ± 3.3                               | detrital                   |
| FF05-39     | 738-04                 | 491015   | 5710508  | 10s                     | 4                                      | Dpar (µm)=2.53: 52.6 ± 8.6               | Dpar (µm)=2.53: ≥52.6 ± 8.6                 | 42.7 ± 5.5                               | igneous                    |
| FF05-40     | 738-05                 | 481831   | 5701760  | 1000s                   | 7                                      | Dpar (µm)=1.40: 42.1 ± 5.4               | Dpar (µm)=1.40: ≥42.1 ± 5.4                 | 88.0 ± 10.8                              | igneous                    |
| FF05-44     | 738-06                 | 473928   | 5714838  | 1000s                   | 3                                      | Dpar (µm)=1.67: 100.0 ± 12.6             | Dpar (µm)=1.67: ≥100.0 ± 12.6               | 77.0 ± 3.9                               | igneous                    |
| FF05-48     | 738-07                 | 486174   | 5724102  | 10s                     | 2                                      | Dpar (µm)=1.52: 81.5 ± 4.1               | Dpar (µm)=1.52: ≥81.5 ± 4.1                 | 55.6 ± 4.9                               | igneous                    |
| FF05-49     | 738-08                 | 479689   | 5719593  | 1000s                   | 9                                      | Dpar (µm)=1.48: 53.8 ± 4.7               | Dpar (µm)=1.48: ≥53.8 ± 4.7                 | 70.4 ± 4.8                               | igneous                    |
| FF05-51     | 738-09                 | 492762   | 5722331  | <20                     | 2                                      | Dpar (µm)=1.33: 68.8 ± 4.7               | Dpar (µm)=1.33: ≥68.8 ± 4.7                 | 58.1 ± 9.7                               | igneous                    |
| FF05-52     | 738-10                 | 506063   | 5723902  | 1000s                   | 8                                      | Dpar (µm)=1.46: 53.8 ± 9.0               | Dpar (µm)=1.46: ≥53.8 ± 9.0                 | 53.9 ± 5.1                               | igneous                    |
| FF05-54     | 738-11                 | 510496   | 5715757  | 1000s                   | 1                                      | Dpar (µm)=1.38: 53.9 ± 5.1               | Dpar (µm)=1.38: ≥53.9 ± 5.1                 | 32.4 ± 1.4                               | igneous                    |
| FF05-55     | 738-12                 | 501888   | 5704608  | 1000s                   | 4                                      | Dpar (µm)=1.72: 31.3 ± 1.4               | Dpar (µm)=1.72: ≥31.3 ± 1.4                 | 38.2 ± 1.7                               | igneous                    |
| FF05-56     | 738-13                 | 501319   | 5704419  | 100s                    | 2                                      | Dpar (µm)=1.40: 39.5 ± 1.8               | Dpar (µm)=1.40: ≥39.5 ± 1.8                 | 28.1 ± 1.7                               | igneous                    |
| FF05-57     | 738-14                 | 493405   | 5746187  | <10                     | 1                                      | Dpar (µm)=1.38: 28.6 ± 1.7               | Dpar (µm)=1.38: ≥28.6 ± 1.7                 | 29.5 ± 4.5                               | igneous                    |
| FF05-60     | 738-15                 | 437930   | 5869933  | 100s                    | 1                                      | Dpar (µm)=1.44: 31.0 ± 4.7               | Dpar (µm)=1.44: ≥31.0 ± 4.7                 | 37.7 ± 4.8                               | detrital                   |
| FF05-66     | 738-16                 | 441154   | 5864344  | 100s                    | 5                                      | Dpar (µm)=1.56: 41.0 ± 6.5               | Dpar (µm)=1.56: ≥41.0 ± 6.5                 | 31.6 ± 3.6                               | igneous                    |
| FF05-70     | 738-17                 | 472028   | 5833656  | 100s                    | 6                                      | Dpar (µm)=2.24: 55.0 ± 12.1              | Dpar (µm)=2.24: ≥55.0 ± 12.1                | 97.4 ± 3.5                               | detrital                   |
| FF05-71     | 738-18                 | 470252   | 5835011  | <10                     | 3                                      | Dpar (µm)=1.51: 30.7 ± 3.5               | Dpar (µm)=1.51: ≥30.7 ± 3.5                 | 83.9 ± 8.2                               | detrital                   |
| FF05-76     | 738-19                 | 469775   | 5846631  | 100s                    | 5                                      | Dpar (µm)=1.42: 105.0 ± 4.2              | Dpar (µm)=1.42: ≥105.0 ± 4.2                | 91.8 ± 3.5                               | detrital                   |
| FF05-78     | 738-20                 | 455908   | 5866539  | <5                      | 3                                      | Dpar (µm)=2.17: 106.0 ± 5.3              | Dpar (µm)=2.17: ≥106.0 ± 5.3                | 190.9 ± 58.0                             | detrital                   |
| FF05-81     | 738-21                 | 451001   | 5783484  | 1000s                   | 5                                      | Dpar (µm)=1.64: 119.0 ± 11.8             | Dpar (µm)=1.64: ≥119.0 ± 11.8               | 40.4 ± 1.8                               | detrital                   |
| FF05-82     | 738-22                 | 461976   | 5768349  | 1000s                   | 4                                      | Dpar (µm)=1.48: 120.0 ± 10.2             | Dpar (µm)=1.48: ≥120.0 ± 10.2               | 49.8 ± 2.8                               | detrital                   |
| 1-1         | (c-75-A 3820-3850)     | 461398   | 5768336  | <20                     | 3                                      | Dpar (µm)=2.38: 121.0 ± 9.8              | Dpar (µm)=2.38: ≥121.0 ± 9.8                | 31.0 ± 3.3                               | detrital                   |
| 1-2         | (c-75-A 2610-2900)     | 461398   | 5768336  | 100s                    | 5                                      | Dpar (µm)=1.72: 147 ± 38                 | Dpar (µm)=1.72: ≥147 ± 38                   | 40.8 ± 2.5                               | detrital                   |
| 1-3         | (c-75-A 1050-1300)     | 461398   | 5768336  | 100s                    | 5                                      | Dpar (µm)=1.35: 38.9 ± 2.0               | Dpar (µm)=1.35: ≥38.9 ± 2.0                 | 42.5 ± 2.9                               | detrital                   |
| 2-1         | (b-16-J 520 - 580 m)   | 480980   | 5740701  | 1000s                   | 8                                      | Dpar (µm)=2.00: 39.3 ± 2.7               | Dpar (µm)=2.00: ≥39.3 ± 2.7                 | 53.6 ± 3.2                               | mixed igneous and detrital |
| 2-2         | (b-16-J 1060 - 1120 m) | 480980   | 5740701  | 100s                    | 6                                      | Dpar (µm)=1.56: 50.1 ± 3.2               | Dpar (µm)=1.56: ≥50.1 ± 3.2                 | 58.5 ± 3.8                               | detrital                   |
| 2-3         | (b-16-J 1640 - 1720 m) | 486398   | 5836290  | 100s                    | 7                                      | Dpar (µm)=2.21: 52.3 ± 5.7               | Dpar (µm)=2.21: ≥52.3 ± 5.7                 | 50.1 ± 3.1                               | detrital                   |
| 2-4         | (b-16-J 2020 - 2090 m) | 486398   | 5836290  | 100s                    | 5                                      | Dpar (µm)=1.88: 52.5 ± 3.3               | Dpar (µm)=1.88: ≥52.5 ± 3.3                 | 62.0 ± 5.6                               | igneous                    |
| 2-5         | (b-16-J 2300 - 2385 m) | 486398   | 5836290  | 100s                    | 4                                      | Dpar (µm)=1.88: 56.5 ± 6.8               | Dpar (µm)=1.88: ≥56.5 ± 6.8                 | 31.6 ± 2.2                               | mixed                      |
|             |                        |          |          |                         |  | Dpar (µm)=2.53: 59.2 ± 7.7               | Dpar (µm)=2.53: ≥59.2 ± 7.7                 |  |                            |
|             |                        |          |          |                         |  | Dpar (µm)=1.64: 44.0 ± 3.2               | Dpar (µm)=1.64: ≥44.0 ± 3.2                 |  |                            |
|             |                        |          |          |                         |  | Dpar (µm)=2.59: 57.4 ± 17.4              | Dpar (µm)=2.59: ≥57.4 ± 17.4                |  |                            |

\*Surface samples were collected 2005 - 2007; locations on Figure 1. Archived well cuttings were sampled in 2006. Analyses were performed by Apatite to Zircon, Inc. of Viola, Idaho. Data with AZZ sample numbers with 738 and 667 prefixes were modeled using AFTSolve v1.4.1. software. Data with AZZ sample numbers with 910 and 965 prefixes were modeled using HeFTy v1.6.7. software.

TABLE 2 CONTINUED

| Field label                   | A2Z Sample Number | Eastings | Northing | Apatite grains observed | Data Quality<br>1=poor<br>10=excellent | Age of Oldest Apatite Fission Track (Ma)   | Timing of Initiation of Uplift/Cooling (Ma)  | Pooled Fission-Track Age (Ma)<br>(Zircon U/Pb age) | Sample type                 |
|-------------------------------|-------------------|----------|----------|-------------------------|--|--|--|--|-----------------------------|
| 3-1<br>(d-94-G 30 – 100 m)    | 738-31            | 453711   | 5723900  | 100s                    | 3                                      | Dpar ( $\mu\text{m}$ )=1.23: 44.0 $\pm$ 5.4<br>Dpar ( $\mu\text{m}$ )=2.18: 45.8 $\pm$ 4.2   | Dpar ( $\mu\text{m}$ )=1.23: $\geq$ 44.0 $\pm$ 5.4<br>Dpar ( $\mu\text{m}$ )=2.18: $\geq$ 45.8 $\pm$ 4.2   | 44.2 $\pm$ 3.4                                     | detrital                    |
| 3-2<br>(d-94-G 635 – 725 m)   | 738-32            | 453711   | 5723900  | 100s                    | 5                                      | Dpar ( $\mu\text{m}$ )=1.44: 59.5 $\pm$ 2.9<br>Dpar ( $\mu\text{m}$ )=2.12: 104 $\pm$ 22     | Dpar ( $\mu\text{m}$ )=1.44: $\geq$ 59.5 $\pm$ 2.9<br>Dpar ( $\mu\text{m}$ )=2.12: $\geq$ 104 $\pm$ 22     | 51.4 $\pm$ 2.5                                     | detrital                    |
| 3-3<br>(d-94-G 1080 – 1180 m) | 738-33            | 453711   | 5723900  | 100s                    | 5                                      | Dpar ( $\mu\text{m}$ )=1.48: 52.5 $\pm$ 2.7  | Dpar ( $\mu\text{m}$ )=1.48: $\geq$ 52.5 $\pm$ 2.7   | 46.8 $\pm$ 2.4                                     | detrital                    |
| 3-4<br>(d-94-G 1470 – 1600 m) | 738-34            | 453711   | 5723900  | 10s                     | 5                                      | Dpar ( $\mu\text{m}$ )=1.40: 33.8 $\pm$ 3.2<br>Dpar ( $\mu\text{m}$ )=1.94: 35.5 $\pm$ 6.7   | Dpar ( $\mu\text{m}$ )=1.40: $\geq$ 33.8 $\pm$ 3.2<br>Dpar ( $\mu\text{m}$ )=1.94: $\geq$ 35.5 $\pm$ 6.7   | 31.4 $\pm$ 2.6                                     | detrital                    |
| 3-5<br>(d-94-G 1800 – 1880 m) | 738-35            | 453711   | 5723900  | 100s                    | 5                                      | Dpar ( $\mu\text{m}$ )=1.47: 42.0 $\pm$ 2.6<br>Dpar ( $\mu\text{m}$ )=2.30: 121 $\pm$ 9.4    | Dpar ( $\mu\text{m}$ )=1.47: $\geq$ 42.0 $\pm$ 2.6<br>Dpar ( $\mu\text{m}$ )=2.30: $\geq$ 121 $\pm$ 9.4    | 39.1 $\pm$ 2.4                                     | detrital                    |
| 3-6<br>(d-94-G 2050 – 2160 m) | 738-36            | 453711   | 5723900  | <20                     | 3                                      | Dpar ( $\mu\text{m}$ )=1.52: 47.2 $\pm$ 15.1<br>Dpar ( $\mu\text{m}$ )=2.07: 58.5 $\pm$ 17.8 | Dpar ( $\mu\text{m}$ )=1.52: $\geq$ 47.2 $\pm$ 15.1<br>Dpar ( $\mu\text{m}$ )=2.07: $\geq$ 58.5 $\pm$ 17.8 | 39.2 $\pm$ 8.7<br>(93.7 $\pm$ 3.2)                 | igneous                     |
| 4-1<br>(d-96-E 950 – 1050 m)  | 738-37            | 470283   | 5834950  | 100s                    | 4                                      | Dpar ( $\mu\text{m}$ )=1.34: 55.5 $\pm$ 3.2<br>Dpar ( $\mu\text{m}$ )=2.36: 116 $\pm$ 10.2   | Dpar ( $\mu\text{m}$ )=1.34: $\geq$ 55.5 $\pm$ 3.2<br>Dpar ( $\mu\text{m}$ )=2.36: $\geq$ 116 $\pm$ 10.2   | 51.1 $\pm$ 2.6                                     | detrital                    |
| 4-2<br>(d-96-E 1440 – 1525 m) | 738-38            | 470283   | 5834950  | 10s                     | 3                                      | Dpar ( $\mu\text{m}$ )=1.49: 41.0 $\pm$ 3.9  | Dpar ( $\mu\text{m}$ )=1.49: $\geq$ 41.0 $\pm$ 3.9   | 32.4 $\pm$ 3.1                                     | detrital                    |
| 4-3<br>(d-96-E 2010 – 2150 m) | 738-39            | 470283   | 5834950  | 10s                     | 4                                      | Dpar ( $\mu\text{m}$ )=1.31: 34.6 $\pm$ 5.8<br>Dpar ( $\mu\text{m}$ )=2.00: 38.7 $\pm$ 4.9   | Dpar ( $\mu\text{m}$ )=1.31: $\geq$ 34.6 $\pm$ 5.8<br>Dpar ( $\mu\text{m}$ )=2.00: $\geq$ 38.7 $\pm$ 4.9   | 38.4 $\pm$ 4.0                                     | detrital                    |
| 4-4<br>(d-96-E 2530 – 2570 m) | 738-40            | 470283   | 5834950  | 10s                     | 5                                      | Dpar ( $\mu\text{m}$ )=1.25: 45.8 $\pm$ 10.4<br>Dpar ( $\mu\text{m}$ )=2.02: 46.4 $\pm$ 5.7  | Dpar ( $\mu\text{m}$ )=1.25: $\geq$ 45.8 $\pm$ 10.4<br>Dpar ( $\mu\text{m}$ )=2.02: $\geq$ 46.4 $\pm$ 5.7  | 48.0 $\pm$ 5.3                                     | detrital                    |
| 4-5<br>(d-96-E 2810 – 2900 m) | 738-41            | 470283   | 5834950  | 100s                    | 5                                      | Dpar ( $\mu\text{m}$ )=1.54: 36.9 $\pm$ 4.1<br>Dpar ( $\mu\text{m}$ )=2.25: 45.5 $\pm$ 9.4   | Dpar ( $\mu\text{m}$ )=1.54: $\geq$ 36.9 $\pm$ 4.1<br>Dpar ( $\mu\text{m}$ )=2.25: $\geq$ 45.5 $\pm$ 9.4   | 31.4 $\pm$ 3.1                                     | detrital                    |
| 4-6<br>(d-96-E 525 – 625 m)   | 738-42            | 470283   | 5834950  | 100s                    | 4                                      | Dpar ( $\mu\text{m}$ )=1.48: 60.0 $\pm$ 4.8<br>Dpar ( $\mu\text{m}$ )=2.23: 125 $\pm$ 19.4   | Dpar ( $\mu\text{m}$ )=1.48: $\geq$ 60.0 $\pm$ 4.8<br>Dpar ( $\mu\text{m}$ )=2.23: $\geq$ 125 $\pm$ 19.4   | 71.4 $\pm$ 4.8                                     | detrital                    |
| 5-1<br>(b-22-K 3625 – 3745 m) | 738-43            | 413936   | 5837969  | 100s                    | 7                                      | Dpar ( $\mu\text{m}$ )=1.68: 6.0 $\pm$ 0.8<br>Dpar ( $\mu\text{m}$ )=2.19: 39.8 $\pm$ 14.1   | Dpar ( $\mu\text{m}$ )=1.68: $\geq$ 6.0 $\pm$ 0.8<br>Dpar ( $\mu\text{m}$ )=2.19: $\geq$ 39.8 $\pm$ 14.1   | 12.2 $\pm$ 1.5<br>(50.6 $\pm$ 1.6)                 | mixed<br>(tuffs, argillite) |
| 5-2<br>(b-22-K 2570 – 2670 m) | 738-44            | 413936   | 5837969  | <10                     | 1                                      | Dpar ( $\mu\text{m}$ )=1.83: 40.7 $\pm$ 20.4   | Dpar ( $\mu\text{m}$ )=1.83: $\geq$ 40.7 $\pm$ 20.4  | 26.7 $\pm$ 13.4<br>(54.0 $\pm$ 2.17)               | igneous                     |
| 5-3<br>(b-22-K 2020 – 2095 m) | 738-45            | 413936   | 5837969  | <10                     | 1                                      | Dpar ( $\mu\text{m}$ )=1.69: 39.3 $\pm$ 5.2  | Dpar ( $\mu\text{m}$ )=1.69: $\geq$ 39.3 $\pm$ 5.2   | 33.0 $\pm$ 4.4<br>(52.4 $\pm$ 1.6)                 | igneous                     |
| 5-4<br>(b-22-K 1210 – 1280 m) | 738-46            | 480980   | 5740701  | 10s                     | 2                                      | Dpar ( $\mu\text{m}$ )=1.46: 28.3 $\pm$ 3.2  | Dpar ( $\mu\text{m}$ )=1.46: $\geq$ 28.3 $\pm$ 3.2   | 24.1 $\pm$ 3.7                                     | igneous                     |
| 6-1<br>(b-82-C 1640 – 1700 m) | 738-47            | 480980   | 5740701  | 1000s                   | 3                                      | Dpar ( $\mu\text{m}$ )=1.85: 102 $\pm$ 10.3  | Dpar ( $\mu\text{m}$ )=1.85: $\geq$ 102 $\pm$ 10.3   | 85.5 $\pm$ 8.5<br>(101.4 $\pm$ 1.9)                | igneous                     |
| 6-2<br>(b-82-C 1275 – 1320 m) | 738-48            | 480980   | 5740701  | 100s                    | 3                                      | Dpar ( $\mu\text{m}$ )=1.50: 92.8 $\pm$ 8.3<br>Dpar ( $\mu\text{m}$ )=2.16: 93.3 $\pm$ 7.0   | Dpar ( $\mu\text{m}$ )=1.50: $\geq$ 92.8 $\pm$ 8.3<br>Dpar ( $\mu\text{m}$ )=2.16: $\geq$ 93.3 $\pm$ 7.0   | 72.1 $\pm$ 4.6                                     | detrital                    |
| 6-3<br>(b-82-C 635 – 730 m)   | 738-49            | 480980   | 5740701  | 100s                    | 6                                      | Dpar ( $\mu\text{m}$ )=1.55: 46.1 $\pm$ 4.3<br>Dpar ( $\mu\text{m}$ )=2.39: 53.6 $\pm$ 6.5   | Dpar ( $\mu\text{m}$ )=1.55: $\geq$ 46.1 $\pm$ 4.3<br>Dpar ( $\mu\text{m}$ )=2.39: $\geq$ 53.6 $\pm$ 6.5   | 37.4 $\pm$ 2.9                                     | detrital                    |
| 6-4<br>(b-82-C 235 – 300 m)   | 738-50            | 480980   | 5740701  | 1000s                   | 8                                      | Dpar ( $\mu\text{m}$ )=1.70: 38.0 $\pm$ 6.9<br>Dpar ( $\mu\text{m}$ )=2.51: 48.5 $\pm$ 6.2   | Dpar ( $\mu\text{m}$ )=1.70: $\geq$ 38.0 $\pm$ 6.9<br>Dpar ( $\mu\text{m}$ )=2.51: $\geq$ 48.5 $\pm$ 6.2   | 41.7 $\pm$ 4.5                                     | detrital                    |

TABLE 2 CONTINUED

| Field label          | AZZ Sample Number | Eastings | Northing | Apatite grains observed | Data Quality<br>1=poor<br>10=excellent | Age of Oldest Apatite Fission Track (Ma)  | Timing of Initiation of Uplift/Cooling (Ma)   | Pooled Fission-Track Age (Ma) | Sample type |
|----------------------|-------------------|----------|----------|-------------------------|--|---|---|-------------------------------|-------------|
| FF06-10              | 857-01            | 357626   | 5904129  | 10s                     | 2                                      | Dpar ( $\mu\text{m}$ )=1.55: 88.8 $\pm$ 19.9  | Dpar ( $\mu\text{m}$ )=1.55: $\geq$ 88.8 $\pm$ 19.9   | 86.6 $\pm$ 19.5               | detrital    |
| FF06-12              | 857-02            | 379434   | 5932897  | 100s                    | 4                                      | Dpar ( $\mu\text{m}$ )=1.88: 83.7 $\pm$ 9.1<br>Dpar ( $\mu\text{m}$ )=2.78: 87.1 $\pm$ 36.1 | Dpar ( $\mu\text{m}$ )=1.88: $\geq$ 83.7 $\pm$ 9.1<br>Dpar ( $\mu\text{m}$ )=2.78: $\geq$ 87.1 $\pm$ 36.1 | 80.4 $\pm$ 8.4                | detrital    |
| FF06-63              | 857-03            | 435864   | 5912238  | 100s                    | 5                                      | Dpar ( $\mu\text{m}$ )=1.64: 104 $\pm$ 6<br>Dpar ( $\mu\text{m}$ )=2.46: 118 $\pm$ 7        | Dpar ( $\mu\text{m}$ )=1.64: $\geq$ 104 $\pm$ 6<br>Dpar ( $\mu\text{m}$ )=2.46: $\geq$ 118 $\pm$ 7        | 107 $\pm$ 5.0                 | detrital    |
| JR06-14              | 857-06            | 392951   | 5918910  | 100s                    | 1                                      | Dpar ( $\mu\text{m}$ )=1.48: 41.2 $\pm$ 5.8<br>Dpar ( $\mu\text{m}$ )=2.03: 41.9 $\pm$ 4.8  | Dpar ( $\mu\text{m}$ )=1.48: $\geq$ 41.2 $\pm$ 5.8<br>Dpar ( $\mu\text{m}$ )=2.03: $\geq$ 41.9 $\pm$ 4.8  | 36.2 $\pm$ 3.3                | detrital    |
| JR06-16              | 857-07            | 394086   | 5918377  | 100s                    | 1                                      | Dpar ( $\mu\text{m}$ )=1.74: 53.2 $\pm$ 4.6<br>Dpar ( $\mu\text{m}$ )=2.60: 54.8 $\pm$ 13.6 | Dpar ( $\mu\text{m}$ )=1.74: $\geq$ 53.2 $\pm$ 4.6<br>Dpar ( $\mu\text{m}$ )=2.60: $\geq$ 54.8 $\pm$ 13.6 | 53.3 $\pm$ 4.4                | detrital    |
| JR06-20              | 857-08            | 394003   | 5919332  | 100s                    | 1                                      | Dpar ( $\mu\text{m}$ )=1.61: 49.4 $\pm$ 7.2<br>Dpar ( $\mu\text{m}$ )=2.46: 52.2 $\pm$ 7.2  | Dpar ( $\mu\text{m}$ )=1.61: $\geq$ 49.4 $\pm$ 7.2<br>Dpar ( $\mu\text{m}$ )=2.46: $\geq$ 52.2 $\pm$ 7.2  | 49.1 $\pm$ 5.0                | detrital    |
| JR06-28              | 857-09            | 422969   | 5917545  | 1000s                   | 9                                      | Dpar ( $\mu\text{m}$ )=2.03: 51.2 $\pm$ 4.0   | Dpar ( $\mu\text{m}$ )=2.03: $\geq$ 51.2 $\pm$ 4.0  | 52.6 $\pm$ 4.1                | igneous     |
| JR06-41              | 857-10            | 452675   | 5857782  | 100s                    | 6                                      | Dpar ( $\mu\text{m}$ )=1.75: 30.4 $\pm$ 2.5   | Dpar ( $\mu\text{m}$ )=1.75: $\geq$ 30.4 $\pm$ 2.5  | 26.4 $\pm$ 2.2                | igneous     |
| JR06-77              | 857-11            | 476496   | 5822759  | <5                      | 6                                      | Dpar ( $\mu\text{m}$ )=1.87: 40.3 $\pm$ 8.4   | Dpar ( $\mu\text{m}$ )=1.87: $\geq$ 40.3 $\pm$ 8.4  | 40.4 $\pm$ 8.3                | detrital    |
| JR07-03              | 910-01            | 615061   | 5955165  | 1000s                   | 5                                      | Dpar ( $\mu\text{m}$ )=2.04: 29.2 $\pm$ 4.2   | Dpar ( $\mu\text{m}$ )=2.04: $\geq$ 29.2 $\pm$ 4.2  | 26.6 $\pm$ 3.7                | detrital    |
| JR07-17              | 910-02            | 642922   | 5956244  | 1000s                   | 7                                      | Dpar ( $\mu\text{m}$ )=1.40: 84.6 $\pm$ 7.4   | Dpar ( $\mu\text{m}$ )=1.40: $\geq$ 84.6 $\pm$ 7.4  | 78.1 $\pm$ 6.8                | igneous     |
| JR07-18              | 910-03            | 639801   | 5955840  | 10s                     | 6                                      | Dpar ( $\mu\text{m}$ )=2.15: 69.1 $\pm$ 8.8<br>Dpar ( $\mu\text{m}$ )=1.41: 42.2 $\pm$ 2.1  | Dpar ( $\mu\text{m}$ )=2.15: $\geq$ 69.1 $\pm$ 8.8<br>Dpar ( $\mu\text{m}$ )=1.41: $\geq$ 42.2 $\pm$ 2.1  | 64.1 $\pm$ 8.2                | detrital    |
| JR07-44              | 910-04            | 614015   | 5986720  | 1000s                   | 6                                      | Dpar ( $\mu\text{m}$ )=2.50: 51.2 $\pm$ 5.0<br>Dpar ( $\mu\text{m}$ )=1.36: 44.4 $\pm$ 2.4  | Dpar ( $\mu\text{m}$ )=2.50: $\geq$ 51.2 $\pm$ 5.0<br>Dpar ( $\mu\text{m}$ )=1.36: $\geq$ 44.4 $\pm$ 2.4  | 40.7 $\pm$ 1.9                | detrital    |
| JR07-47              | 910-05            | 614667   | 5990358  | 1000s                   | 6                                      | Dpar ( $\mu\text{m}$ )=2.08: 47.0 $\pm$ 4.1   | Dpar ( $\mu\text{m}$ )=2.08: $\geq$ 47.0 $\pm$ 4.1  | 42.2 $\pm$ 2.0                | detrital    |
| JR07-62              | 910-06            | 619260   | 5998870  | 1000s                   | 6                                      | Dpar ( $\mu\text{m}$ )=1.62: 46.5 $\pm$ 2.5<br>Dpar ( $\mu\text{m}$ )=1.25: 109 $\pm$ 6     | Dpar ( $\mu\text{m}$ )=1.62: $\geq$ 46.5 $\pm$ 2.5<br>Dpar ( $\mu\text{m}$ )=1.25: $\geq$ 109 $\pm$ 6     | 43.2 $\pm$ 2.3                | detrital    |
| JR07-64              | 910-07            | 621975   | 5998688  | 1000s                   | 7                                      | Dpar ( $\mu\text{m}$ )=2.20: 120 $\pm$ 8  | Dpar ( $\mu\text{m}$ )=2.20: $\geq$ 120 $\pm$ 8   | 96.8 $\pm$ 4.1                | detrital    |
| a-4-L 4800 – 5305'   | 965-01            | 471599   | 5835406  | 10s                     | 4                                      | Dpar ( $\mu\text{m}$ )=1.490: 49.4 $\pm$ 2.8<br>Dpar ( $\mu\text{m}$ )=2.20: 112 $\pm$ 6.5  | Dpar ( $\mu\text{m}$ )=1.490: $\geq$ 49.4 $\pm$ 2.8<br>Dpar ( $\mu\text{m}$ )=2.20: $\geq$ 112 $\pm$ 6.5  | 48.3 $\pm$ 2.8                | detrital    |
| a-4-L 7180 – 7520'   | 965-02            | 471599   | 5835406  | 10s                     | 5                                      | Dpar ( $\mu\text{m}$ )=1.40: 38.5 $\pm$ 3.1<br>Dpar ( $\mu\text{m}$ )=2.42: 57.5 $\pm$ 4.8  | Dpar ( $\mu\text{m}$ )=1.40: $\geq$ 38.5 $\pm$ 3.1<br>Dpar ( $\mu\text{m}$ )=2.42: $\geq$ 57.5 $\pm$ 4.8  | 35.1 $\pm$ 2.9                | detrital    |
| a-4-L 10625 – 10864' | 965-03            | 471599   | 5835406  | 1000s                   | 2                                      | Dpar ( $\mu\text{m}$ )=1.80: 26.7 $\pm$ 3.0<br>Dpar ( $\mu\text{m}$ )=2.27: 34.7 $\pm$ 3.8  | Dpar ( $\mu\text{m}$ )=1.80: $\geq$ 26.7 $\pm$ 3.0<br>Dpar ( $\mu\text{m}$ )=2.27: $\geq$ 34.7 $\pm$ 3.8  | 16.2 $\pm$ 1.8                | igneous     |

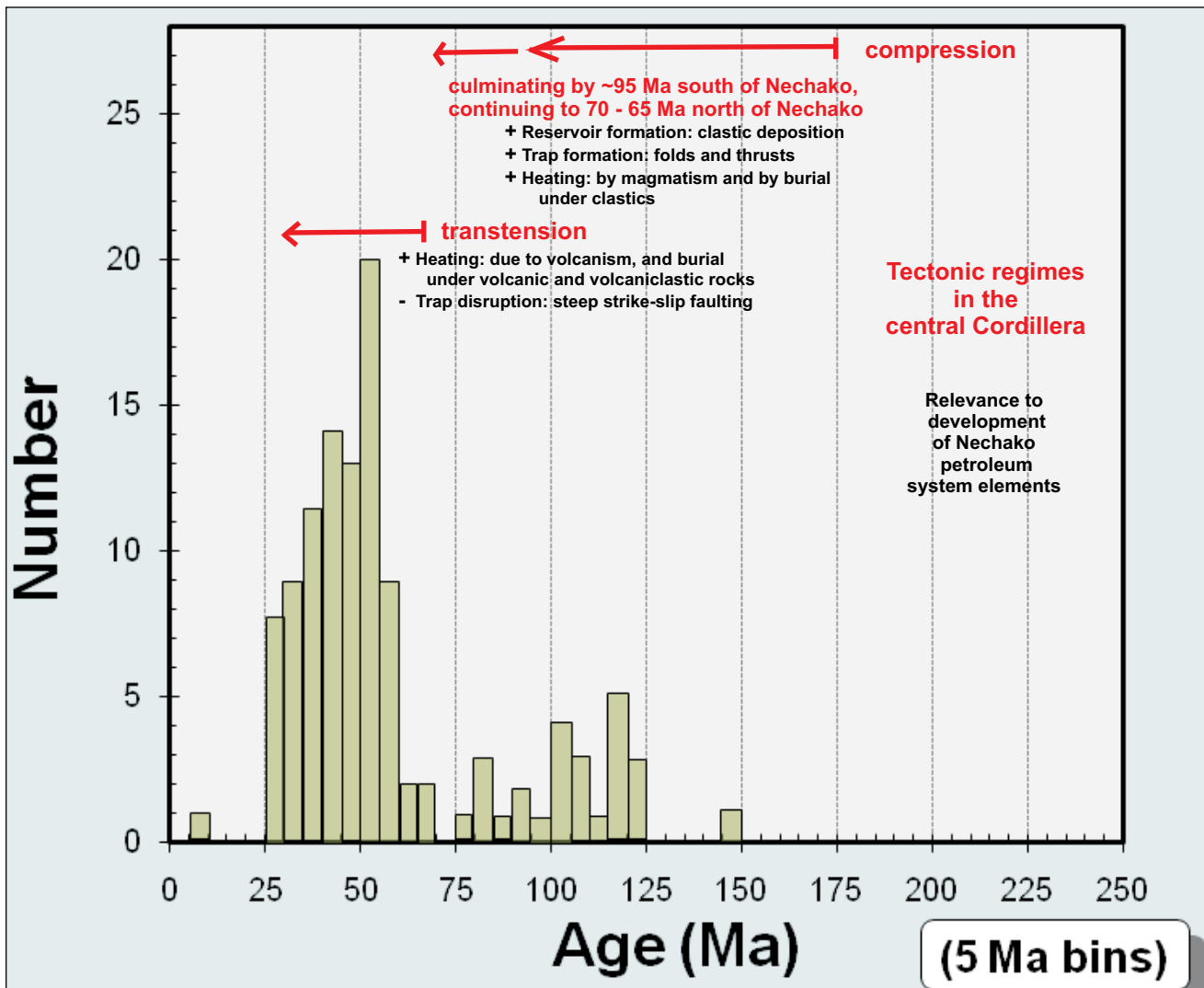


Figure 2. Histogram of ages of oldest apatite fission tracks in Nechako samples. The age of the oldest apatite in a sample is an indication of the last time the sample cooled through the higher end of the apatite annealing temperature range, about 160° C.

## ACKNOWLEDGMENTS

All radiometric dates and apatite fission-track analyses were undertaken by Paul O’Sullivan, Raymond Donelick and Margaret Donelick at the Apatite to Zircon Lab of Viola, Idaho. Helpful comments on earlier versions of the manuscript were provided by Fil Ferri, Nathan Hayward, Paul Schiarizza and Paul O’Sullivan.

## REFERENCES

- Brown, D., Simpson, J., Daniels, H. and Riddell, J. (2008): Petrographic analyses of potential reservoir units of the Nechako region of British Columbia; *BC Ministry of Energy, Mines and Petroleum Resources*, Petroleum Geology Open File 2008-09, 110 pages.
- Evenchick, C.A., McMechan, M.E., McNicoll, V.J. and Carr, S.D. (2007): A synthesis of the Jurassic-Cretaceous tectonic evolution of the central and southeastern Canadian Cordillera: exploring links across the orogen; in *Whence the Mountains? Inquiries into the Evolution of Orogenic Systems; A Volume in Honor of Raymond A. Price, Sears, J.W., Harms, T.A. and Evenchick, C.A., Editors Geological Society of America, Special Paper 433*, pages 117–145.
- Ferri, F. and Riddell, J. (2006): The Nechako Basin project: new insights from the southern Nechako Basin; in *Summary of Activities 2006, BC Ministry of Energy, Mines and Petroleum Resources*, pages 89–124.
- Friedman, R.M. and Armstrong, R.L. (1988): Tatla Lake metamorphic complex: an Eocene metamorphic complex on the southwestern edge of the Intermontane Belt of British Columbia, *Tectonics*, Volume 7, Number 6, pages 1141–1166.
- Grainger, N.C., Villeneuve, M.E., Heaman, L.M. and R.G. Anderson (2001): New U-Pb and Ar-Ar isotopic age constraints on the timing of Eocene magmatism, Fort Fraser and Nechako River map areas, central British Columbia; *Canadian Journal of Earth Sciences*, Volume 38, pages 679–696.
- Hayward, N. and Calvert, A. (in prep): Structure of the southeastern Nechako Basin, British Columbia: interpretation of the Canadian Hunter seismic surveys; *Canadian Journal of Earth Sciences*, 2011.
- Hickson, C.J. and Higman, S. (1993): Geology of the northwest quadrant, Taseko Lakes map area, west-central British Columbia; in *Current Research, Part A, Geological Survey of Canada*, Paper 93-1A, pages 63–67.
- Ketcham, R.A., Donelick, R.A., and Carlson, W.D. (1999): Variability of apatite fission-track annealing kinetics: III. Extrapolation to geological time scales, *American Mineralogist*, Volume 84, pages 1235-1255.
- Lowe, C., Enkin, R.J. and Struik, L.C. (2001): Tertiary extension in the central British Columbia Intermontane Belt: magnetic and paleomagnetic evidence from the Endako region; *Canadian Journal of Earth Sciences*, Volume 38, pages 657–678.
- O’Sullivan, P.B., Evenchick, C.A., Osadetz, K.G., Ferri, F. and Donelick, R.A. (2009): Apatite fission track data for seventeen rocks from the Bowser and Sustut basins, British Columbia; *Geological Survey of Canada*, Open File 6325, 119 pages.
- Riesterer, J.W., Mahoney, J.B. and Link, P.K. (2001): The conglomerate of Churn Creek: Late Cretaceous basin evolution along the Insular–Intermontane superterrane boundary, southern British Columbia; *Canadian Journal of Earth Sciences*, Volume 38, Number 1, pages 59–73.
- Riddell, J. and Ferri, F. (2008): Nechako Project update; in *Geoscience Reports 2008, BC Ministry of Energy, Mines and Petroleum Resources*, pages 67–78.
- Riddell, J., Ferri, F., Sweet, A. and O’Sullivan, P. (2007): New geoscience data from the Nechako Basin Project; in *The Nechako Initiative — Geoscience Update, BC Ministry of Energy, Mines and Petroleum Resources*, Open File 2007-1, pages 59–98.
- Schiarizza, P., Riddell, J., Gaba, R.G., Melville, D.M., Umhoefer, P.J., Robinson M.J., Jennings, B.K. and D. Hick (2002): Geology of the Beece Creek-Nuit Mountain area, B.C. (NTS 92N/8, 9, 10; 92O/5, 6, 12); *BC Ministry of Energy, Mines and Petroleum Resources*, Geoscience Map 2002-3, 1:100 000 scale.
- Schiarizza, P., Gaba, R.G., Glover, J.K., Garver, J.I. and Umhoefer, P.J. (1997): Geology and mineral occurrences of the Taseko-Bridge River area; *BC Ministry of Employment and Investment, Bulletin 100*, 292 pages.
- Struik, L.C. (1993): Intersecting intracontinental Tertiary transform fault systems in the North American Cordillera; *Canadian Journal of Earth Sciences*, Volume 30, pages 1262–1274.
- Tipper, H.W. (1959): Geology, Anahim Lake, British Columbia; *Geological Survey of Canada*, Map 1202, scale 1” : 4 mi.
- Tipper, H.W. (1968): Geology, Mount Waddington, British Columbia; *Geological Survey of Canada*, Map 5-1968, scale 1” : 2 mi.
- Umhoefer, P.J. and Schiarizza, P. (1996): Latest Cretaceous to early Tertiary dextral strike-slip faulting on the southeastern Yalakom fault system, southeastern Coast Belt, British Columbia; *Geological Society of America Bulletin*, Volume 108, Number 7, pages 768–785.





